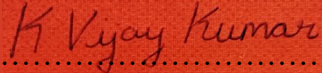




FACULTY OF SCIENCE AND TECHNOLOGY

MASTER'S THESIS

Study program/ Specialization: Master of Science in Petroleum Engineering/ Drilling and Well Engineering	Spring Semester, 2018 Confidential
Author: Vijay Kumar Keerthivasan	 (signature of author)
Faculty Supervisor: Kjell Kåre Fjelde, University of Stavanger External Supervisor: Geirmund Sætre, NOV Completion Tools	
Title of Master's thesis: Applications and Selection of Dissolvable Materials in Well Completions	
Credits: 30 ECTS	
Key words: Dissolvable materials Degradable frac balls Multistage stimulation Fracturing/Fracking Analytical model Empirical model	Number of Pages: 149 + Supplemental material/Other: 6 Stavanger, 15/06/2018

Acknowledgement

I would like to take this opportunity to express my gratitude to those who have played a key role in the completion of this Master's thesis.

Firstly, I would like to thank the management at National Oilwell Varco (NOV) Completion Tools – Tore Sørheim and Geirmund Sætre, for providing the necessary resources and laboratory facility for undertaking this research. Without Geirmund's support and understanding, it would not have been possible for me to work on the thesis while simultaneously juggling a full-time position at NOV. Additionally, his technical insights during our brainstorming sessions helped steer me towards the right direction.

As my faculty supervisor, Professor Kjell Kåre Fjelde's constructive feedback and valuable critique of my work has had a profound impact on the scientific soundness and overall quality of the end product. Even before I started conducting experiments, his advice to clearly define the objectives and plan the thesis chapters was an influential piece of advice that enabled me to be efficient and effective.

Last but not least, I would like to thank my parents – Santha Keerthivasan and Keerthivasan Venkatramani, whose continued support and encouragement motivate me to stay focussed on my goals.

Abstract

Dissolvable materials are an emerging technology in the petroleum industry with multiple areas of application, the chief among them being multistage well stimulation. The challenges associated with removal of traditional frac balls in sleeve-based multistage stimulation has seen a surge in demand for the use of dissolvable balls.

Selecting the right dissolvable frac ball for a given operational constraint and downhole condition has been a major barrier to their widespread adoption and commercialization. The present qualification process of dissolvable balls involves multiple iterations of extensive full-scale tests on several materials until the acceptance criteria for the specific application are fulfilled. There is a distinct lack of information in existing scientific literature on how to systematically select the optimal dissolvable ball. The main goal of this thesis is to simplify this tedious selection process.

A series of experiments were conducted on four dissolvable cylindrical samples from National Oilwell Varco (NOV) to characterize their responses to various test conditions. Empirical models of the dissolution rates were developed based on regression analysis of the experimental data. Thereafter, an analytical model was formulated to forecast the downhole performance of dissolvable frac balls. Finally, the empirical and analytical models were utilized to devise a stepwise workflow that enables selection of the most suitable dissolvable ball type to fulfil the operator's requirements.

This novel workflow eliminates the need for excessive full-scale qualification testing, thereby resulting in substantial cost-savings for the company while drastically improving the overall efficiency and reliability of the selection process.

Table of Contents

Acknowledgement	i
Abstract.....	ii
Table of Contents	iii
List of Figures.....	vi
List of Tables	xii
Nomenclature	xiii
Abbreviations	xv
1 Introduction.....	1
1.1 Background and Research Motivation.....	1
1.2 Thesis Concept and Problem Formulation.....	3
1.3 Thesis Objectives	5
1.4 Thesis Structure	6
2 State of the Art	9
2.1 Well Completions – An Introduction.....	9
2.2 Stimulation	13
2.2.1 Types of Stimulation Techniques	13
2.2.2 Well Completion Design for Stimulation	18
2.3 Dissolvable Materials - Applications in Petroleum Industry	24
2.3.1 Dissolvable Balls in MSF Applications – The Need	24
2.3.2 Current Developments in Dissolvable Materials	28
2.3.3 Other Applications of Dissolvable Materials in Petroleum Industry	33

3 Materials and Experimental Methods.....37

3.1	Materials Used	37
3.1.1	Dissolvable Material Samples.....	37
3.1.2	Test Fluids.....	39
3.2	Apparatus & Methods of Measurement	41
3.2.1	Heating and Temperature Measurement	41
3.2.2	Mass Measurement	43
3.2.3	Dimensional Measurement	44
3.2.4	Other Apparatus	45
3.3	Experimental Procedure	46
3.3.1	Detailed Procedure – Sample Dissolution Tests	46
3.3.2	Test Program.....	52

4 Results and Discussion.....56

4.1	Stage I - Variations in Critical Parameters during the Dissolution Process	56
4.1.1	Initial Observations from Dissolution Tests	56
4.1.2	Variation in Measured Parameters with Time	59
4.1.3	Defining the rate of dissolution reaction.....	68
4.1.4	ROD Comparison at 80 °C in 1% NaCl	76
4.2	Stage II - Investigating the Effect of Concentration on Dissolution Rate	79
4.2.1	Results: Stage II Experiments.....	80
4.2.2	Discussion: Stage II Experiments	86
4.3	Stage III - Examining the Effect of Temperature on Dissolution Rate.....	90
4.3.1	Results: Stage III Experiments.....	91
4.3.2	Discussion: Stage III Experiments.....	97
4.4	Stage IV - Combined Effect of Temperature and Concentration	102

4.4.1	Results and Discussion: Stage IV Experiments	103
4.4.2	Developing a Dissolve Rate Predictor	108
4.5	Dissolvable Ball Selection based on Sample Dissolution Test Results	125
4.5.1	Developing a Dissolvable Ball Size Calculator	125
4.5.2	Dissolvable Ball Selection Workflow.....	136
5	Conclusions and Recommendations	140
5.1	Conclusions.....	140
5.2	Recommendations.....	143
	Bibliography	144
	Appendix I	I
	Appendix II.....	V

List of Figures

Figure 1-1: Multistage stimulation using ball-actuated sleeves in a horizontal well [3] 2

Figure 1-2: Overview of Chapters 6

Figure 1-3: Overview of Chapter 2: State of the Art 7

Figure 1-4: Overview of Chapter 3: Materials and Experimental Methods 7

Figure 1-5: Overview of Chapter 4: Results and Discussion..... 8

Figure 2-1: Well Completion Design showing Upper, Middle & Lower completions [14]..... 10

Figure 2-2: Reservoir completion methods [15]..... 11

Figure 2-3: Upper Completion Methods [15] 12

Figure 2-4: Classifying Well Stimulation Techniques..... 14

Figure 2-5: Reservoir Stimulation Treatment by Fracturing [18]..... 15

Figure 2-6: Proppants used in Hydraulic Fracturing [19]..... 16

Figure 2-7: Going down to perforate with perforating guns after setting a frac-plug [25]..... 19

Figure 2-8: Plug and Perf method deployed in a cemented cased-hole completion [24] 19

Figure 2-9: Schematic of Ball-drop Activated Sleeves in an open-hole completion [2] 21

Figure 2-10: 5-stage Ball-drop Activated Sleeve Completion in cemented completions [6] 21

Figure 2-11: Automatic Remote-actuated Ball-launcher [27] 22

Figure 2-12: Ball shown landed on an NOV i-Seat™ [28] 24

Figure 2-13: Ball catcher [30]..... 26

Figure 2-14: ‘Egging’ of a ball on seat with pressure. Photo shown of a composite ball that has experienced egging during testing [5]..... 26

Figure 2-15: SEM image of cellular nano-matrix with metallic grains dispersed [8] 28

Figure 2-16: Cylindrical samples for qualification testing [4]..... 29

Figure 2-17: Tensile strength comparison between Dissolvable metal, PGA and an Aluminum alloy (6016-T6) [10] 30

Figure 2-18: Results from impact testing. a) Showing the metallic and plastic balls on seat b) Showing the metallic and plastic balls after impact testing [9] 31

Figure 2-19: Composite Frac Plugs – Halliburton Fas Drill® [35] 33

Figure 2-20: Dissolvable Frac Plugs - Halliburton Illusion® [39] 34

Figure 2-21: Gas Lift Valve with Dissolvable Material [41].....	35
Figure 2-22: Pre-perforated liner with dissolvable plugs [41].....	36
Figure 3-1: Cylindrical Sample made from NOV Dissolve 105.....	38
Figure 3-2: Heater	41
Figure 3-3: Heater used to heat and maintain a water bath at required temperature	42
Figure 3-4: Thermostat used to monitor temperature of test fluid.....	42
Figure 3-5: Weighing scale to measure cylindrical sample mass	43
Figure 3-6: Scale used to weigh NaCl crystals for test fluid preparation	44
Figure 3-7: Digital Vernier Caliper.....	44
Figure 3-8: Heat Gun used to dry samples.....	45
Figure 3-9: Test fluid inside the jar being heated using a water bath	47
Figure 3-10: Test Data Sheet Example – Pre-test data	48
Figure 3-11: Lowering the dissolvable material sample into the test fluid using sample holder .	49
Figure 3-12: Test Data Sheet Example – Completed Test Data	50
Figure 3-13: Schematic of Stage I Test Outline.....	52
Figure 3-14: Schematic of Stage II Test Outline	53
Figure 3-15: Schematic of Stage III Test Outline	54
Figure 3-16: Schematic of Stage IV Test Outline.....	55
Figure 4-1: Cloud of gas bubbles as soon as sample is lowered into the test fluid	57
Figure 4-2: Dissociation of NaCl when dissolved in water. The chloride ions and sodium ions dissociate and are surrounded by hydrogen and oxygen atoms respectively [44]	57
Figure 4-3: NOV Dissolve 105 – Untested Sample vs Tested Sample (80 °C, 1% NaCl)	59
Figure 4-4: Length measurements during dissolution test of NOV Dissolve 105 in 1% NaCl at 80 °C.....	60
Figure 4-5: Diameter measurements during dissolution test of NOV Dissolve 105 in 1% NaCl at 80 °C.....	61
Figure 4-6: NOV Dissolve 105 weight as a function of time at 80 °C in 1% aq. NaCl.....	62
Figure 4-7: NOV Dissolve 105 weight (% of initial sample mass) as a function of time at 80 °C in 1% aq. NaCl	62
Figure 4-8: The effect of surface area in a solid-liquid reaction [46]	63
Figure 4-9: NOV 105 sample’s surface area as a function of time at 80 °C in 1% aq. NaCl	64

Figure 4-10: Perforated sample holder to ensure uniform exposure of sample's surface area to test fluid	65
Figure 4-11: Measured weight as a function of time for the four dissolvable samples at 80 °C and 1% NaCl solution	66
Figure 4-12: Surface area as a function of time for the four dissolvable samples at 80 °C and 1% NaCl solution	67
Figure 4-13: NOV Dissolve 105 mass rate as a function of time at 80 °C in 1% aq. NaCl.....	68
Figure 4-14: NOV Dissolve 105 surface area as a function of time at 80 °C in 1% aq. NaCl	69
Figure 4-15: NOV Dissolve 105 mass rate and surface area as a function of time at 80 °C in 1% aq. NaCl	70
Figure 4-16: NOV Dissolve 105 ROD as a function of time at 80 °C in 1% aq. NaCl	72
Figure 4-17: Transient Period versus Steady State Period: NOV Dissolve 105 at 80 °C in 1% aq. NaCl	73
Figure 4-18: ROD as a function of time for the four dissolvable samples at 80 °C and 1% NaCl solution.....	76
Figure 4-19: Schematic of Stage II Test Outline	79
Figure 4-20: Steady State ROD (ROD_{ss}) plotted as a function of NaCl concentration at 80 °C for Material 105	80
Figure 4-21: Steady State ROD (Normalized w.r.t to the ROD_{ss} in 1% NaCl) plotted as a function of NaCl concentration at 80 °C for Material 105.....	81
Figure 4-22: Steady State ROD (ROD_{ss}) plotted as a function of NaCl concentration at 80 °C for Material 106	82
Figure 4-23: Steady State ROD (Normalized w.r.t to the ROD_{ss} in 1% NaCl) plotted as a function of NaCl concentration at 80 °C for Material 106.....	82
Figure 4-24: ROD_{ss} plotted as a function of NaCl concentration at 80 °C for Material 202.....	83
Figure 4-25: Steady State ROD (Normalized w.r.t to the ROD_{ss} in 1% NaCl) plotted as a function of NaCl concentration at 80 °C for Material 202.....	83
Figure 4-26: ROD_{ss} plotted as a function of NaCl concentration at 80 °C for Material 301	84
Figure 4-27: Steady State ROD (Normalized w.r.t to the ROD_{ss} in 1% NaCl) plotted as a function of NaCl concentration at 80 °C for Material 301.....	84

Figure 4-28: Steady State ROD (Normalized w.r.t to the corresponding ROD_{ss} in 1% NaCl) plotted as a function of NaCl concentration at 80 °C for all materials	85
Figure 4-29: Catalytic mechanism of chloride ions during the dissolution reaction [48]	87
Figure 4-30: Schematic of Stage III Test Outline	90
Figure 4-31: Steady State ROD plotted as a function of temperature for Material 105 with the test fluid being 1% aqueous solution of NaCl	91
Figure 4-32: Steady State ROD (Normalized w.r.t to the ROD_{ss} at 50 °C) plotted as a function of temperature for Material 105 with the test fluid being 1% aq. solution of NaCl	92
Figure 4-33: Steady State ROD plotted as a function of temperature for Material 106 with the test fluid being 1% aqueous solution of NaCl	92
Figure 4-34: Steady State ROD (Normalized w.r.t to the ROD_{ss} at 50 °C) plotted as a function of temperature for Material 106 with the test fluid being 1% aq. solution of NaCl	93
Figure 4-35: Steady State ROD plotted as a function of temperature for Material 106 with the test fluid being 1% aqueous solution of NaCl	93
Figure 4-36: Steady State ROD (Normalized w.r.t to the ROD_{ss} at 50 °C) plotted as a function of temperature for Material 202 with the test fluid being 1% aq. solution of NaCl	94
Figure 4-37: Steady State ROD plotted as a function of temperature for Material 301 with the test fluid being 1% aqueous solution of NaCl	94
Figure 4-38: Steady State ROD (Normalized w.r.t to the ROD_{ss} at 50 °C) plotted as a function of temperature for Material 301 with the test fluid being 1% aq. solution of NaCl	95
Figure 4-39: Steady State ROD (Normalized w.r.t to the corresponding ROD_{ss} at 50 °C) plotted as a function of temperature for all materials with the test fluid being 1% aq. solution of NaCl	95
Figure 4-40: Activation energy of a chemical reaction [50]	97
Figure 4-41: Maxwell- Boltzmann Distribution definition [50]	98
Figure 4-42: Activation energy represented on a Maxwell- Boltzmann Distribution [50]	98
Figure 4-43: Shift in Maxwell- Boltzmann Distribution with increase in temperature [51]	99
Figure 4-44: $\ln(ROD_{ss})$ vs $1/T_K$ in 1% aq. NaCl solution	100
Figure 4-45: Schematic of Stage IV Test Outline (Repeated from Section 3.3.2)	102
Figure 4-46: Steady State ROD plotted as a function of NaCl concentration at 3 different temperatures for Material 301	103

Figure 4-47: Steady State ROD plotted as a function of NaCl concentration at 3 different temperatures for Material 202.....	104
Figure 4-48: Steady State ROD plotted as a function of NaCl concentration at 3 different temperatures for Material 106.....	104
Figure 4-49: Steady State ROD plotted as a function of NaCl concentration at 3 different temperatures for Material 105.....	105
Figure 4-50: Steady State ROD plotted as a function of test temperature in various test fluid concentrations for Material 105	105
Figure 4-51: Steady State ROD plotted as a function of test temperature in various test fluid concentrations for Material 106	106
Figure 4-52: Steady State ROD plotted as a function of test temperature in various test fluid concentrations for Material 202	106
Figure 4-53: Steady State ROD plotted as a function of test temperature in various test fluid concentrations for Material 301	107
Figure 4-54: Regression analysis equations and trendline expressing ROD_{ss} as a function of NaCl concentration when temperature is constant for NOV Dissolve 105.....	110
Figure 4-55: Regression analysis equations and trendline expressing ROD_{ss} as a function of NaCl concentration when temperature is constant for NOV Dissolve 106.....	111
Figure 4-56: Regression analysis equations and trendline expressing ROD_{ss} as a function of NaCl concentration when temperature is constant for NOV Dissolve 202.....	111
Figure 4-57: Regression analysis equations and trendline expressing ROD_{ss} as a function of NaCl concentration when temperature is constant for NOV Dissolve 301	112
Figure 4-58: Regression analysis equations and trendline modelling ROD_{ss} as a function of temperature when NaCl concentration is constant for NOV Dissolve 105	113
Figure 4-59: Regression analysis equations and trendline modelling ROD_{ss} as a function of temperature when NaCl concentration is constant for NOV Dissolve 106	114
Figure 4-60: Regression analysis equations and trendline modelling ROD_{ss} as a function of temperature when NaCl concentration is constant for NOV Dissolve 202	114
Figure 4-61: Regression analysis equations and trendline modelling ROD_{ss} as a function of temperature when NaCl concentration is constant for NOV Dissolve 301	115

Figure 4-62: 3-D Surface plot showing ROD_{ss} as a function of both temperature and concentration for material 105.....	119
Figure 4-63: Rotated surface plot shown perpendicular to the ROD-Concentration (Z-X) plane for material 105	120
Figure 4-64: Rotated surface plot shown perpendicular to the ROD-Temperature (Z-Y) plane for material 105	120
Figure 4-65: Surface plot showing ROD_{ss} as a function of both temperature and concentration for material 106	121
Figure 4-66: Surface plot showing ROD_{ss} as a function of both temperature and concentration for material 202	122
Figure 4-67: Surface plot showing ROD_{ss} as a function of both temperature and concentration for material 301	123
Figure 4-68: Ball shown landed on an NOV i-Seat [28]	126
Figure 4-69: Variation of ROD with time under constant temperature and fluid conditions	128
Figure 4-70: Diameter of a 3.625” NOV Dissolve 105 ball as a function of time at 80 °C in 1% NaCl	134
Figure 4-71: Dissolvable Ball Selection Workflow	138

List of Tables

Table 1: Inputs from Operator for Dissolvable ball application	3
Table 2: Dissolvable Materials Tested.....	38
Table 3: NOV Dissolve 105 dissolution test results at 80 °C in 1% aq. NaCl.....	71
Table 4: ROD_{ss} and t_{ss} values at 80 °C and 1% NaCl solution	77
Table 5: Surface fitting options used in Matlab.....	117
Table 6: Material coefficients for NOV Dissolve 105.....	118
Table 7: Material coefficients for NOV Dissolve 106.....	121
Table 8: Material coefficients for NOV Dissolve 202.....	122
Table 9: Material coefficients for NOV Dissolve 301	123
Table 10: Dissolve Rate Predictor Summary	124
Table 11: Diameter of the ball at different times	130
Table 12: Dissolvable Ball Size Calculator Summary.....	135
Table 13: Inputs required for implementing the Dissolvable Ball Selection Workflow	136

Nomenclature

A	Surface Area of dissolvable material, cm^2 .
A(t) or A_t	Surface Area at a given time, t expressed in cm^2 .
a_1	Material constant for a given dissolvable material at a specific temperature.
a_2	Material constant for a given dissolvable material at a specific temperature.
a_3	Material constant for a given dissolvable material at a specific NaCl concentration.
a_4	Material constant for a given dissolvable material at a specific NaCl concentration.
A_{rr}	Arrhenius pre-exponential factor or frequency factor.
b_1	Material Coefficient / Material Constant for a given dissolvable material. Independent of Temperature & NaCl concentration.
b_2	Material Coefficient / Material Constant for a given dissolvable material. Independent of Temperature & NaCl concentration.
b_3	Material Coefficient / Material Constant for a given dissolvable material. Independent of Temperature & NaCl concentration.
C	Concentration, g/ml.
d	Diameter of Cylindrical Sample, cm.
D(t) or D_t	Diameter of ball at time=t. Expressed in cm.
D_{ball}	Diameter of Ball, cm.
D_i	Initial diameter of ball when t=0. Expressed in cm.
D_{seat}	Inner Diameter of Seat, cm.
D_{ss}	Diameter of ball at start of steady state period when time= t_{ss} . Expressed in cm.
E_A	Activation Energy, J/mol.
h	Height of Cylindrical Sample, cm.
k_A	Rate of a Chemical Reaction (Arrhenius Equation).
m	Mass of dissolvable material, mg.

$m(t)$ or m_t	Mass at a given time, t expressed in mg.
M_{Cl}	Molar mass of Chloride, g/mol.
M_{NaCl}	Molar mass of Sodium Chloride, g/mol.
R	Universal Gas Constant, $J.K^{-1}.mol^{-1}$.
R^2	R-squared.
ROD_{ss}	Steady State Rate of Dissolution, expressed in $mg.cm^{-2}.hr^{-1}$ or $mg/cm^2/hr$.
ROD_t	Rate of Dissolution at time, t expressed in $mg.cm^{-2}.hr^{-1}$ or $mg/cm^2/hr$.
ROD_{tr}	Transient Rate of Dissolution, expressed in $mg.cm^{-2}.hr^{-1}$ or $mg/cm^2/hr$.
t	Time, hours,
T	Temperature, °C.
t_{end}	Time in hours when the ball is completely dissolved.
t_{final}	Time at which ball passes through seat, i.e., ball-on-seat time. Expressed in hours.
T_K	Temperature, Kelvin.
t_{max}	Maximum time period before which the ball is required to pass through seat. Expressed in hours.
t_{min}	Minimum time period the ball is required to stay on seat. Expressed in hours.
t_{ss}	Time to Reach Steady State or End of Transient State, hours.
Δm	Mass Loss, mg.
Δt	Time interval, hours.
ρ	Density of the dissolvable material, $mg.cm^{-3}$.

Abbreviations

CEM	Controlled Electrolytic Metallic
Cl ⁻	Chloride Ion
ERW	Extended Reach Wells
H ₂	Hydrogen
HCl	Hydrochloric Acid
HF	Hydrofluoric Acid
HNBR	Hydrogenated Nitrile Rubber
HRTEM	High Resolution Transmission Electron Microscopy
HSCC	High-Strength Corrodible Composite
HSE	Health, Safety and Environment
HT	High Temperature
IUPAC	International Union of Pure and Applied Chemistry
LCM	Lost Circulation Material
Mg	Magnesium
Mg(OH) ₂	Magnesium Hydroxide
MSF	Multistage Fracturing
Na ⁺	Sodium Ion
NaCl	Sodium Chloride
NCS	Norwegian Continental Shelf
NOV	National Oilwell Varco
PGA	Polyglycolic Acid
ROC	Rate of Corrosion
ROD	Rate of Dissolution or Rate of Dissolve
SAS	Stand-alone Screens
SEM	Scanning Electron Microscope
XRD	X-Ray Diffraction

1 Introduction

Multistage well stimulation combined with developments in horizontal drilling have played a key role in increasing the global oil output. Frac balls play a key role in the actuation of sleeves used in multistage stimulation operations. However, eliminating these balls afterwards to open-up the wellbore for production is a challenging and time-consuming process. As a result, there has been a growing demand in the industry for the development and use of dissolvable frac balls for stimulation applications.

In this thesis, the behaviour of dissolvable materials developed by National Oilwell Varco (NOV) have been examined under varying conditions through a series of experimental investigations. Both empirical and analytical methods have been employed to model the performance of dissolvable balls. A systematic workflow has been devised to select the correct dissolvable balls based on downhole conditions and operational requirements.

1.1 Background and Research Motivation

The use of well stimulation methods to improve reservoir productivity has become increasingly common in oilfields worldwide. Multistage stimulation techniques such as hydraulic/acid fracturing and matrix acidizing are necessary for tackling deficiencies like low formation permeability and near-wellbore damage caused during drilling [1]. Technology developments in horizontal drilling and multistage stimulation have enabled extraction of hydrocarbons from low permeable formations such as shale or tight sandstone which were previously considered to be either inaccessible or uneconomical.

Multistage stimulation involves splitting up the well into several stages and stimulating each of the stages individually. Ball-drop activated sleeve completion is a type of multistage stimulation technique wherein communication to the formation is established by opening sliding sleeves which are run as part of the lower completion string. Within each stage, a ball is dropped from the surface to land on a seat and open the corresponding sleeve, thereby allowing communication between the wellbore and formation [2]. After landing on seat, the ball isolates the stages below allowing for focussed stimulation of the stage. Stimulation fluids are then pumped into the formation at that

stage after which the next slightly larger-sized ball is dropped to open the sleeve further above to stimulate the next stage. Thus, balls of gradually increasing sizes are dropped from surface to open corresponding sleeves at each stage starting from the bottom of the well to top (or from the toe to heel in horizontal wells). Figure 1-1 illustrates ball-activated sliding sleeves separated by swell packers in an open-hole horizontal well for multistage stimulation. Horizontal wells can have up to 40 stages with the average number in the US being 16 stages per well [3, 4].

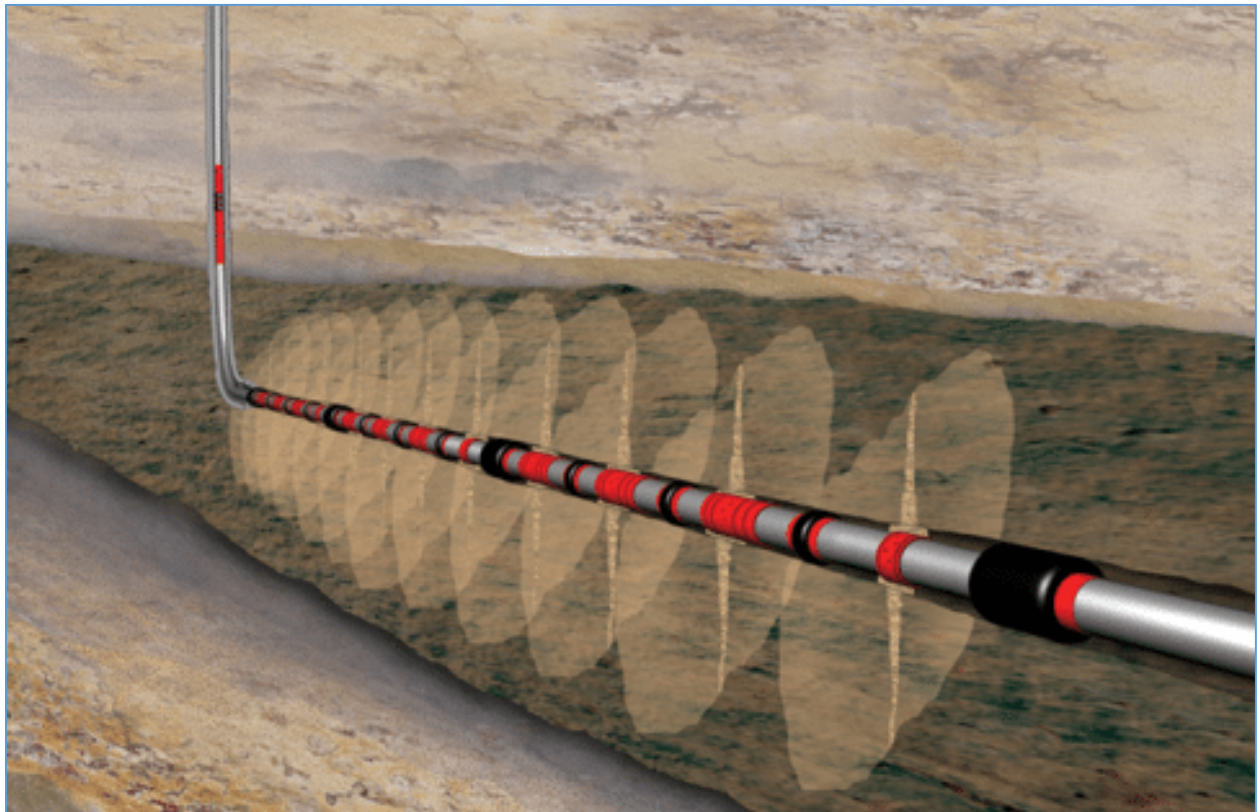


Figure 1-1: Multistage stimulation using ball-actuated sleeves in a horizontal well [3]

Upon completion of these multistage stimulation operations, there are numerous balls left in the completion string which need to be removed before production can begin. There are 2 possible approaches used to remove them. The first method is using the well pressure to allow the balls to flow back to the surface. However, flowback is often unreliable and unsuccessful due to one of several reasons such as the ball being stuck on the seat, high density of the ball, low reservoir pressure, low production rate or if the size of the ball is too small relative to flow area through the production tubing [4, 5]. As a result, balls stuck in the well become an obstacle to hydrocarbon flow and reduce the overall well productivity.

The second method involves drilling out the balls by using milling tools run on coiled tubing. Milling out several balls in multiple stages is a risky and time-consuming operation. This reduces the operational efficiency due to the high rig and personnel costs especially in offshore fields such as those in the Norwegian Continental Shelf [6, 7].

Thus, both of these current methods of ball removal are inefficient and not optimal. Challenges associated with the removal of frac balls necessitated the petroleum industry to innovate and look towards developing degradable/dissolvable frac balls. Ideally, a suitable dissolvable frac ball should be strong enough to withstand the high pressures experienced during stimulation. Once the required operations have been completed, these dissolvable balls should then gradually dissolve in the well fluid after which hydrocarbon production can begin without any wellbore obstructions.

1.2 Thesis Concept and Problem Formulation

Due to the growing industry demand for dissolvable frac balls, National Oilwell Varco (NOV) has recently developed a new generation of proprietary metallic dissolvable materials with Magnesium being the main constituent. However, the process of selecting the right dissolvable material for a given application has been a major challenge in commercializing these dissolvable frac balls. The main inputs from the operator for a dissolvable ball application can be grouped into downhole conditions and operational requirements as shown in Table 1.

Table 1: Inputs from Operator for Dissolvable ball application

Inputs to Dissolvable Ball Selection Workflow	
I. Downhole Conditions	a. Downhole Temperature
	b. Downhole Fluid Type
II. Operational Requirements	c. Seat Inner Diameter / Ball diameter
	d. Required Pressure Differential across ball
	e. Time Period, t_{min} and t_{max}

Of the listed operational requirements, the most challenging one to meet is the time window between t_{min} and t_{max} that the ball is expected to remain on the ball seat. The dissolvable ball is expected to stay on seat for a minimum period, t_{min} , to allow the operator sufficient time to carry out the stimulation operations that require the ball hold pressure from above. The dissolvable ball

should not stay on seat for more than a certain maximum period, t_{\max} . In other words, by this maximum period, the ball must dissolve enough such that the reduction in its size allows it to pass through the seat. This is to allow subsequent well operations to be carried out and/or to allow production. This time window requirement is challenging to achieve because the reduction in diameter of the dissolvable ball varies considerably depending on downhole conditions.

The present process of qualification of dissolvable frac balls involves multiple iterations of extensive full-scale tests on several different dissolvable materials until the acceptance criteria for the specific application are fulfilled. Dissolvable balls are high-priced and it is a tedious, time-consuming and expensive process to perform full-scale testing on the numerous dissolvable ball materials for every specific downhole condition and operational requirement.

Since the start of this decade, several service companies have invested significant efforts towards the development of dissolvable frac balls for use in multistage stimulation operations [4, 5, 8-10]. While the available literature on dissolvable materials do qualitatively document the effects of certain downhole conditions on their performance, there is a distinct lack of information on how this information can be effectively used to select the correct dissolvable ball material for a given application. This is the main knowledge gap that this thesis aims to bridge and examine for the new generation of metallic dissolvable balls being developed by NOV.

The unique aspect of this thesis is the development of a novel approach to enable the selection of the correct dissolvable frac ball for any given application environment without the need for multiple iterations of full-scale tests on several types of expensive dissolvable balls. This shall be achieved by the following four steps -

- i. The first step is to map out the response of dissolvable materials to variations in downhole conditions by conducting a series of experiments on small cylindrical samples. Four different NOV dissolvable materials shall be selected for this purpose.
- ii. The second step is to develop empirical models of the dissolution rates by performing regression analysis of the experimental data. These empirical models would allow one to forecast how slowly or quickly these materials dissolve at different temperatures and fluid conditions.

- iii. In the third step, an analytical model shall be developed to translate the results from cylindrical sample testing and express them in terms of size reduction of dissolvable balls. This analytical model can be used to determine how long a dissolvable frac ball can last on seat under given downhole conditions. This is to address the time window criterion which is critical for operational requirements (Table 1).
- iv. The final step is to devise a systematic workflow that enables one to directly select the most suitable dissolvable ball type to fulfil the operational requirements under given downhole conditions. This workflow shall be based on the empirical and analytical models developed in previous steps.

The workflow presented in this thesis shall eliminate the need for excessive full-scale tests on various dissolvable ball types for various combinations of downhole environment and operational requirements. Consequently, this would result in substantial cost-savings for the company and drastically improve the overall efficiency of the selection process.

For the sake of clarity, it must be stated here that the development and manufacturing of NOV's proprietary dissolvable materials were not done as part of the thesis and are beyond the scope of discussion. However, all the dissolution experiments, subsequent analysis of the results, development of empirical and analytical tools, and the dissolvable ball selection workflow documented in Chapters 3 and 4 were specifically executed as part of this thesis work.

1.3 Thesis Objectives

Based on the thesis concept and problem formulation described in Section 1.2, the main objectives of the thesis have been listed below:

- i. Identify and define key parameters required to characterize the performance of dissolvable materials in a quantifiable manner.
- ii. Investigate the effect of variations in composition of downhole brines on the performance of the four dissolvable materials from NOV.
- iii. Examine how variations in temperature affect the performance of dissolvable materials.
- iv. Compare the relative performances of the four dissolvable materials tested in this work.
- v. Use the experimental data to develop an empirical model to predict the performance of the tested dissolvable materials under different temperatures and brine compositions.

- vi. Formulate an analytical model to evaluate how long a dissolvable frac ball can last on seat under given downhole conditions.
- vii. The final objective of the thesis is to create a stepwise workflow to select the correct dissolvable ball material for any given downhole condition and operational requirement. This is done by consolidating the experimental results, empirical models and analytical calculators.

1.4 Thesis Structure

In addition to this chapter, this thesis comprises of four main chapters as shown in Figure 1-2.

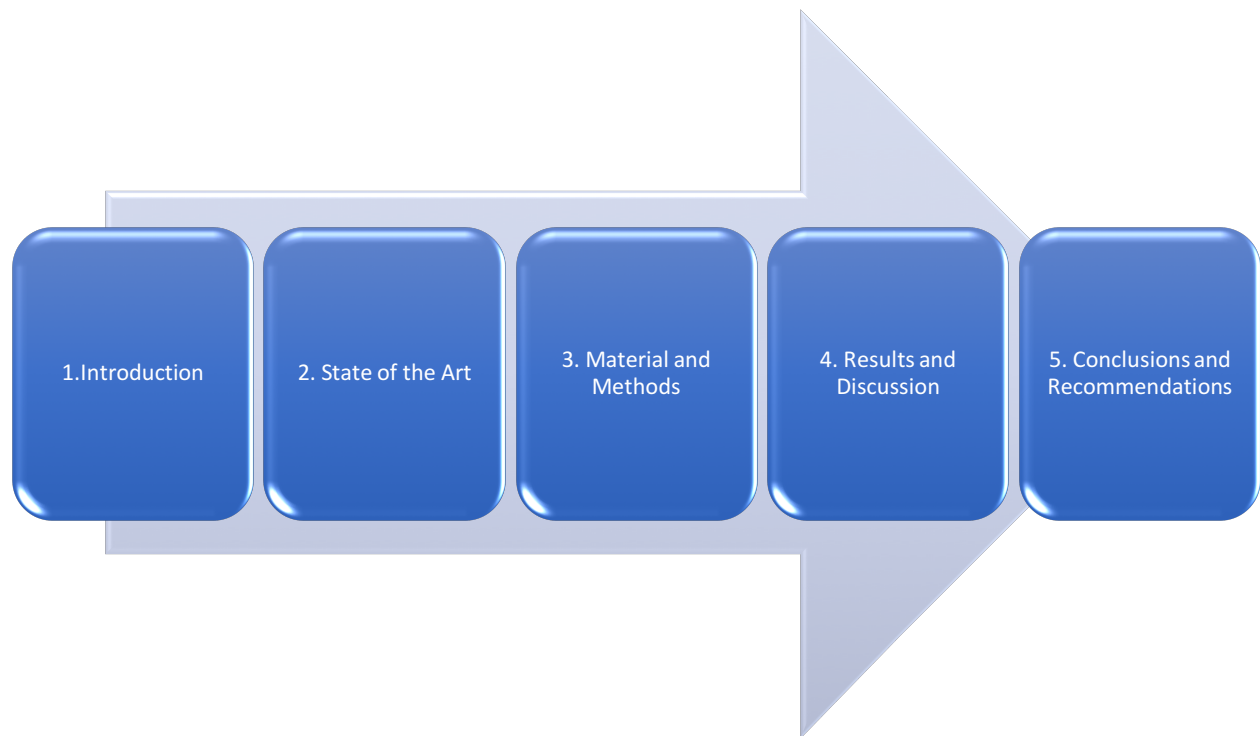


Figure 1-2: Overview of Chapters

Chapter 2 documents the current state of the art with regards to dissolvable materials and their usage in the petroleum industry. The main application area of dissolvable materials is in well completions, specifically during the reservoir stimulation process. In order to provide appropriate context to the reader, this chapter also briefly introduces relevant topics of well completions, stimulation techniques and completion design for stimulation operations (Figure 1-3).

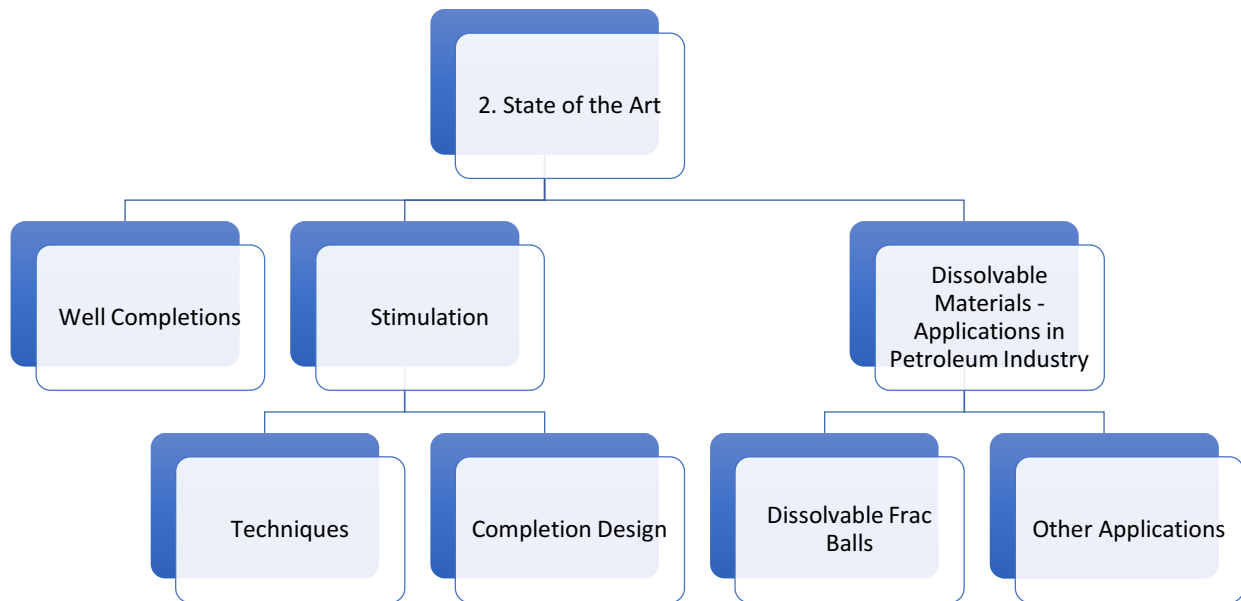


Figure 1-3: Overview of Chapter 2: State of the Art

In Chapter 3, the materials and procedure used for the experimental portion of the thesis are covered (Figure 1-4). This chapter also documents the test program consisting of four distinct stages which were devised to methodically analyse the behaviour of the dissolvable materials.

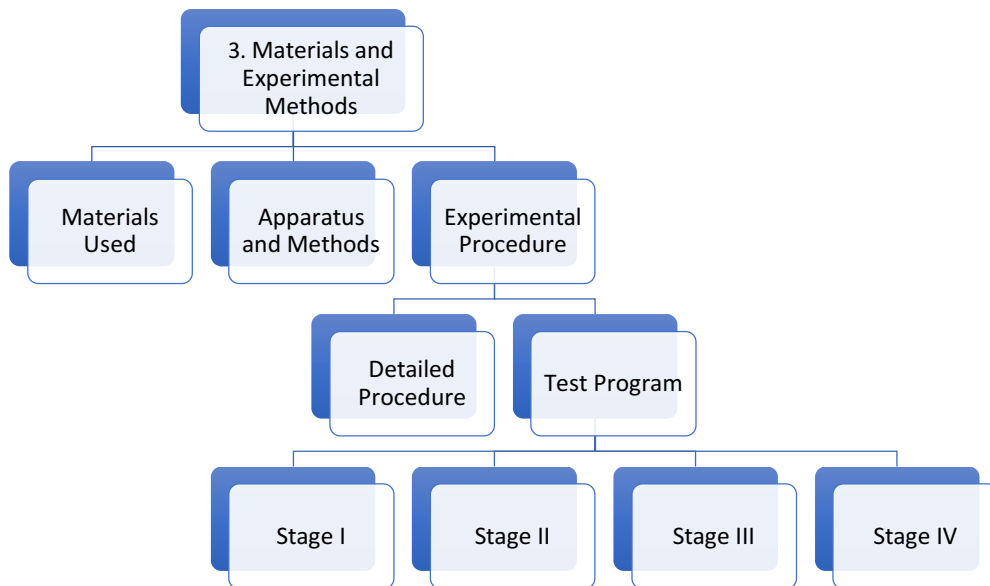


Figure 1-4: Overview of Chapter 3: Materials and Experimental Methods

Chapter 4 is the crux of this thesis which documents and examines the outcomes from a four-stage experimental program to characterize the performance of dissolvable materials. Sections 4.1 - 4.4 correspond to the experimental results of Stage I to Stage IV of the test program.

Empirical models of the dissolution rates, termed ‘Dissolve Rate Predictors’, are developed based on regression analysis of the experimental data. Thereafter, an analytical model is developed to translate the results from cylindrical sample testing and express them in terms of size reduction of dissolvable balls. This model is labelled as the ‘Dissolvable Ball Size Calculator’. The thesis work culminates with the presentation of a selection flowchart in Section 4.5 that enables one to systematically select the most suitable dissolvable ball type to fulfil the operational requirements under given downhole conditions. This workflow is based on the empirical and analytical models developed in previous steps.

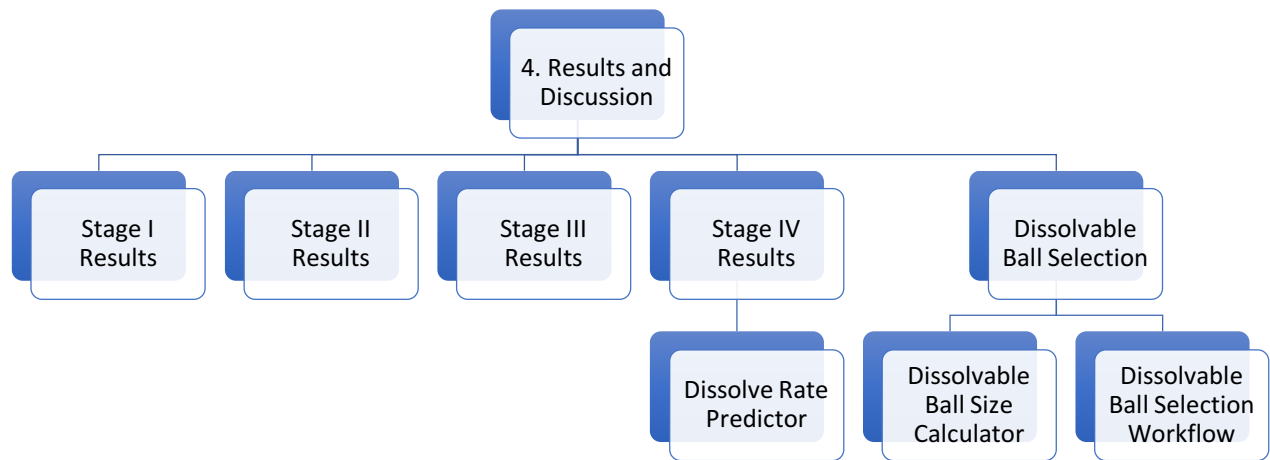


Figure 1-5: Overview of Chapter 4: Results and Discussion

Chapter 5 draws conclusions from current work and presents recommendations for future work.

2 State of the Art

Chapter 2 aims to provide a summary of the current state of technology on dissolvable materials pertaining to applications within the oil and gas industry. The predominant use of dissolvable materials has been in well completions, specifically, during the reservoir stimulation process. Hence, it is important to provide the reader with appropriate background on this specific area of application.

Consequently, this review chapter starts out with a broad introduction to well completions. This is followed by an overview of reservoir stimulation techniques followed by recent developments in well completion designs to implement these techniques. Finally, the last section of this chapter focusses on reviewing the existing literature related to dissolvable materials along with other potential areas of applications of the same within the upstream petroleum business.

2.1 Well Completions – An Introduction

Well completion is the process of putting a well into production in a safe and efficient manner. It typically comes after the well has been drilled. Depending on the geological structure, complexity and production strategy, completions designs can range from being as simple as open-hole designs to more complicated ones such as intricate multilaterals or deepwater completions with subsea manifolds. A comprehensive completion design involves multiple disciplines such as reservoir engineering, geology and well engineering in order to identify the type of lithology, pore configuration and fluid flow characteristic to minimize formation damage and maximize productivity. Knowledge of petroleum production further aids the different understanding of long-term well requirements such as water injection, steam injection or the need for artificial lift [11].

An effective design for completions must uphold the mechanical integrity of the wellbore against the industry's standard without compromising the economy of production in terms of flow capacity [12]. While a well is drilled from top to bottom, well completions is performed from bottom to top. A common misconception is that there is always a tubing string installed inside the production casing when completing a well. However, that is not always true as development of technology and workover techniques allow for smaller casing sizes such as 2 7/8 inches. The small casing size

negates the need for the use of conventional tubing and without compromising the possibility of future stimulation operations as well as sand control [13]. Well completion is typically categorized into 3 sections depending on their purpose – lower, middle and upper completions. Figure 2-1 shows a completion schematic used by an operator for a subsea well in the Norwegian Continental Shelf. The lower completion is installed first followed by the middle completion and finally, the upper completion.

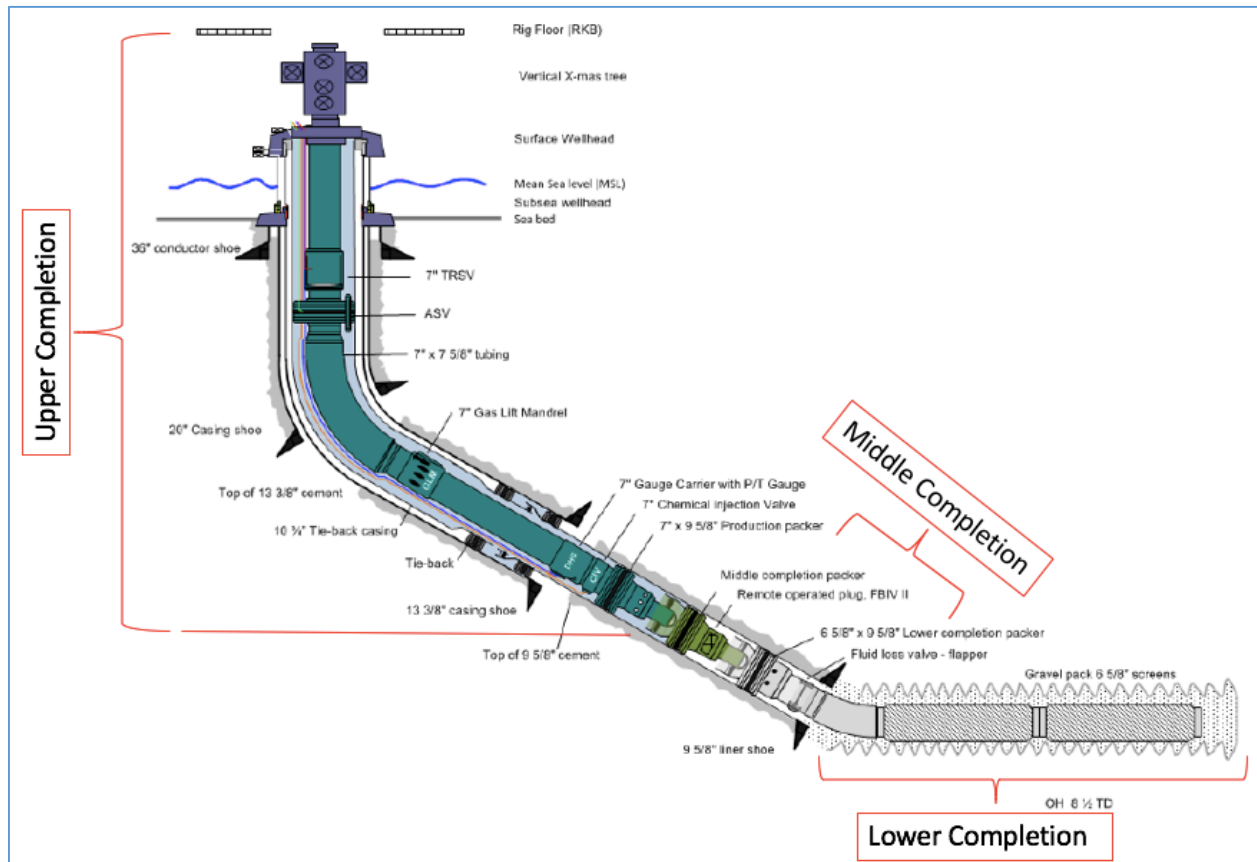


Figure 2-1: Well Completion Design showing Upper, Middle & Lower completions [14]

Lower completion is the section of the completion which is in direct contact with the reservoir. A few types of lower completion (also referred to as reservoir completion) is shown in Figure 2-2. As lower completion is in immediate contact with the reservoir, the design considerations on whether it should be an open hole completion or cased and perforated can be of paramount importance as it affects the inflow performance and long-term well productivity [15]. Open hole completions which includes slotted liners as well as stand-alone screens (SAS) are often chosen when the target formation is not suitable or capable of handling the inherent damage that is

commonly associated with cement operation [16]. On the other hand, although there can be significant skin damages that comes with cased hole and perforated completions design, it is still widely applicable as it allows selective reservoir perforation in order to manage the different pressure and petrochemical properties of complex interlayer target zones [11].

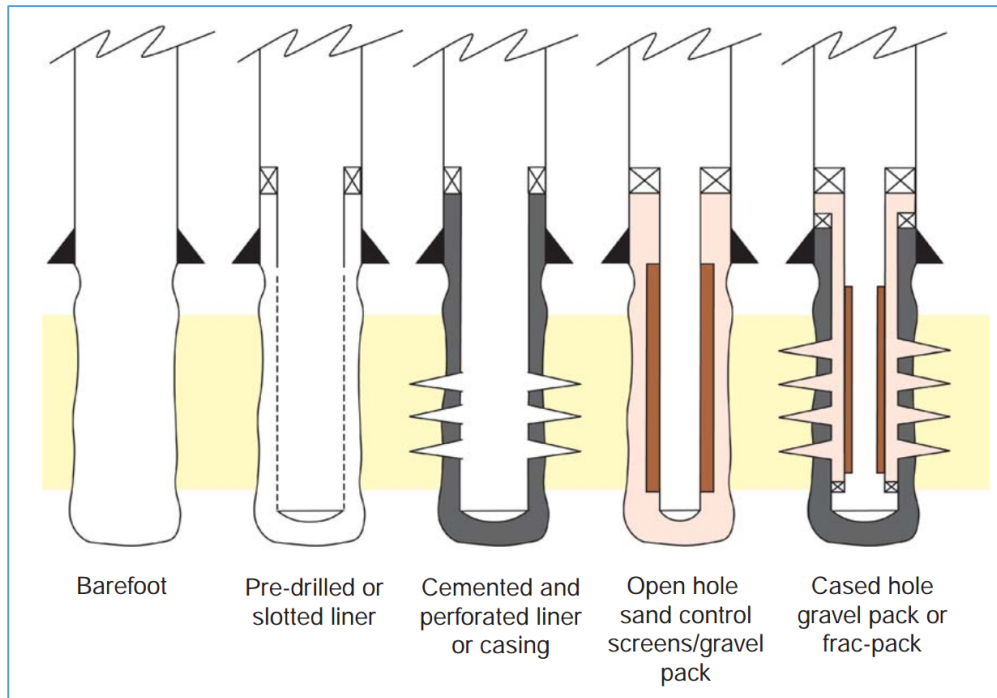


Figure 2-2: Reservoir completion methods [15]

Middle completion comprises of barrier elements required to isolate the reservoir at various times such as when installing upper completions and during intervention operations. Typical barrier elements used in middle completions include middle-completion packer and fluid-loss valves as shown in Figure 2-1.

Upper completion is for flow control and acts as a conduit to bring the hydrocarbons up to surface. It includes all the components of the completion string from production packer up to the X-mas tree (Figure 2-1). A clear communication between the teams planning the lower completion and upper completion is crucial to avoid any mismatch which can have a severe negative effect on productivity and operation costs [17]. The safety valves used in upper completion is also an important barrier element for well control throughout the subsequent life of the well. Figure 2-3 illustrates a few types of upper completion methods.

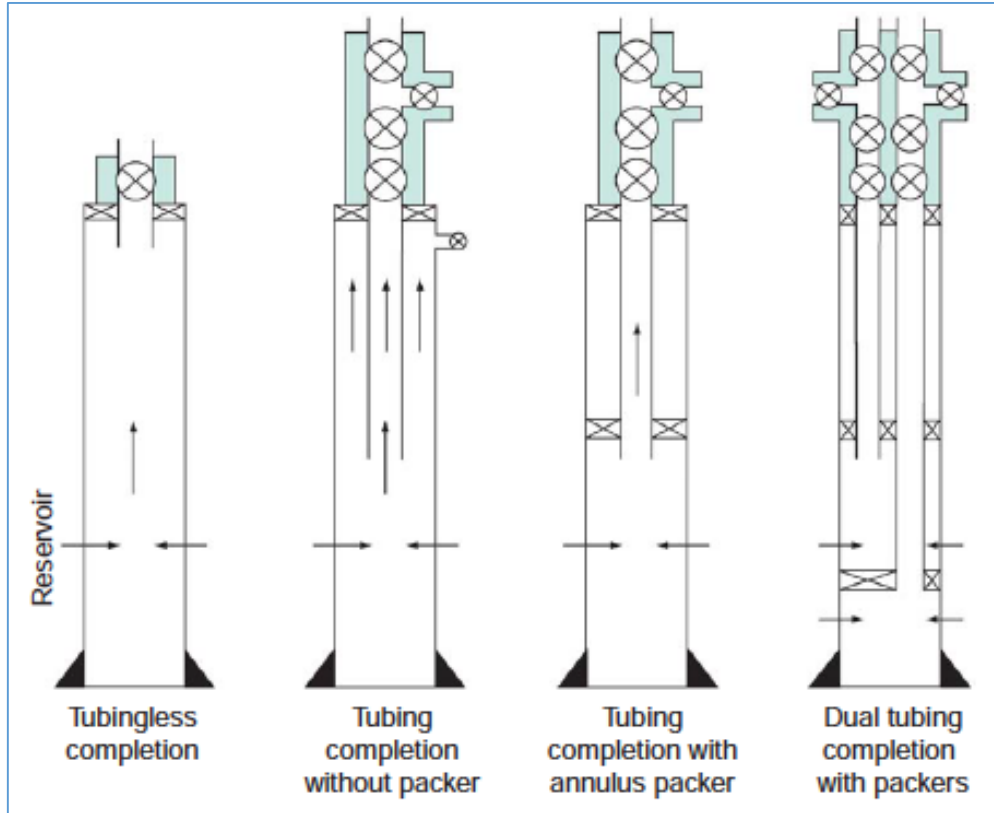


Figure 2-3: Upper Completion Methods [15]

Much emphasis has been placed on optimizing the drilling process as the operational costs associated is several orders of magnitude higher than a typical conventional completion [17]. However, without a well-thought-out completions design, the productive life of the well can be diminished and its financial implications are far-reaching. Given the relatively small cost in implementing a comprehensive completions system with sufficient safety features, the potential overall benefits are well worth the effort and expense.

2.2 Stimulation

Currently, the largest application and market for dissolvable materials is during multistage stimulation operations. One of the primary goals of this thesis is to provide a basis for selection of the right dissolvable materials for such applications. Hence, to provide appropriate context to this main application area of dissolvables, Section 2.2.1 has been devoted to introducing reservoir stimulation methods. In addition to this, Section 2.2.2 delves in the current well completion designs used to implement these reservoir stimulation methods.

The need for well stimulation stems from one of the following reasons -

- i. **Low formation Permeability:** Sometimes wells are drilled into tight formations (eg. shale) which are found to have low permeability. In such cases, reservoir stimulation techniques such as hydraulic fracturing or acid fracturing are used to overcome this deficiency and improve the well productivity [1]. Reservoir stimulation plays a key role in making these low permeable hydrocarbon reservoirs economically viable.
- ii. **Near-Wellbore Damage:** In this scenario, the well has been drilled and completed in a formation with sufficient permeability. However, near-wellbore damage results in the formation having a low productivity index. Near-wellbore damage can occur from several sources such as fines invasion during drilling or perforation, and chemical incompatibility between the formation and drilling fluids. Natural reservoir processes such as changes in saturation arising due to low near-wellbore reservoir pressure, scale deposition and formation fines are also possible sources of damage [18]. Near-wellbore damage is undesirable and reduces the overall productivity and economic viability of a well. In such cases, a damage removal technique, such as matrix acidizing is employed [1].

2.2.1 Types of Stimulation Techniques

While there are different approaches to grouping stimulation techniques, this thesis groups the stimulation methods based on the purpose that they serve as seen in Figure 2-4. This chart has been inspired by the work of Gidley [1]. Formations having average effective permeability less or equal to 1 millidarcy require reservoir stimulation methods whereas those with average effective permeability more than or equal to 10 millidarcy require damage removal treatments.

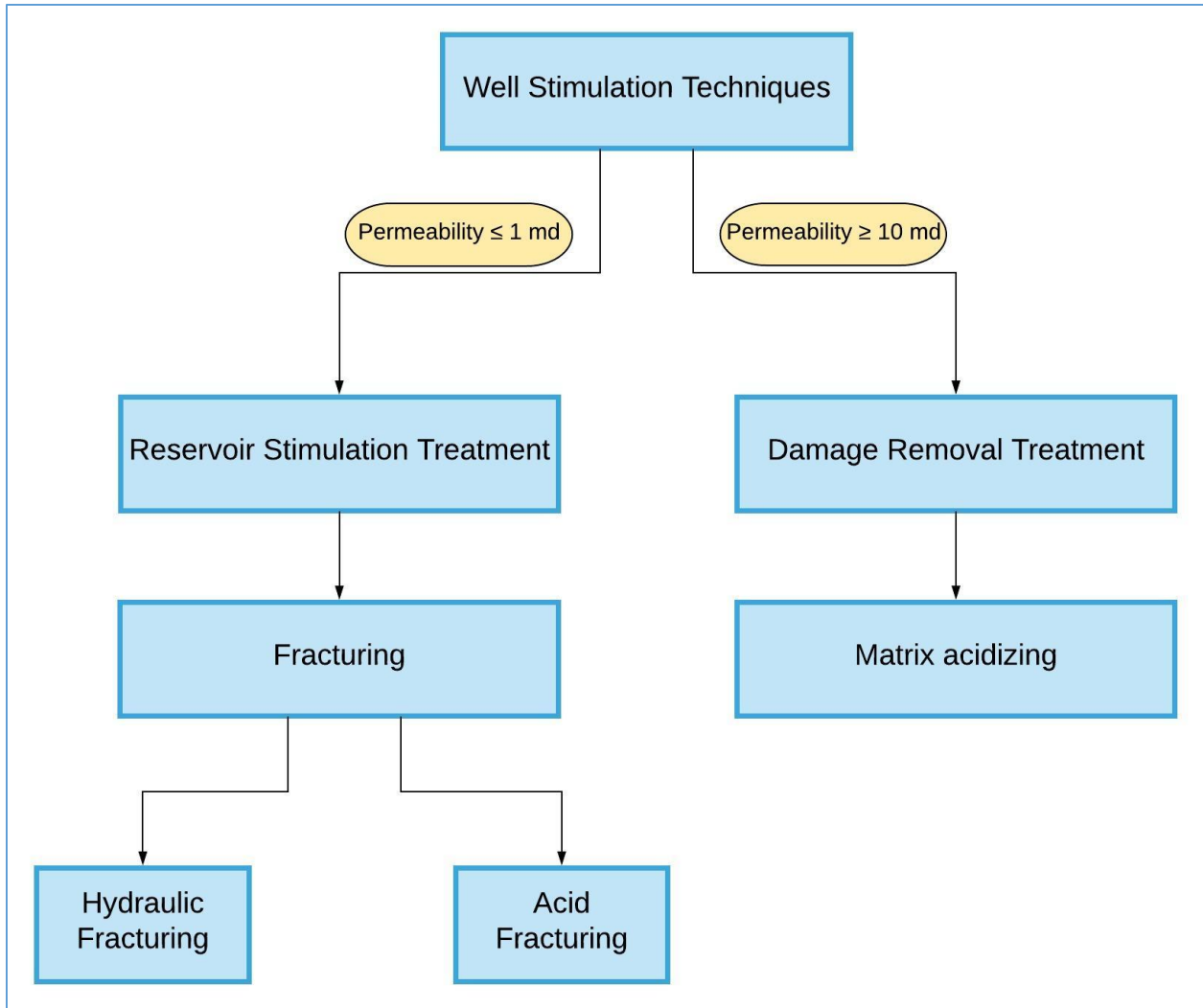


Figure 2-4: Classifying Well Stimulation Techniques

2.2.1.1 Fracturing

When fluid is pumped into the well faster than the fluid can escape into the formation, the pressure in the well rises. Eventually the wellbore pressure gets higher than the formation breakdown pressure which causes the rocks to fracture. This process of breaking down the formation through hydraulic action is called fracturing [18].

If the pumping rate is maintained higher than the fluid-loss rate, then the created fractures propagate and grow further into the formation as seen in Figure 2-5 [18]. Thus, the effective area of the communication channel between the wellbore and formation can be increased through fracturing as a result of which the productivity is improved.

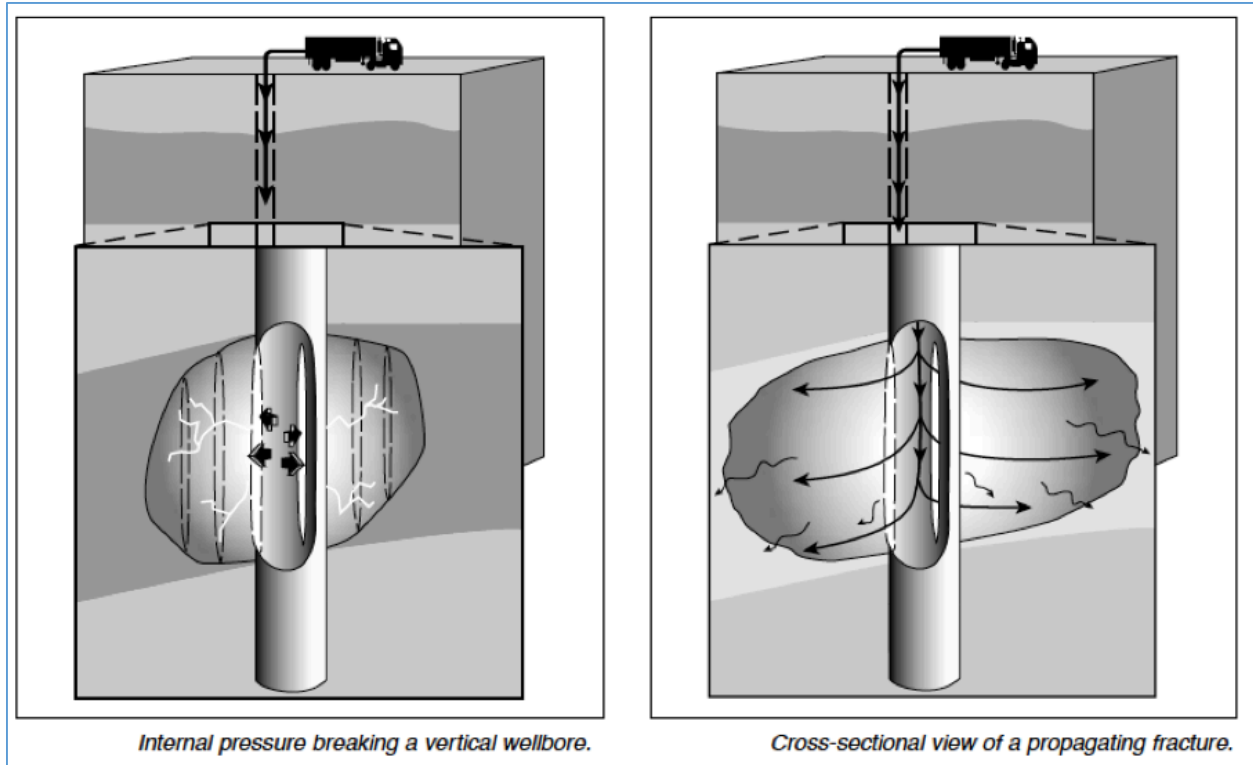


Figure 2-5: Reservoir Stimulation Treatment by Fracturing [18]

There are 2 main types of fracturing used for reservoir stimulation – Hydraulic fracturing and Acid fracturing.

Hydraulic Fracturing

In hydraulic fracturing, fluids mixed with small round particles called proppants are pumped into the well. The purpose of these proppants is to hold open the fractures even after the pumping has stopped (Figure 2-6). Common proppant materials include ceramic beads, resin-coated sand and sintered bauxite [1, 19]. Thus, in hydraulic fracturing, fluid mixed with proppant are pumped to create and maintain long conductive flow paths into the formation. These paths can extend several hundred meters out from the wellbore.

After the fracturing operation is complete, pumping is stopped. The well is shut-in for a few hours after which the surface valves are opened and fluid is produced at the surface from the fractures. This clean-up operation is to remove the fracturing fluid from the formation and to initiate the production of hydrocarbons from the reservoir. The success of a fracturing treatment depends on

the extent of the fracture propagation, how successfully the proppants were placed in the fracture and the remaining reservoir pressure [1].

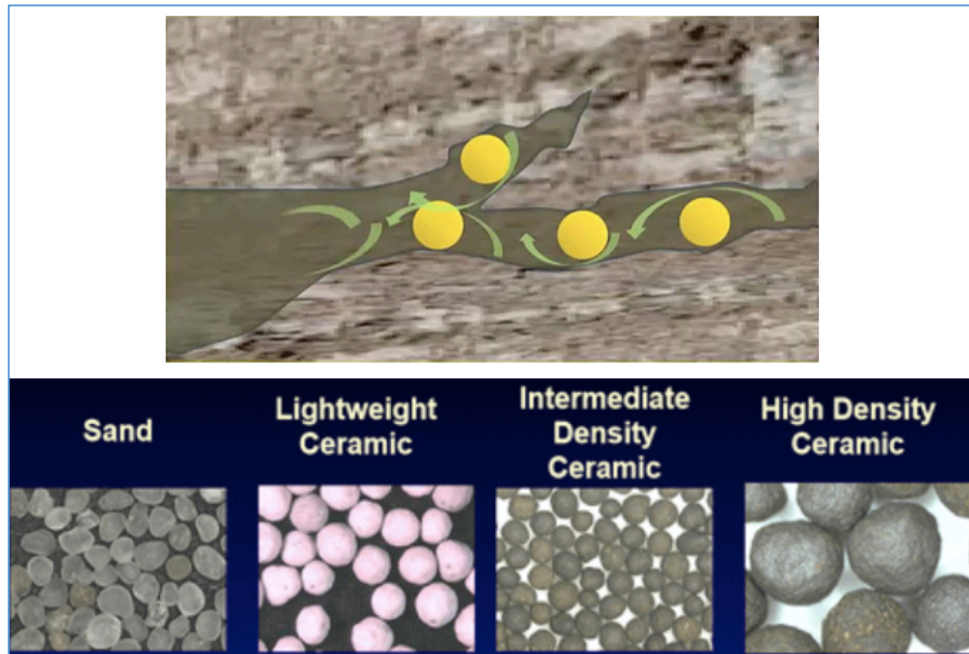


Figure 2-6: Proppants used in Hydraulic Fracturing [19]

Acid Fracturing

Acid fracturing is an operation very similar to hydraulic fracturing in that fluid is pumped down the well at pressures above the formation breakdown pressure resulting in fracture propagation into the reservoir rocks. However, in acid fracturing the fluid pumped down is acid and no proppants are used. Acid fracturing is performed on formations which are soluble in acid. As the acid travels through the fractures, it etches the face of the fracture [1]. These acid-etched channels improve the fracture porosity and conductivity which improves the subsequent hydrocarbon flow into the wellbore. Typical acid fracture radial lengths range from 9-61m from the wellbore [20].

Hydrochloric acids of 7.5%, 15% or 28% concentration (by weight) are the most commonly used acids for fracturing. In some cases, organic acids may be used in high temperature wells due to their reduced corrosiveness. Acid fracturing is used to stimulate carbonate reservoirs since the acid is effective in etching formations with at least 60% carbonate content (limestone, dolomite or chalk) [20, 21]. This method is seldom employed in sandstone formations since these acids are unable to create effective channels in sandstones.

Hydraulic Fracturing versus Acid Fracturing – For Carbonates [1]

When it comes to carbonates, the operator has two options for reservoir treatment, namely, hydraulic fracturing and acid fracturing. The decision has to be made evaluating the comparative advantages and disadvantages between these two options.

During hydraulic fracturing, there are higher risks of mechanical failures due to screen out of the proppant carrying fluid. Furthermore, acid fracturing is less expensive and requires lesser equipment than hydraulic fracturing since the latter requires proppant handling equipment, blenders etc.

However, the advantage of hydraulic fracturing is that it provides better control of the fluid losses during fracturing operations. On the other hand, during acid fracturing since the acid reacts with the formation, LCM (Lost Circulation Material) used to prevent fluid losses are less effective. This is because the acid etches and dissolves the formation making it difficult for the LCM to act as a bridging agent. Additionally, acid fracturing is not as effective as hydraulic fracturing to create long fractures in reservoirs with temperatures above 93 °C. Thus, these factors must be kept in mind while deciding between the hydraulic fracturing and acid fracturing for carbonate reservoirs.

2.2.1.2 Matrix Acidizing

Matrix acidizing is a damage removal treatment where acid is pumped into the well at low pressures below the formation breakdown pressure. Thus, the intent here is to restore near-wellbore permeability without fracturing the producing formation. Matrix acidizing is distinct from acid fracturing where fracturing the formation is the main objective. The effect of matrix acidizing is confined to a radius of under a metre [20]. The acid dissolves the particles (such as clay) plugging the pores that are responsible for the wellbore damage. This opens up pore spaces and improves productivity [22].

Matrix acidizing is mainly used in sandstone formations. They are not as useful in carbonate formations since carbonates are less susceptible to near-wellbore damage. The acid used for matrix acidizing is a mixture of hydrochloric (HCl) and hydrofluoric acid (HF) [1].

In this thesis, the term stimulation has been used to denote fracturing (acid/hydraulic) as well as matrix acidizing treatments. The completion design for these operations is described next.

2.2.2 Well Completion Design for Stimulation

The earliest methods of implementing well stimulation involved displacing the entire tubing with the treatment fluid and continued pumping which forced the stimulation fluid into the entire formation [21, 23]. This method of stimulating the entire well at the same time required millions of gallons of stimulation fluids which was not only expensive but also a logistical challenge especially on offshore rigs where the available storage space on-board was scarce. This procedure also does not allow any control over which zones of the formations are stimulated. As a result, the stimulation treatment is not uniform since the bulk of the treatment fluids get diverted into the most permeable section of the pay zones. Furthermore, the operator could not customize the stimulation parameters such as fluid types and stimulation pressures for the different zones.

As a result of these shortcomings, the lower completion design of wells which required stimulation gradually evolved into what is now called multistage completions or multistage fracturing (MSF) systems. In an MSF completion, the well is split into several stages and the stimulation treatment is applied separately to each of the different stages/zones. This enables the operator to customize the treatment fluids as well as treatment pressure for the different zones to maximise the chances of success of the stimulation job [23].

Note: The commonly used oilfield terminology for abovementioned completions, '*Multistage Fracturing (MSF)*', is a slight misnomer since these completions are used for not only fracturing applications but also matrix acidizing operations.

The two most popular completion techniques to perform multistage stimulations are Plug and Perf Completion and Ball-drop Activated Sleeve Completion. Both these methods may be applied for fracturing as well as matrix acidizing operations. These techniques have been discussed below.

Plug and Perf Completion Method

The plug and perf method is the traditionally standard method of performing multistage stimulation operations. Referring to Figure 2-7 and Figure 2-8, the typical steps involved in a Plug & Perf completion have been listed below [2, 24]:

- i. Production liner/casing is cemented in place.

- ii. An isolation device (called frac-plug) and perforating guns are lowered into the wellbore by slickline or electric line.
- iii. At the desired depth, the plug is set.
- iv. The zone/interval is then perforated.
- v. The perforating guns is pulled back up to surface.
- vi. The interval is stimulated using the appropriate fluids and required treatment pressures for this interval.
- vii. Convey another frac-plug via wireline along with perforating guns.
- viii. Set the second plug a certain distance above the first and retrieve the perforation assembly.
- ix. Perform the second stimulation operation for the second stage.
- x. This process is repeated for each of the subsequent stages/zones.
- xi. After the stimulation operation has been completed for all the stages, mill out all the plugs by using coiled-tubing-run milling tools.
- xii. The well is now cleaned and put on production.

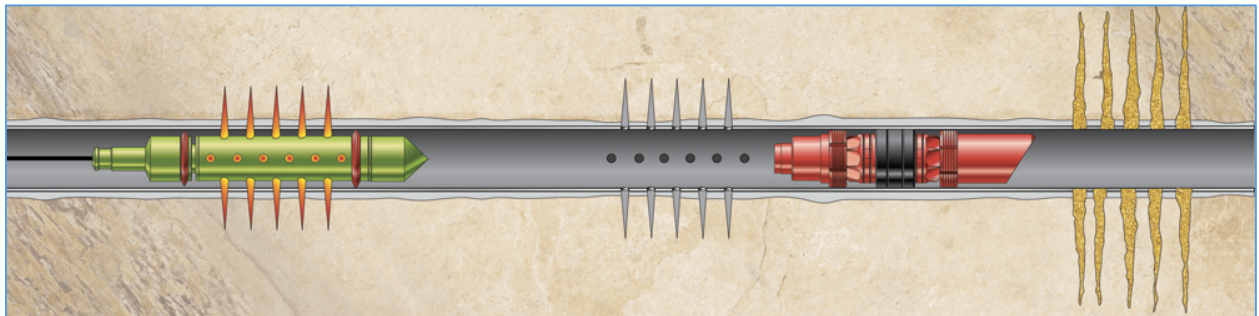


Figure 2-7: Going down to perforate with perforating guns after setting a frac-plug [25]

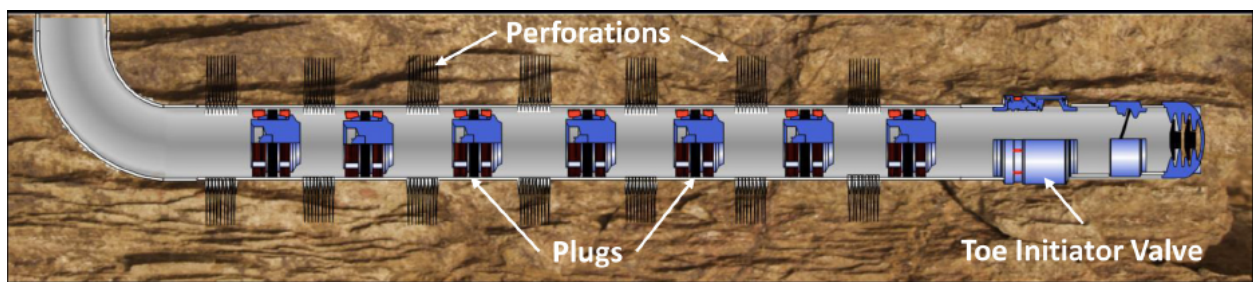


Figure 2-8: Plug and Perf method deployed in a cemented cased-hole completion [24]

The plug and perf method can also be adapted to be deployed on open hole completions by making use of open-hole packers such as swell packers or external casing packer.

Advantages: The advantage of plug and perf method is that it ensures proper isolation of various stages ensuring the travel of the stimulation fluids only into the isolated interval. As a result, the treatment pressures are focussed in one interval resulting in far-reaching travel of the stimulation fluids & fractures. Additionally, if any operational problems are encountered during a plug & perf operation, it is less disruptive since intervention wireline services are already available to perform any required fixes.

Disadvantages: However, there are several disadvantages to this method. The foremost is that it is a very time-consuming process due to the several slickline or electric line runs that are required to stimulate the various stages. The average turnaround times for performing a 20-stage stimulation operation using this method is 5 days [25, 26]. In offshore wells like those in the Norwegian Continental Shelf, this translates to high expenses due to the steep rig rentals. Moreover, in extended reach wells (ERW) having long horizontal sections, it is a challenge to have access and run frac-plugs and perforation assemblies. The operational steps needed for plug and perf stimulations require simultaneous operations between fracturing personnel and wireline crews. This would require repeated rigging up and down of the wireline equipment and the stimulation equipment, alternating back and forth for each stage. There are additional operational risks such as pre-setting of plugs and perforating guns misfiring [7]. Removal of the frac-plugs after stimulation is often a risky and time-consuming operation.

Ball-drop Activated Sleeve Completion

This is a relatively newer type of multi-stage completions where a number of sleeves are run as part of the lower completion string. Within each stage, a ball dropped from the surface opens the corresponding sleeve and lands on a ball-seat tubular at the bottom of the stage. The dropped ball passes through all the seats which are larger than its diameter on its way to reach its intended target location where the seat has a smaller diameter than the ball (See Figure 2-9) [2]. When the sleeve is opened by the correspondingly sized ball, ports on the sleeve body allow communication to the formation. This is followed by pumping stimulation fluids down the well into the specific formation interval (a.k.a stage) at which the sleeve has been opened. Thereafter, the next slightly larger-sized ball is dropped to stimulate the next stage higher up in the well. Thus, due to the graduated seat sizes, the stimulation operations are performed starting at the lowermost stage

(corresponding to the smallest ball size), and gradually moving up the well by dropping increasingly larger-sized balls. This is known as toe-to-heel stimulation operations.

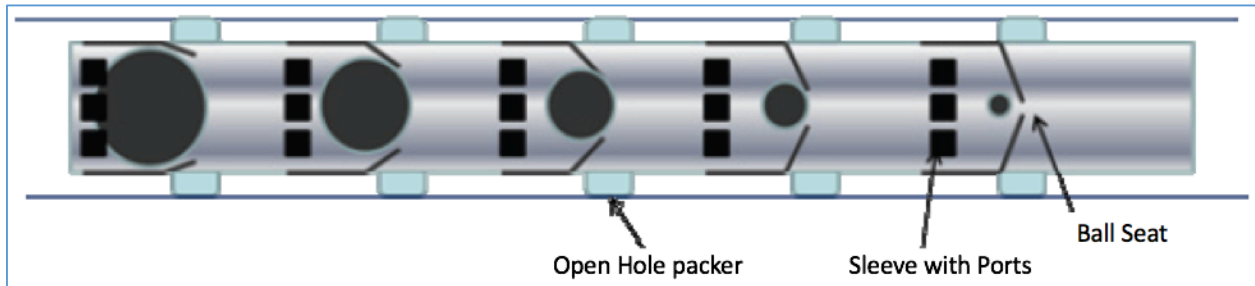


Figure 2-9: Schematic of Ball-drop Activated Sleeves in an open-hole completion [2]

Koloy et al. has described in detail the development and implementation process of the first cementable multistage ball-activated sleeve completion in the NCS in 2011 by NOV Completion Tools [6]. Prior to 2011, all MSF completions in the region had been in open hole completions. Referring to Figure 2-10, this MSF completions consisted of 5 stages with 3 ball-activated sleeves per stage. These ball-activated sleeves, called ‘i-Frac™ flex’, were designed to be opened by a single ball after which the ball can pass through the sleeves and land on a fixed seat (‘i-Seat™’).

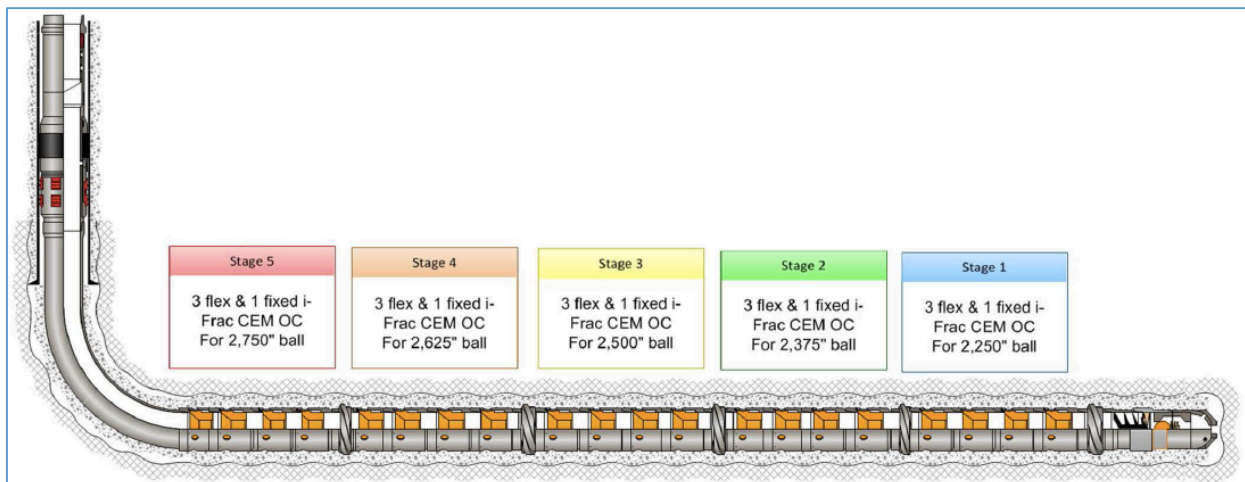


Figure 2-10: 5-stage Ball-drop Activated Sleeve Completion in cemented completions [6]

The stimulation procedure for the above MSF completion has been summarized below:

- i. Stage 1 stimulation: A 2.250 in. ball is dropped. The ball opens the 3 sleeves (‘i-Frac™ flex’) and lands on a fixed seat (‘i-Seat™’) at the bottom. Thereafter, treatment fluid is pumped down the well for fracturing of the Stage 1 interval.

- ii. Stage 2 stimulation: A slightly larger 2.375 in. ball is dropped. The ball passes through the sleeves and seats located between Stage 5 to Stage 3. The ball opens the corresponding 3 sleeves in Stage 2 and lands on a fixed seat at the bottom of Stage 2. Thereafter, treatment fluid is pumped down the well for fracturing of the Stage 2 interval. Note that during treatment of Stage 2, Stage 1 is isolated by the 2.375 in. ball on the seat.
- iii. Stage 3, 4 and 5 stimulations: The previous steps are repeated by dropping correspondingly larger ball sizes (2.500 in., 2.625 in. and 2.750 in.).

Thus, all 5 stages can be individually isolated and stimulated by dropping 5 gradually larger sized balls. Balls are typically introduced into the well through wing valves or isolation valves within the pump flowlines. In order to eliminate manual errors in dropping the correct sequence of balls, remote-automatic ball-launchers like the one in Figure 2-11 have been developed. These can be pre-loaded to deploy the balls in a specific sequence [27].

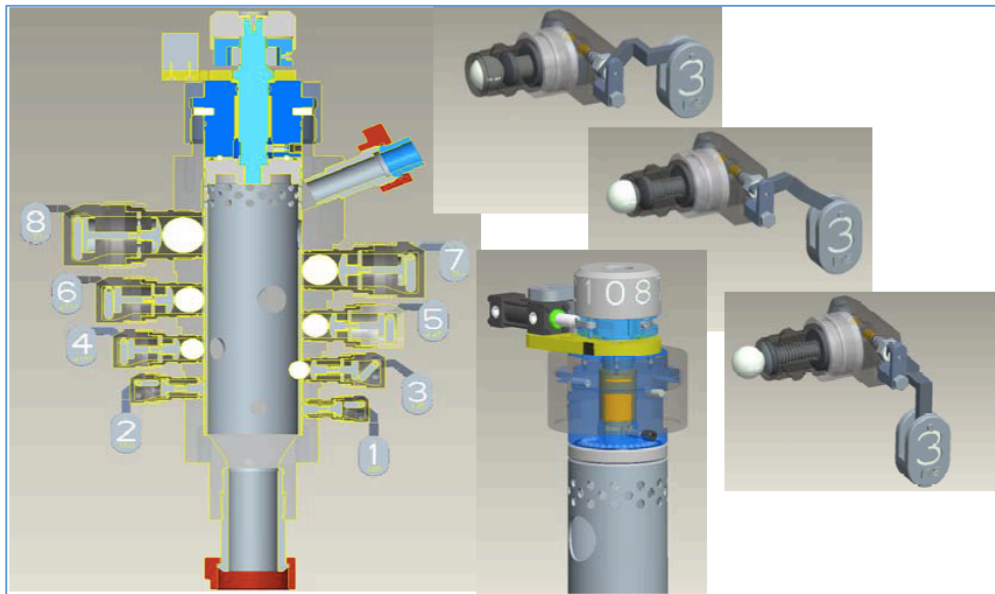


Figure 2-11: Automatic Remote-actuated Ball-launcher [27]

Advantages: As one can appreciate, the ball-drop activated sleeve system is a much faster way of performing stimulation operations relative to the plug and perf method. A 20-stage ball-activated sleeve stimulation can be completed in a single, continuous pumping operation within 24 hours whereas a comparable plug and perf stimulation operation can extend up to 5 days [25]. There is no requirement for wireline or coiled tubing services and this would considerably reduce the required rig-time for performing these stimulations. It has been reported that sleeve-based

fracturing systems require much lesser treatment fluids and water per stage [25]. Unlike the plug and perf, this method is better from an HSE point of view since no explosives are required for perforation. Additionally, re-closeable frac-sleeves are available in the market which can be closed back by wireline shifting tools. These frac-sleeves can be closed and re-fractured by ball-drop at a later stage of the well's life.

Disadvantages: During stimulation operations, there is less flexibility in case of operational problems. Presence of ball seats makes it difficult and expensive to enter the well in order to remove fluid obstructions [2]. Frac balls are typically recovered by flowing them back to surface. However, recovery of the frac balls can be a problem especially in wells with high number of stages. As a result, balls can get stuck in the wellbore causing obstructions to flow.

Thus, before selecting one of these well completion designs for reservoir stimulation, the operator has to evaluate their pros and cons including factors such as costs, time, operational risks, HSE and long-term well productivity.

2.3 Dissolvable Materials - Applications in Petroleum Industry

2.3.1 Dissolvable Balls in MSF Applications – The Need

As detailed in Section 2.2.2, frac balls play a key role in Multistage Fracturing (MSF) completions that comprise of sliding sleeves and seats. They serve two key purposes in these types of MSF completions. The first is to actuate the right sliding sleeves and open up communication ports to the formation. Thereafter, stimulation fluids are pumped through these zones into the reservoir. The second purpose is for the balls to provide a barrier in order to divert the pumped stimulation fluids through these communication ports into the selected zone. Thus, the balls-drop sequence allows one to individually stimulate specific zones while isolating the zones that have already been treated [5].

Current developments in completion technology has enabled the operator to individually stimulate as many as 40 different stages in a well. These frac balls are circulated down at high flow rates and are expected to withstand pressures as high as 10 000 psi (689 bars) when on the ball seat [4].

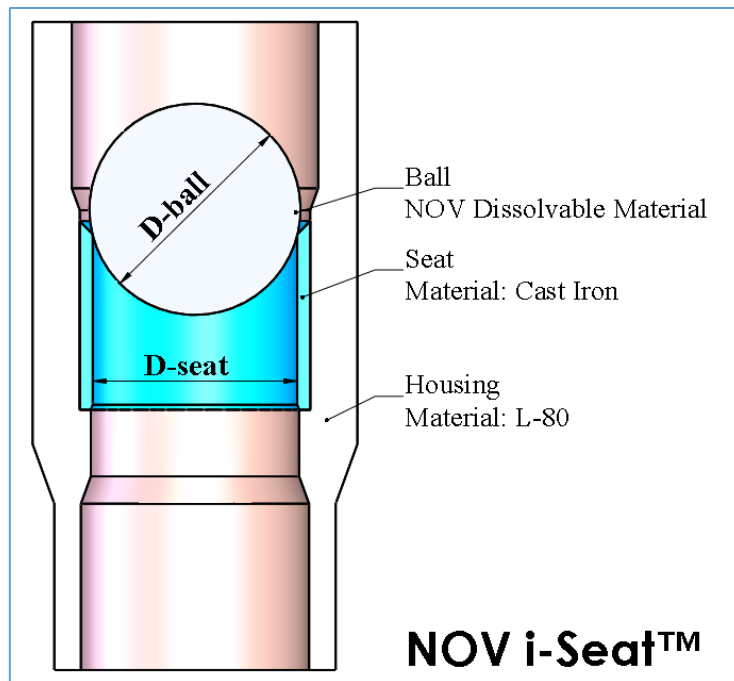


Figure 2-12: Ball shown landed on an NOV i-Seat™[28]

Figure 2-12 shows a ball landed on an NOV i-Seat™. This is a standard ball-seat tubular and is run downhole as an integral part of the MSF completion string below the fracturing sleeves. The i-Seat™ consists of a housing made from similar material to that of the completion tubing string. A cast iron seat is installed inside this housing. The top and bottom of the i-Seat™ has premium tubing connection threads for connecting with the tubing string. Frac balls are circulated down from surface and open a number of fracturing sleeves before landing on the fixed i-Seat™ (Figure 2-10). The contact area between the ball and the seat is such that it forms a complete seal thereby isolating zones/stages below it (Figure 2-12).

The size of the ball is chosen based on the required maximum pressure from above that the ball-seat system is expected to experience. The size of the ball (D_{ball}) relative to the seat inner diameter (D_{seat}) is commonly described by the term ‘overlap’. Ball-seat systems with higher overlaps will be able to withstand higher pressure values before failure. In addition to the overlap, the maximum pressure rating of a ball-seat system is also a function of the yield strength and the ultimate tensile strength for metallic balls. Thus, the ball size is chosen such that there is sufficient overlap to be able to achieve the required maximum pressure rating.

The standard materials that these stimulation/frac balls are typically available in are phenolic, metallic and composite materials. The pros and cons of the different options were tested by means of laboratory tests as well as finite element analysis by Baihly et al., in [29]. Expectedly, metallic balls were found to be the strongest of the three. However, the use of composite and phenolic balls is widespread for fracturing due to the fact that these are lighter and much easier to mill out than metallic balls [23].

Once all the well stimulation operations for the different stages have been completed, there are several frac balls in the well that need to be cleared out to allow a full-bore path for hydrocarbon production. There are two possible approaches to achieve this. The first method is to allow the production balls to flow back upstream and these are retrieved at the surface using specialized equipment called ball catchers [30, 31]. Figure 2-13 shows a Seaboard™ AJ7 ball catcher.



Figure 2-13: Ball catcher [30]

However, flowback is not always successful as the ball may get stuck on the seat due to deformation at high stimulation pressures. This deformation, commonly referred to as “egging” of the ball prevent flowback of the ball as illustrated in Figure 2-14.

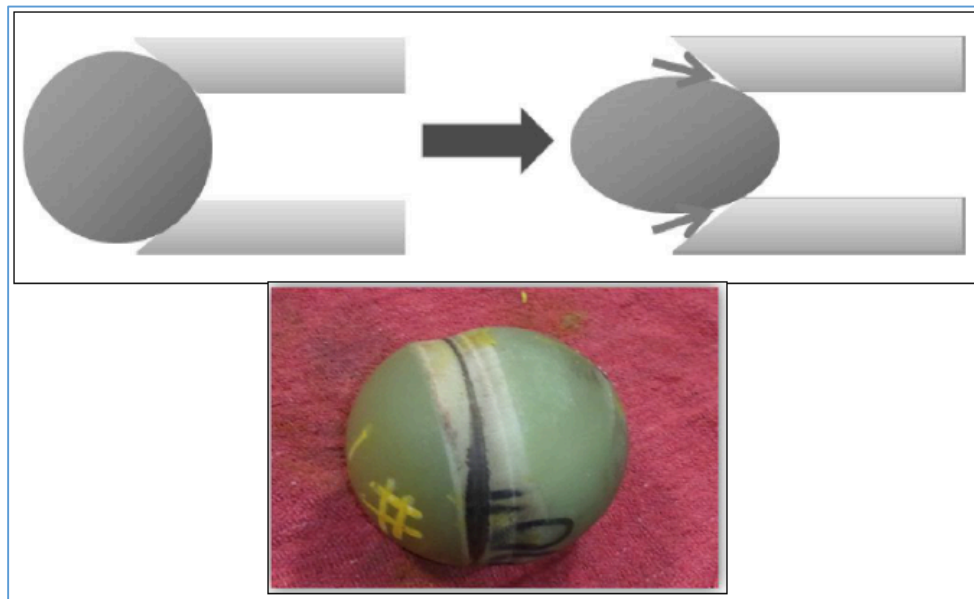


Figure 2-14: ‘Egging’ of a ball on seat with pressure. Photo shown of a composite ball that has experienced egging during testing [5].

Some operational observations indicate that the balls flow from the heel of a horizontal well until they get stuck in a particular deviation of the well at which point they smash against the tubing and break into pieces. In such cases, only ball fragments are recovered in the ball catcher [5].

Another challenge with flowing back is it might not be possible to generate sufficient lift forces due to high relative density of the ball, low reservoir pressure, low production rate or if the size of the ball is too small relative to the production tubing's inner diameter. Thus, it is possible that the ball becomes an obstacle to production and can affect the long-term productivity of the well due to the reduction in effective flow area through the production tubing. Additionally, this can also prevent the future passage of logging or intervention tools through the tubing string [4, 32]. Therefore, this retrieval method of flow back of frac balls is not always reliable and reduces the overall production efficiency of the stimulated well.

The second approach to removing frac balls after stimulation is to do an intervention operation during which the balls are milled out of the seats to provide full-bore access for later hydrocarbon production. This approach is usually adopted in cases when poor ball flowback of the frac balls is observed. The main drawbacks of this method are the high expenses and times associated with rig costs especially in offshore fields such as those in the Norwegian Continental Shelf. Additionally, milling operations are inherently risky and involve considerable personnel involvement as a result of which the overall operational efficiency of the stimulation operation is adversely affected [6, 7].

The effect on production due to failed ball flowback has been documented by Wozniak [33]. He discovered that poor flowback of frac balls was the cause of low production in approximately 142 lateral wells in the eastern Kentucky play. The production of the wells increased significantly after milling operations were undertaken.

In conclusion, the use of the traditional frac balls adversely affects both the operational efficiency as well as the production efficiency of wells due to the challenges associated with removal of these balls after the stimulation operations have been completed as elaborated previously.

This motivated the oil and gas industry to look towards degradable/dissolvable balls as a solution to address these inefficiencies. Ideally, a suitable dissolvable frac ball should be strong enough to withstand the high pressures experienced during stimulation. Once the required operations have been completed, these dissolvable balls should then gradually dissolve in the well fluid after which well production can begin without any wellbore obstructions.

2.3.2 Current Developments in Dissolvable Materials

Motivated by the shortcomings of traditional phenolic/composite frac balls, several oil and gas companies and suppliers began investing their R&D efforts in an attempt to develop high-strength dissolvable materials since the start of this decade.

Dissolvable balls for downhole use need to have 3 key properties - high strength, controlled degradation and be lightweight. The challenging aspect to developing such a material is that a high strength material often does not degrade fast enough and vice versa. Xu et al. [8] developed a prototype material at Baker Hughes Inc. based on nanostructured material technology called controlled electrolytic metallic (CEM). The material consisted of a continuous cellular nano-matrix with metallic grains dispersed in the nano-matrix as shown in Figure 2-15. The dissolvable material with nano-matrix was found to have a compressive strength that was 5-6 times more than a reference material without the nano-matrix. This work in 2011 is one of the earliest documented efforts of dissolvable material development specifically, for frac ball applications. CEM balls were field tested in multistage fracturing systems in the Bakken shale field with reported success.

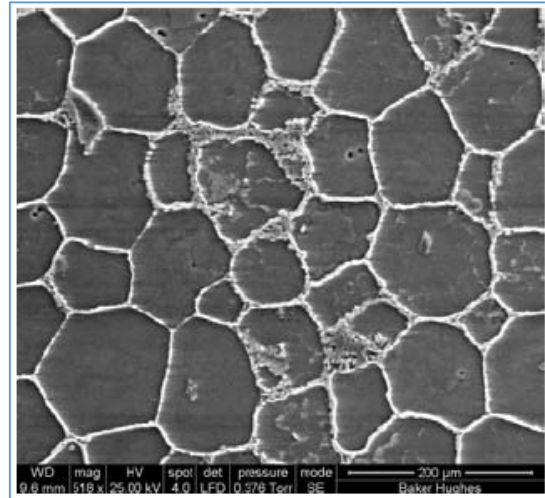


Figure 2-15: SEM image of cellular nano-matrix with metallic grains dispersed [8]

However, there is not much details in the work of Xu et al. [8] about the factors that affect how quickly a material dissolves and how the material's properties were customized to accommodate specific operational design criteria. This is possibly due to the sensitive nature of this novel technology with major commercial implications. This is a recurring aspect of the other literature

that has been reviewed in this section that companies maintain a certain level of confidentiality and do not reveal the exact composition of their dissolvable materials as well as the exact approach to selecting the right dissolvable material for the right application.

While at Baker Hughes, Carrejo et al. [4] developed another high-strength corrodible composite (HSCC) by forging of individually treated granules. The initial qualification of the dissolution rate of the material was performed on small cylindrical samples that were 2.54 cm in height and 1.27 diameter. The sample was immersed in brines at 93 °C. The weight of the sample was taken at the beginning of the test and at the conclusion of the test. The average surface area was calculated by taking the mean of the surface area measurements at the start of the test and at the end of the test, i.e., $A_{avg} = (A_{start} + A_{end})/2$. Thereafter, a term called the Rate of Corrosion (ROC) was defined per Eq. 2.1. The change in time, i.e., test duration was 4 hours.

$$\begin{aligned} \text{Rate of Corrosion, ROC (mg/hr/cm}^2\text{)} \\ = \frac{\text{Change in Weight (mg)}}{\text{Change in Time (hrs)} * \text{Average Surface Area(cm}^2\text{)}} \end{aligned} \quad (2.1)$$

While the above definition of ROC is a reasonable initial indication of the dissolution speed of the material, a more refined formula to characterise dissolution rate has been presented and compared with Eq. 2.1 in Section 4.1.3 of this thesis. It was found that for these HSCC materials from Baker Hughes, monovalent brines (Sodium Chloride & Potassium Chloride) were more effective in dissolving the samples than divalent brines (Calcium Chloride). The dissolution process was found to be quicker at higher temperatures for the HSCC materials in brines.



Figure 2-16: Cylindrical samples for qualification testing [4]

In 2013, Aviles et al. developed a metallic degradable material at Schlumberger to enter the market for dissolvable stimulation balls [5]. Though Aviles et al. started out developing degradable polymeric composites, it was found that such materials could not provide the sufficient material strengths for applications in stimulation operations. The mechanism of degradation of this metallic alloy is reported to be an intra-galvanic cell wherein the different crystallographic phases of the material undergo electrochemical reactions and is described as being “car-battery like”.

The metallic degradable material was reported to have been field tested in US and Canada in temperatures ranging from 30 °C to 98 °C. Application of dissolvable balls in low temperatures was identified as a key challenge since the balls could take several weeks to dissolve.

In addition to metal-based degradables, dissolvable materials have also been developed based on polymers (plastics) [9, 10]. The main component of dissolvable plastics is PGA (Polyglycolic Acid) and its dissolution mechanism is driven mainly by temperature effects on the polymer causing it to lose shape and ‘flow’. Dissolvable PGA was found to be almost 4 times weaker in terms of the tensile strength than dissolvable metal as seen in Figure 2-17.

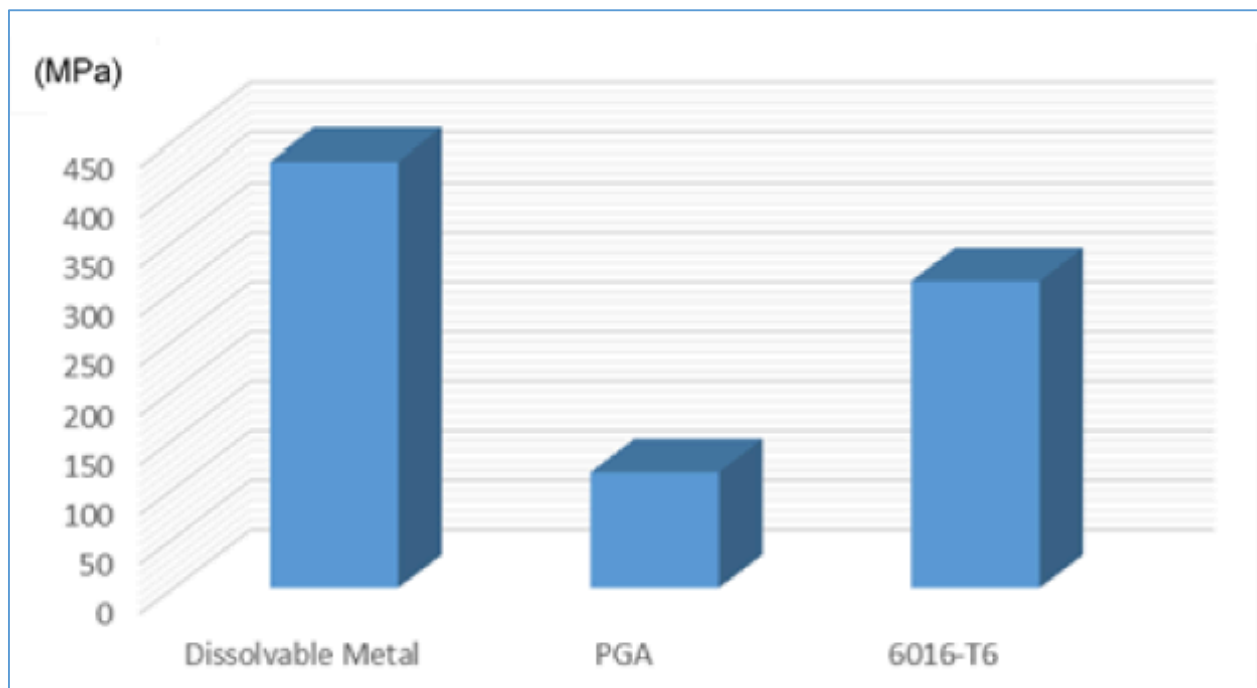


Figure 2-17: Tensile strength comparison between Dissolvable metal, PGA and an Aluminum alloy (6016-T6) [10]

Zachary et al. performed comparative impact testing on Halliburton's dissolvable metals and dissolvable plastics [9]. The balls were pumped through a 5000-ft. long flow-loop at 15-19 BPM to eventually land on seats to simulate real-life stimulation scenarios. The dissolvable metallic balls were found to pass all the impact tests whereas the dissolvable plastics failed in majority of the impact tests as shown in Figure 2-18.

Therefore, while dissolvable plastics are possible cheaper, dissolvable metals are the way forward for degradable technology. Hence, in this thesis, dissolvable metals have been tested & characterized.

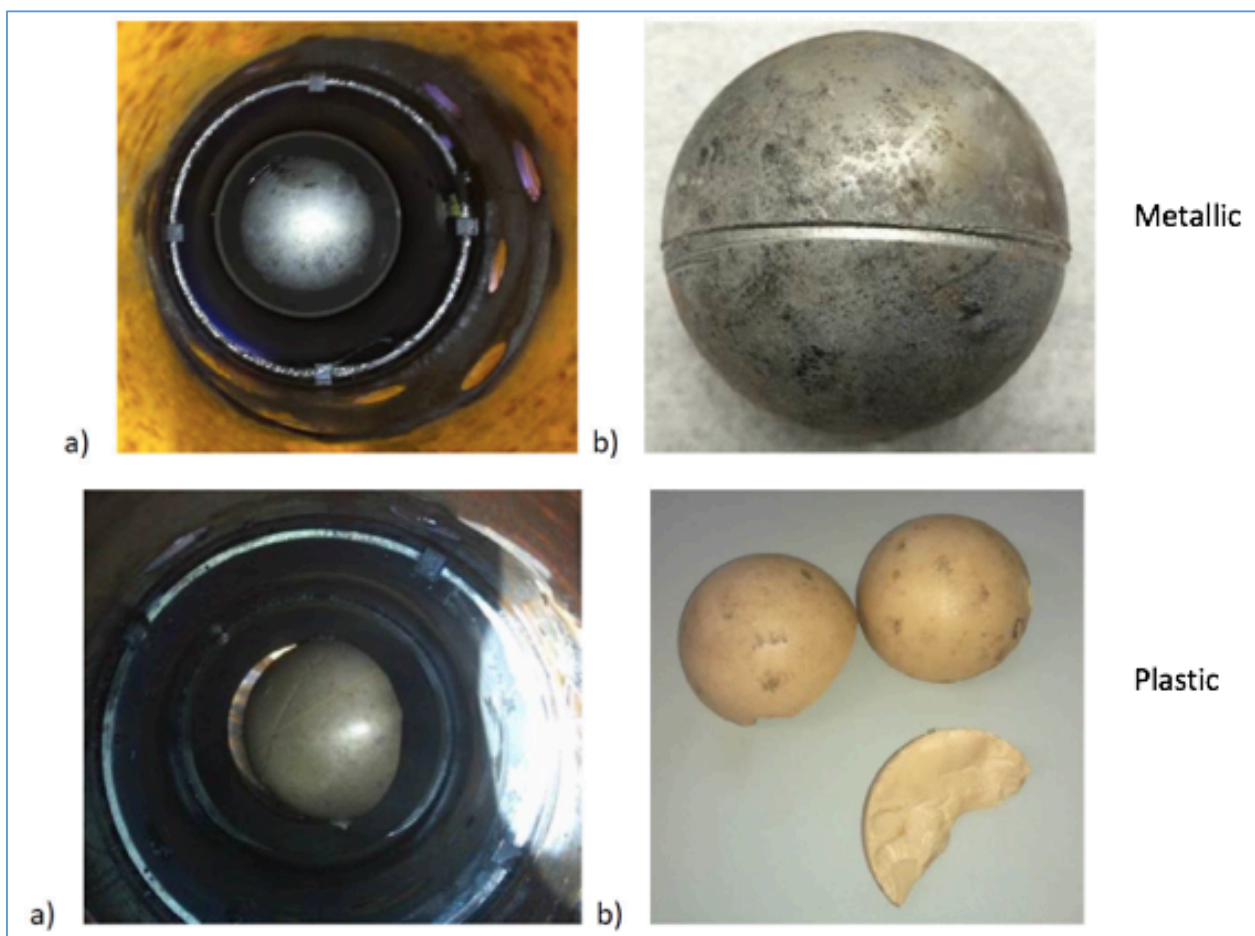


Figure 2-18: Results from impact testing. a) Showing the metallic and plastic balls on seat b) Showing the metallic and plastic balls after impact testing [9]

In this section, the publicly available literature on the recent efforts to develop dissolvable materials for application in stimulation operations have been documented. There are also multiple examples of field deployment of the dissolvable ball technology with varying levels of success [5-8].

However, none of the existing literature provide a detailed description of how to select the correct dissolvable ball material for given downhole conditions and operational requirements. That is the main knowledge gap that this thesis aims to examine and document for the new generation metallic degradable balls being developed by National Oilwell Varco (NOV). In order to do this, it is important to investigate and understand exactly how the dissolution process of the NOV Dissolve balls is affected by the downhole conditions. This is undertaken in this thesis by a combination of laboratory experiments followed by the development of empirical and analytical models.

This thesis work culminates in the presentation of a systematic workflow based on empirical and analytical models to directly select a suitable dissolvable material for a ball. This ensures that one does not have to spend excessive amounts of time and money on performing full-scale testing on expensive dissolvable balls for various combinations of downhole conditions and operational requirements.

2.3.3 Other Applications of Dissolvable Materials in Petroleum Industry

As previously discussed, the predominant driver towards development of dissolvable materials was driven by their need in multistage stimulation operations comprising of ball-actuated sliding sleeves. However, in recent years oil and gas companies have been looking into other applications for these dissolvable materials in order to maximise the R&D efforts that have been invested into developing these materials. This section provides a brief overview of the other applications of dissolvable materials within the upstream oil and gas sector.

Plug and Perf

The plug and perf method introduced in Section 2.2.2 is the traditionally standard method of performing multistage stimulation operations, especially in land wells where rig costs are not as expensive as in offshore wells. In this method, frac-plugs are set at each stage followed by perforations to established a pathway to the formation. Thereafter, the stimulation fluid is pumped into the formation. After all the stages have been stimulated, all the plugs are milled out [34].

The current industry standard material for frac-plugs is composites since they can be easily milled out and the previously common cast-iron plugs are now obsolete (Figure 2-19). The sealing elements of the frac-plugs are made up of standard elastomers like Hydrogenated Nitrile rubber (HNBR) and fluoroelastomers [24].



Figure 2-19: Composite Frac Plugs – Halliburton Fas Drill® [35]

However, milling out several of these composite plugs is an extremely time-consuming and risky operation, especially in extended reach wells and wells with depleted reservoirs [24]. Several companies have since developed and field tested fully dissolvable frac-plugs [10, 24, 34, 36, 37]. The body of these frac-plugs are made from dissolvable metals similar to those developed for dissolvable frac balls. In addition to the degradable metallic body, significant work has been done in developing fully degradable rubber elements to fulfil the sealing functionality [38].



Figure 2-20: Dissolvable Frac Plugs - Halliburton Illusion® [39]

Gas Lift Valves

In conventional gas-lift systems, dummy valves are installed in side-pocket mandrels to form a part of the barrier during completion operations such as tubing testing, annulus testing or setting of a hydraulic packer. At a later stage, these dummy valves are replaced with live valves by means

of wireline intervention after which the gas-lift string becomes active. In order to eliminate this step of intervention, Xu. et al. [40] proposed a smart gas lift valve with an inbuilt dissolvable plug. This dissolvable dummy valve has a high pressure and temperature rating to isolate tubing from annulus. Once the completion operations are complete, the dissolvable material in the gas lift valve disintegrates when in contact with brine, thus automatically converting the dummy valve into a live valve without the need for intervention. This smart gas lift valve has been field tested in the Gulf of Thailand.

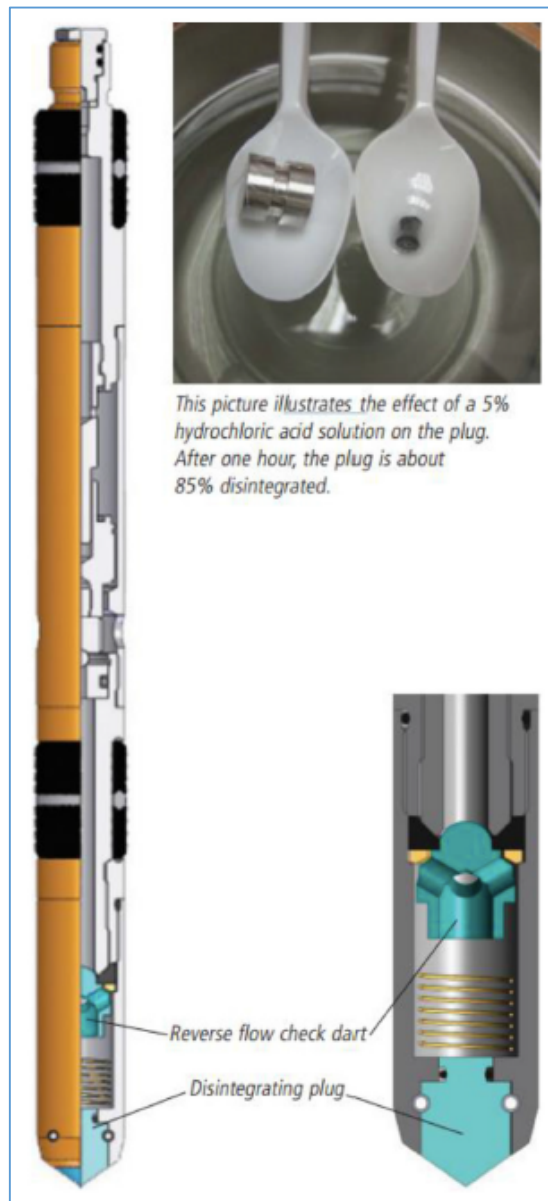


Figure 2-21: Gas Lift Valve with Dissolvable Material [41]

Pre-Perforated Drill-in Liner

Pre-perforated liner with dissolvable material plugging the holes can prevent fluid loss while drilling the well. Thus, this is an interventionless alternative to perforation systems. This concept has been experimented with in test wells under controlled conditions but has not yet been field tested [41, 42].

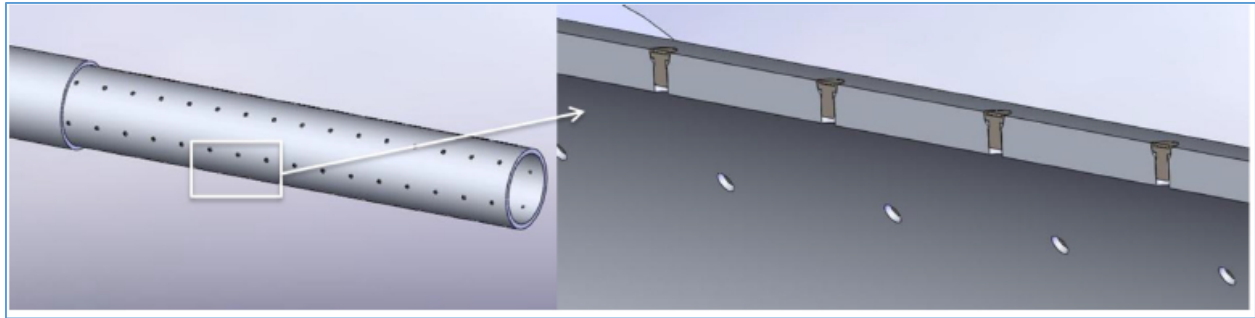


Figure 2-22: Pre-perforated liner with dissolvable plugs [41]

This chapter provided a brief overview of the various applications of the dissolvable technology within upstream oil and gas industry. Keeping in mind the huge potential of dissolvable materials, this thesis aims to systematically examine and characterize the behaviour of the dissolvable materials developed by National Oilwell Varco. While this thesis primarily focuses on the application of dissolvable balls, several aspects of the methodologies, results and analyses presented in this thesis are applicable for the aforementioned diverse applications of this technology.

3 Materials and Experimental Methods

The core of this thesis lies in understanding the behaviour of dissolvable materials in order to select the right material type for a specific oil and gas application. The aim of the experimental work performed in this chapter is three-fold. The first objective is to identify key parameters required to quantify the dissolution behaviour of these materials. The second goal is to examine the various factors that affect the performance of dissolvable materials and establish the nature of this relationship. The third goal of these experiments is to analyse the experimental data using regression methods in order to develop a model to predict the performance of dissolvable materials. The final target of the thesis is to develop a stepwise workflow to select the correct dissolvable ball material for any given downhole condition and operational requirement. Empirical and analytical models shall be developed to formulate this material selection methodology.

3.1 Materials Used

3.1.1 Dissolvable Material Samples

A series of experiments were conducted on selected dissolvable materials developed by National Oilwell Varco (NOV). In typical applications of dissolvable materials in the oil and gas industry in the North Sea, they are in the form of balls ranging from 2 in. – 4.5 in. Owing to the steep material prices and intricate manufacturing process involved in manufacturing these balls, the average cost of manufacturing a dissolvable frac ball is upwards of 1200 USD (10 000 NOK).

Keeping this in mind, the experiments in this section were performed on small cylindrical samples which are significantly cheaper to manufacture. These cylindrical samples measured approximately 12-16 mm (0.5-0.6 in) in diameter and 25 mm (0.98 in) long as illustrated in Figure 3-1. The analytical model developed in a subsequent section (Chapter 4.5) translates the results from cylindrical sample testing to predict the dissolution behaviour of frac balls.

These cylindrical samples made from dissolvable materials were stored in vacuum sealed packaging to ensure that they were not exposed to air for extended periods of time before actual usage.

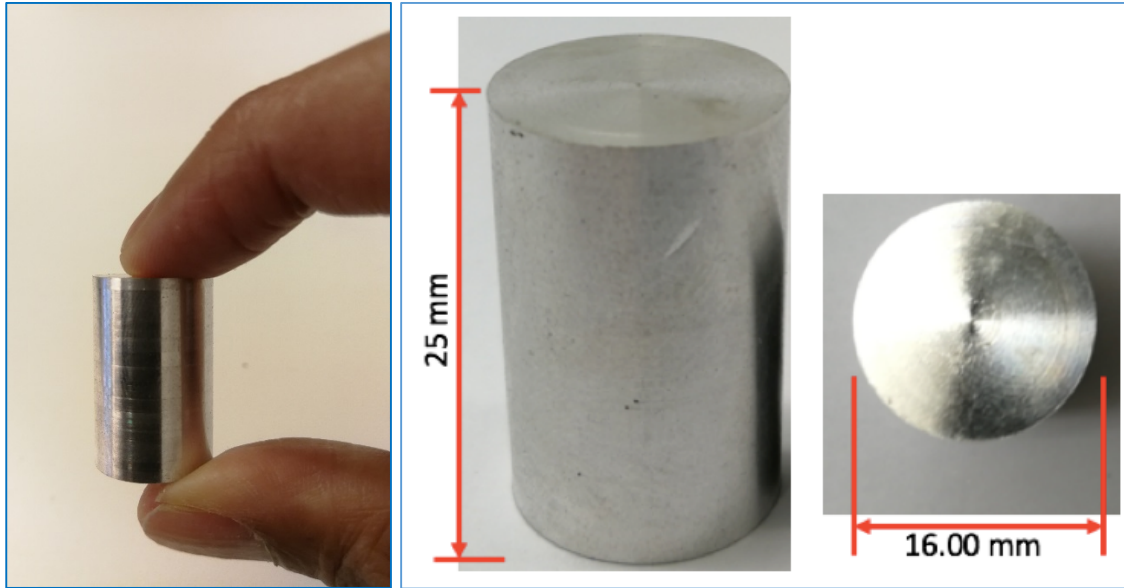


Figure 3-1: Cylindrical Sample made from NOV Dissolve 105

Four different types of proprietary materials developed by NOV were selected for this purpose. The materials and their description have been tabulated in Table 2. This information has been obtained from the company's internal data sheets on these materials.

Table 2: Dissolvable Materials Tested

Material	General Description	Manufacturing Method	0.2% Yield Strength (MPa)*	Ultimate Tensile Strength (MPa)*
NOV Dissolve 105	Composite of Nano-structured Mg-based metallic materials	Powder consolidation	225	307
NOV Dissolve 106	Composite of Nano-structured Mg-based metallic materials	Powder consolidation	201	279
NOV Dissolve 202	Magnesium Alloy	Extruded & Machined to shape	212	296

NOV Dissolve 301	Magnesium Alloy	Extruded & Machined to shape	180	290
---------------------	-----------------	---------------------------------	-----	-----

* Measured at 20 °C

The main difference between the 4 materials is that the percentages of Magnesium and other constituents vary substantially and hence, are expected to display diverse dissolution behaviours as well as mechanical properties. The reason behind selecting these materials as candidates for experiments was the expectation that due to their varying mechanical properties and composition, these specimens would be able to capture a spectrum of varied responses during dissolution testing.

To obtain the most accurate experimental results, within each material type, the samples were selected from the same manufacturing batch. For instance, all the NOV Dissolve 106 samples were selected from the batch manufactured together on a specific date as part of the same order. This is to ensure that when comparing the experimental results between the same material while varying an external factor (eg. temperature), the variations in manufacturing processes do not lead to erroneous results. This is one of the steps taken to ensure the quality control of experimental data.

3.1.2 Test Fluids

The behaviour of dissolvable materials is influenced by the fluids that they are exposed to. In order to better understand this effect, simple Sodium Chloride (NaCl) based brines were chosen as the test fluid for the experiments conducted. The main reason for selecting this fluid is because it is one of the most common type of downhole completion fluid and is often used for circulating down frac balls. Hence, it is a good starting point to systematically analyse the fluid effects on dissolvable materials. In addition to this, preparation of aqueous NaCl solutions poses no safety concerns and can be done in a precise and controlled manner.

Pure NaCl crystals were weighed and mixed into a pre-measured volume of distilled water to obtain the required concentration of aqueous NaCl solution. At this juncture, it is important to clearly define how concentration has been defined in this thesis. Solution concentration has been defined in several ways depending on the field of study, preference and region. In the current work, concentration of the NaCl solution is defined as follows –

$$\text{Concentration (\%)} = \frac{\text{Mass of NaCl crystals (g)}}{\text{Volume of water (ml)}} * 100 \quad (3.1)$$

Since this study involves solids dissolved in liquid, the above definition made the most sense in terms of ease of measurement of the solute's mass and solvent's volume. A mixer was used to ensure uniform mixing to obtain a homogenous solution of the required concentration.

3.2 Apparatus & Methods of Measurement

3.2.1 Heating and Temperature Measurement

In this thesis, a series of dissolution tests were conducted at various temperatures ranging from 50 °C to 80 °C. In order to heat the test fluid to the required temperature and maintain it at that level, a heater was used as shown in Figure 3-2. Once the desired setpoint is programmed into the heater, it heats up the fluid inside to the desired temperature and maintains it at the setpoint.



Figure 3-2: Heater

However, it was found that directly having test fluid (NaCl brine) inside the heater damaged the inside surfaces and affected its longevity. Hence, an alternative method was devised where water inside the heater was used as a water bath to heat glass jars containing the test fluid. This is illustrated in Figure 3-3.



Figure 3-3: Heater used to heat and maintain a water bath at required temperature

However, in order to ensure that the temperature of the test fluid inside the glass jar was maintained at the desired setpoint, a temperature sensor was immersed inside the glass jar to monitor this (Figure 3-4).



Figure 3-4: Thermostat used to monitor temperature of test fluid

3.2.2 Mass Measurement

The cylindrical samples of dissolvable materials were weighed on an hourly basis throughout the duration of the dissolution experiments. A digital weighing scale with high precision was required for this purpose. This requirement stems from the fact that the weight of all the measured samples were under 10 grams and to monitor the extent of dissolution, the mass changes were monitored regularly during the course of the experiments. A reasonably sensitive measurement device was used in order to capture the slight changes in mass with a precision of 2 decimal places for weight measured in grams (Figure 3-5). Care was taken to ensure that the scale was always zeroed before taking any measurements.



Figure 3-5: Weighing scale to measure cylindrical sample mass

During the preparation of test fluids, a scale with a larger range of measurement was required to be able to weigh the NaCl crystals to obtain the required concentration. This was measured using a scale shown below in Figure 3-6.



Figure 3-6: Scale used to weigh NaCl crystals for test fluid preparation

3.2.3 Dimensional Measurement

The length and diameter of the cylindrical sample were measured using a digital Vernier caliper with a precision of 2 decimal places for measurements displayed in millimetres (See Figure 3-7). The diameter was measured at 3 different places along the length of the sample and the average value was used as experimental data.



Figure 3-7: Digital Vernier Caliper

3.2.4 Other Apparatus

During the dissolution test, the cylindrical samples were taken out from the test fluid to monitor the changes in mass and dimensions. Prior to recording these measurements, the samples were dried using a heat gun (or hot air gun). The heat gun blows a stream of hot air that dries the sample within a period of 5-7 seconds.



Figure 3-8: Heat Gun used to dry samples

In addition to the abovementioned pieces of apparatus, safety gloves and the appropriate ventilation system must be used to ensure safety of personnel and to prevent overheating of the lab during high temperature experiments.

3.3 Experimental Procedure

The experiments performed on the cylindrical test pieces of the dissolvable material are referred to as ‘Sample Dissolution Tests’ in this work. Various sample dissolution tests were performed as part of Chapter 3 and the experimental results have been elaborated on in Chapter 4.

Section 3.3.1 lists the various steps in a typical sample dissolution test. Section 3.3.2 provides an overall picture of the various sample dissolution tests that were performed on different materials types under varying experimental conditions. The objective behind performing these different dissolution tests have also been listed.

3.3.1 Detailed Procedure – Sample Dissolution Tests

The steps documented below were followed in every sample dissolution test that was conducted as part of this work. The steps were followed meticulously while avoiding any variations in them. This was to ensure that consistent and reliable results were obtained in order to make accurate correlations and conclusions about the parameters that affect the performance of dissolvable materials.

- Step 1. A clean jar is filled with 2 litres of distilled water.
- Step 2. The appropriate amount of NaCl crystals is weighed using the scale to achieve the desired concentration.

For example - Referring to Eq. 3.1, to achieve a concentration of 1% NaCl brine, 20 grams of NaCl crystals are added to 2 litres of water.

$$\text{Concentration (\%)} = \frac{20 \text{ (g)}}{2000 \text{ (ml)}} \times 100 = 1\%$$

- Step 3. Weighed salt is added into the jar and mixed thoroughly to ensure that the salt has fully dissolved in the solution.
- Step 4. The heater is filled with water and programmed to heat up to the desired test temperature.
- Step 5. The jar with the 2 litres of test fluid is placed inside the heater as shown in Figure 3-9.



Figure 3-9: Test fluid inside the jar being heated using a water bath

- Step 6. The temperature of the test fluid inside the jar is monitored using a temperature sensor (Figure 3-4) until it reaches the test temperature.
- Step 7. Meanwhile, the cylindrical sample of the desired test material is taken from its packaging. The material information and manufacturing batch number (LOT #) is recorded in the test data sheet.

Note: A test data sheet is used to record the experimental data for every dissolution test experiment. This data sheet shall be referred to in subsequent steps as well. As an example, the test data sheet from an experiment conducted on NOV Dissolve 105 in 3% NaCl solution at 70 °C is shown in Figure 3-10.

- Step 8. The pre-test diameter and length of the cylindrical sample are measured using a digital vernier caliper. There may be very slight variations in the diameter along the length of the sample. Hence, three diameter readings are taken along the length and the average value is recorded in the test data sheet.

TEST DATA SHEET - Cylindrical Sample Dissolution Test						
Pre testing Data						
Date of test:		06/02/2018				
Sample Material:		NOV Dissolve 105 Lot#445305				
Fluid Data:		3% NaCl Additional info - Mixed 60 gms of NaCl in 2 lites of water				
Fluid Temperature:		70 °C				
Initial Sample Mass and Dimensions:			Initial Values:			
OD (mm)	16.05	Volume of Cylindrical sample [cm ³]	5.01			
Length (mm)	24.74	Area of Cylindrical sample [cm ²]	16.52			
Weight (g)	9.15	Density of Cylindrical sample [g/cm ³]	1.83			
Start time (hh:mm)	10:25					
Recorded Values During Dissolution Test						
Reading#	Weight(g)	Length (mm)	OD (mm)	Sample date	Sample Time	Comments

Figure 3-10: Test Data Sheet Example – Pre-test data

- Step 9. The initial mass of the sample is also measured and recorded in the test data sheet.
- Step 10. Other pre-test information recorded in the test data sheet include the test date, test fluid data and test temperature (Figure 3-10).
- Step 11. Once the test fluid has reached the required test temperature, the cylindrical sample is lowered into the jar using a sample holder as shown in Figure 3-11.
- Note:** The sample holder is made from stainless steel to ensure that the holder material does not corrode, or in any way alter the dissolution reaction between the dissolvable material and the test fluid. Furthermore, the sample holder has a number of perforations at the bottom. This is to make sure that when the sample is suspended at mid-height in the jar, the cylinder is exposed to the test fluid in all directions and hence, the dissolution reaction between the dissolvable material and the test fluid will be uniform.
- Step 12. The jar's lid is closed to minimize evaporation of the test fluid as this might affect the concentration of NaCl. The time when the cylindrical sample is first lowered into the test fluid is recorded in the test data sheet as the 'Start Time'. The test has now commenced and the temperature sensor is monitored continuously to ensure that the test temperature is maintained constant throughout the test duration.



Figure 3-11: Lowering the dissolvable material sample into the test fluid using sample holder

Step 13. Thereafter, at approximately every 1 hour, the sample is taken out and dried using the hot air gun (See 3.2.4). The duration of the drying process is short and last approximately 5-10 seconds.

This is to ensure that when measuring the weight, the test fluid’s mass does not distort the reading. The material is only slightly porous once the dissolution reaction has commenced. However, it has been observed that there is a slight variation in the weight of the sample before and after using the hot air gun due to a slight fluid penetration into the outer edges of the sample surface. Hence, this step was included in the test procedure.

Step 14. The dried sample’s average outer diameter, length and mass are measured and recorded in the test data sheet along with the time when the measurement was taken as shown below in Figure 3-12.

TEST DATA SHEET - Cylindrical Sample Dissolution Test						
Pre testing Data						
Date of test:			06/02/2018			
Sample Material:			NOV Dissolve 105 Lot#445305			
Fluid Data:			3% NaCl Additional info - Mixed 60 gms of NaCl in 2 lites of water			
Fluid Temperature:			70 °C			
Initial Sample Mass and Dimensions:			Initial Values:			
OD (mm)	16.05	Volume of Cylindrical sample [cm ³]				5.01
Length (mm)	24.74	Area of Cylindrical sample [cm ²]				16.52
Weight (g)	9.15	Density of Cylindrical sample [g/cm ³]				1.83
Start time (hh:mm)	10:25					
Recorded Values During Dissolution Test						
Reading#	Weight(g)	Length (mm)	OD (mm)	Sample date	Sample Time	Comments
1	7.75	24.12	15.20	06/02/2018	11:34	
2	5.68	22.56	13.58	06/02/2018	12:56	
3	4.31	21.03	12.26	06/02/2018	14:06	
4	3.14	19.72	10.88	06/02/2018	15:18	
5	2.41	18.62	9.73	06/02/2018	16:14	
6	2.01	17.68	9.18	06/02/2018	16:52	
7	1.48	16.87	8.34	06/02/2018	17:47	

Figure 3-12: Test Data Sheet Example – Completed Test Data

Step 15. Measurements are taken about every hour throughout the test duration. The test is performed continuously for a period of at least 7 hours. The test is not performed overnight due to safety concerns related to leaving the heater switched on in the lab overnight. However, it is expected that the 7-hour experimental duration is sufficient to establish the dissolution behaviour of the test samples under a given set of test conditions.

3.3.2 Test Program

A test program consisting of 4 distinct stages was devised in order to systematically understand and quantify the dissolution behaviour of the materials listed in Section 3.1.1. Each stage of the test program involved conducting a series of sample dissolution tests with specific objectives in mind. The test procedure outlined in Section 3.3.1 was consistently followed in order to obtain reliable results that could be analysed to derive meaningful relationships between the factors that the dissolution behaviour depends upon.

Stage I - Variations in Critical Parameters (Mass & Geometry) during Dissolution Process

The first objective of this stage was to make initial observations regarding the nature of the dissolution process and how the dissolvable materials react when exposed to brine. The second objective was to examine the variations in key parameters such as mass and geometry (diameter, length) during the dissolution process. This was done in order determine which of the parameters measured as part of the dissolution tests were critical to characterize the dissolution performance of a material under specific experimental conditions. A third objective was to compare the performance of the 4 dissolvable materials at this identical test condition.

In order to meet the first and second objectives, a first dissolution test was conducted on NOV Dissolve 105 material at a test temperature of 80 °C with 1% NaCl as the test fluid. Thereafter, to address the third objective, dissolution tests were conducted on NOV Dissolve 106, 202 and 301 at the same test conditions as illustrated in Figure 3-13. Stage I results are discussed in Section 4.1.

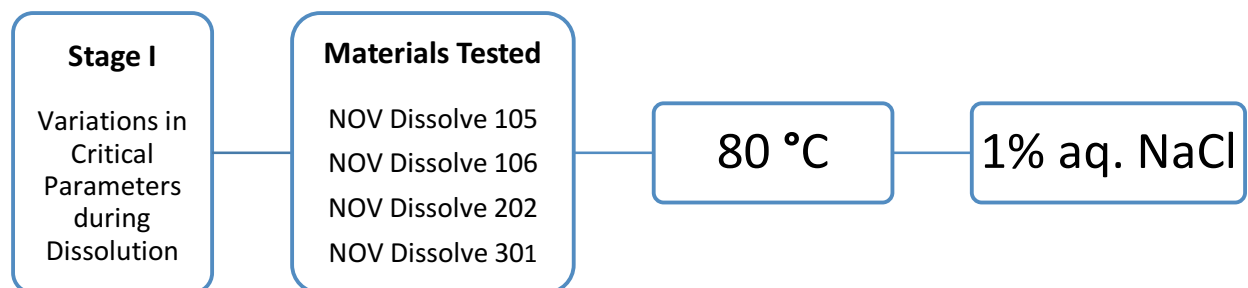


Figure 3-13: Schematic of Stage I Test Outline

Stage II - Investigating the Effect of Concentration

Since the application of dissolvable materials in upstream oil and gas sector is the main focus area here, one key operational parameter that is likely to affect the performance of these materials is the composition of downhole fluids. Chloride-based brines of different concentrations (eg. seawater) are one of the most commonly used type of fluids during the well completion process. Therefore, the main objective of this stage was to determine how variations in the concentration of aqueous NaCl solutions affect the performance of dissolvable materials. In addition to this, the responses of the four different materials to variation in concentrations were compared.

In order to isolate the effect of concentration, sample dissolution tests were conducted on each of the four different materials at a constant temperature of 80 °C while the NaCl concentration in the test fluid concentration was varied – 1%, 3%, 6% and 9%. These specific concentrations were chosen to cover the typical maximum and minimum ranges of chloride based brines used in completion. This has been illustrated below in Figure 3-14. Stage II results are discussed in Section 4.2.

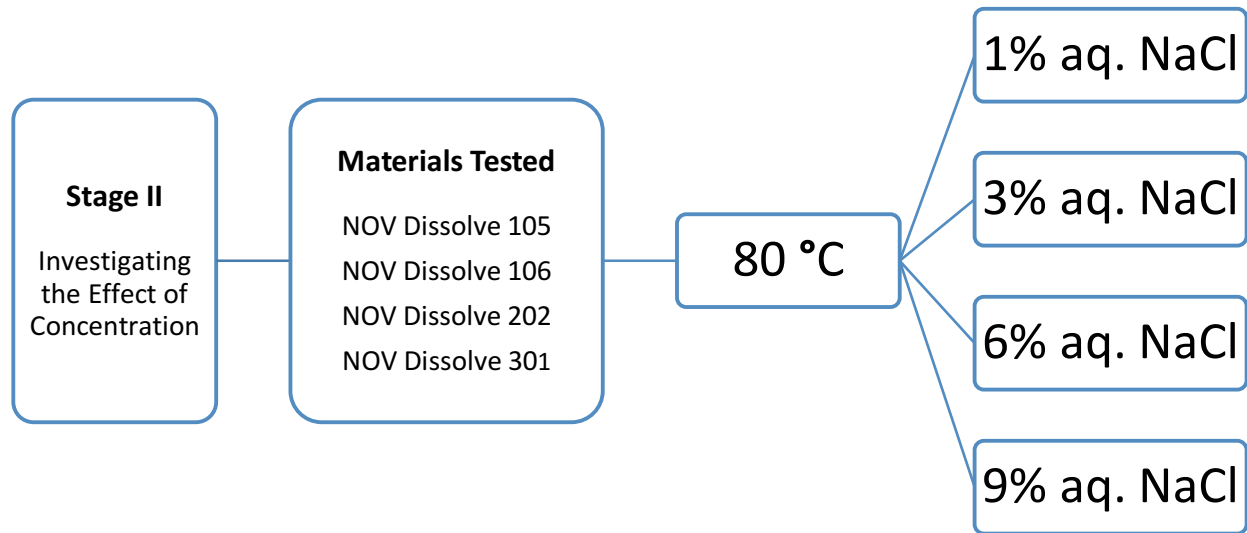


Figure 3-14: Schematic of Stage II Test Outline

Stage III - Examining the Effect of Temperature

In addition to the fluid composition, the other key operational criteria that could have an effect on the dissolution performance is the downhole temperature. Thus, the main objective of this stage was delving into the variations in the dissolution behaviour of the different dissolvable materials with changing temperatures.

Downhole temperatures can span a wide spectrum ranging from 50 °C to as high as 200 °C depending on the depth and temperature gradient in a particular field. Wells with temperatures higher than 150 °C are classified as High-Temperature (HT) wells. However, owing to the limitations of the test equipment and safety concerns, the dissolution tests were performed at 50 °C, 70 °C and 80 °C.

Referring to Figure 3-15, dissolution tests were performed on each of the four dissolvable materials at a constant concentration of 1% aq. NaCl but at 3 different test temperatures of 50 °C, 70 °C and 80 °C. In addition to this, the response of the four different materials to variation in temperatures were compared. Stage III results are discussed in Section 4.3.

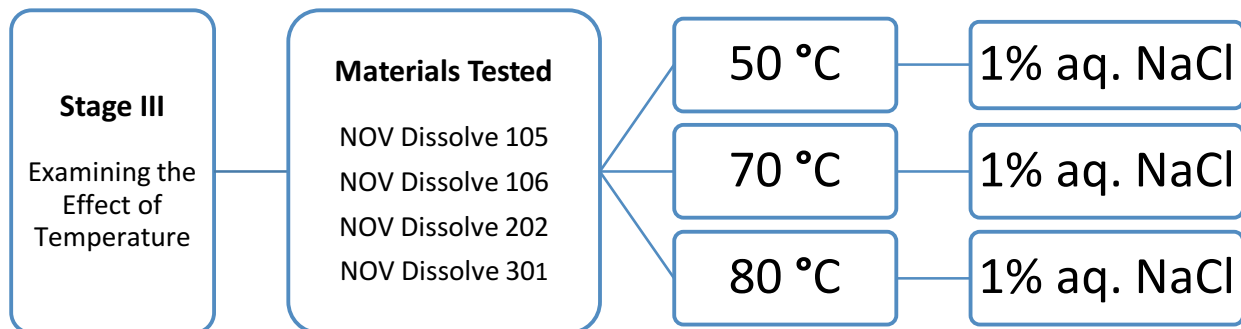


Figure 3-15: Schematic of Stage III Test Outline

Stage IV - Investigating the Combined Effects of Temperature & Concentration

As a natural progression from the experiments conducted in Stages I-III, a final stage of testing was planned with the objective of exploring the combined effects of both temperature and concentration on the performance of dissolvable materials. The final goal of this stage was to use the experimental data to develop an empirical model which allows one to predict of performance of the tested dissolvable materials under different temperatures and brine compositions.

In this stage, a series of 48 different experiments were conducted wherein each of the four dissolvable materials were tested at the 3 test temperatures of 50 °C, 70 °C and 80 °C, and in four different test fluid concentrations of 1% aq. NaCl, 3% aq. NaCl, 6% aq. NaCl and 9% aq. NaCl. The schematic shown below (Figure 3-16) succinctly captures the tests conducted in this stage. Stage IV results are discussed in Section 4.4.

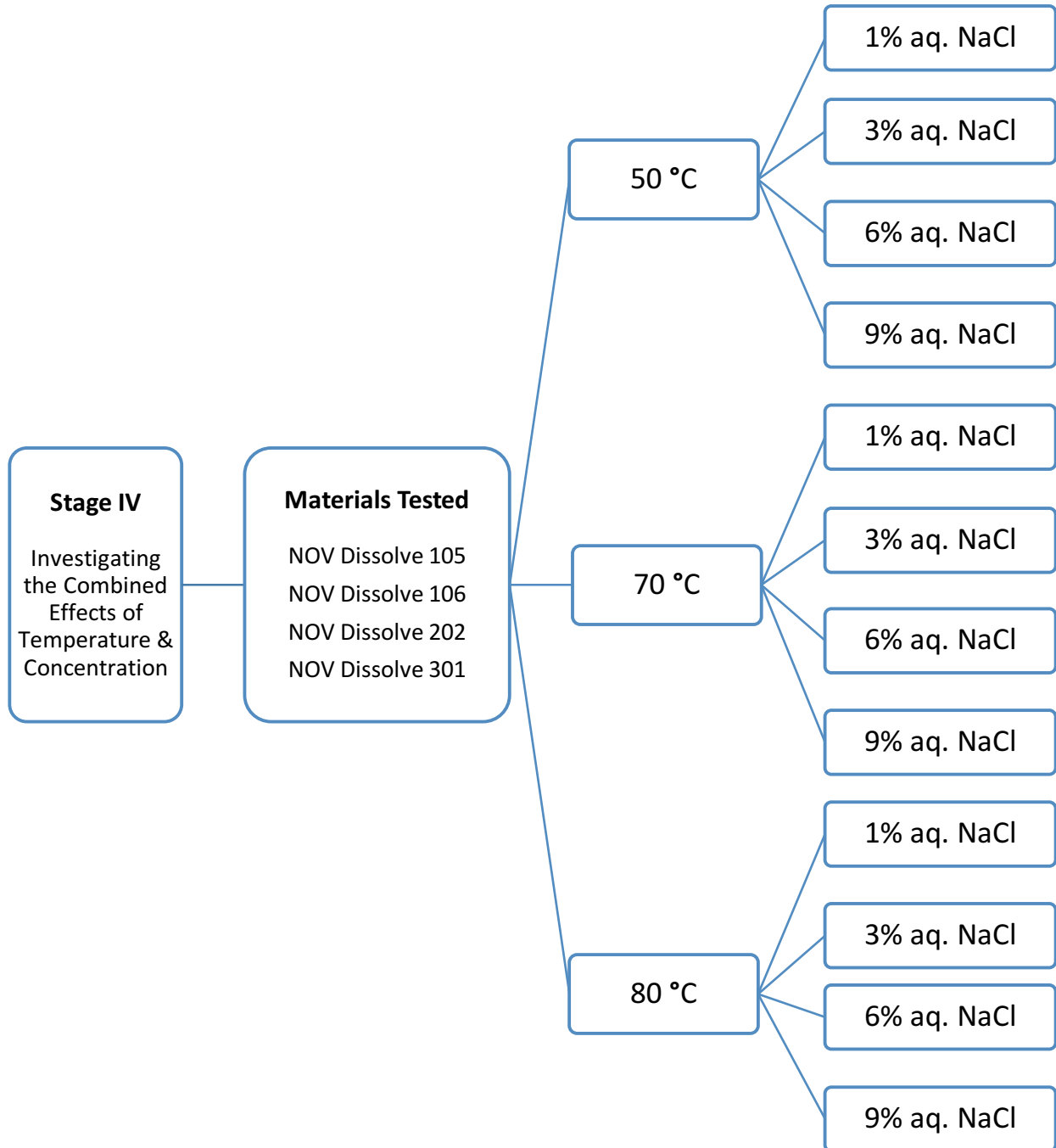


Figure 3-16: Schematic of Stage IV Test Outline

4 Results and Discussion

A test program consisting of four different stages was devised with specific objectives as enumerated in Section 3.3.2. Within each stage, a series of dissolution tests on cylindrical samples were performed following the prescribed steps in Section 3.3.1 in order to obtain consistent and comparable results. In Section 4, the results from the test program's various experiments are presented along with discussions and analyses. Sections 4.1 - 4.4 correspond to the experimental results of Stage I to Stage IV of the test program. Empirical and analytical methods are used to model the performance of dissolvable balls in Section 4.5.

Note that while certain areas of fundamental chemistry are briefly touched in this work to explain the experimental results, the main focus shall remain on the behaviour of the dissolvable materials that have practical implications to their applications in downhole completions.

4.1 Stage I - Variations in Critical Parameters during the Dissolution Process

4.1.1 Initial Observations from Dissolution Tests

At the start of Stage I, a dissolution test was performed on NOV Dissolve 105 cylindrical sample at a test temperature of 80 °C with 1% aqueous solution of NaCl as the test fluid. As soon as the sample was lowered into the test fluid, a cloud of bubbles was observed indicating that at this test condition, the dissolution reaction was initiated almost instantaneously as seen in Figure 4-1.

When sodium chloride (NaCl) is mixed in water to prepare the test fluid, a dissociation process occurs. Since NaCl is an ionic compound, the ions physically separate from each other and get surrounded by water molecules [43]. Thus, the products of this reaction are positively charged sodium ions (cation) and negatively charged chloride ions (anions), and this process is termed as dissociation. The more negative oxygen atoms from water are attracted to the positively charged sodium ions whereas water's hydrogen atoms are attracted to the negatively charged chloride ions as seen in Figure 4-2 [44].

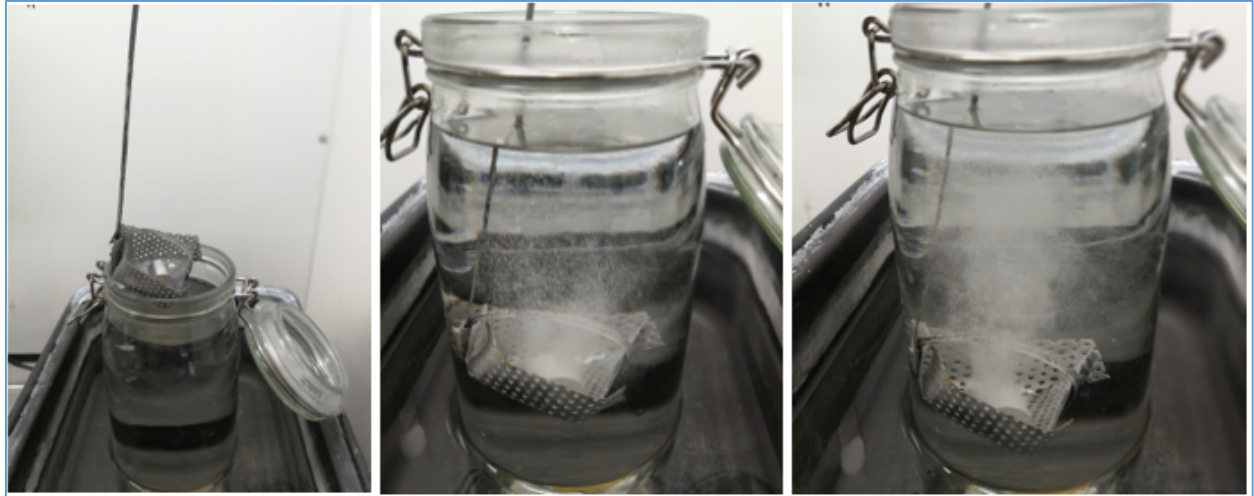


Figure 4-1: Cloud of gas bubbles as soon as sample is lowered into the test fluid

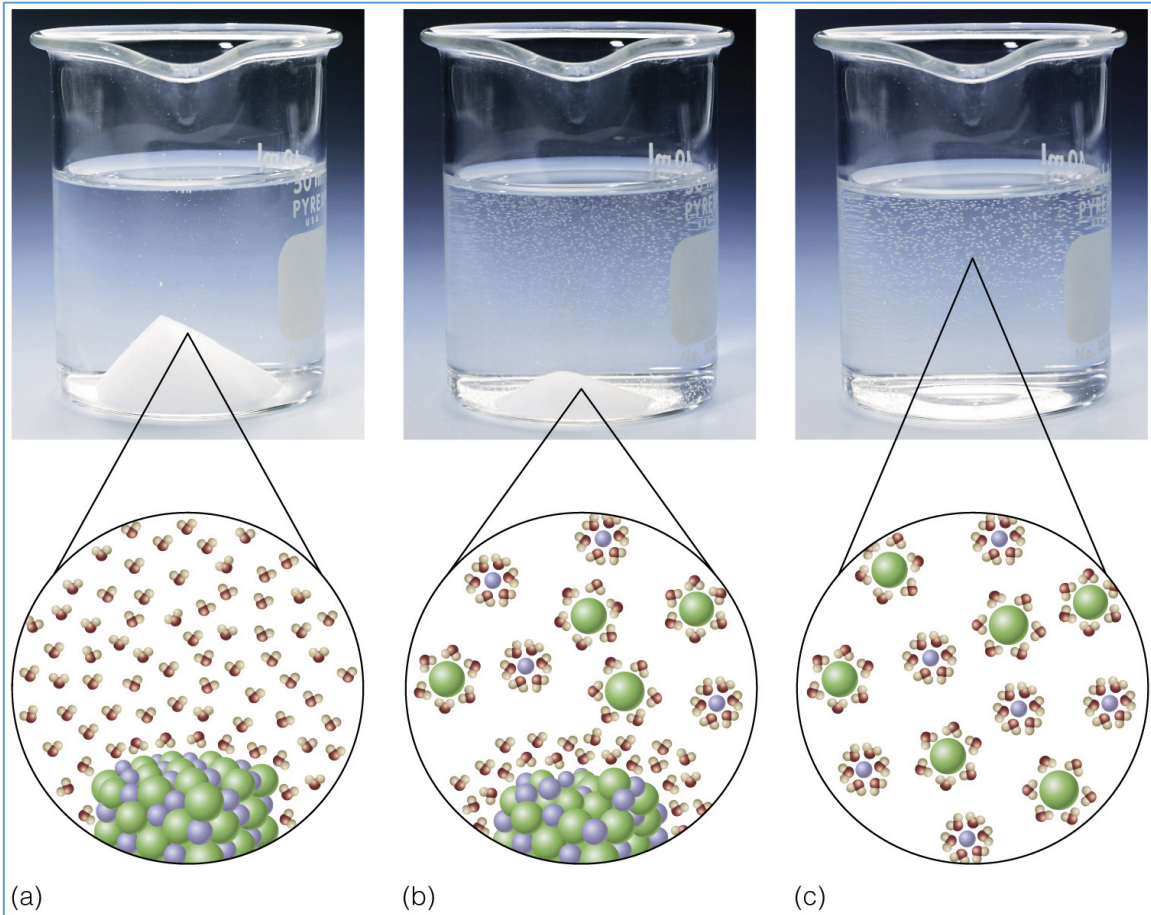
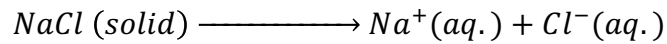


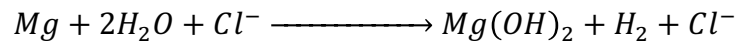
Figure 4-2: Dissociation of NaCl when dissolved in water. The chloride ions and sodium ions dissociate and are surrounded by hydrogen and oxygen atoms respectively [44]

This dissociation reaction occurring when preparing the test fluid can be represented by the following equation –



The dissolvable materials tested in this experiment are metallic alloys with Magnesium as the primary constituent (Section 3.1.1). The reaction occurring during the dissolution process is the magnesium in the cylindrical sample reacting with the water to form Magnesium Hydroxide and Hydrogen as derivatives [5, 10]. During this reaction, the free chloride ions in the water act as catalysts to drive the dissolution reaction forward.

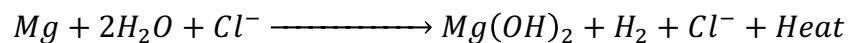
Thus, the dissolution reaction can be represented by the equation below –



Therefore, the gas bubbles emanating from the sample during the test are postulated to be hydrogen gas produced as a by-product of the dissolution reaction shown above. However, the amount of hydrogen produced during the course of a dissolution test is very small and does not pose any safety risks when using these dissolvable materials.

Another observation during the experiment was an increase in local temperature inside the test jar during the dissolution reaction. This was measured using the temperature sensor which was placed closed to the sample that was undergoing the reaction. However, since the sample volume is small compared to the overall test fluid volume inside the jar, the overall temperature of the test fluid was relatively constant. However, this point must be kept in mind when performing future dissolution tests where the dissolvable material volume is comparable to the test fluid volume (such as a dissolvable ball) and appropriate measures must be used to ensure that the temperature is kept constant.

Noting its exothermic nature, the dissolution reaction can be more accurately described as -



4.1.2 Variation in Measured Parameters with Time

During the dissolution test of NOV Dissolve 105 in 1% NaCl at 80 °C the sample's mass, length and average diameter were recorded in the test data sheet throughout the experimental duration of ≈ 7 hours. Before each measurement, the sample is taken out from the test jar and dried using a hot air gun to ensure that the mass of test fluid is not included in mass measurements.

During the test, the sample's mass reduced from 9.22 grams to 1.04 grams. The variation in length was from an initial value of 25 mm down to 15.53 mm at the end of the experiment. The corresponding change in sample diameter was from 15.98 mm to 7.16 mm. Figure 4-4 and Figure 4-5 show the progressive mass, length and diameter measurements taken of the NOV Dissolve 105 sample at the test conditions.

It can be observed that the dissolution is generally uniform with the sample maintaining its cylindrical shape throughout the test duration. This is more apparent from Figure 4-3 below showing the comparative photos of an untested 105 sample and a tested sample of the same material. This is due to the fact that a perforated sample holder was used as a result of which the entire sample's surface area was exposed to the test fluid throughout the test duration.

It can also be observed that the surface of the sample is of ashiny metallic nature at the start but soon after the commencement of the dissolution reaction, it is replaced by a dull charcoal-coloured inner core.

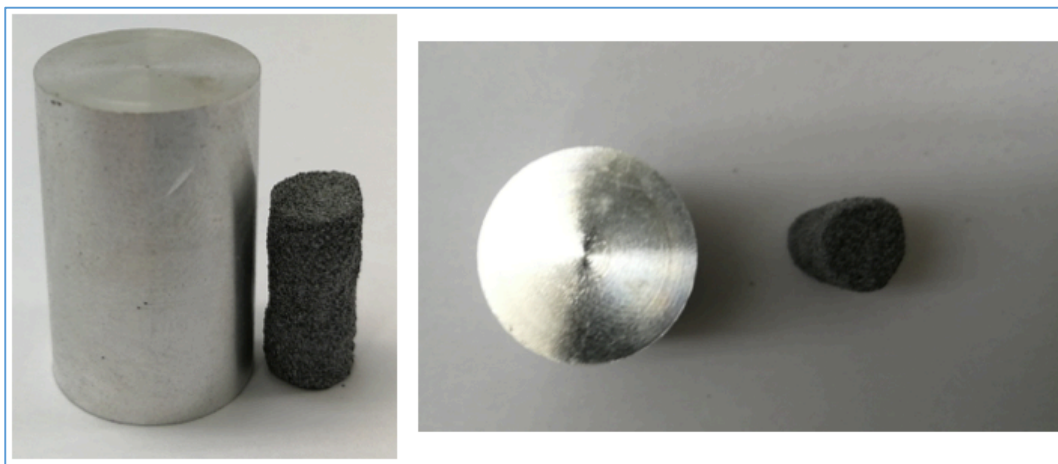


Figure 4-3: NOV Dissolve 105 – Untested Sample vs Tested Sample (80 °C, 1% NaCl)

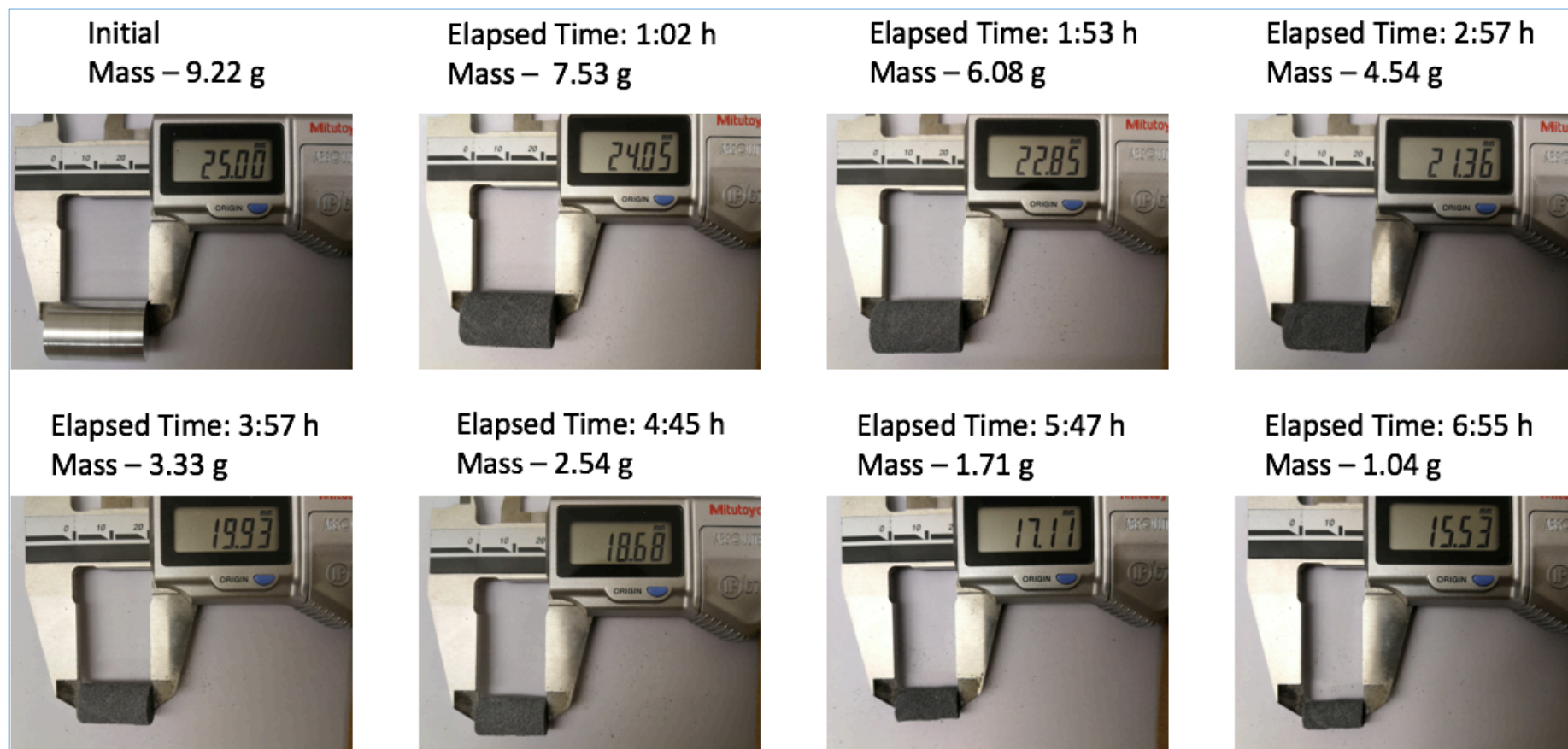


Figure 4-4: Length measurements during dissolution test of NOV Dissolve 105 in 1% NaCl at 80 °C

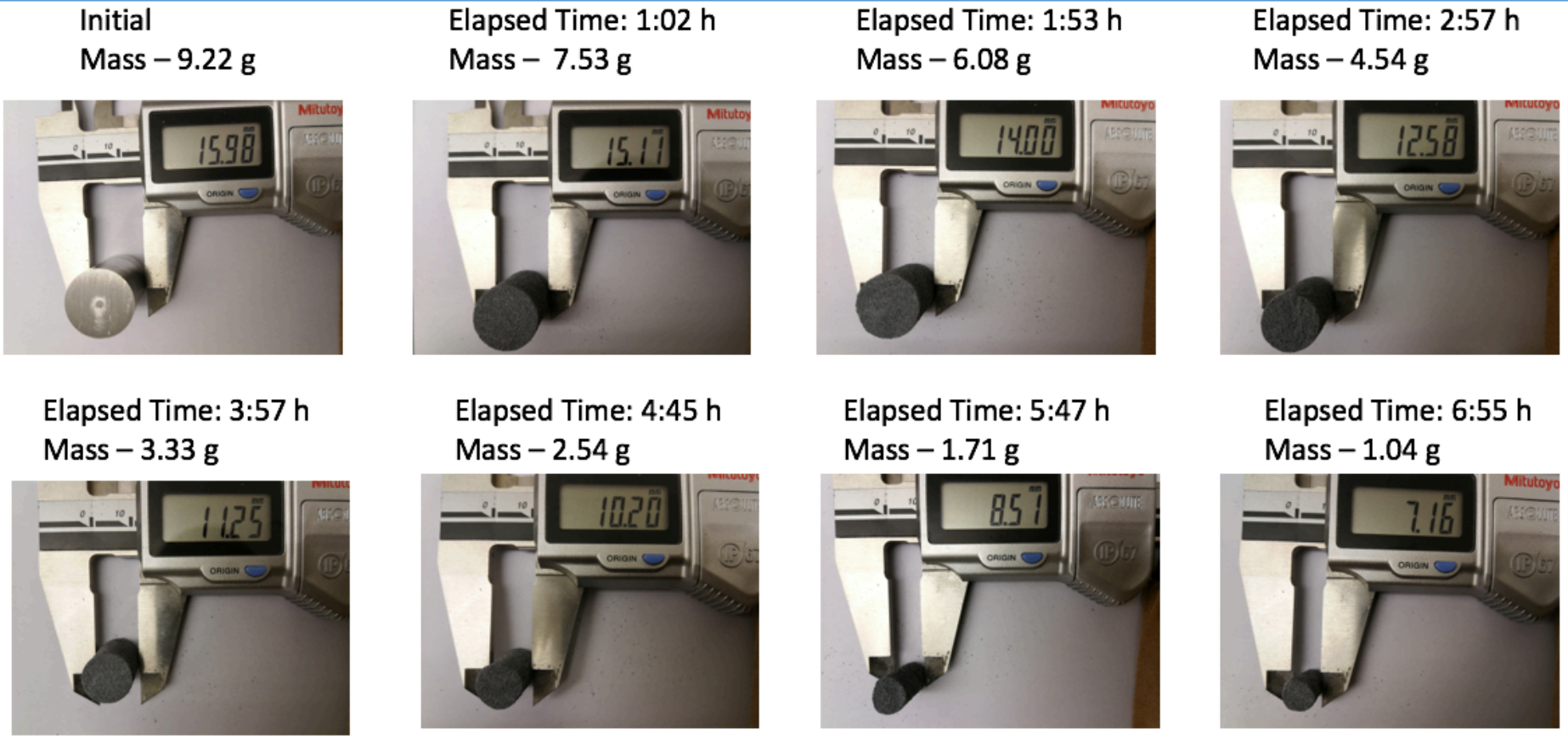


Figure 4-5: Diameter measurements during dissolution test of NOV Dissolve 105 in 1% NaCl at 80 °C

Figure 4-6 below shows the mass of the 105 sample plotted as a function of time using the information recorded in the test data sheet. While the mass decreases with time as expected, the rate of reduction is not constant. The slope of the curve is steep at the beginning and as the reaction progresses it gets more gradual.

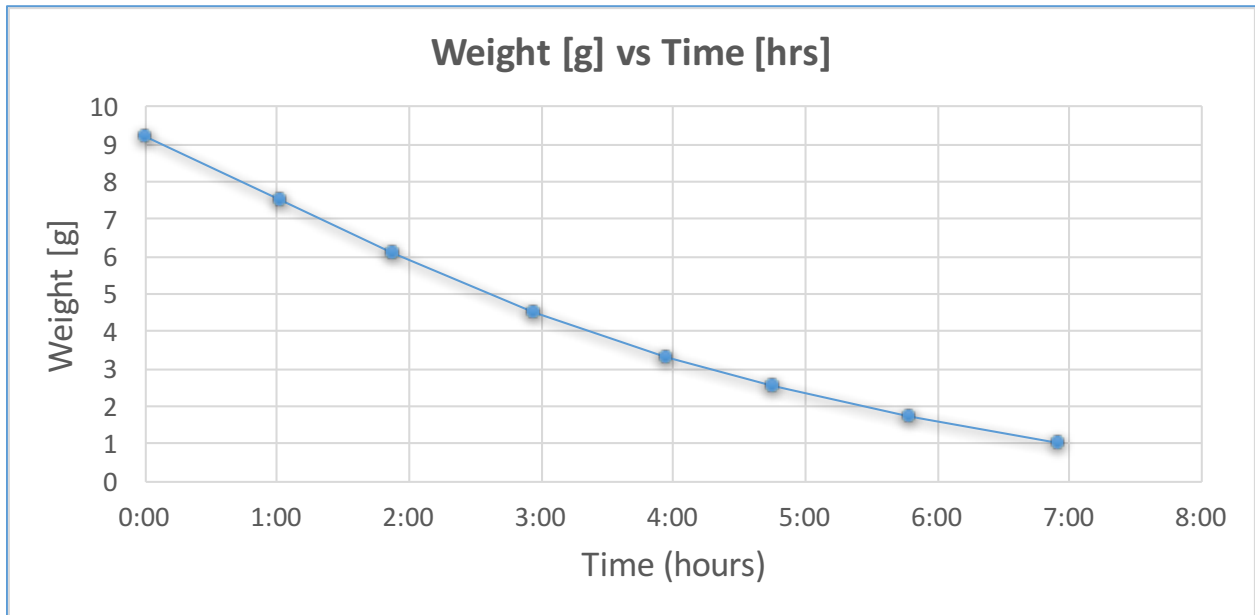


Figure 4-6: NOV Dissolve 105 weight as a function of time at 80 °C in 1% aq. NaCl

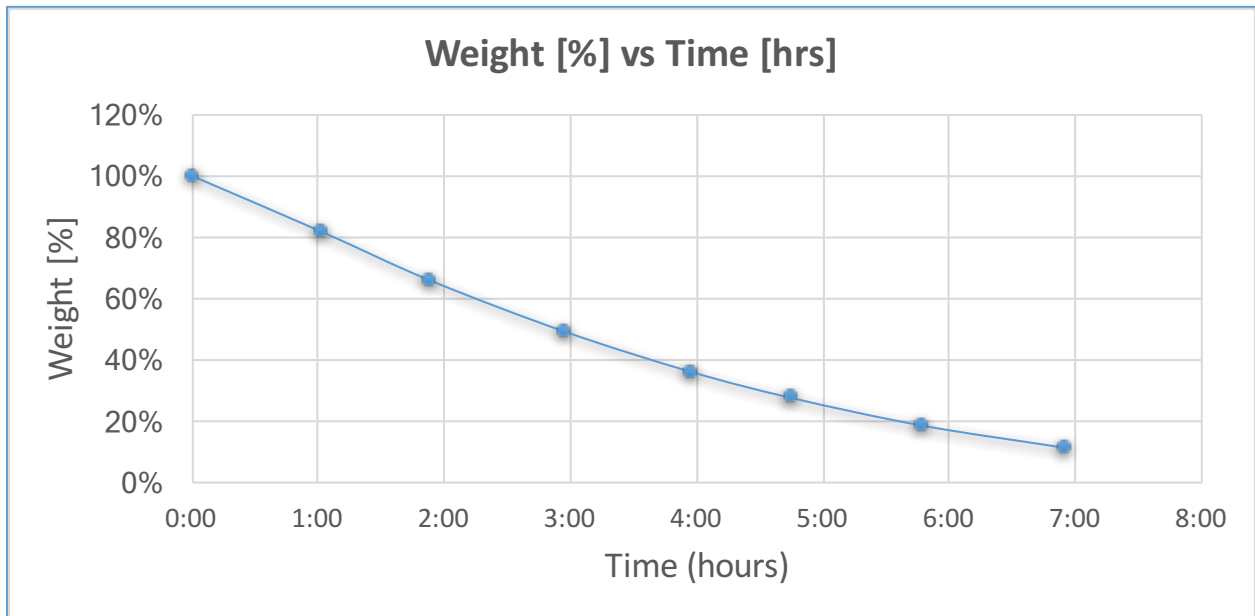


Figure 4-7: NOV Dissolve 105 weight (% of initial sample mass) as a function of time at 80 °C in 1% aq. NaCl

Figure 4-7 plots the mass from the same experiment but expressed as a percentage of the initial sample mass. During the first hour of the experiment, the sample weight was reduced by 18% relative to the initial value. During the second hour, the sample lost a further 18%. On the other hand, during the 6th and 7th hours of the experiment, the sample only lost 9% and 8% of the initial weight, respectively. This variation in the rate of mass loss can be attributed to another key parameter that is changing during the course of the experiment - the surface area of the cylindrical sample that is exposed to test fluid.

Collision theory of reactivity states that chemical reactions take place when the molecules of the reacting substances (aka reactants) collide with a certain minimum amount of molecular energy [43]. The number of collisions occurring in a given time interval, known as collision rate, directly affects the rate of a chemical reaction [45]. For chemical reactions where one of the reactant is a solid and the other is in liquid state, as is the case in the dissolution reaction, surface area plays a key role in determining the reaction rate. In these two-phase reactions, the collision between the reactants' molecules can only occur at the boundary between the solid and liquid, i.e., the surface of the solid reactant. When the surface area of the solid reactant is increased, the probability of collision as well as the collision rate increase resulting in an increased rate of reaction. This has been illustrated in Figure 4-8.

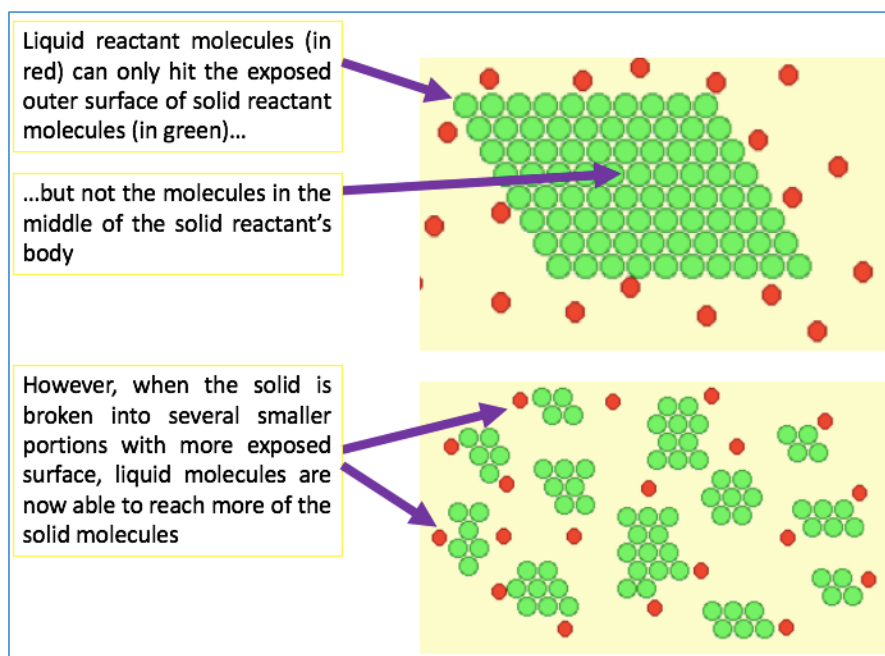


Figure 4-8: The effect of surface area in a solid-liquid reaction [46]

In the sample dissolution reaction, where magnesium reacts with water, the surface area of the sample has a direct effect of the reaction rate. However, since this reaction ‘dissolves’ the cylindrical sample, the surface area of the sample is continuously changing with time. Figure 4-9 plots the surface area of the 105 cylindrical sample calculated from the measured diameter and length values recorded in the test data sheet. The total surface area of the cylindrical sample of diameter, d and height, h was calculated using the following standard formula:

Total Surface Area = (2 · Area of end faces) + Area of Cylindrical surface

$$Total\ Surface\ Area = \left(2 \cdot \frac{\pi \cdot d^2}{4} \right) + (\pi \cdot d \cdot h) \quad (4.1)$$

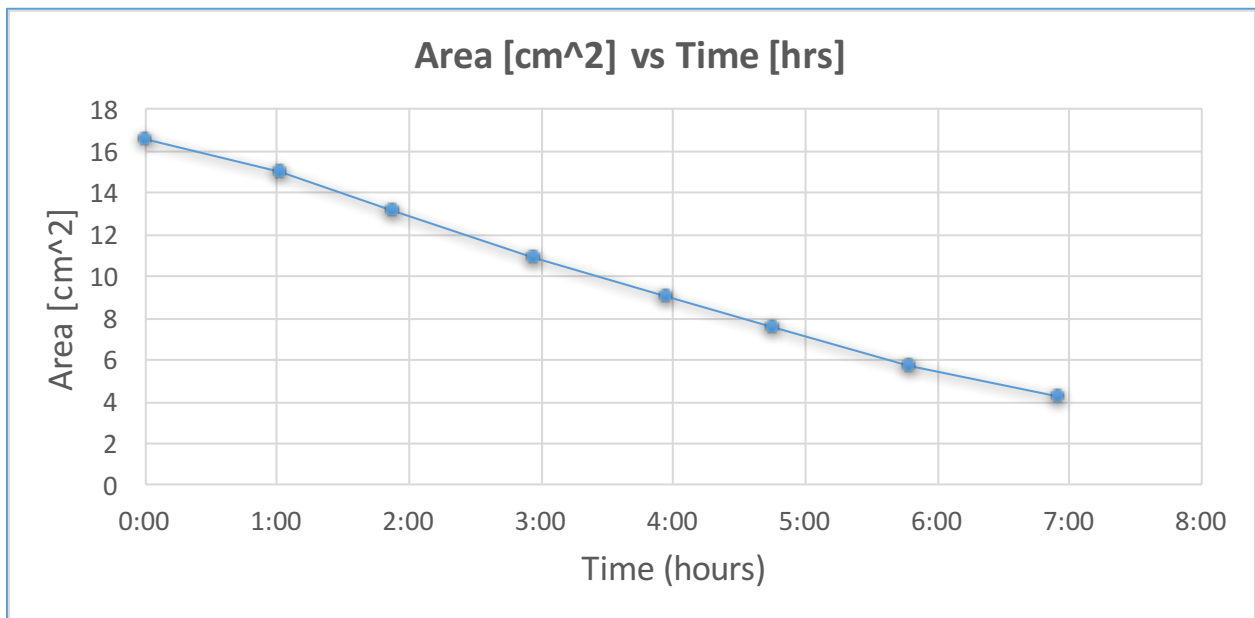


Figure 4-9: NOV 105 sample’s surface area as a function of time at 80 °C in 1% aq. NaCl

A steady decrease in surface area can be seen as the dissolution reaction progresses. Therefore, as per the collision theory introduced earlier, the collisions between the molecules of water and magnesium reduce with time. As a result, the dissolution reaction slows down with time. Thus, this theory can be used to explain why the rate of reduction of mass observed in Figure 4-6 and Figure 4-7 becomes progressively slower with time.

It is to be noted here that initially the test plan was to merely place the cylindrical sample at the bottom of the jar containing test fluid during the dissolution tests. However, the importance of the sample surface area exposed to the test fluid was recognized early on prior to beginning the experiments. Placing the cylinder at the bottom of the jar would not have exposed the entire surface area of the cylinder to test fluid. Furthermore, an additional variable as to how the cylinder is placed at the bottom, i.e., vertically or horizontally, would have resulted in inconsistent test results. Keeping this in mind, the perforated sample holder (Figure 4-10) was made to ensure that during the dissolution tests, the entire surface of the cylindrical sample was uniformly accessible to the test fluid.



Figure 4-10: Perforated sample holder to ensure uniform exposure of sample's surface area to test fluid

Continuing on with Stage I of the test program shown in Figure 3-13, the three-other materials NOV Dissolve 106, 202 and 301 were taken through the identical experimental conditions of 80 °C with 1% aqueous solution of NaCl as the test fluid.

Figure 4-11 plots the measured weight of the four dissolvable materials while undergoing a dissolution test at the identical test conditions of 80 °C with 1% aq. NaCl as the test fluid. For ease of comparison, the weight values have been expressed as a percentage of the initial pre-test weight of the respective sample.

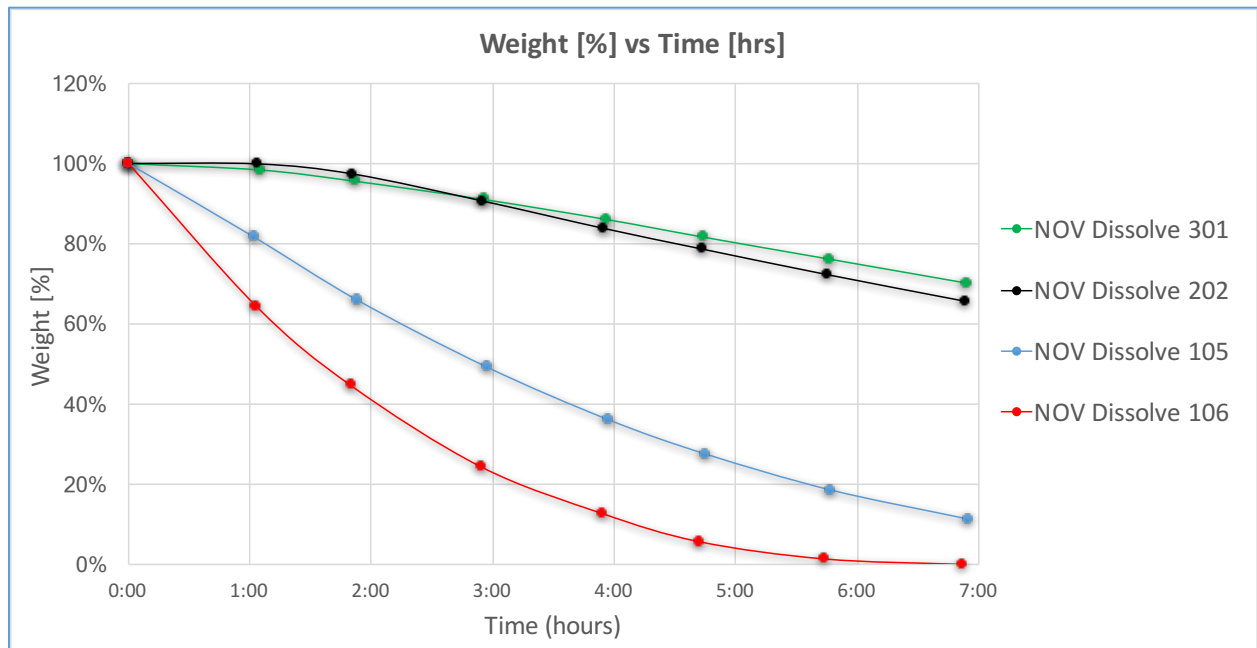


Figure 4-11: Measured weight as a function of time for the four dissolvable samples at 80 °C and 1% NaCl solution

From initial analysis of the plot, material 106 was found to be the fastest dissolving material among the tested samples since the sample completely dissolved within the test duration of 6h 52 minutes. Material 105 is the second fastest material with the final measured weight being 11% of the initial weight. Between materials 202 and 301, material 301 lost more weight during the initial 2 hours. Thereafter, material 202 lost weight at a higher rate than 301 such that at the end of the test 65% of material 202 was left which is marginally smaller than the 70% of material 301 that was remaining.

Figure 4-12 plots the surface area of the four dissolvable materials while undergoing a dissolution test at the identical test conditions of 80 °C with 1% aq. NaCl as the test fluid. For ease of

comparison, the surface area values have been expressed as a percentage of the initial pre-test surface area of the respective cylindrical sample.

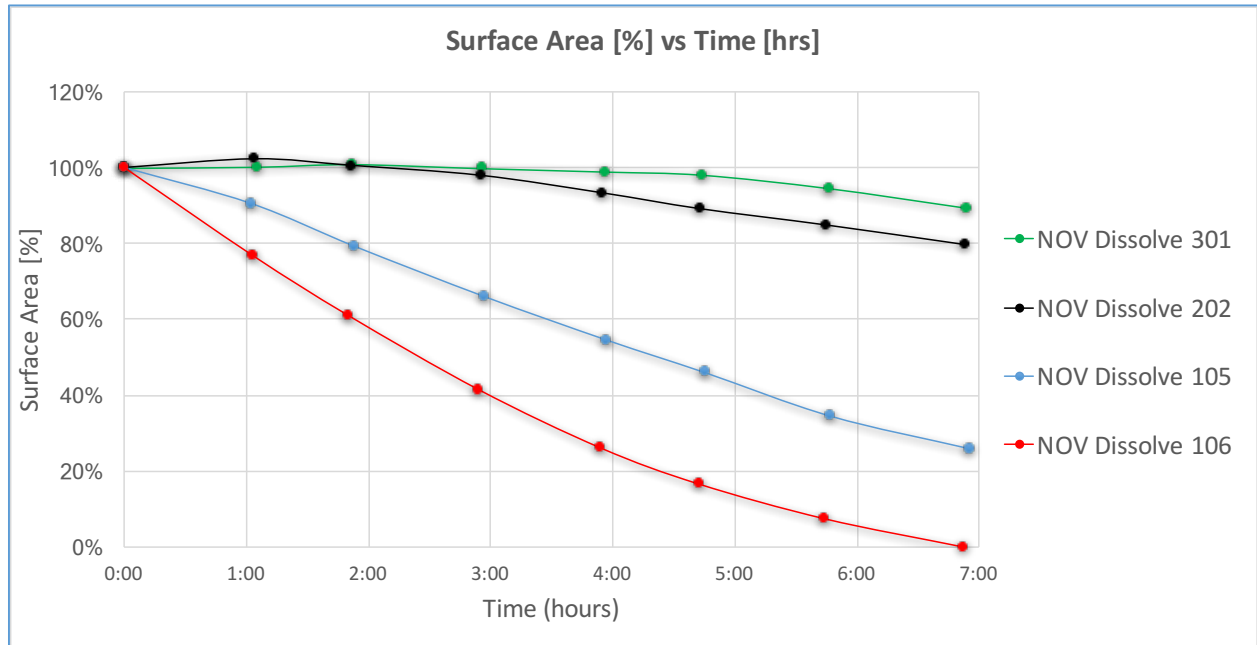


Figure 4-12: Surface area as a function of time for the four dissolvable samples at 80 °C and 1% NaCl solution

The reduction in surface area is the highest for NOV Dissolve 106 since the surface area goes down to 0 due to complete dissolution of the sample. The next highest reduction in surface area is seen in NOV Dissolve 105 (26%) followed by materials 202 (80%) and 301 (89%). In material 202, it can be seen that there was an initial increase in the surface area to 102% before it began reducing. For this material, during the test an initial swelling was observed possibly due to the fact that the outer surface initially absorbed small quantities of test fluid before the dissolution reaction commenced. Similar behavior was observed in other tests conducted (discussed in subsequent sections) on this specific material. This behavior was not found in any of the other 3 materials.

The ranking of the materials when looking at the reduction in surface area corresponds qualitatively with the reduction in mass chart (Figure 4-11) at the given test conditions. Both in terms of loss in surface area and reduction in mass, material 106 is the fastest dissolving followed by materials 105, 202 and 301. From the discussions and results in this sub-section, it has been established that the changes in mass and surface area are two of the main measured parameters

from the dissolution tests. These parameters are instrumental in quantifying the extent and speed at which these materials dissolve under given conditions.

4.1.3 Defining the rate of dissolution reaction

The parameters analysed in the previous section, i.e., mass and surface area give us an indication of how quickly/slowly a particular material dissolves under given conditions of NaCl concentration and test temperature. In this sub-section, it is attempted to define a term that shall be a more robust way of quantifying the rate of the dissolution reaction. Defining such a term is of paramount importance to make it easier to model the effects of varying temperatures and NaCl concentrations in the subsequent sections.

As a first step towards this goal, from the mass versus time plot of the 105 material (Figure 4-6), the mass rate was plotted as a function of time. The experimental data from the 105 material dissolution test at 80 °C and 1% NaCl was used in these plots. Mass rate is defined as follows:

$$\text{Mass rate (mg/hr)} = \frac{\Delta m \text{ (mg)}}{\Delta t \text{ (hrs)}} \quad (4.2)$$

where Δm is the different in mass (in mg) between consecutive mass readings recorded in the test data sheet during the dissolution test and Δt is the corresponding time interval in hours.

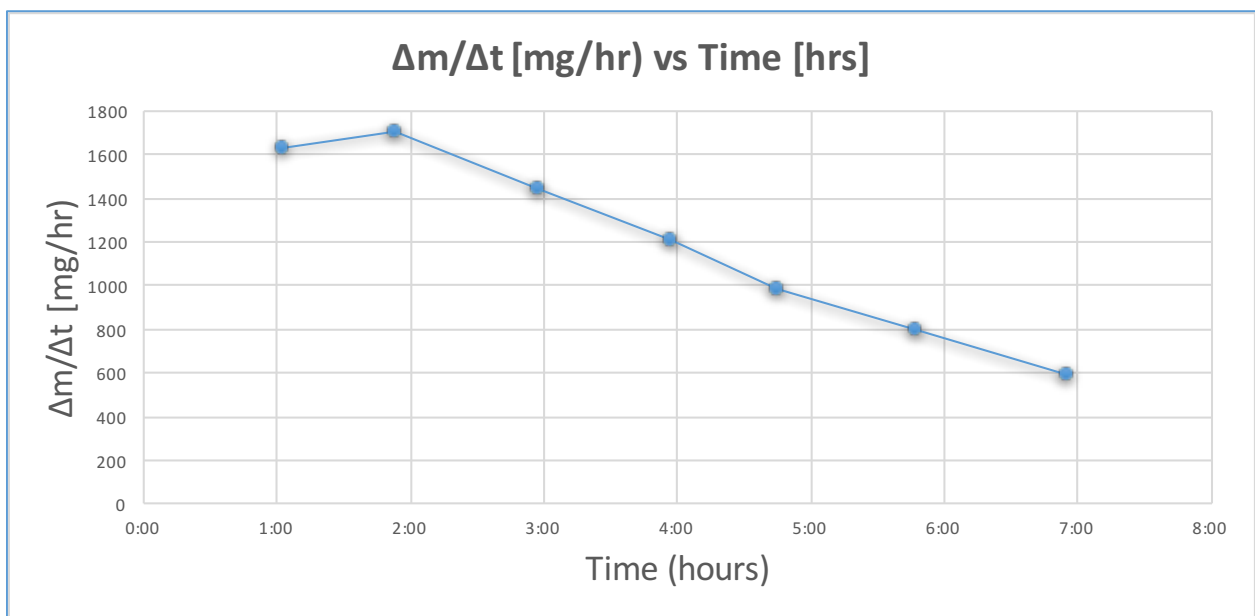


Figure 4-13: NOV Dissolve 105 mass rate as a function of time at 80 °C in 1% aq. NaCl

When the mass rate is plotted as a function of time in Figure 4-13, it can be seen have a slight increase upto ≈ 2 hours after which the mass rate steadily decreases until the end of the dissolution experiment at 7 hours. The decrease in mass rate between 2 – 7 hours is largely linear in nature. However, it is not optimal to directly define the mass rate as the rate of the dissolution reaction due to the fact that the mass rate is continuously changing with time. Furthermore, the mass rate does not completely take into account the variation in surface area which is another key parameter that affects the dissolution rate. The ideal characteristic parameter that describes the rate of the dissolution reaction should be able to capture the effects of both the changing mass rates as well the changing surface area values with respect to time.

Having discussed the effect of surface area on the dissolution reaction in Section 4.1.2, the next logical step in this endeavour to formulate a rate of dissolution reaction term was to plot the total surface area (Eq. 4.1) as a function of time. This is shown below in Figure 4-14. The surface area decreases steadily with time and the variation is also largely linear in nature throughout the duration of the experiment.

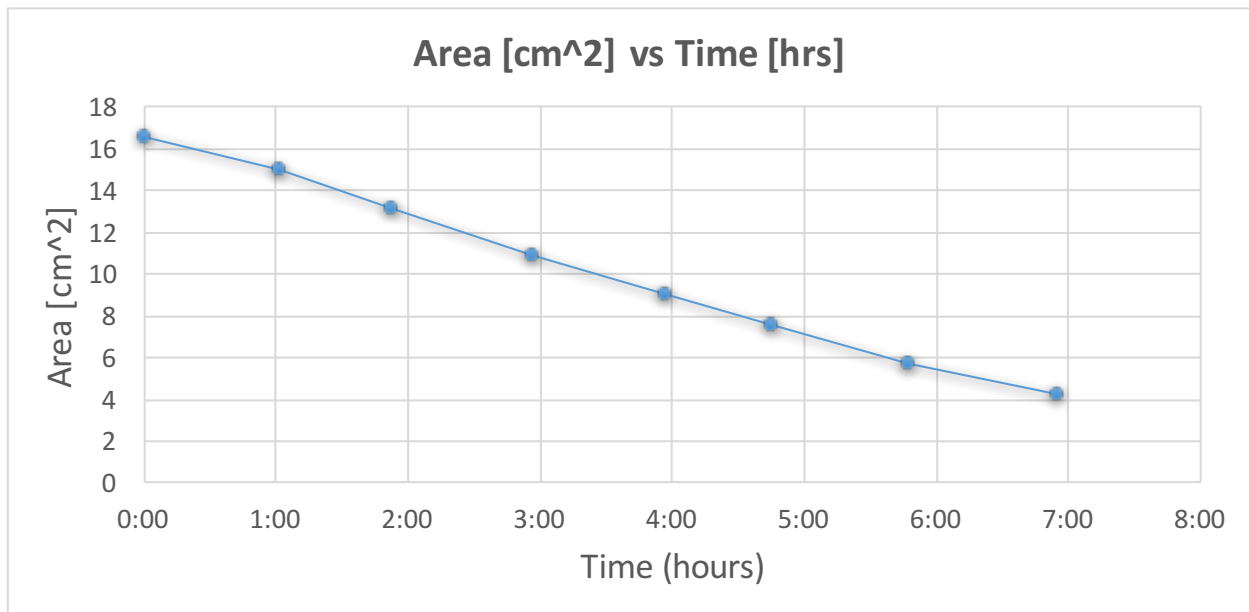


Figure 4-14: NOV Dissolve 105 surface area as a function of time at 80 °C in 1% aq. NaCl

Comparing the plots in Figure 4-13 and Figure 4-14, we have two critical parameters that are decreasing linearly with time for most of the experimental duration. The two plots were combined as shown below maintaining their values by using different axes as shown in Figure 4-15. The

values were plotted from the experimental data between approximately 2 hours to 7 hours. The initial behaviour up to 2 hours shall be addressed later on in this sub-section.

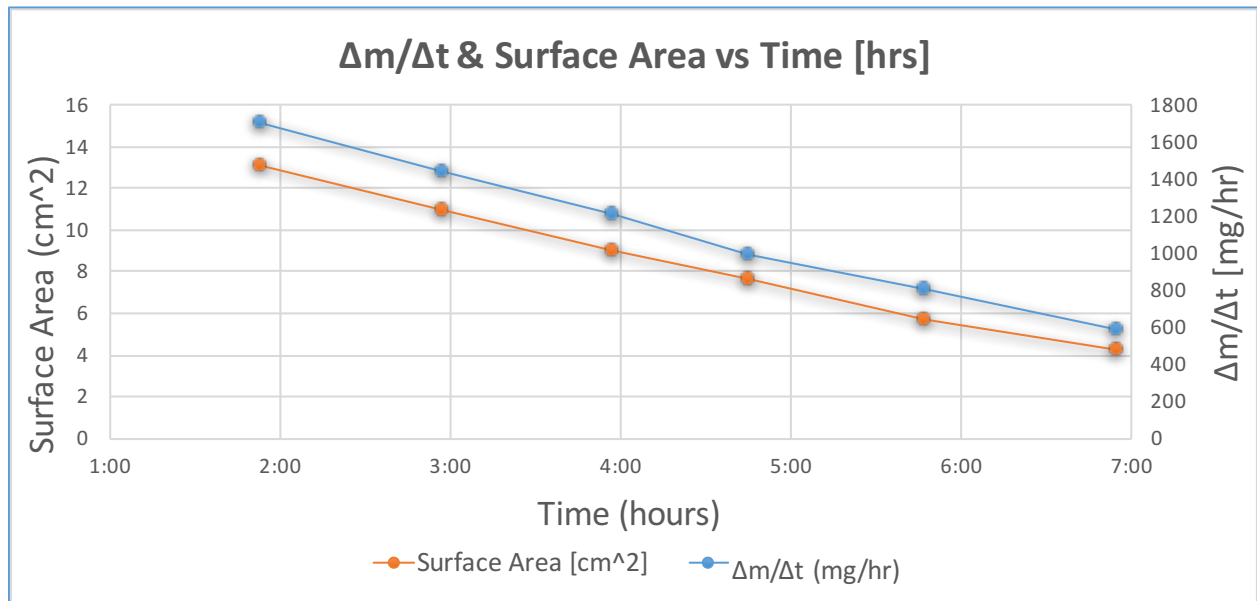


Figure 4-15: NOV Dissolve 105 mass rate and surface area as a function of time at 80 °C in 1% aq. NaCl

A new insight can be observed from this combined plot of surface area and mass rate. There is a clear correlation between the two parameters between 2 to 7 hours. Between each measurement interval, the two lines are parallel, i.e., the slope angles are virtually identical. In other words, the extent of reduction in surface area is directly proportional to the extent of reduction in mass rate.

Therefore, normalizing one of these parameters with respect to the other within the same interval should output a constant value. This is intuitively expected since if two terms are reducing linearly at a similar rate, dividing one by the other will result in a constant.

Based on this analysis, the value of mass rate normalised with respect to the corresponding surface area shall be a constant that will effectively describe the rate of the dissolution reaction. This term is defined as Rate of Dissolution (ROD). The ROD shall be calculated for each measurement interval using the following formula:

$$\text{Rate of Dissolution, ROD} \quad (\text{mg/cm}^2/\text{hr}) \text{ or } (\text{mg} \cdot \text{cm}^{-2} \cdot \text{hr}^{-1}) = \frac{\Delta m \text{ (in mg)}}{\Delta t \text{ (in hrs)} \cdot A \text{ (in cm}^2\text{)}} \quad (4.3)$$

The formula variables have been outlined below:

- t is the experimental running time in hours. The value of t starts at 0 h when the dissolution sample is first lowered in the test fluid.
- Δt is the corresponding time interval in hours.
- Δm is the difference in mass in mg between consecutive mass readings recorded in the test data sheet during the dissolution test, i.e., $|m_t - m_{t-\Delta t}|$. The absolute value is taken to ensure ROD is a positive value.
- A is the average surface area in cm^2 between the consecutive experimental measurements from the test data sheet, i.e., $(A_t + A_{t-\Delta t})/2$. The average surface area between consecutive readings has been used to reduce the impact of measurement errors on the calculated ROD value.

Based on the above definitions, the Rate of Dissolution at any given experimental running time, t can be accurately described as shown below:

$$ROD_t = \frac{|m_t - m_{t-\Delta t}|}{\Delta t \cdot \left(\frac{A_t + A_{t-\Delta t}}{2}\right)} \quad (4.4)$$

From the test data of the dissolution experiment on the NOV Dissolve 105 material at 80 °C in 1% NaCl, the following results table has been generated including the calculated ROD values.

Table 3: NOV Dissolve 105 dissolution test results at 80 °C in 1% aq. NaCl

Running Time t [hours]	Time Interval Δt [hours]	Sample Mass m_t [g]	Surface Area A_t [cm^2]	ROD [$\text{mg}/\text{cm}^2/\text{hr}$]
0:00	-	9.22	16.562	-
1:02	1:02	7.53	15.003	103.63
1:53	0:51	6.08	13.129	121.28
2:57	1:04	4.54	10.928	120.03
3:57	1:00	3.33	9.032	121.25
4:45	0:48	2.54	7.620	118.60

5:47	1:02	1.71	5.712	120.50
6:55	1:08	1.04	4.299	118.11

Note that the ROD value can only be defined from the second reading onwards since at least two readings are required to calculate ROD based on the formula.

The calculated ROD values were plotted as a function of time from Table 3 data.

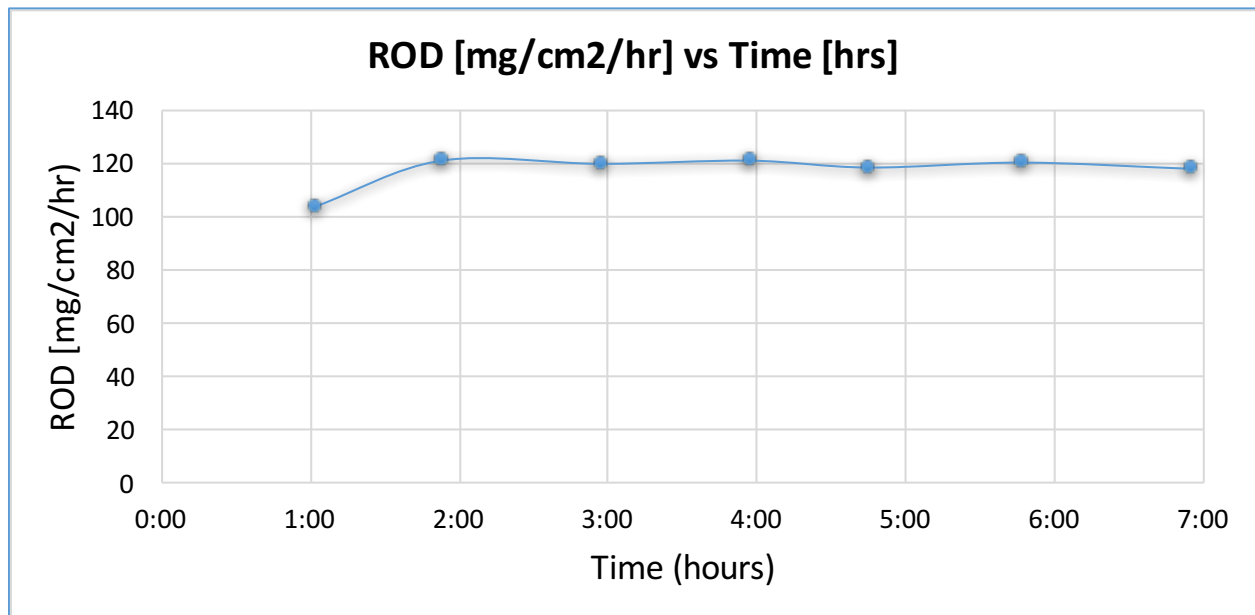


Figure 4-16: NOV Dissolve 105 ROD as a function of time at 80 °C in 1% aq. NaCl

As expected, the ROD is constant at a value of ≈ 120 mg/cm²/hr in the duration between 1.88 hours to end of experiment at 6.9 hours. This is due to the steady linear decrease in both mass rate and surface area with the same slope angle with respect to time as analysed earlier in this section.

The dissolution reaction's timeframe can be broken down into two distinct phases based on the ROD behaviour as illustrated in Figure 4-17:

- Transient Period:** The first portion is the time period between 0-1.88 hours when the ROD value is climbing up is a transient phase. This is when the dissolution reaction is being initiated and hence, occurring at a slower pace. The ROD value in this period is continuously increasing and is a function of time. This ROD value shall be defined as 'Transient Rate of Dissolution' denoted by ROD_{tr}.

- Steady State Period:** The second portion is the time period after 1.88 hours when the ROD value remains at a constant value. In this phase, the dissolution reaction has fully commenced and is occurring at a steady rate based on the test conditions. This ROD value shall be defined as the ‘Steady State Rate of Dissolution’ abbreviated as ROD_{ss} . For the sake of consistency, henceforth in this work, the ROD value is considered as being in steady state when the variation in ROD value is within $\pm 5\%$ of the final ROD value. Additionally, the time when the steady state period commences is termed as ‘Time to Reach Steady State’ and is denoted by t_{ss} . The steady state ROD (ROD_{ss}) is determined by averaging the ROD values from t_{ss} to end of the dissolution test.

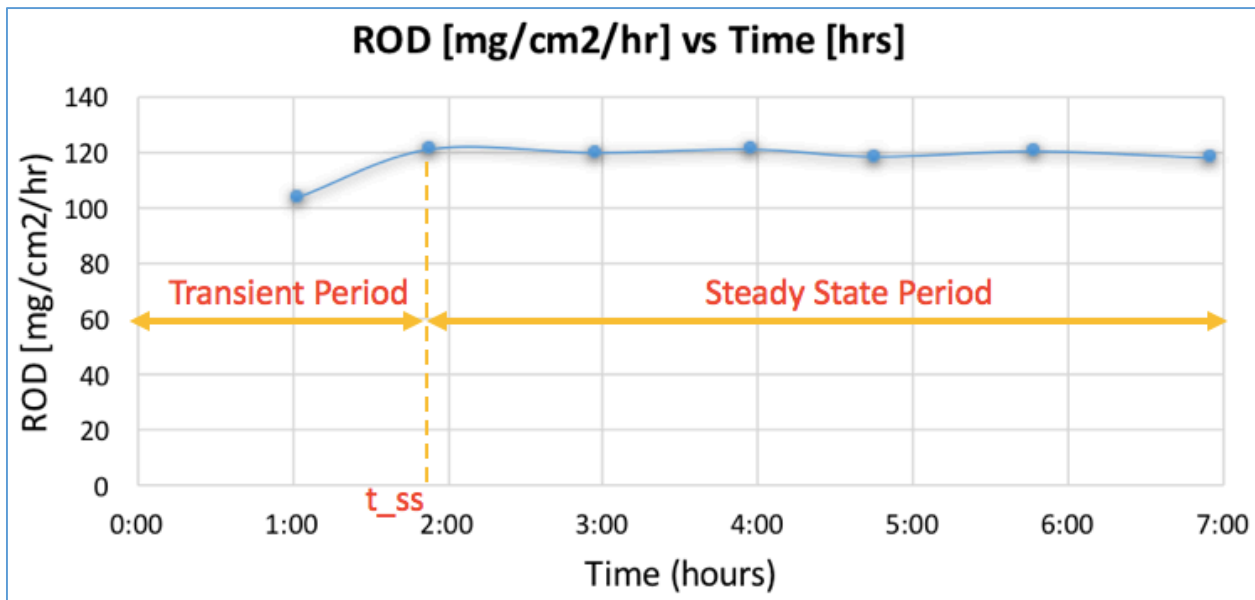


Figure 4-17: Transient Period versus Steady State Period: NOV Dissolve 105 at 80 °C in 1% aq. NaCl

In case of dissolution test of 105 material at 80 °C in a test fluid with 1% NaCl:

- Start of steady state is at $t_{ss} = 1\text{h } 53\text{m}$ or 1.88 hours
- Steady state $ROD_{ss} = 119.96\text{ mg/cm}^2/\text{hr}$

Therefore, the steady state ROD_{ss} shall be used as the main characteristic parameter to define the speed at which dissolvable materials react with test fluids.

In Section 2.3.2, the definition of a term Rate of Corrosion (ROC) by Carrejo et al. was introduced [4]. The definition of ROC by Carrejo et al. in Eq. 2.1 is insufficient in completely capturing the

dissolution behaviour of these materials. The problem with this ROC definition is that this is an average dissolution rate which only considers the sample mass at the start and end of the test. Thus, it is an average value of mass rate normalised with respect to surface area. In other words, the ROC is the dissolution rate averaged across the entire test duration. While this average value gives an approximate indication of how quickly a material loses mass during dissolution, it does not capture the nuances of the transient period and steady-state period.

On the other hand, the definition of ROD presented here in Eq. 4.4 is an instantaneous ROD value which captures the dissolution rate at every interval of the dissolution test. This enables one to clearly differentiate between the ROD values during the transient phase and the steady-state phase. This distinction is important to get the most representative value of ROD in order to aid the selection of the right material for a particular application.

The justification and advantages behind using ROD_{ss} to characterize the dissolution process are:

- i. The steady state ROD term's formula captures the variation in mass rate as the reaction progresses.
- ii. Since ROD_{ss} term, by definition, has the dissolvable material's current surface area value (A_t) embedded within, it also accounts for the effects on rate of dissolution reaction due to the variations in surface area as discussed in Section 4.1.2.
- iii. As a corollary to the above point, the steady state ROD_{ss} is also independent of the shape and size of the dissolvable material since the surface area of exposure is part of the ROD formula. Though the dissolution tests in this work were performed on cylindrical samples, the ROD_{ss} values would not have been different had the samples been ball-shaped. For this exact same reason, the initial sample dimensions will also not affect the ROD_{ss} value. This is an important advantage because the idea behind the dissolution tests is to characterize the dissolution rate in such a way so as to be able to use the results from the sample dissolution tests to predict the behaviour of actual full-scale dissolvable balls.
- iv. From the above arguments, it can be concluded that ROD_{ss} is constant for a given dissolvable material at a specific temperature and test fluid type (NaCl concentration), irrespective of the size or shape of the tested material.

According to the International Union of Pure and Applied Chemistry (IUPAC), an intensive property is defined as a bulk property whose magnitude is independent of the size or the amount of the material present. Some examples of this are hardness and density. In contrast, an extrinsic property is dependent on the amount of material present and is additive for sub-systems. Some examples of this are mass and volume [47]. Therefore, ROD_{ss} is an intensive property of the dissolvable material since it is independent of the size or quantity of the samples.

- v. Having a single critical parameter to characterise the dissolution behaviour makes it convenient to quantify and compare the various factors that influence this reaction. In subsequent Sections 4.2, 4.3 and 4.4 where the effects of temperature and concentration on the dissolution reaction of the various materials have been investigated, the variations on the ROD_{ss} value is the main characteristic parameter analysed.

4.1.4 ROD Comparison at 80 °C in 1% NaCl

As part of Stage I experiments, the dissolution test was repeated on all four dissolvable materials at 80 °C in aqueous solution with 1% NaCl concentration. The ROD of all four materials at these test conditions were calculated as described in Section 4.1.3.

In Figure 4-18, the ROD has been plotted as a function of time for NOV Dissolve 106, 105, 202 and 303 materials. It can be observed that the ROD curve follows the same trend for all materials as described in the previous section. The ROD value increases initially in the transient period. Once the transient time period has ended and the steady state has been reached, i.e., at t_{ss} , the ROD value stays constant for the remainder of the experiment.

The exception is material 106 which does not appear to have a transient phase. However, this can be easily explained by the fact that since this is a highly reactive material (as demonstrated by the high ROD value), the transient phase is too short at these test conditions. Therefore, the transient phase had ended before the first experimental measurement was taken at ≈ 1 hour. The ROD trends seen below are further evidence that the analyses presented in Section 4.1.3 is applicable to all the dissolvable materials explored in this work.

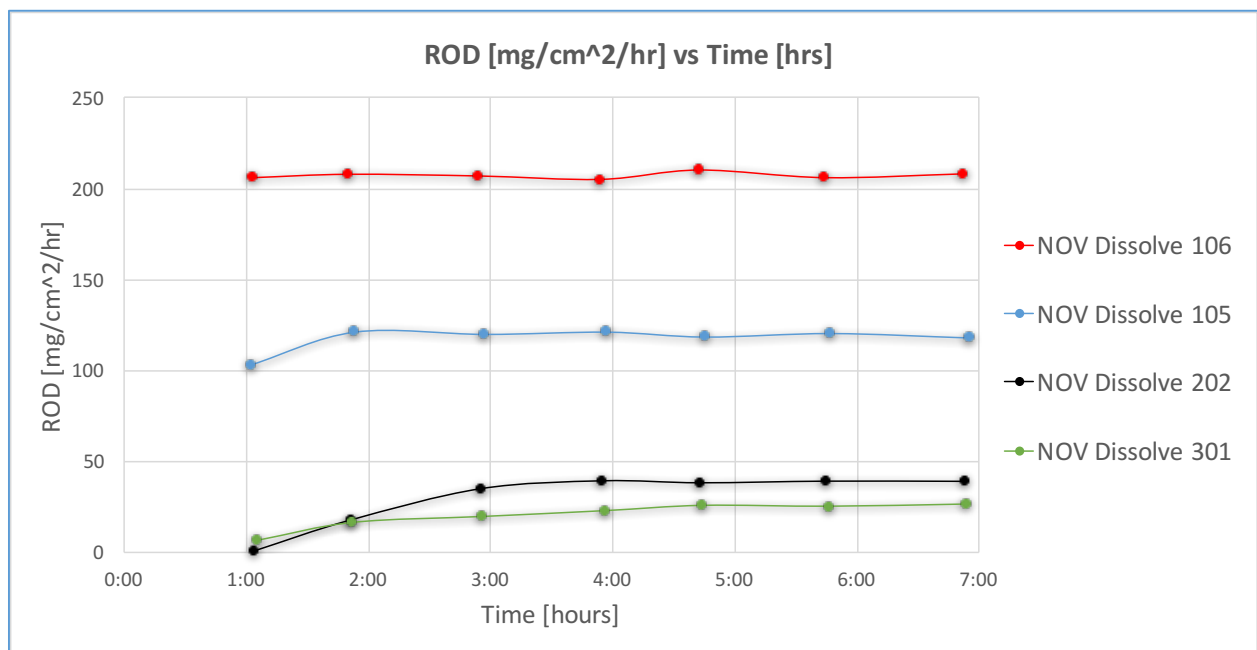


Figure 4-18: ROD as a function of time for the four dissolvable samples at 80 °C and 1% NaCl solution

The times to reach steady state (t_{ss}) and steady state ROD_{ss} have been tabulated based on the above data in Table 4.

Table 4: ROD_{ss} and t_{ss} values at 80 °C and 1% NaCl solution

Material	t_{ss} [hours]	ROD_{ss} [mg/cm²/hr]
NOV Dissolve 106	<1	207.25
NOV Dissolve 105	1.88	119.96
NOV Dissolve 202	3.92	38.96
NOV Dissolve 301	4.73	25.80

NOV Dissolve 106 is the material with the highest steady state ROD followed by materials 105, 202 and 301 in that specific order. The time to reach steady state (t_{ss}) has a reverse ranking with material 301 taking the longest time to reach steady state dissolution followed by materials 202, 105 and 106. This is unsurprising since the material with the highest ROD_{ss} has the fastest dissolution reaction and hence, is expected to reach steady state quickest.

In the subsequent sections, the steady state ROD value shall be the main parameter based on which the responses of the different materials to variations in temperature and NaCl concentration shall be examined. During these experiments, it shall be ensured that the ROD values have reached the steady state period during the dissolution test before making use of them for comparison.

The objectives achieved and conclusions drawn at the end of Stage I experiments have been listed below:

- Initial observations were made regarding the nature of the dissolution process based on NOV Dissolve 105 material at 80 °C in 1% NaCl. The underlying chemical reaction was introduced.

- The variations in key measured data was plotted as functions of time based on which it was found that the mass rate and surface area were key measured parameters governing the dissolution reaction.
- Rate of Dissolution (ROD) was defined and found to be the most convenient way of expressing the performance of dissolvable materials while accounting for the influences of geometry, mass loss and surface area.
- Steady state ROD (ROD_{ss}) shall be used as the main characteristic parameter to define the speed at which dissolvable materials react with fluids. ROD_{ss} is an intensive property which is constant for a given material under specific test conditions of temperature and NaCl concentration.
- The performance of the four dissolvable materials at this identical test condition was compared based on ROD_{ss} and t_{ss} values. NOV Dissolve 106 was found to be most reactive followed by materials 105, 202 and 301 in that specific order.

4.2 Stage II - Investigating the Effect of Concentration on Dissolution Rate

Chloride-based fluids are commonly used in downhole oilfield applications with NaCl being a prevalent component. The main objective of Stage II of the test program is to determine how variations in the concentration of aqueous NaCl solutions affect the performance of dissolvable materials.

In order to isolate the effect of concentration, sample dissolution tests were conducted on each of the four different materials at a constant temperature of 80 °C while the NaCl concentration in the test fluid concentration was varied – 1%, 3% 6% and 9%. The Stage II test program schematic from Section 3.3.2 has been repeated below for recap.

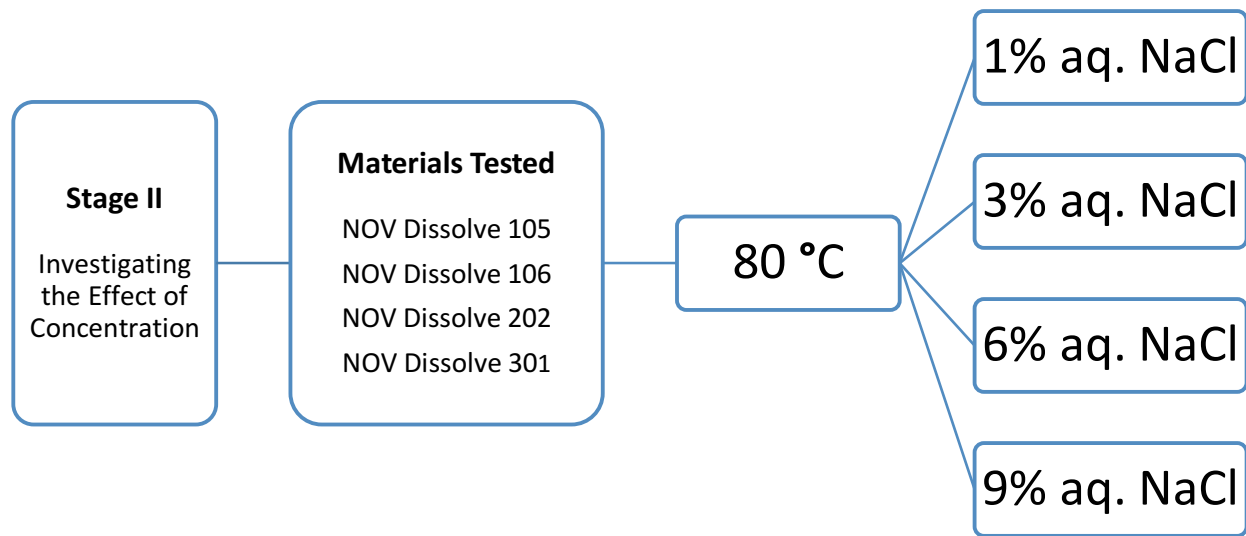


Figure 4-19: Schematic of Stage II Test Outline

The steady state Rate of Dissolution values (ROD_{ss}) defined in the Section 4.1.3 is the primary characteristic that has been compared in this stage. During these experiments, it was ensured that the ROD values had reached steady state period during the dissolution test before utilising the values for assessment.

4.2.1 Results: Stage II Experiments

First, considering just the results from the Stage II experiments performed on NOV Dissolve 105 samples, the Rate of Dissolution value in the steady state phase (ROD_{ss}) has been charted at test fluid concentrations of 1%, 3%, 6% and 9% aqueous NaCl solutions.

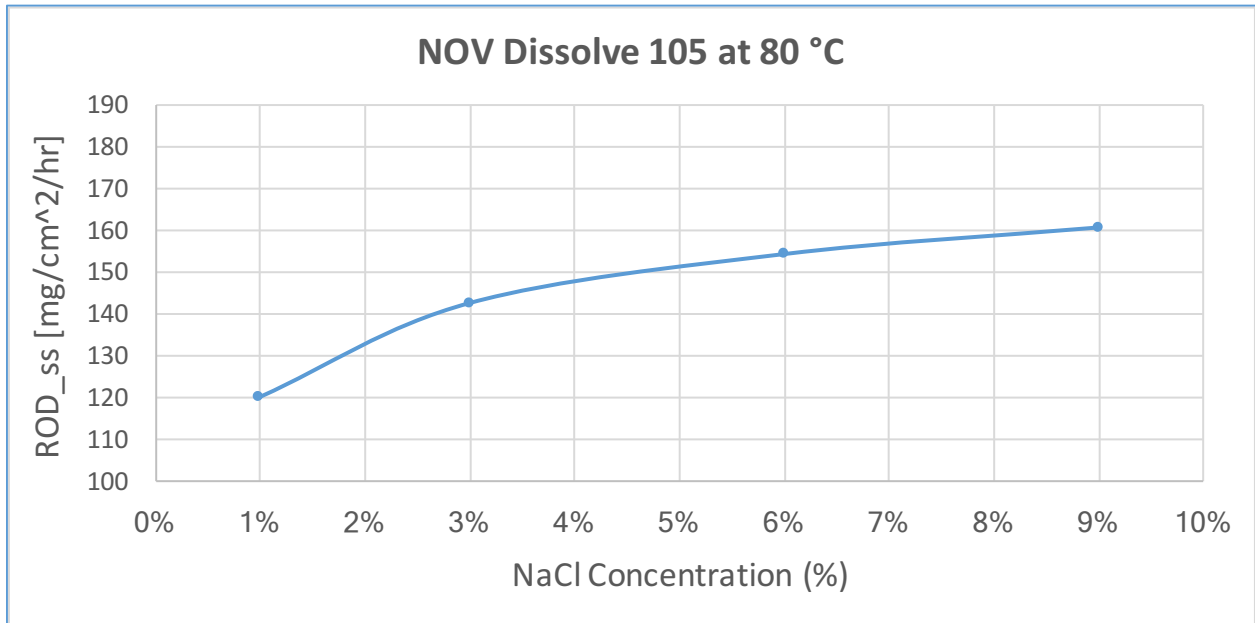


Figure 4-20: Steady State ROD (ROD_{ss}) plotted as a function of NaCl concentration at 80 °C for Material 105

Referring to Figure 4-20, ROD_{ss} steadily increases as the amount of NaCl increases in the test fluid. The value of ROD_{ss} is 119.96 mg/cm²/hr in 1% NaCl solution and increases to 160.35 mg/cm²/hr when the test fluid is changed to 9% NaCl. This translates to a 34% increase in steady state ROD at 9% relative to the value at 1% NaCl.

For ease of comparison, the ROD_{ss} values have been normalized with respect to the ROD_{ss} value in 1% NaCl and plotted in Figure 4-21. It can be seen that the slope of the curve decreases as the concentration increases and becomes progressively flatter. Increase in the concentration from 1% NaCl to 3% NaCl results in a 19% increase in ROD_{ss} . However, when the concentration is increased from 3% NaCl to 6% NaCl, only a 10% increase in ROD_{ss} is seen. This trend continues when we consider that increasing the concentration from 6% NaCl to 9% NaCl only results in a

6% increase in the ROD_{ss} value. In other words, as the concentration of the NaCl is increased, the impact of this increase on the rate of dissolution gets progressively less profound.

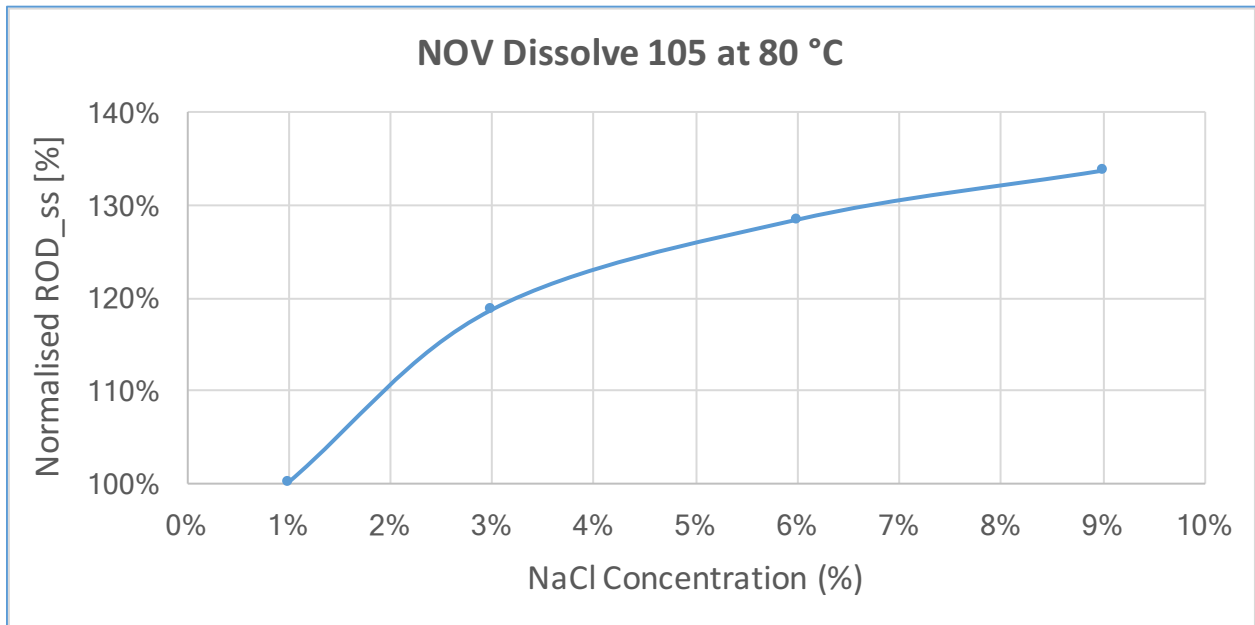


Figure 4-21: Steady State ROD (Normalized w.r.t to the ROD_{ss} in 1% NaCl) plotted as a function of NaCl concentration at 80 °C for Material 105

In case of material 106, the ROD_{ss} increases from 207.25 mg/cm²/hr in 1% NaCl to 365.12 mg/cm²/hr in 9% NaCl. This is illustrated in Figure 4-22 and Figure 4-23. Thus, ROD_{ss} shows a steady increase in value with increase in NaCl concentration.

Thus, the steady state ROD increases by 76% relative to the value at 1% NaCl. Of this 76% increase, the major share (43%) can be attributed to the increase in concentration from 1% NaCl to 3% NaCl. Only 24% increase in ROD_{ss} is seen when the concentration is increased from 3% NaCl to 6% NaCl. This increase is further lowered to 9% when the concentration is changed from 6% NaCl to 9% NaCl.

Thus, in case of NOV Dissolve 106 material as well, it can be seen that as the concentration increases, the effect on ROD_{ss} due to increasing the concentration of NaCl gradually decreases.

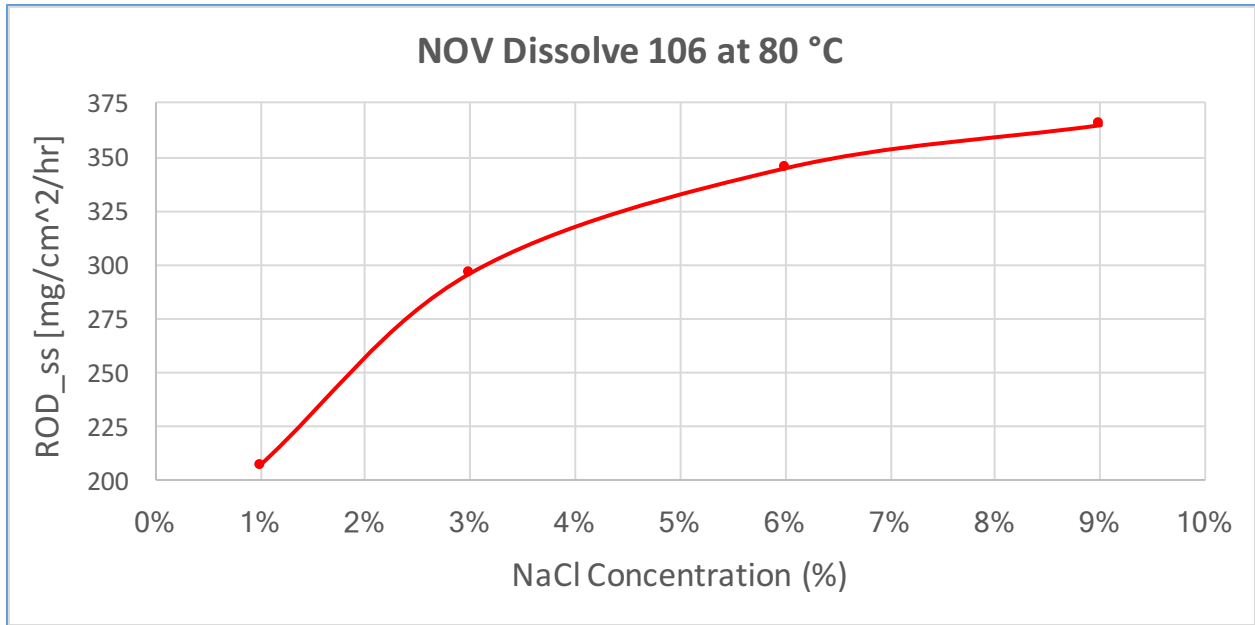


Figure 4-22: Steady State ROD (ROD_{ss}) plotted as a function of NaCl concentration at 80 °C for Material 106

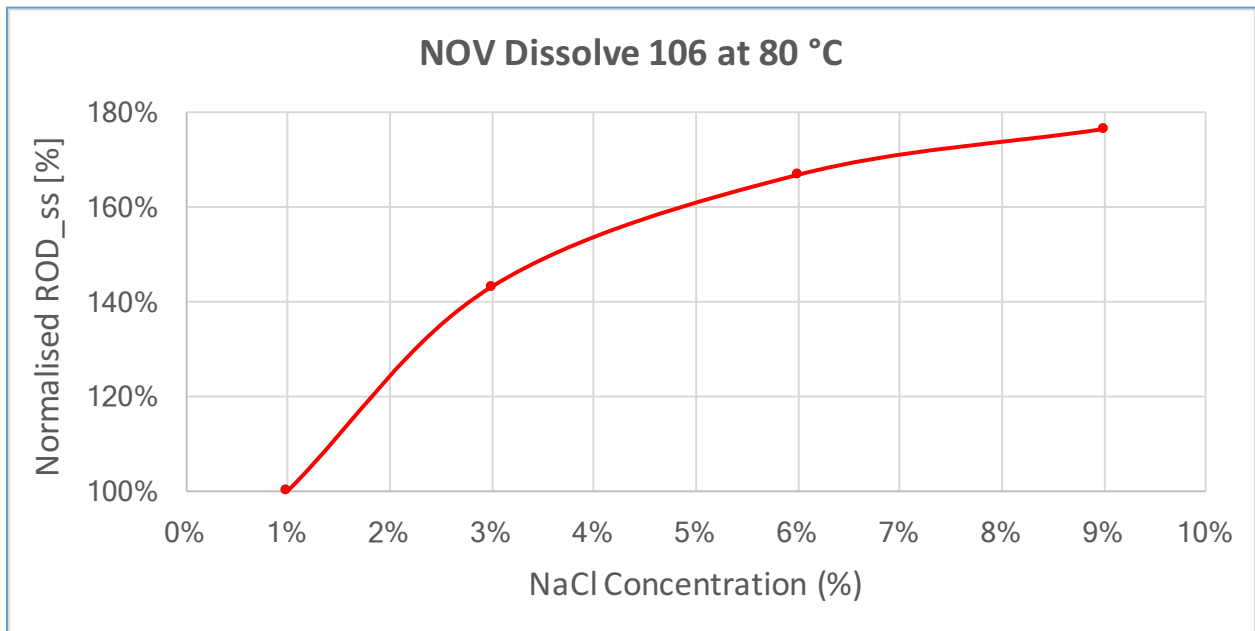


Figure 4-23: Steady State ROD (Normalized w.r.t to the ROD_{ss} in 1% NaCl) plotted as a function of NaCl concentration at 80 °C for Material 106

For material 202 (Figure 4-24 and Figure 4-25), the ROD_{ss} value increases by 61% when the concentration is increased from 1% to 9% NaCl. Additionally, as seen in the previous two materials, the slope of the curve gets progressively flatter as the concentration increases.

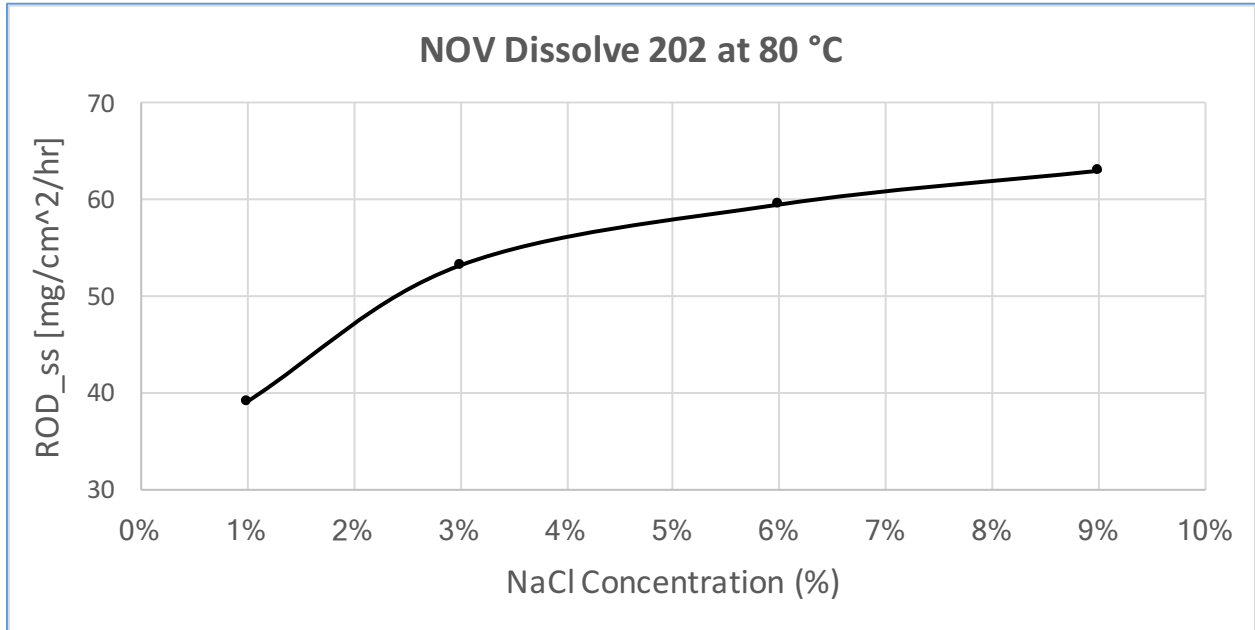


Figure 4-24: ROD_{ss} plotted as a function of NaCl concentration at 80 °C for Material 202

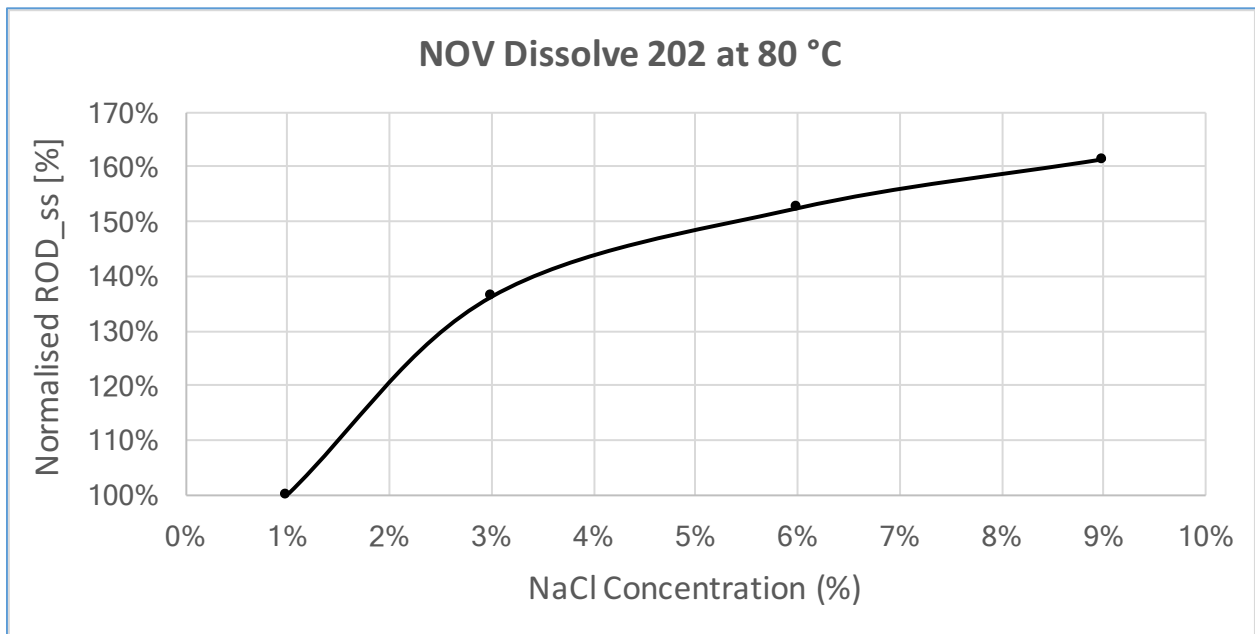


Figure 4-25: Steady State ROD (Normalized w.r.t to the ROD_{ss} in 1% NaCl) plotted as a function of NaCl concentration at 80 °C for Material 202

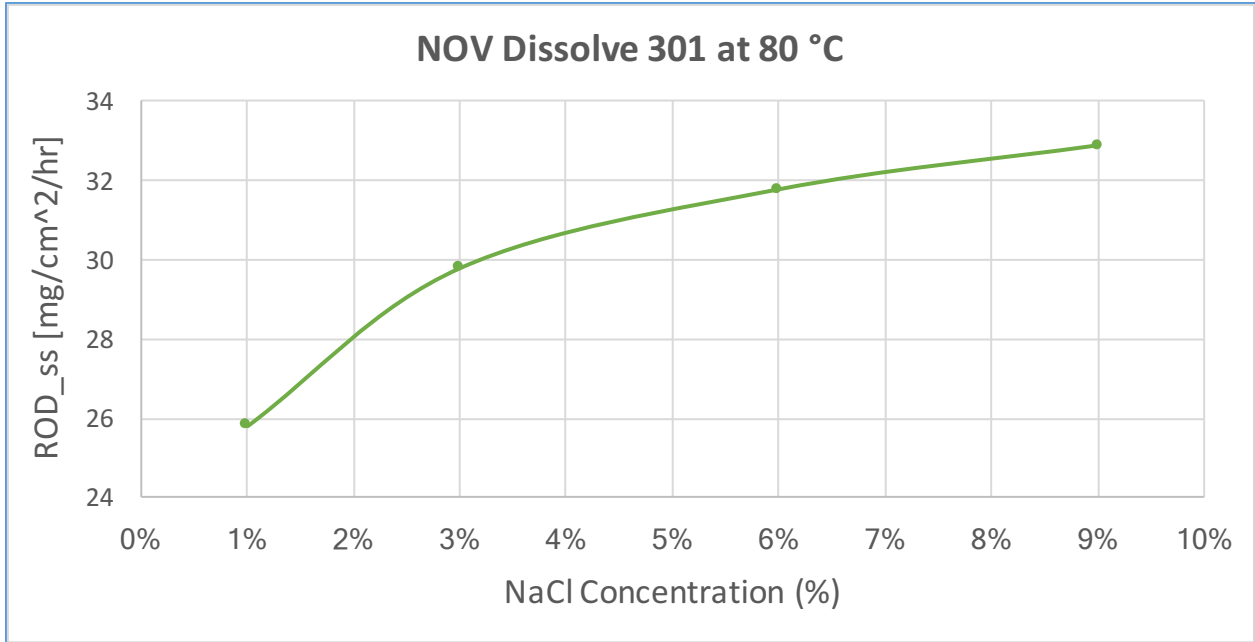


Figure 4-26: ROD_{ss} plotted as a function of NaCl concentration at 80 °C for Material 301

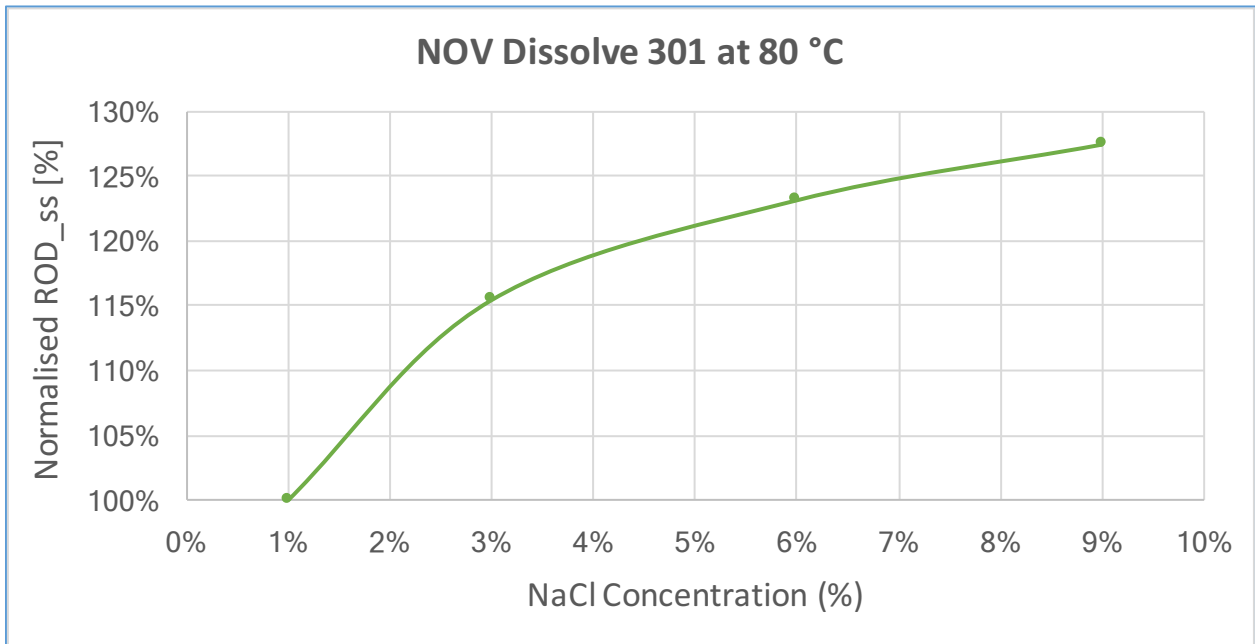


Figure 4-27: Steady State ROD (Normalized w.r.t to the ROD_{ss} in 1% NaCl) plotted as a function of NaCl concentration at 80 °C for Material 301

Referring to Figure 4-26 and Figure 4-27, the value of ROD_{ss} is 25.80 mg/cm²/hr in 1% NaCl solution and increases to 32.89 mg/cm²/hr when the test fluid is changed to 9% NaCl. This equates to a 27% increase in the steady state ROD at 9% NaCl relative to the value at 1% NaCl.

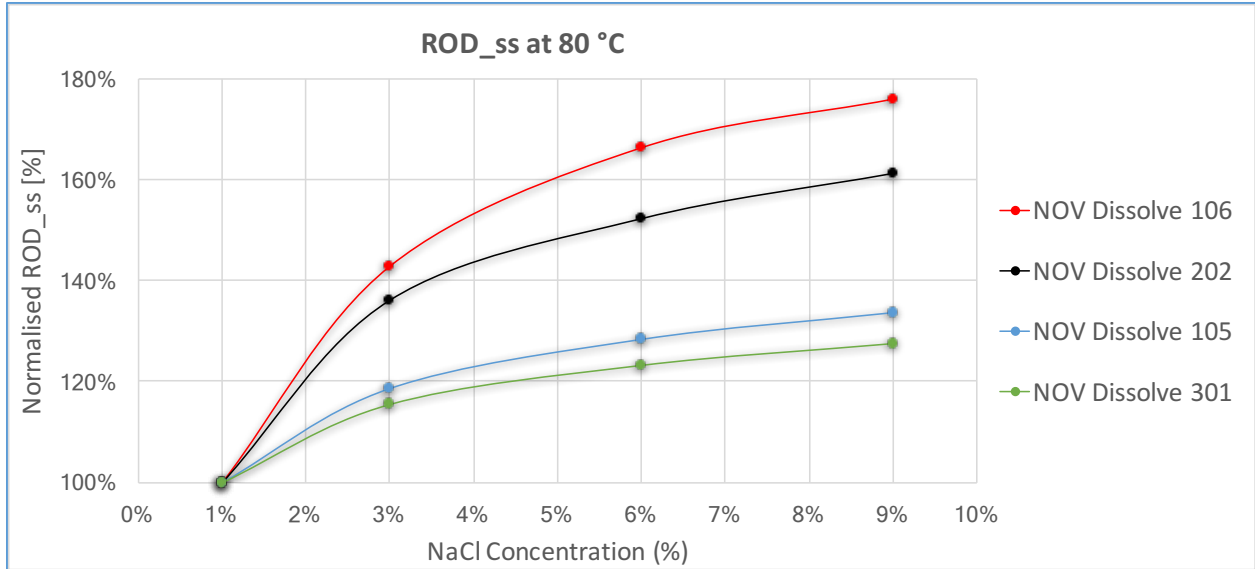


Figure 4-28: Steady State ROD (Normalized w.r.t to the corresponding ROD_{ss} in 1% NaCl) plotted as a function of NaCl concentration at 80 °C for all materials

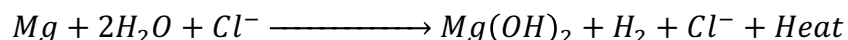
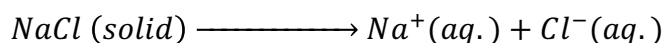
Figure 4-28 plots the steady state ROD values for all materials normalized with respect to their respective values at 1% NaCl concentration. This plot can be used to give an indication of how sensitive each of the material is to changes in NaCl concentration. Material 106 is the most sensitive to changes in concentration and it is followed by materials 202, 105 and 301 in descending order. Another observation from this plot is the distinct similarity in the general nature of the curves for all the four materials. This aspect shall be explored further as part of Stage IV in Section 4.4.

Thus, for all the dissolvable materials examined in this study, two distinct effects of varying NaCl concentration in the test fluid were observed:

- i. Increasing the concentration of NaCl increases the rate of dissolution process as reflected by the increase in ROD_{ss} values.
- ii. The dependence of ROD_{ss} on NaCl concentration gradually decreases as the NaCl concentration gets higher. The slope of the curve gets progressively flatter and at some high concentration value (beyond the 9% NaCl investigated here), the ROD_{ss} value is expected to become constant. Beyond this point, it is hypothesized that any further increase in NaCl concentration would have negligible effect on the speed of the dissolution process.

4.2.2 Discussion: Stage II Experiments

In order to explain this behavior, one needs to go back to the underlying chemical reactions driving the dissolution of these materials. The dissociation of sodium chloride in the test fluid and the subsequent dissolution reaction have been represented in Section 4.1.1 as shown below:



The chloride ions (Cl^-) are formed via the dissociation process when the NaCl salt is dissolved in water. Thereafter, these chloride ions act as catalysts during the dissolution reaction. However, in order to examine the mechanism through which the chloride ions catalyze the dissolution reaction, the work of Liu et al. shall be referred to in this section [48].

In his work, Liu et al. developed a method to synthesize magnesium hydroxide [$Mg(OH)_2$] nanostructures. Magnesium hydroxide has several applications in the pharmaceutical and polymer industries. It was discovered that a simple and efficient way of synthesizing magnesium hydroxide was immersing a foil of magnesium in a solution of water containing dissolved NaCl. The reaction occurring would be identical to the dissolution reaction that is being investigated in this thesis. It was found that increasing the concentration of NaCl increased the rate of reaction. This is in line with what has been observed in Section 4.2.1.

Additionally, by using High Resolution Transmission Electron Microscopy (HRTEM), Scanning Electron Microscope (SEM) and X-Ray Diffraction (XRD) imaging techniques, Liu et al. uncovered the underlying catalytic role of chloride ions in the reaction between magnesium and water. This shall be used to de-construct the dissolution reaction of the dissolvable materials investigated in this thesis.

Referring to Figure 4-29, when magnesium is immersed in aqueous NaCl solution, $Mg(OH)_2$ is formed almost immediately. A layer of $Mg(OH)_2$ is formed over the surface of magnesium as seen in Figure 4-29 (b). However, this layer is insoluble in water. As it gets thicker, the insoluble $Mg(OH)_2$ layer prevents water from reaching the magnesium and as a result, stops the dissolution reaction between magnesium and water from continuing any further. This is where the chloride

ions come in. Chloride ions can generate channels through the $\text{Mg}(\text{OH})_2$ layer by replacing OH^- to form $\text{Mg}(\text{OH})\text{Cl}$ which is soluble in water as represented in Figure 4-29 (c). Thus, through these channels or pathways generated by the chloride ions, water can reach the surface of the magnesium and the dissolution reaction continues as seen in Figure 4-29 (d) [48].

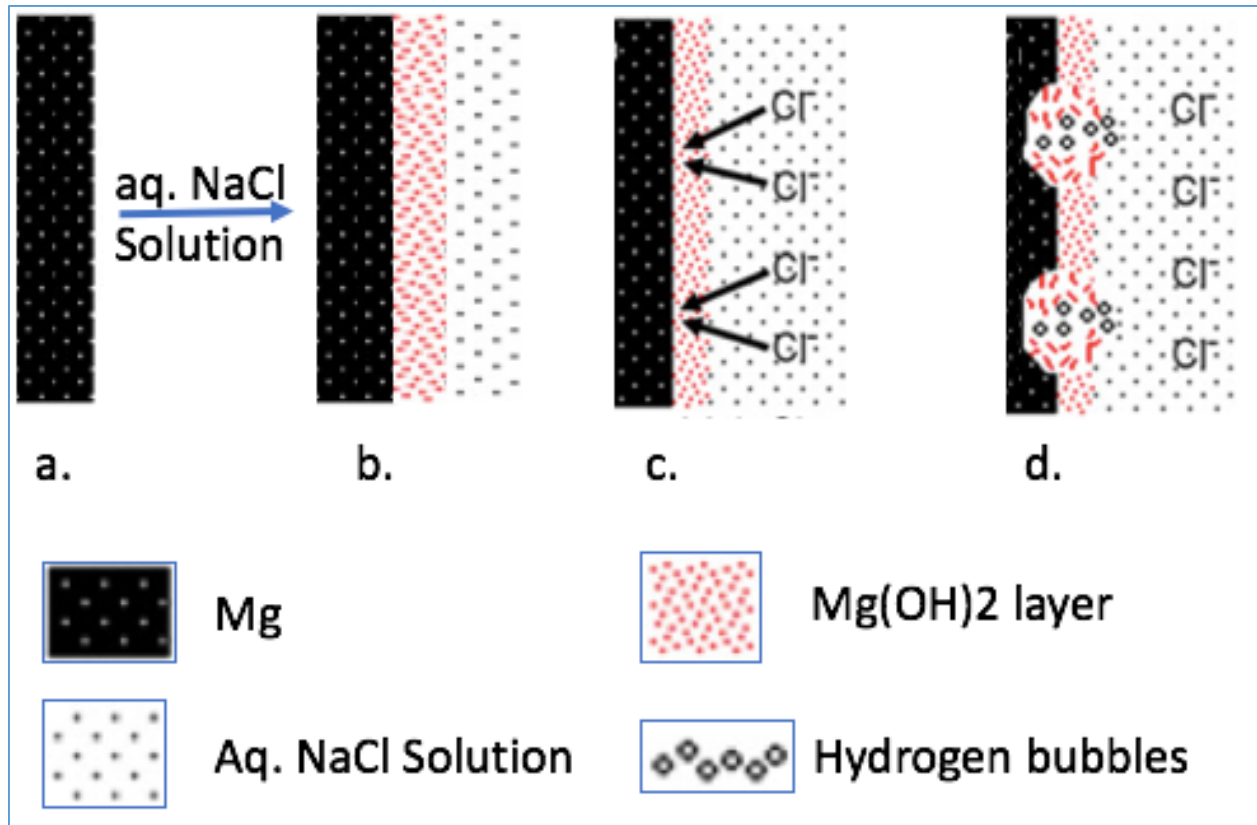


Figure 4-29: Catalytic mechanism of chloride ions during the dissolution reaction [48]

The above catalytic mechanism can be utilized to explain the results of the Stage II experiments. Increasing the concentration of the NaCl results in increase in concentration of the dissociated chloride ions in the solution. These chloride ions continually work to remove the insoluble $\text{Mg}(\text{OH})_2$ layer, thereby catalysing the dissolution reaction and increasing the overall reaction rate (ROD_{ss}). This explains why increasing the concentration of NaCl increases the rate of dissolution process as reflected by the increase in the ROD_{ss} values.

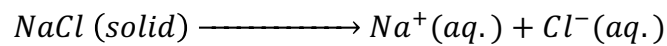
At the start, when the chloride ion concentration is low/medium they are busy and constantly working to remove the $\text{Mg}(\text{OH})_2$ layer to facilitate the dissolution reaction. However, as the chloride ion concentration increases, they are more efficient in removing the $\text{Mg}(\text{OH})_2$ layer. In

fluid with substantial NaCl content, the chloride ion concentration is high relative to the Mg(OH)₂ layers produced from the dissolution reaction. In such cases, the rate at which the chloride ions remove the Mg(OH)₂ layers is higher than the rate at which the layers are being formed. Thus, at this point there are more than enough chloride ion catalysts and not as much work that needs to be done by them, i.e., not as much Mg(OH)₂ layers to remove.

This explains why the effect of increasing the NaCl concentration gets progressively less pronounced as the concentration increases. The slope of the ROD_{ss} versus concentration curves gets gradually flatter at high concentration values due to this effect. At high chloride concentrations, there are sufficient chloride ions catalyzing the dissolution reaction and adding more chloride to the system has little to no effect on the reaction rate.

Based on the above discussed mechanism of the dissolution reaction, it can be concluded that the concentration of the chloride ions in the test fluid has a critical influence on the rate of the dissolution reaction.

While the plots and experiments in this work discuss the concentration of NaCl in the test fluid, it is possible to obtain the equivalent concentration of chloride ions in the solution.



Referring to the above dissociation reaction, 1 mole of NaCl dissolved in water produces 1 mole of Na⁺ ions and 1 mole of Cl⁻ ions. This statement is based on well-established concepts of mole ratios and stoichiometry in chemistry [43]. Based on these concepts, a simple equation is formulated below to convert the concentration of NaCl to the concentration of chloride ions in the solution:

$$C_{Cl} = C_{NaCl} * \frac{M_{Cl}}{M_{NaCl}} \quad (4.5)$$

where

- C_{NaCl} is the concentration of sodium chloride in solution (%)
- C_{Cl} is the concentration of chloride ions in solution (%)
- M_{Cl} is the molar mass of chloride (g/mol). This value is a constant and is 35.453 g/mol [49].

- M_{NaCl} is the molar mass of sodium chloride (g/mol). This value is a constant and is 58.443 g/mol [49].

Example: When the concentration of NaCl dissolved in water is 9%, the concentration of chloride ions in the solution is calculated as shown below:

$$C_{Cl} = C_{NaCl} * \frac{M_{Cl}}{M_{NaCl}} = 9\% * \frac{35.453}{58.443} = 5.46\%$$

Thus, the ‘ROD_{ss} versus NaCl concentration charts’ presented in the Stage II results section, can easily be expressed as ROD_{ss} versus Cl⁻ concentration charts. However, for the sake of consistency and clarity, this work shall continue to refer to NaCl concentration in subsequent chapters when discussing variations in the test fluid concentration.

The objectives achieved and conclusions drawn at the end of Stage II experiments have been summarised below:

- Increasing the NaCl concentration increases the rate of dissolution process as reflected by the increase in the ROD_{ss} values
- The dependence of ROD_{ss} on NaCl concentration gradually decreases as the NaCl concentration gets higher.
- The above results were rationalized by examining the role of chloride ions in catalyzing the dissolution reaction by removing the inhibiting magnesium hydroxide [Mg(OH)₂] layers.
- Chloride ion concentration is the key factor in determining the dissolution behavior and a simple formula was presented to convert NaCl concentration to chloride ion concentration.
- The dissolvable materials listed in the decreasing order of sensitivity to changes in concentration are: Material 106, 202, 105 and 301.

4.3 Stage III - Examining the Effect of Temperature on Dissolution Rate

The temperature of the downhole environment is a key operational variable that needs to be addressed when discussing the application of dissolvable materials in oil and gas applications. The main objective of Stage III experiments is to examine the influence of temperature on the performance of dissolvable materials.

In order to isolate the effect of temperature, sample dissolution tests were performed on each of the four dissolvable materials at a constant concentration of 1% aq. NaCl at three different test temperatures of 50 °C, 70 °C and 80 °C. The Stage III test program schematic from Section 3.3.2 has been recapped below.

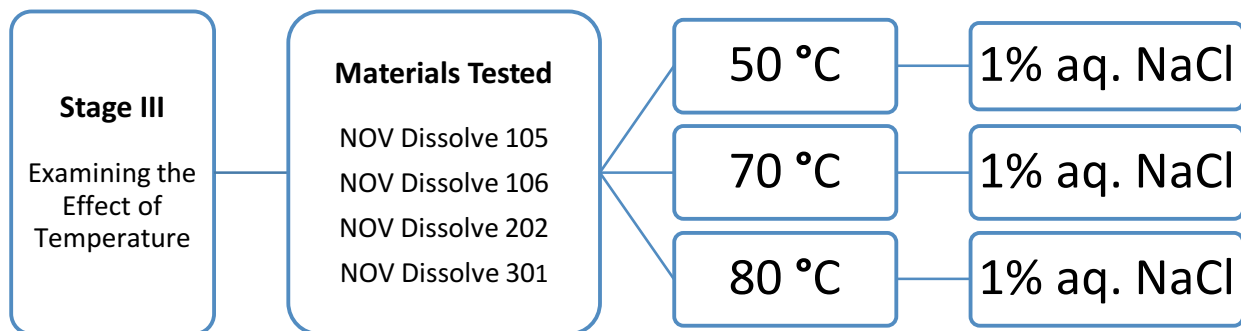


Figure 4-30: Schematic of Stage III Test Outline

As with the Stage II analysis, the steady state Rate of Dissolution (ROD_{ss}) has been used as the main basis in this stage to scrutinize the response of dissolvable materials to variations in temperature. During these experiments, it was ensured that the ROD values had reached the steady state period during the dissolution test prior to utilizing the values for assessment.

4.3.1 Results: Stage III Experiments

The results from the Stage III experiments on NOV Dissolve 105 material have been charted. Figure 4-31 shows the steady state ROD plotted as a function of test temperatures 50 °C, 70 °C and 80 °C while the NaCl concentration has been maintained constant at 1%.

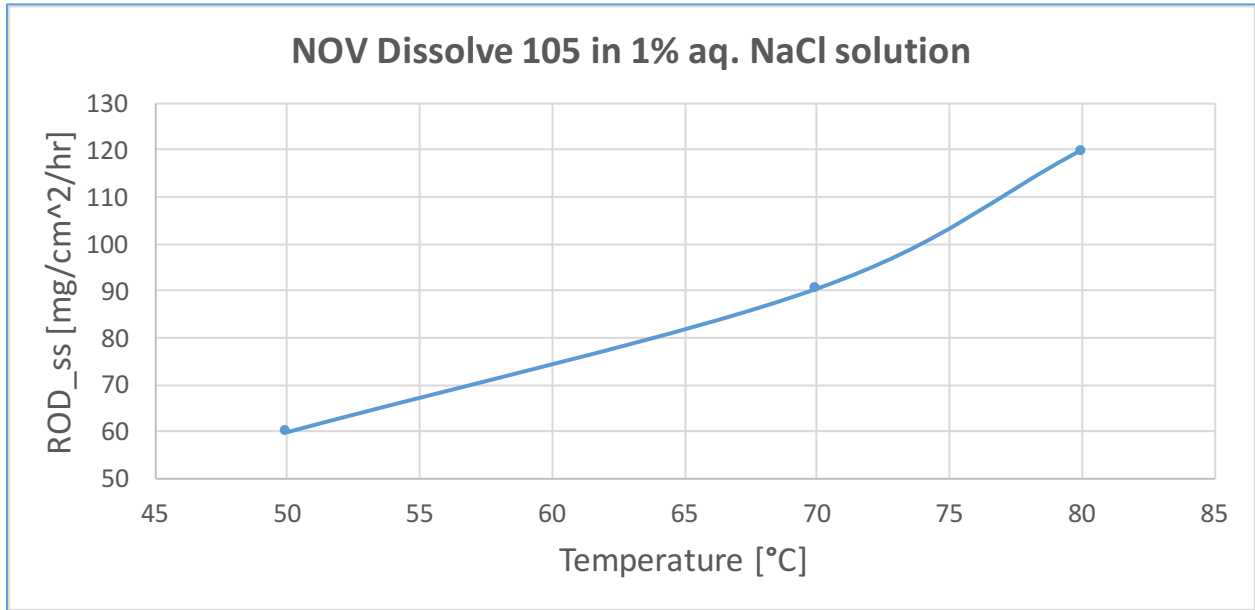


Figure 4-31: Steady State ROD plotted as a function of temperature for Material 105 with the test fluid being 1% aqueous solution of NaCl

The ROD_{ss} value increases considerably with temperature. The ROD_{ss} is seen to increase from 60 mg/cm²/hr at 50 °C to 119.96 mg/cm²/hr at 80 °C. The ROD_{ss} value has almost doubled due to this 30 °C increase in test temperature.

For further interpretation, the same experimental data has been presented in terms of ROD_{ss} values normalized with respect to the ROD_{ss} value at 50 °C in 1% NaCl as shown in Figure 4-32. It can be observed that the slope of the curve gradually increases as the temperature increases. When the temperature is increased from 50 °C to 70 °C, the ROD_{ss} value increases by 51%. However, a smaller temperature change from 70 °C to 80 °C also results in a 49% increase in the steady state ROD. Thus, the influence of temperature on the dissolution reaction gets progressively more dominant at higher temperature values.

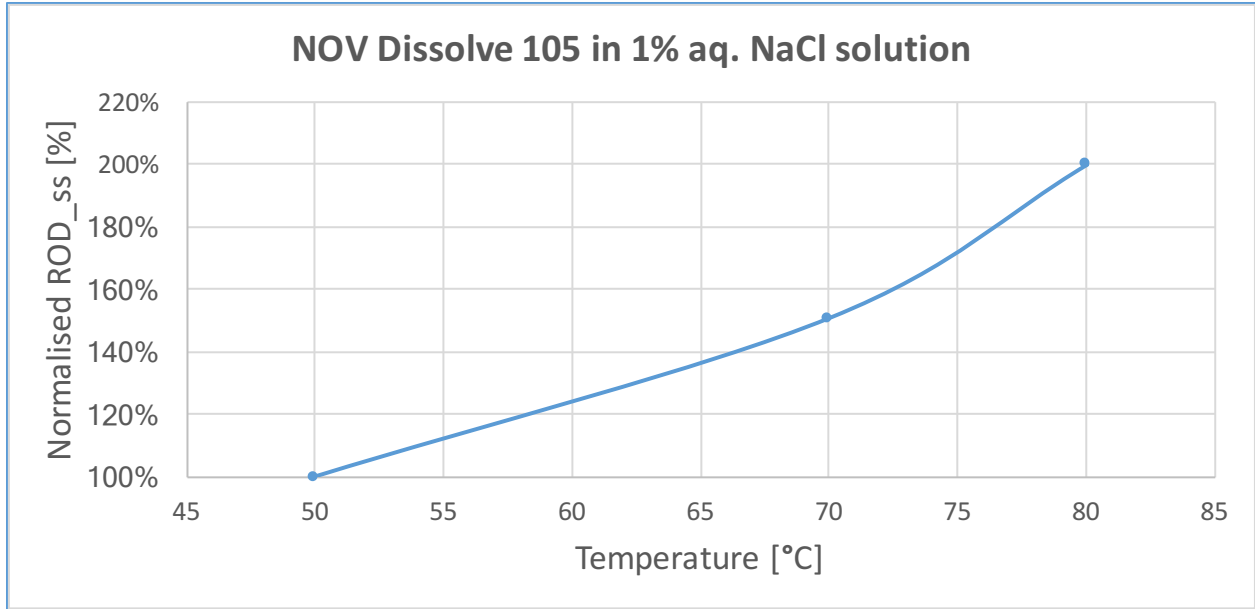


Figure 4-32: Steady State ROD (Normalized w.r.t to the ROD_{ss} at 50 °C) plotted as a function of temperature for Material 105 with the test fluid being 1% aq. solution of NaCl

Referring to the ROD_{ss} versus temperature plot for material 106 (Figure 4-33), the steady state ROD increases from 108.8 mg/cm²/hr at 50 °C to 207.25 mg/cm²/hr at 80 °C. This is a net increase in the ROD_{ss} value of 90% due to the 30 °C temperature raise.

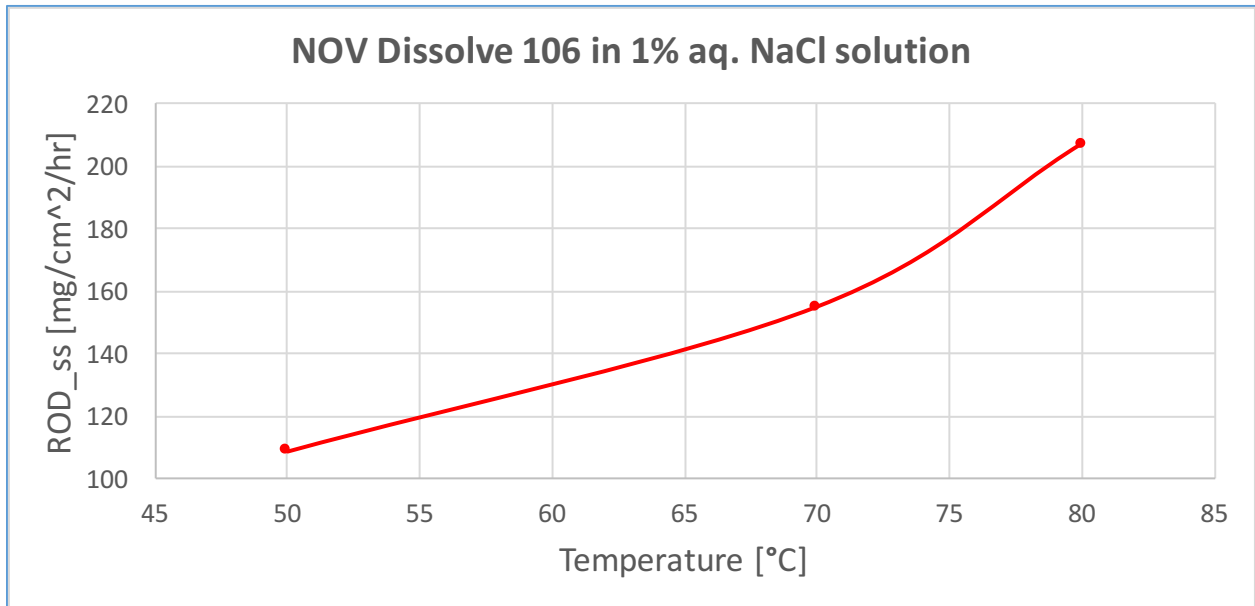


Figure 4-33: Steady State ROD plotted as a function of temperature for Material 106 with the test fluid being 1% aqueous solution of NaCl

Of this 90% increase in ROD_{ss} , 43% occurs during the first temperature change from 50 °C to 70 °C and 47% occurs during the second smaller temperature change from 70 °C to 80 °C. This has been captured in Figure 4-34 which is a plot of normalized ROD_{ss} versus temperature. Thus, the effect of temperature increase is seen to get more profound at higher temperatures.

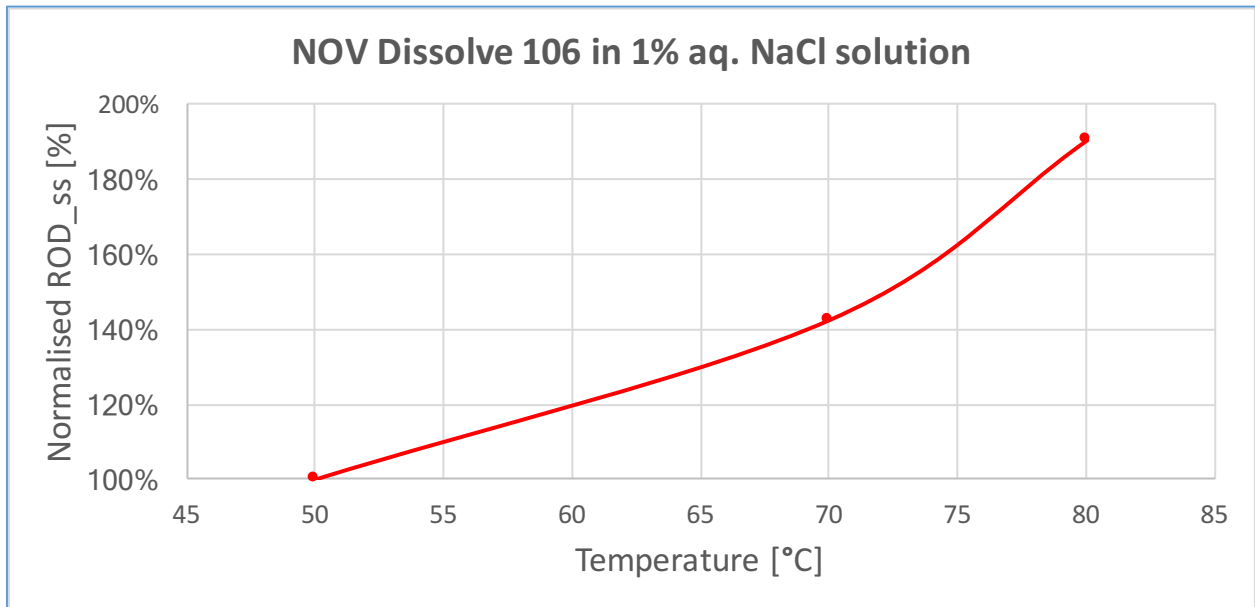


Figure 4-34: Steady State ROD (Normalized w.r.t to the ROD_{ss} at 50 °C) plotted as a function of temperature for Material 106 with the test fluid being 1% aq. solution of NaCl

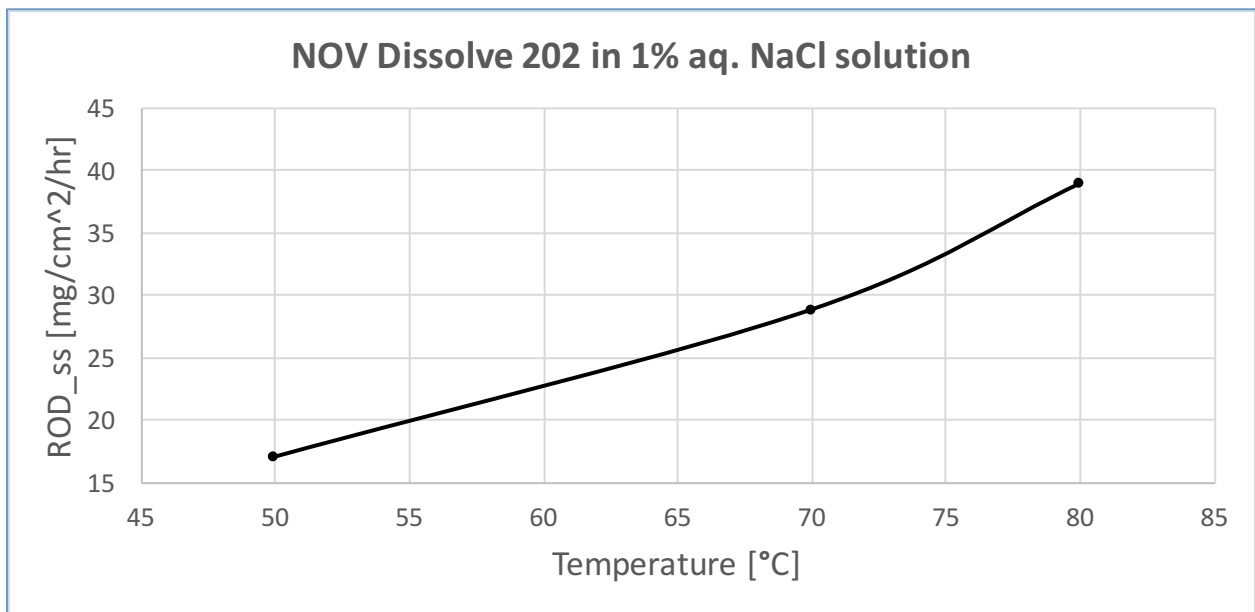


Figure 4-35: Steady State ROD plotted as a function of temperature for Material 106 with the test fluid being 1% aqueous solution of NaCl

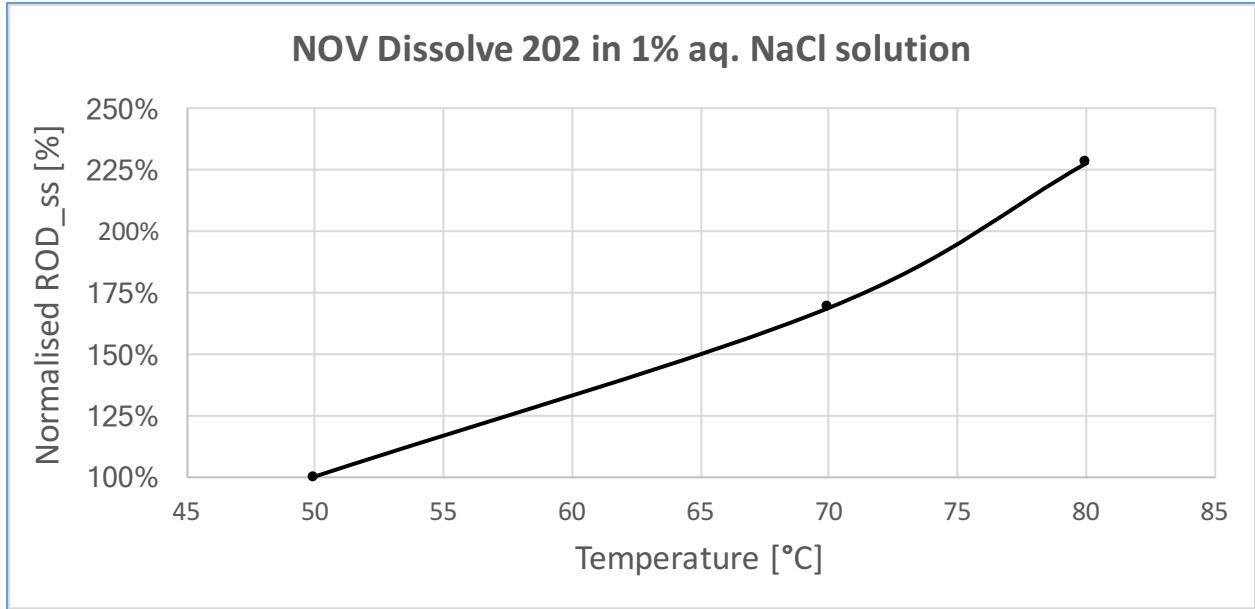


Figure 4-36: Steady State ROD (Normalized w.r.t to the ROD_{ss} at 50 °C) plotted as a function of temperature for Material 202 with the test fluid being 1% aq. solution of NaCl

For material 202 (Figure 4-35 and Figure 4-36), the ROD_{ss} value increases by 128% when the test temperature is changed from 50 °C to 80 °C. Additionally, as seen in the previous two materials, the slope of the curve gets progressively steeper as the temperature increases.

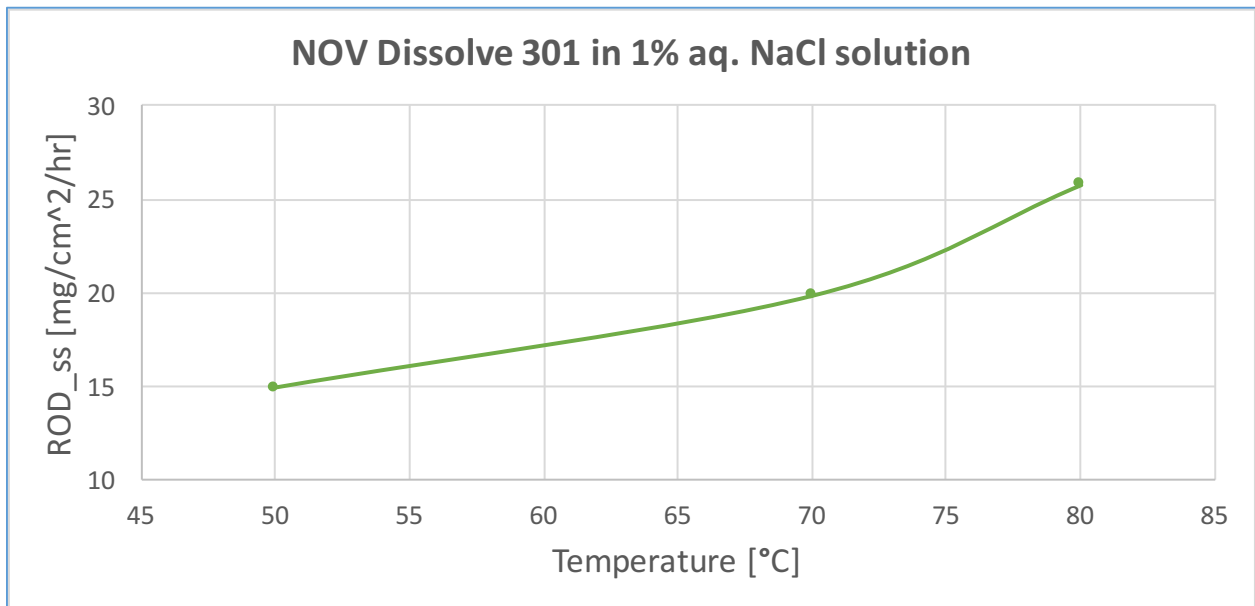


Figure 4-37: Steady State ROD plotted as a function of temperature for Material 301 with the test fluid being 1% aqueous solution of NaCl

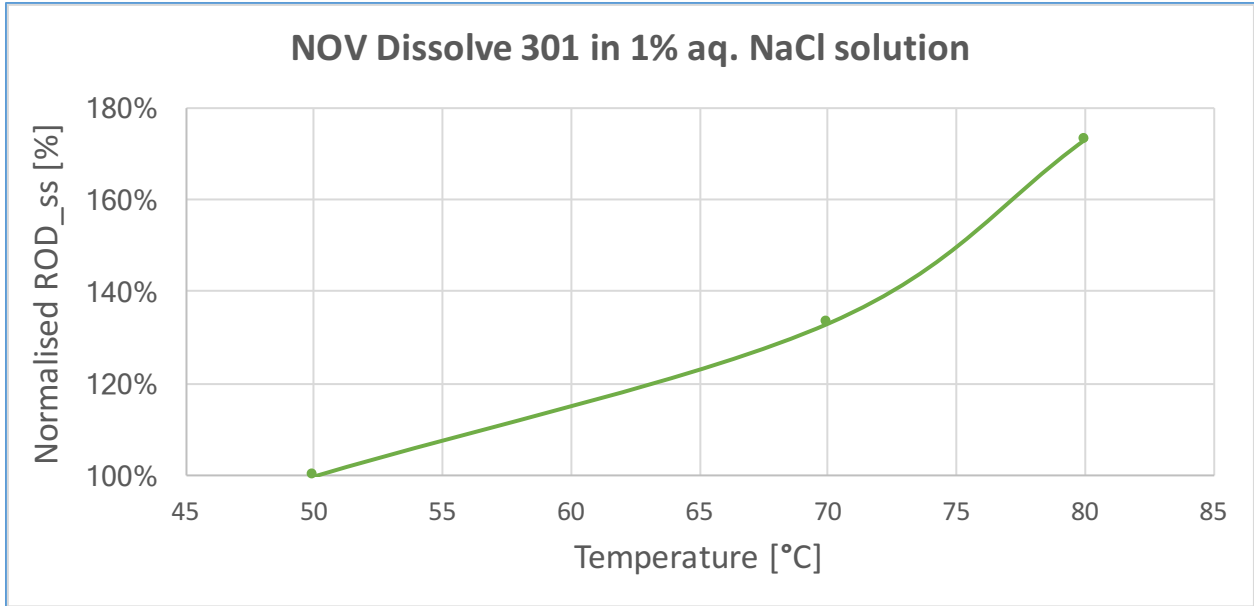


Figure 4-38: Steady State ROD (Normalized w.r.t to the ROD_{ss} at 50 °C) plotted as a function of temperature for Material 301 with the test fluid being 1% aq. solution of NaCl

In case of material 301, as seen in Figure 4-37 and Figure 4-38, the value of ROD_{ss} is 14.91 mg/cm²/hr at 50 °C and increases to 25.80 mg/cm²/hr when the test temperature is changed to 80 °C. This translates to a 73% increase in ROD_{ss} at 80 °C relative to the value at 50 °C.

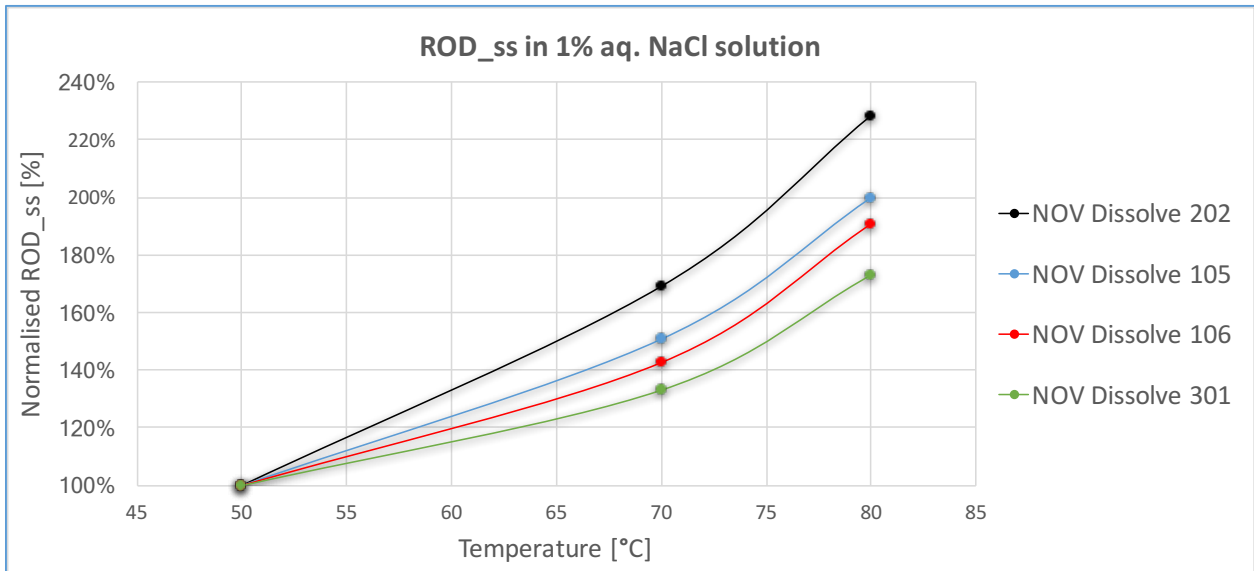


Figure 4-39: Steady State ROD (Normalized w.r.t to the corresponding ROD_{ss} at 50 °C) plotted as a function of temperature for all materials with the test fluid being 1% aq. solution of NaCl

Figure 4-39 plots the steady state ROD values for all materials normalized with respect to their corresponding values at 50 °C in 1% NaCl concentration. This plot can be used to give an indication of how sensitive each of the material is to changes in test temperature. Material 202 is the most sensitive to changes in temperature and it is followed by materials 105, 106 and 301 in descending order. Another observation from this plot is the clear likeness in the general nature of the curves for all the four materials. This aspect shall be explored further as part of Stage IV in Section 4.4.

Thus, for all the dissolvable materials examined in this study, two distinct effects of varying the test temperature were observed:

- i. The dissolution reaction's speed increased with increase in temperatures as reflected by the increase in steady state ROD values.
- ii. The influence of increasing the temperature became progressively more dominant at higher temperatures. This was observed through the continued increase in slope of ROD_{ss} versus temperature curve for all four materials.

4.3.2 Discussion: Stage III Experiments

The results from the Stage III experiments can be explained by making use of the collision theory briefly introduced in Section 4.1.2. According to collision theory, chemical reactions occur when the reactant molecules collide effectively with a certain minimum amount of kinetic energy. This energy threshold varies for each reaction and is defined as the activation energy (E_A) [43]. Referring to Figure 4-40, the energy profile of an exothermic reaction like the dissolution reaction is represented where the reactants need to possess the activation energy in order for the reaction to progress.

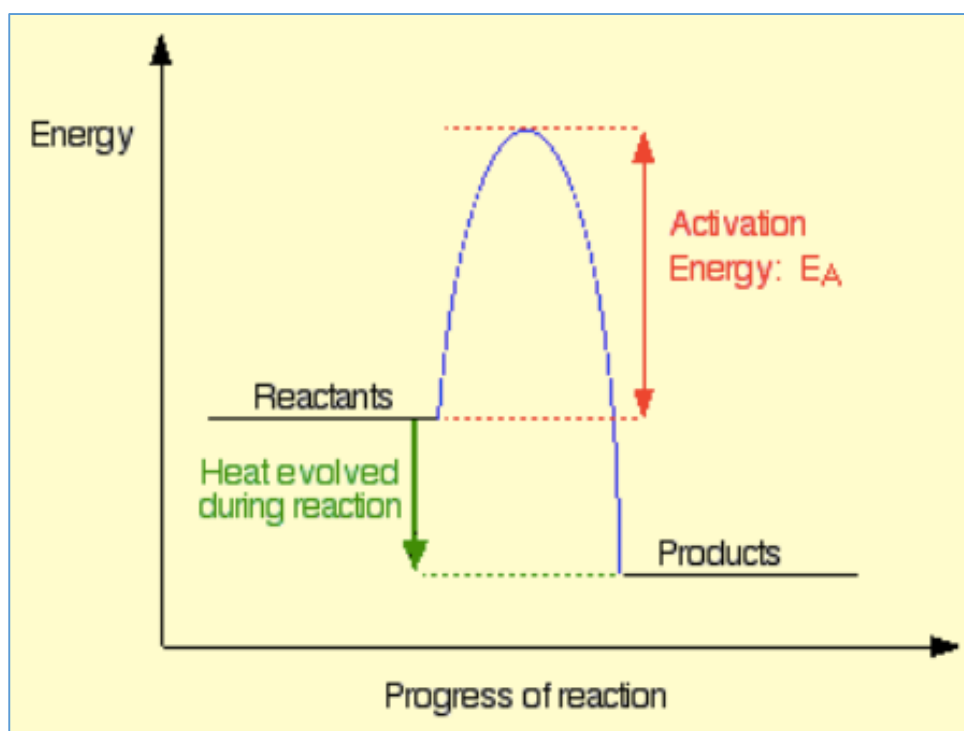


Figure 4-40: Activation energy of a chemical reaction [50]

The activation energy can be further understood by making use of the Maxwell-Boltzmann distribution shown in Figure 4-41. The curve plots the number of particles having a certain kinetic energy versus the kinetic energy of these particles. The area under the curve represents the total number of molecules or particles. While the graph applies to gases, the interpretations and conclusions drawn can be used to explain the behaviour of liquids undergoing chemical reactions as well [50].

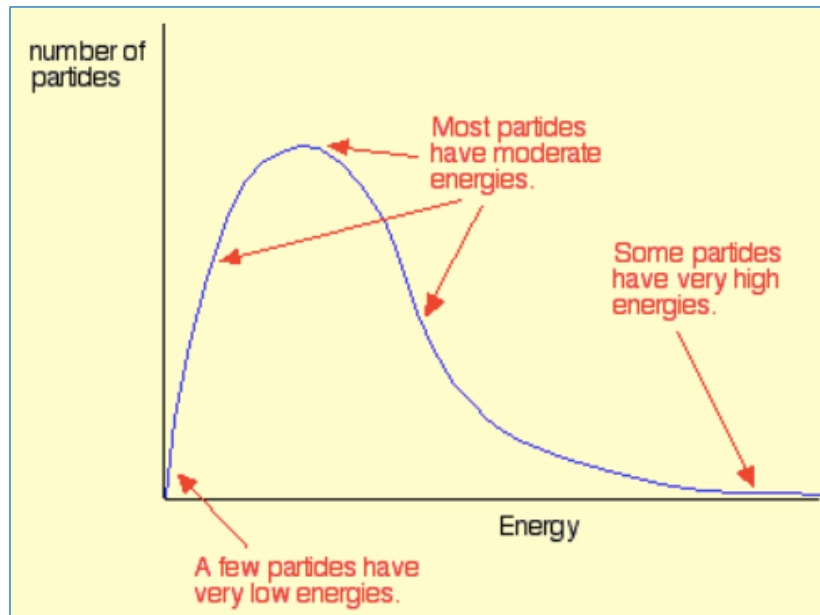


Figure 4-41: Maxwell- Boltzmann Distribution definition [50]

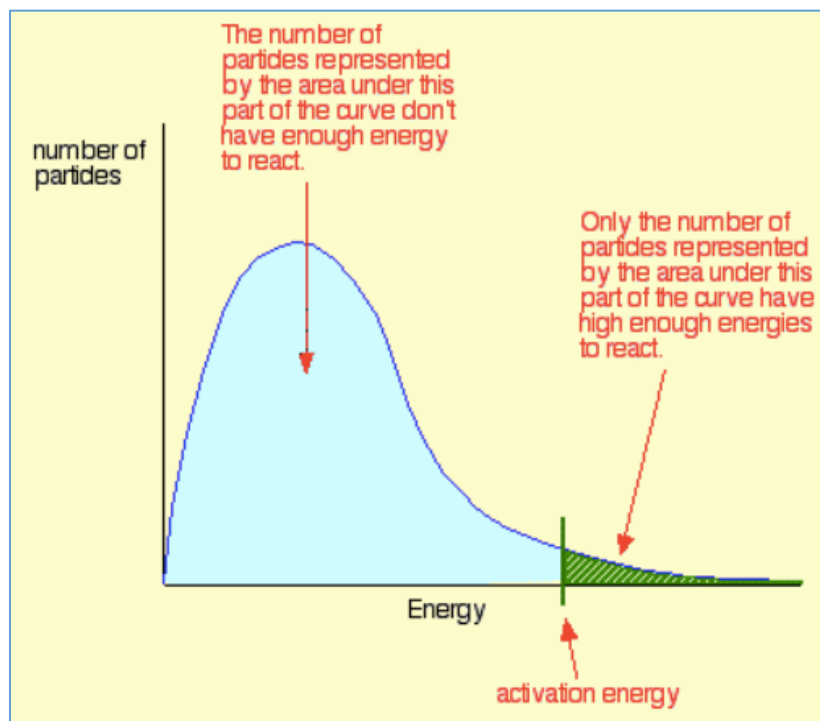


Figure 4-42: Activation energy represented on a Maxwell- Boltzmann Distribution [50]

Referring to Figure 4-42, only those molecules with the kinetic energy equal to or greater than the activation energy participate in the chemical reaction. This is represented by the area under the curve section shaded in green.

Increasing the temperature of the reaction increases the kinetic energy of the reactant molecules. This can be seen in Figure 4-43 where the Maxwell-Boltzmann distribution curve has a greater proportion of particles in the high energy zone when the temperature is increased to 'T+t'. Note that the area under the curve, which represents the total number of particles, does not change. Thus, at a higher temperature (T+t), the number of particles with energy greater than the activation energy threshold is greater. As a result, the number and frequency of collisions between the reactant molecules increases resulting in an increased rate of reaction [43, 51]. Therefore, this theory can be used to explain why the rate of the dissolution reaction increases with increase in temperatures resulting in higher steady state ROD values.

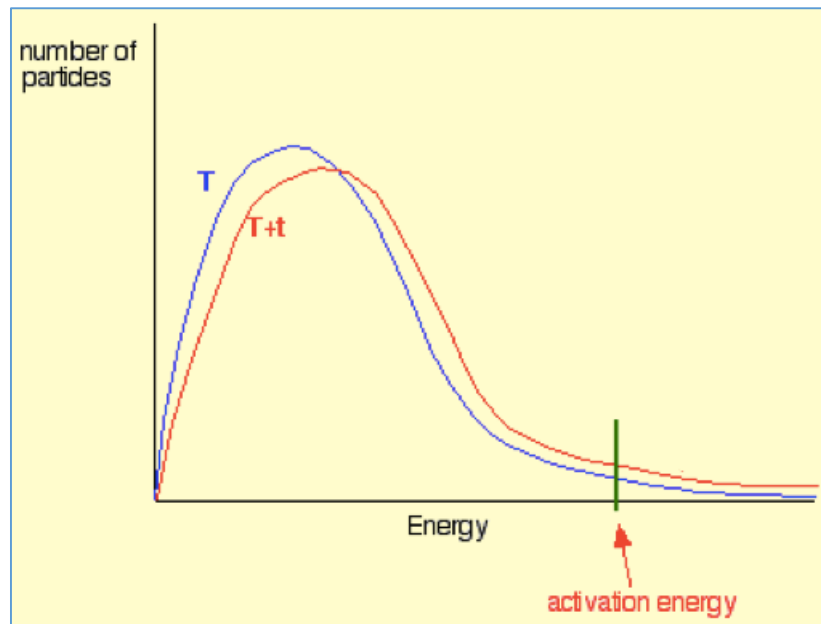


Figure 4-43: Shift in Maxwell- Boltzmann Distribution with increase in temperature [51]

Furthermore, it was observed in the results from the Stage III results (Section 4.3.1), that the slope of the ROD_{ss} versus temperature curves gradually increased at higher temperatures. This can be rationalised by the Arrhenius equation which captures the effect of temperature on chemical reactions.

The Arrhenius equation states that the chemical reaction increases exponentially with temperature as presented by the equation below [52]:

$$k_A = A_{rr} \cdot \exp\left(-\frac{E_A}{R \cdot T_K}\right) \quad (4.6)$$

In the Arrhenius equation:

- k_A is the rate of a chemical reaction expressed in sec^{-1}
- A_{rr} is the Arrhenius pre-exponential factor or frequency factor expressed in sec^{-1}
- E_A is the activation energy commonly expressed in $\text{J} \cdot \text{mol}^{-1}$
- A_{rr} and E_A together are often referred to as Arrhenius parameters and are experimentally determined
- T_K is the temperature expressed in Kelvin
- R is the universal gas constant and is $8.314 \text{ J} \cdot \text{K}^{-1} \cdot \text{mol}^{-1}$

This equation is more conveniently represented in a linear form as shown in the modified Arrhenius equation [53]:

$$\ln k_A = \ln A_{rr} - \frac{E_A}{R \cdot T_K} \quad (4.7)$$

Thus, if the natural logarithm of the reaction rate is plotted against the reciprocal of temperature (expressed in Kelvin), a straight line with a negative slope is expected.

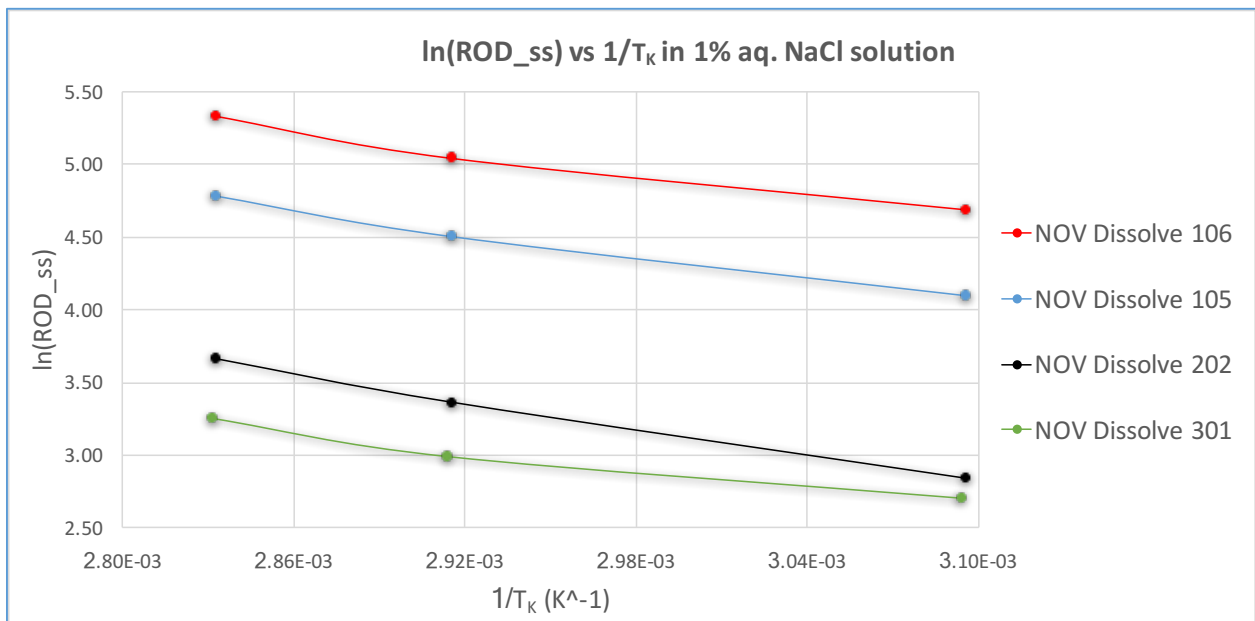


Figure 4-44: $\ln(\text{ROD}_{ss})$ vs $1/T_K$ in 1% aq. NaCl solution

In case of the dissolution reaction, while the steady state Rate of Dissolution (ROD_{ss}) is not defined in the exact way that the rate of a chemical reaction (k_A) is traditionally defined [45], the ROD_{ss} serves the same purpose since it is representative of the rate of the dissolution reaction. Hence, using the Stage III experimental results, the natural logarithm of ROD_{ss} is plotted versus the reciprocal of the experimental temperatures in Figure 4-44. The trend is found to be largely linear for all the tested dissolvable materials. Thus, the natural logarithm of ROD_{ss} varies linearly with the inverse of temperature as predicted by the modified Arrhenius equation.

Therefore, it follows that the ROD_{ss} is expected to increase exponentially with temperature as per the Arrhenius equation. This is reflected in the plots charting the ROD_{ss} as a function of temperature for the different materials recorded in Section 4.3.1. The exponential nature of the relationship between the ROD_{ss} and temperature explains increasing slope of the curve and why the effect of increasing the temperature gets progressively more dominant at higher temperatures.

The objectives achieved and conclusions drawn at the end of Stage III experiments have been summarised below:

- The rate of dissolution reaction was found to increase with temperature as reflected by the increase in ROD_{ss} values.
- The dependence of ROD_{ss} on temperature progressively increases as the temperature gets higher.
- The above results were explained by means of the collision theory, the role of activation energy as well as the Arrhenius equation. Based on the latter, the ROD_{ss} value was found to increase exponentially with temperature.
- The dissolvable materials listed in the decreasing order of sensitivity to changes in temperature are: Material 202, 105, 106 and 301.

4.4 Stage IV - Combined Effect of Temperature and Concentration

In Stage II, the effect of concentration on dissolve rate was investigated by varying the NaCl concentration in a series experiments conducted at a constant temperature 80 °C. In Stage III, the influence of temperature on ROD_{ss} was examined through experiments at different temperatures while using a test fluid with fixed concentration of 1% aq. NaCl. As a next step, in Stage IV the combined effects of varying both temperature and concentration were investigated. A series of 48 different experiments were conducted wherein each of the four dissolvable materials were tested at the three test temperatures of 50 °C, 70 °C and 80 °C, and in four different test fluid concentrations of 1% aq. NaCl, 3% aq. NaCl, 6% aq. NaCl and 9% aq. NaCl.

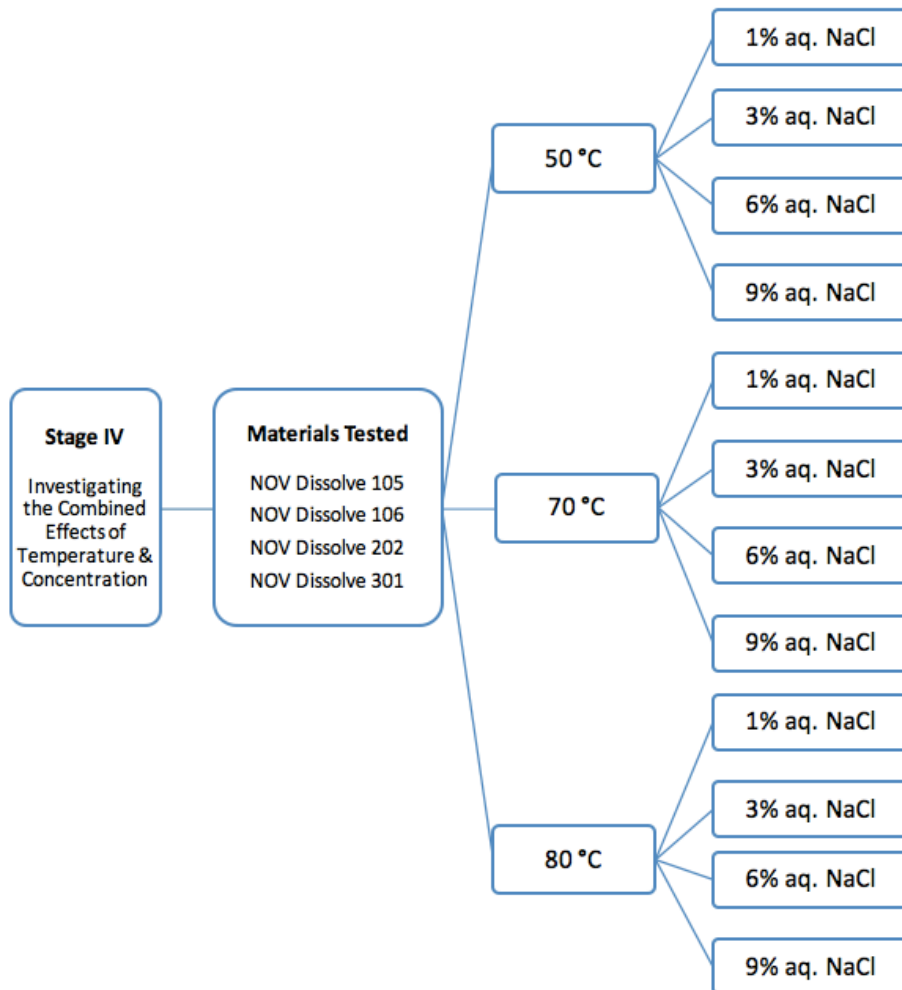


Figure 4-45: Schematic of Stage IV Test Outline (Repeated from Section 3.3.2)

4.4.1 Results and Discussion: Stage IV Experiments

Based on the 48 dissolution tests conducted in Stage IV, the variation in ROD_{ss} as a function of NaCl concentration at different temperatures have been charted below in Figure 4-46 to Figure 4-49 for the four different dissolvable materials.

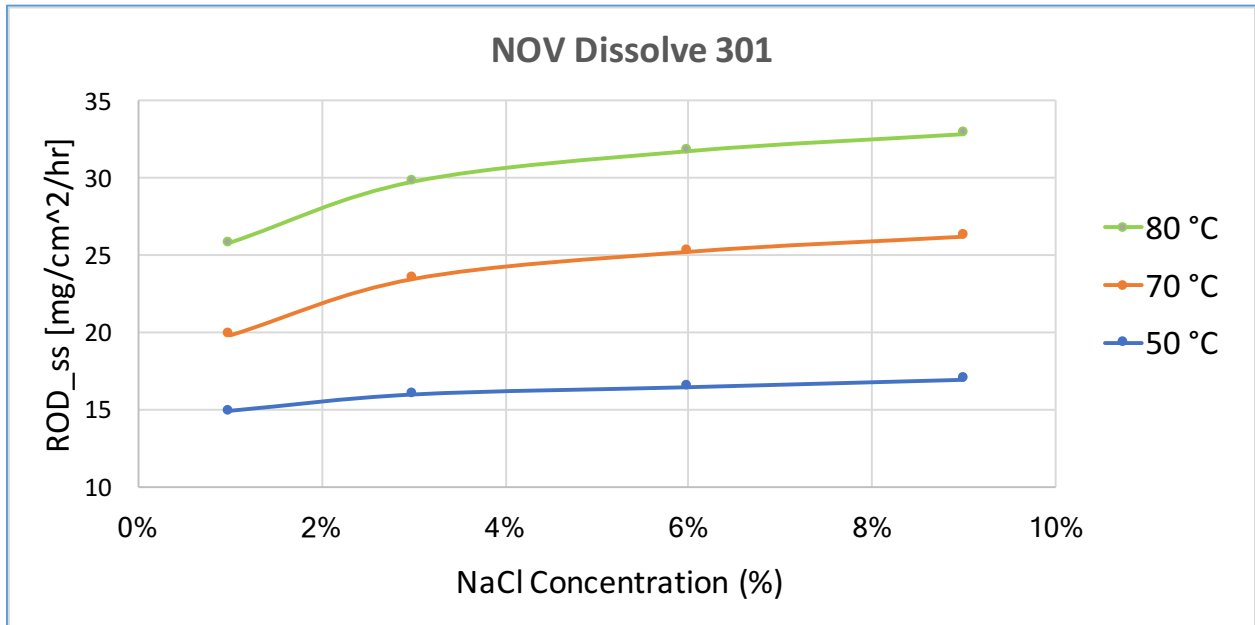


Figure 4-46: Steady State ROD plotted as a function of NaCl concentration at 3 different temperatures for Material 301

The following observations can be drawn from these four charts:

- Increasing the concentration of NaCl increases the rate of dissolution process as reflected by the increase in the ROD_{ss} values.
- The dependence of ROD_{ss} on NaCl concentration gradually decreases as the NaCl concentration gets higher.
- The ROD_{ss} increases as the temperature increases.

These results are consistent with the Stage II and Stage III results as discussed in Section 4.2.1 and 4.3.1. The variation of ROD_{ss} with concentration can be explained based on the catalytic role of the chloride ions in facilitating the dissolution reaction as elaborated in Section 4.2.2. The effect of temperature has been previously analyzed in Section 4.3.2.

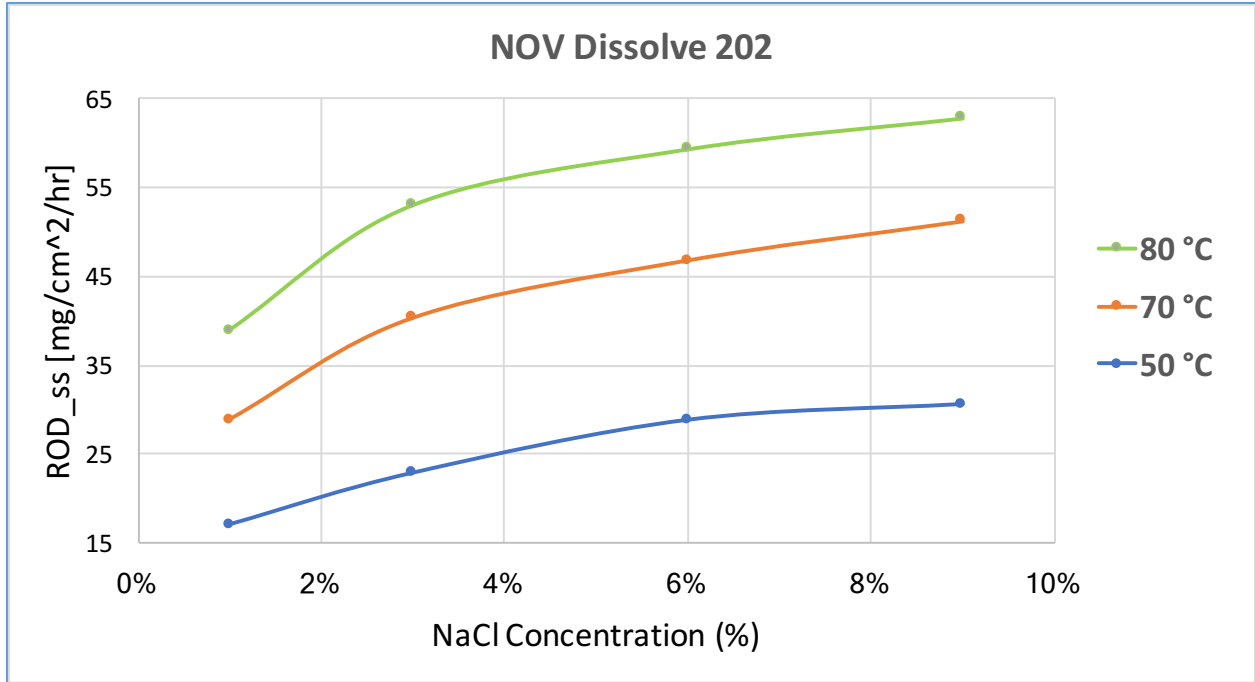


Figure 4-47: Steady State ROD plotted as a function of NaCl concentration at 3 different temperatures for Material 202

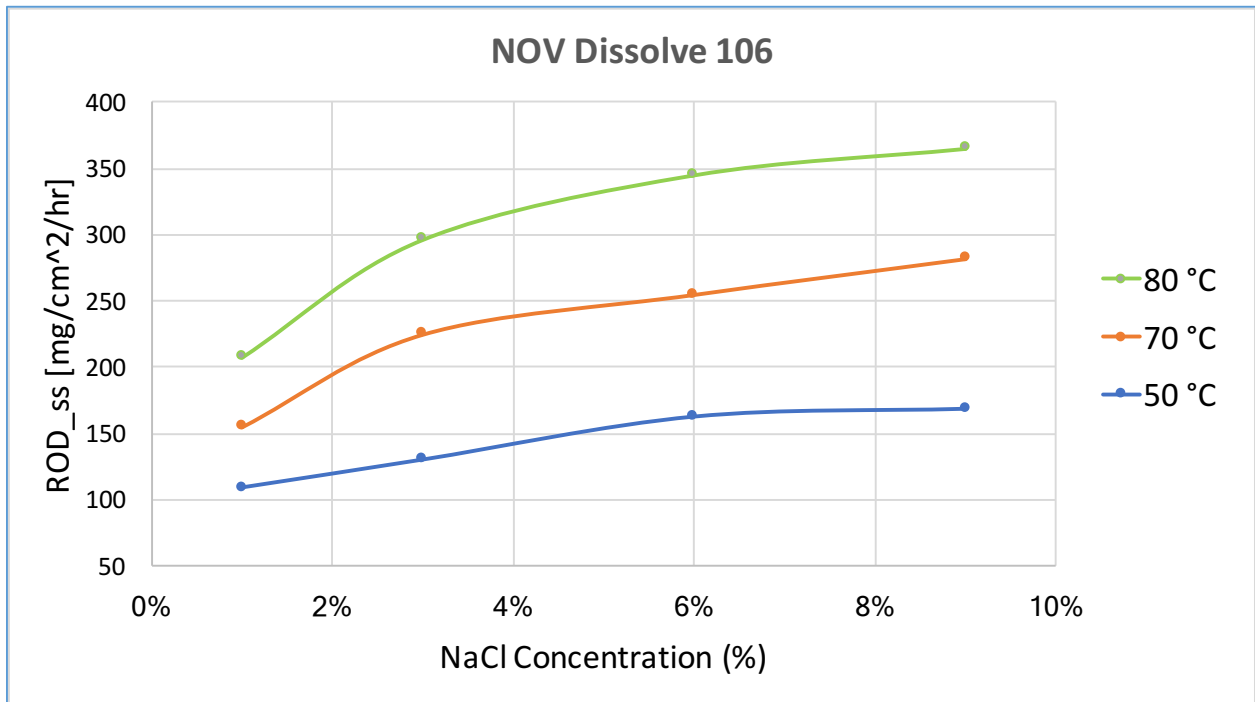


Figure 4-48: Steady State ROD plotted as a function of NaCl concentration at 3 different temperatures for Material 106

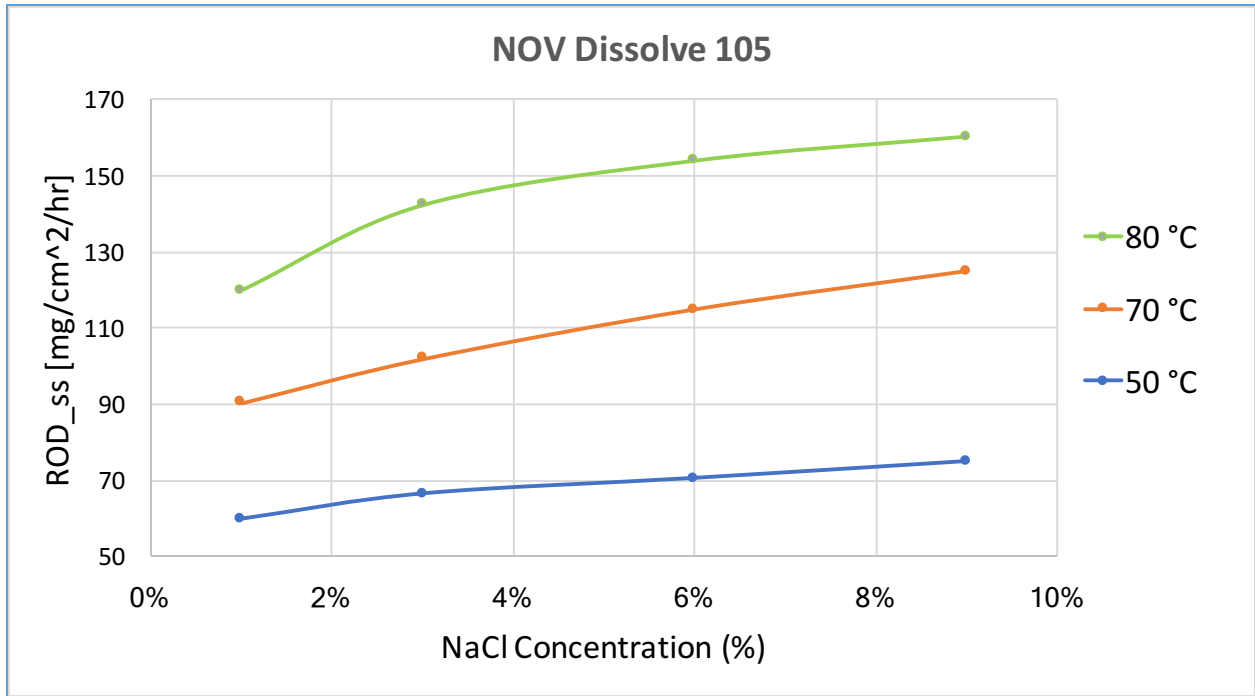


Figure 4-49: Steady State ROD plotted as a function of NaCl concentration at 3 different temperatures for Material 105

In Figure 4-50 to Figure 4-53, the ROD_{ss} values have been plotted as a function of temperature for test fluids with different NaCl concentrations.

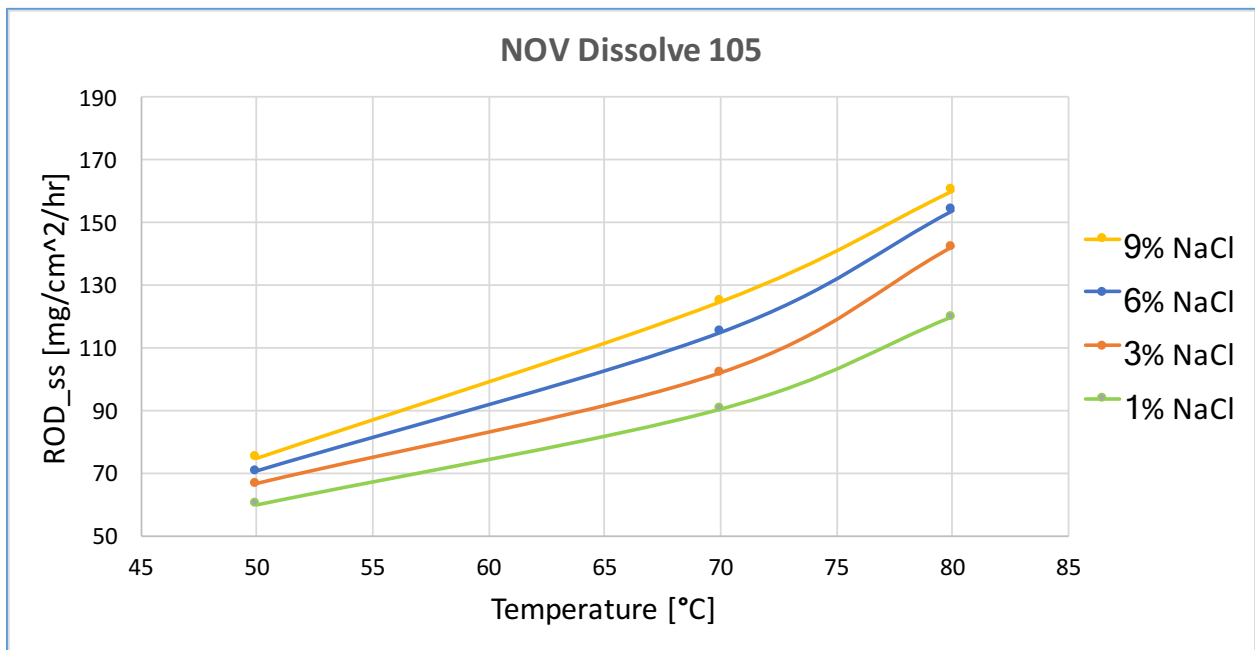


Figure 4-50: Steady State ROD plotted as a function of test temperature in various test fluid concentrations for Material 105

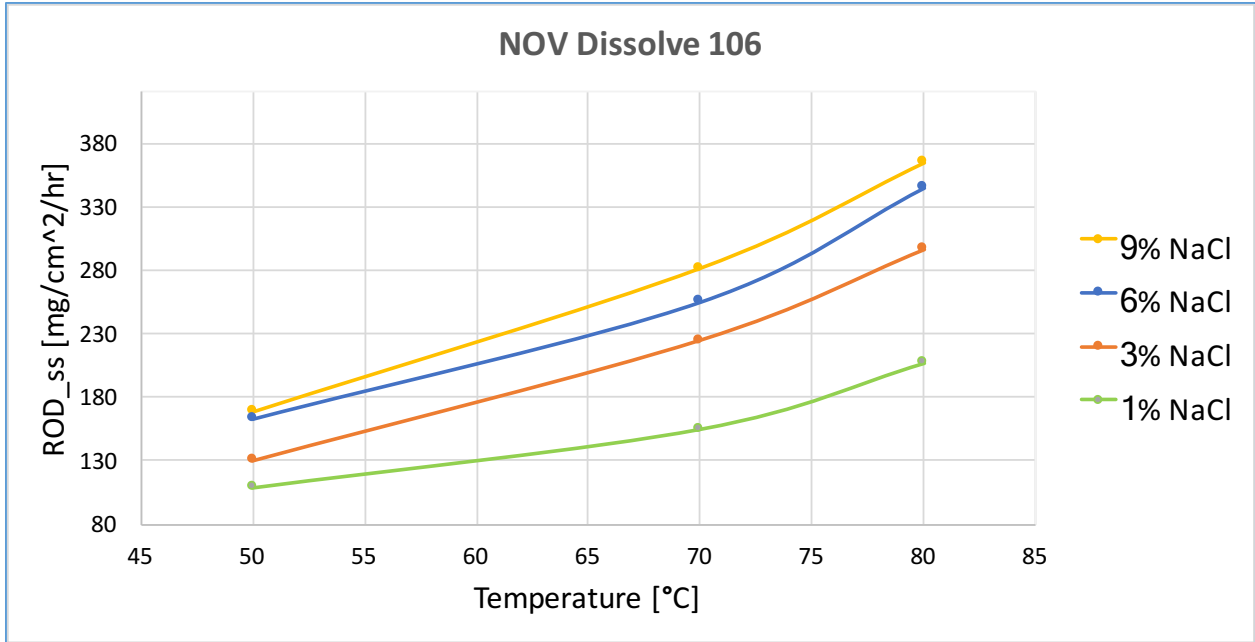


Figure 4-51: Steady State ROD plotted as a function of test temperature in various test fluid concentrations for Material 106

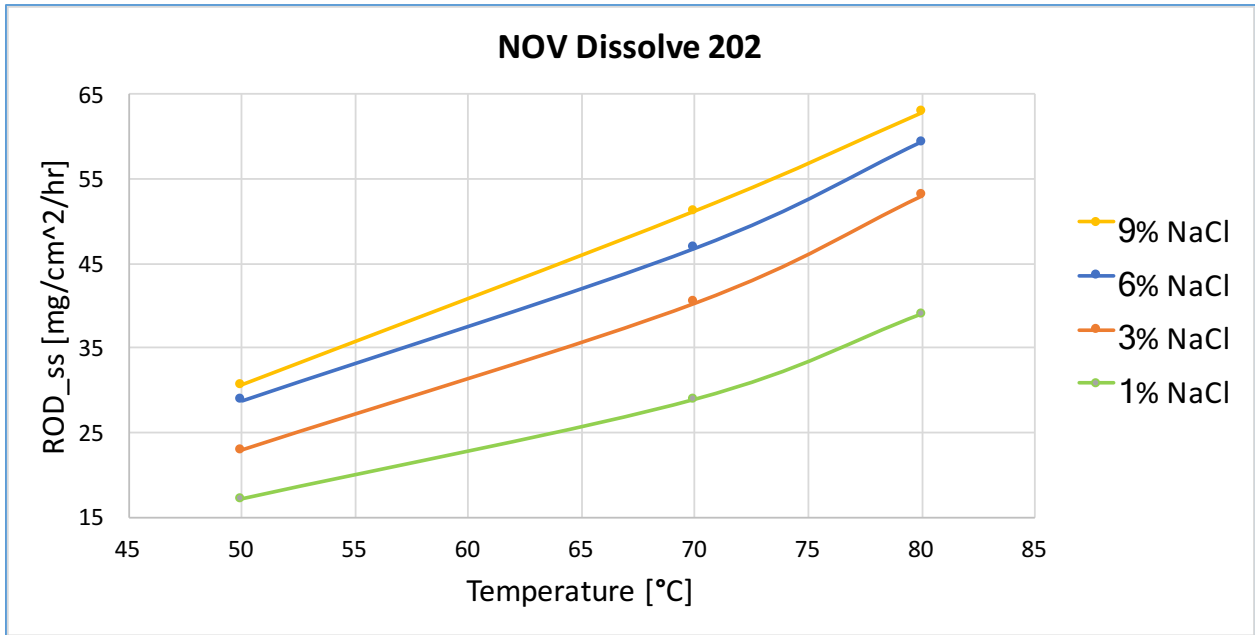


Figure 4-52: Steady State ROD plotted as a function of test temperature in various test fluid concentrations for Material 202

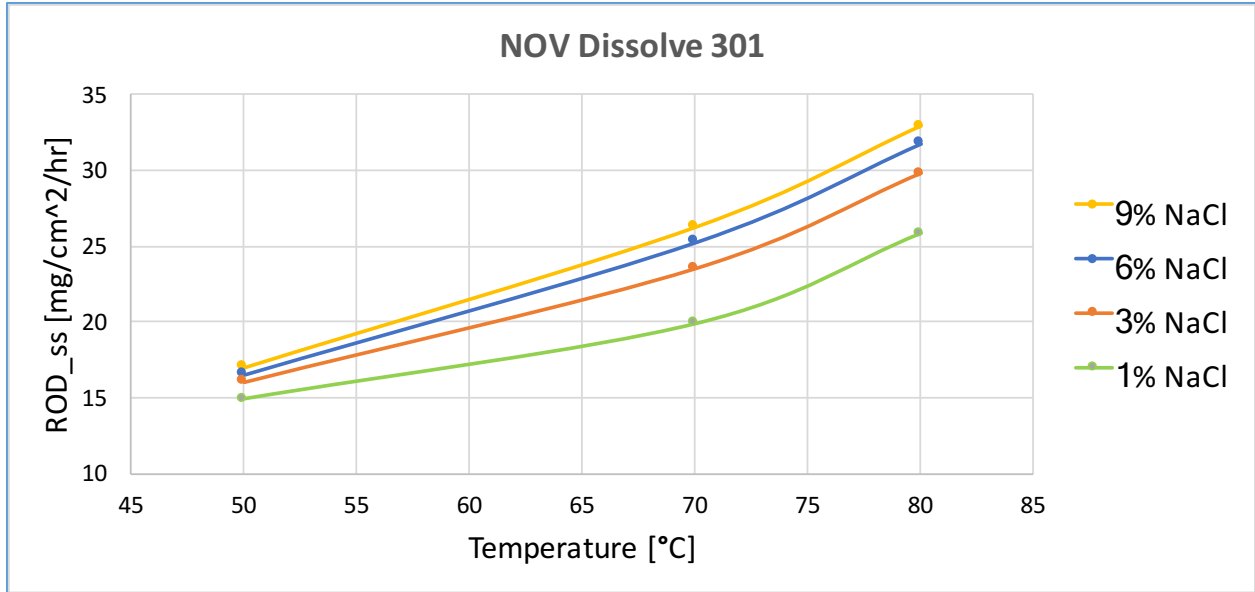


Figure 4-53: Steady State ROD plotted as a function of test temperature in various test fluid concentrations for Material 301

The following statements can be made based on these four charts:

- The dissolution reaction's speed increased with increase in temperatures as reflected by the increase in the steady state ROD values.
- The influence of increasing the temperature gets progressively more dominant at higher temperatures. This can be seen in the continued increase in slope of ROD_{ss} versus temperature curve for all the four materials.

These results are in line with the observations made previously in the Stage III results (Section 4.3.1). The above results were explained by means of the collision theory, the role of activation energy as well the Arrhenius equation in Section 4.3.2.

4.4.2 Developing a Dissolve Rate Predictor

In this section, a Dissolve Rate Predictor has been developed based on experimental data by using regression methods. It has been established that temperature and the test fluid's NaCl concentration are two of the most influential factors affecting the performance of dissolvable materials. An empirical model that captures this dependence is developed for each of the four dissolvable materials. The steady-state ROD values from the sample dissolution experiments performed at different temperatures and concentration are analysed to develop this model.

4.4.2.1 Outline of Methodology

The goal is to develop an empirical model to forecast the dissolution rate of a dissolvable material at a given temperature and NaCl concentration in the test fluid. To achieve this, the subsequent three steps are implemented for each of the four dissolvable materials -

Step 1: $ROD_{ss} = f(C)$; Constant T

Determine the dependence of ROD_{ss} on NaCl concentration (C) when the temperature (T) is held constant

Step 2: $ROD_{ss} = f(T)$; Constant C

Establish the relationship between ROD_{ss} and temperature (T) when the NaCl concentration in test fluid is held constant

Step 3: $ROD_{ss} = f(C, T)$

Use the results from Steps 1 and 2 to develop a predictive model for the steady state Rate of Dissolution when both concentration and temperature are varying.

4.4.2.2 Regression Analysis: Some definitions

Regression analysis is a well-established area of statistics which is used to develop predictive models based on observed experimental data. Some relevant terminologies used in regression analysis and their concise definitions have been compiled below for reference:

- i. **Regression Analysis:** This is a statistical tool used to establish the effect of independent variables on a dependant variable and quantify the nature of this relationship [54].

ii. **Simple versus Multiple regression:** When we want to examine the relationship between the dependent variable and a single independent variable, this is known as simple regression.

On the other hand, when the dependent variable depends on more than 1 independent variable and we want to analyse the combined dependence of the dependent variable on both the independent variables, this is known as multiple regression [54].

In Section 4.4.2.1, we start off with simple regression in Steps 1 and 2 before moving on to multiple regression analysis in Step 3.

iii. **Empirical versus Mechanistic models:** The models obtained from regression analysis are based solely on collected and observed data. These regression analysis-based models are called empirical models and are used to model the relationship between the various variables in complicated phenomena.

On the other hand, those models which can be derived or analytically explained by means of physical, chemical or other scientific theory are called mechanistic models [55].

In this chapter, an empirical approach is used to establish the relationship between temperature, NaCl concentration and the Rate of Dissolution.

iv. **Linear versus Non-Linear Regression Models:** Linear regression model is a model which is linear in its parameters. On the other hand, all other equations which cannot be categorized as linear-regression models are collectively termed as non-linear regression models [56].

v. **R-squared:** R-squared value (sometimes referred to as Coefficient of Determination or Goodness-of-fit) is a measure of how well the empirical model captures the observed experimental data. The value of R-squared is between 0 and 1. The closer the value is to 1, the more accurate the empirical model is in capturing the behaviour of the phenomenon being observed [54].

A brief introduction to common regression analysis terminologies has been provided above. Detailed information about methods in regression analysis are beyond the scope of this thesis. For in-depth information on this topic, the books by Rawling et al. [57] and Montgomery et al. [55] are recommended. The statistical tools available in Microsoft Excel and Matlab have been used extensively in this thesis and the underlying algorithms for the regression functions used in these programs can be found in their respective product documentation manuals.

4.4.2.3 Implementation of Methodology

Step 1: $ROD_{ss} = f(C)$; Constant T

Using the non-linear regression tools in Microsoft Excel, the steady state ROD has been expressed as a function of the NaCl concentration (C) at a constant temperature value (T). This has been done for all four materials as shown in Figure 4-54 to Figure 4-57.

At each constant temperature, Power-Law model was found to represent the best fit of the experimental data. The R-squared values were found to be above 0.97 indicating excellent correlation with between the experimental data and the generated Power-Law model. In these figures, the dotted lines represent the predicted Power-Law model trendline while the solid markers represent the actual experimental ROD_{ss} values.

Note that these curve-fitted equations are valid in the temperature range of 50-80 °C and when the NaCl concentration is in the range of 1% - 9%.

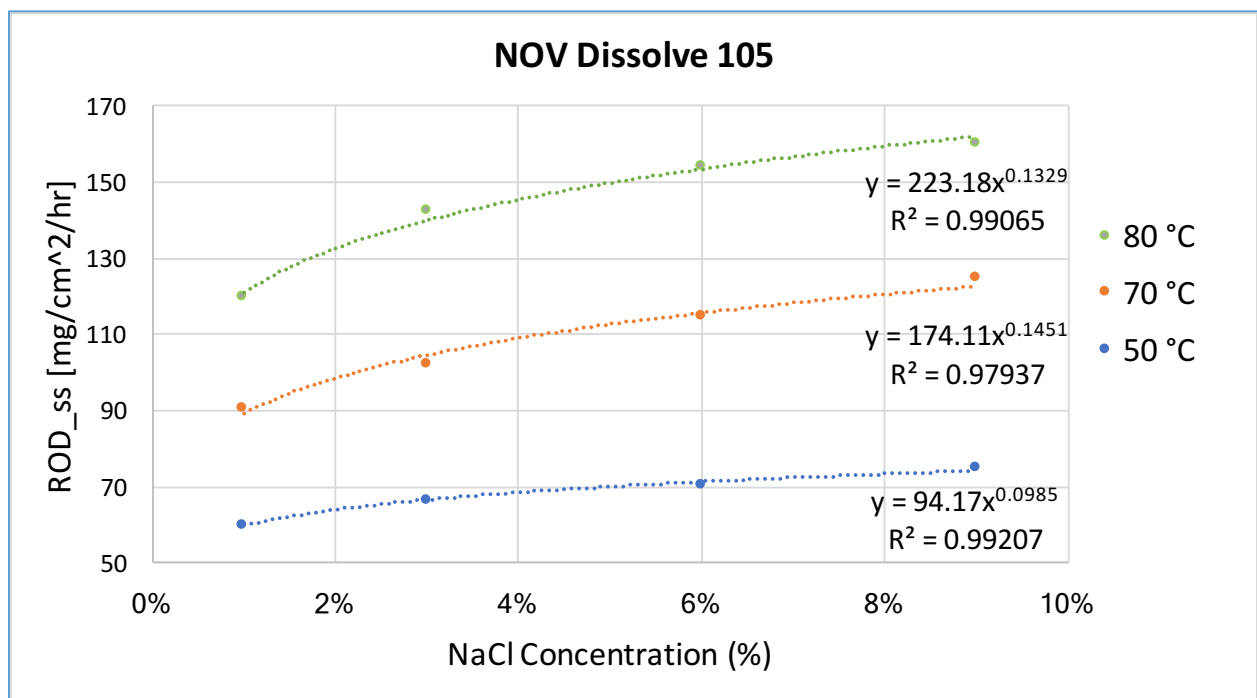


Figure 4-54: Regression analysis equations and trendline expressing ROD_{ss} as a function of NaCl concentration when temperature is constant for NOV Dissolve 105

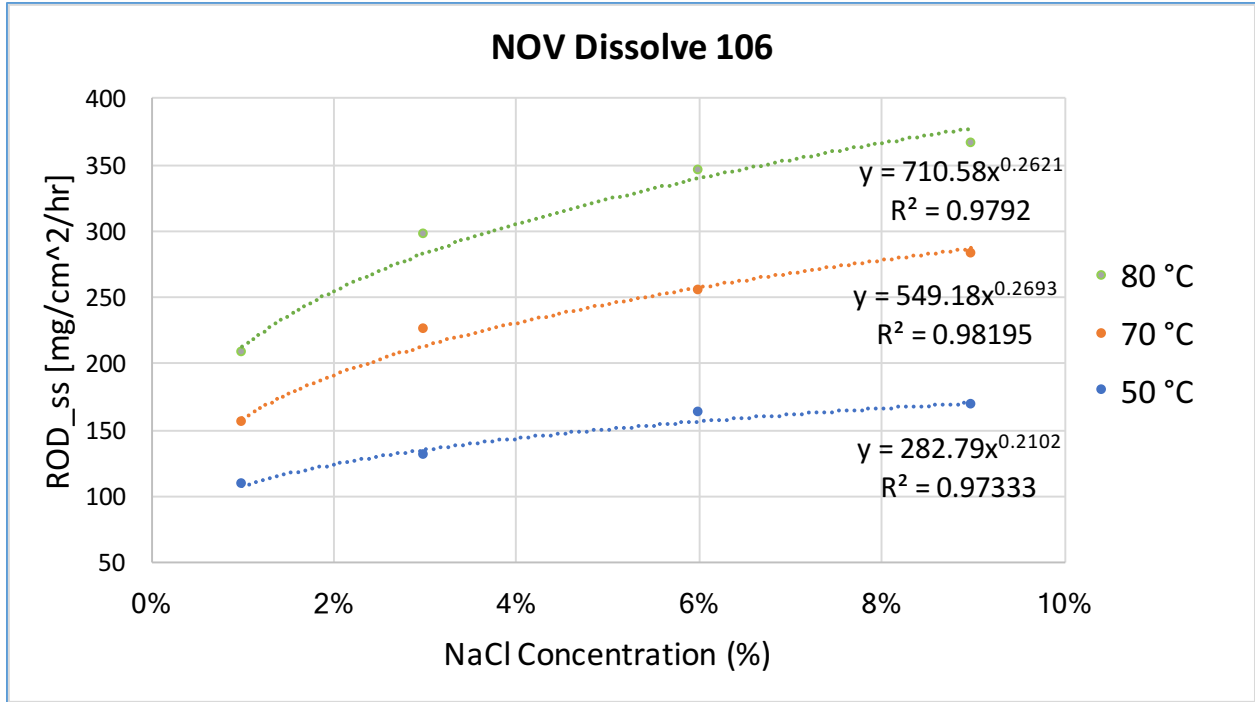


Figure 4-55: Regression analysis equations and trendline expressing ROD_{ss} as a function of NaCl concentration when temperature is constant for NOV Dissolve 106

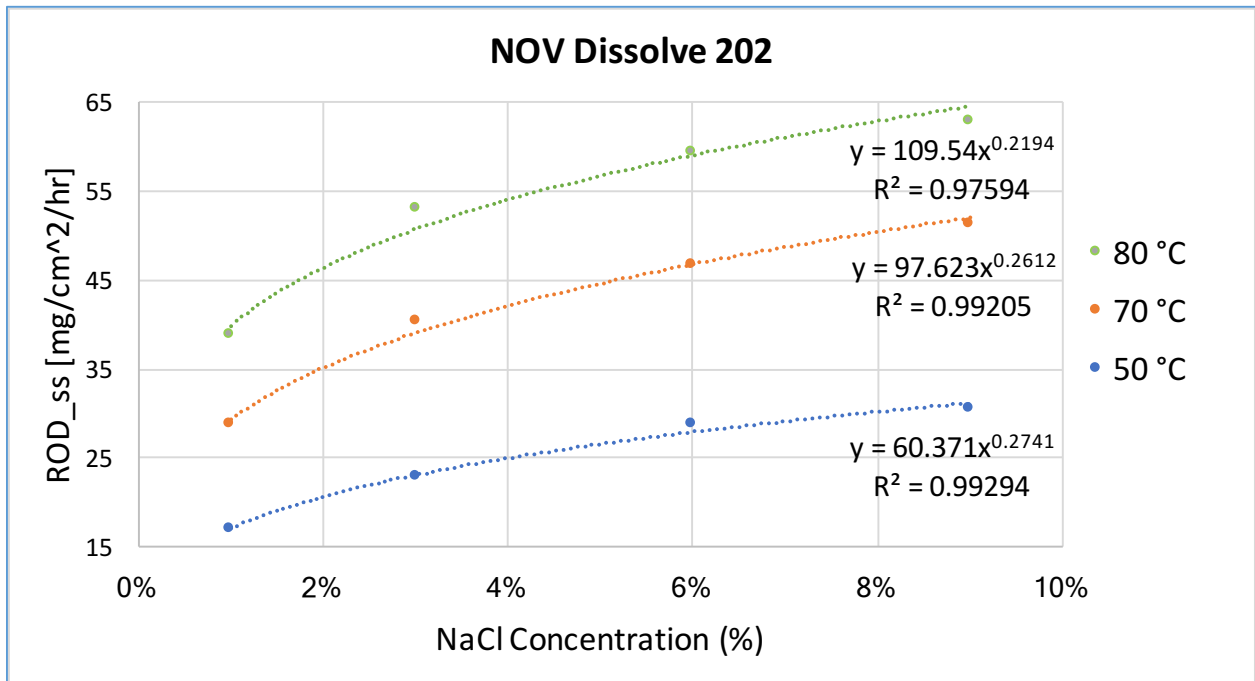


Figure 4-56: Regression analysis equations and trendline expressing ROD_{ss} as a function of NaCl concentration when temperature is constant for NOV Dissolve 202

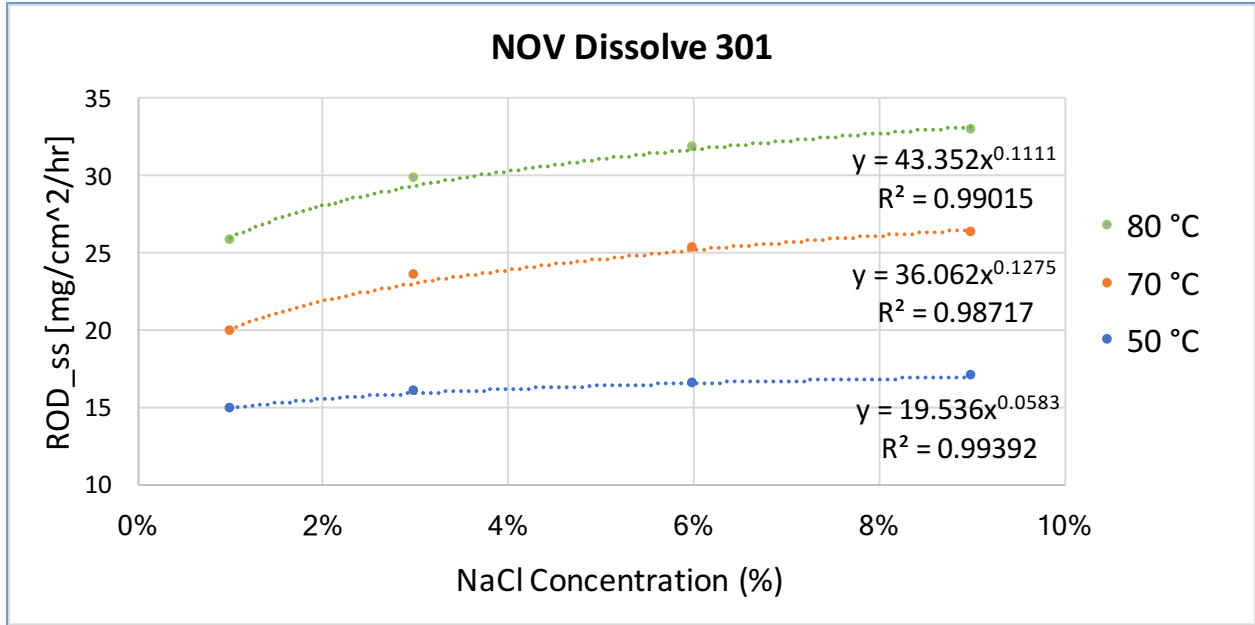


Figure 4-57: Regression analysis equations and trendline expressing ROD_{ss} as a function of NaCl concentration when temperature is constant for NOV Dissolve 301

Based on the above analysis, the relationship between ROD_{ss} and NaCl concentration at a constant temperature was found to be of the form:

$$ROD_{ss} = f(C) = a_1 * C^{a_2}; \text{Constant } T \quad (4.8)$$

where:

- ROD_{ss} : The steady state Rate of Dissolution expressed in $mg/cm^2/hr$
- C : Concentration of NaCl in the test fluid expressed in grams per millilitre according the definition presented in Equation 3.1. As an example, the value of C is 0.03 for a 3% aqueous solution of NaCl formed by mixing 3 grams of NaCl in 100 ml of water
- T : Temperature in °C
- a_1 and a_2 are constants for a given material at a specific temperature

Step 2: $ROD_{ss} = f(T)$; Constant C

In this section, the aforementioned regression analysis tools in Microsoft Excel have been used to express the steady state ROD as a function of the test temperature (T) for constant values of NaCl concentration in the test fluid. This has been performed for all four materials as shown in Figure 4-58 to Figure 4-61.

An exponential relationship was found between the rate of dissolution (ROD_{ss}) and the test temperature when the test fluid concentration is constant. The R-squared values were found to be above 0.97, thereby demonstrating excellent correspondence with the experimental data. The exponential increase in rate of dissolution is as predicted by the Arrhenius equation which is based on collision theory and the role of activation energy (discussed in Section 4.3.2).

In the figures below, the dotted lines represent the predicted exponential model trendline while the solid markers represent the actual experimental ROD_{ss} values. Note that these curve-fitted equations are valid in the temperature range of 50-80 °C and when the NaCl concentration is in the range of 1% - 9%.

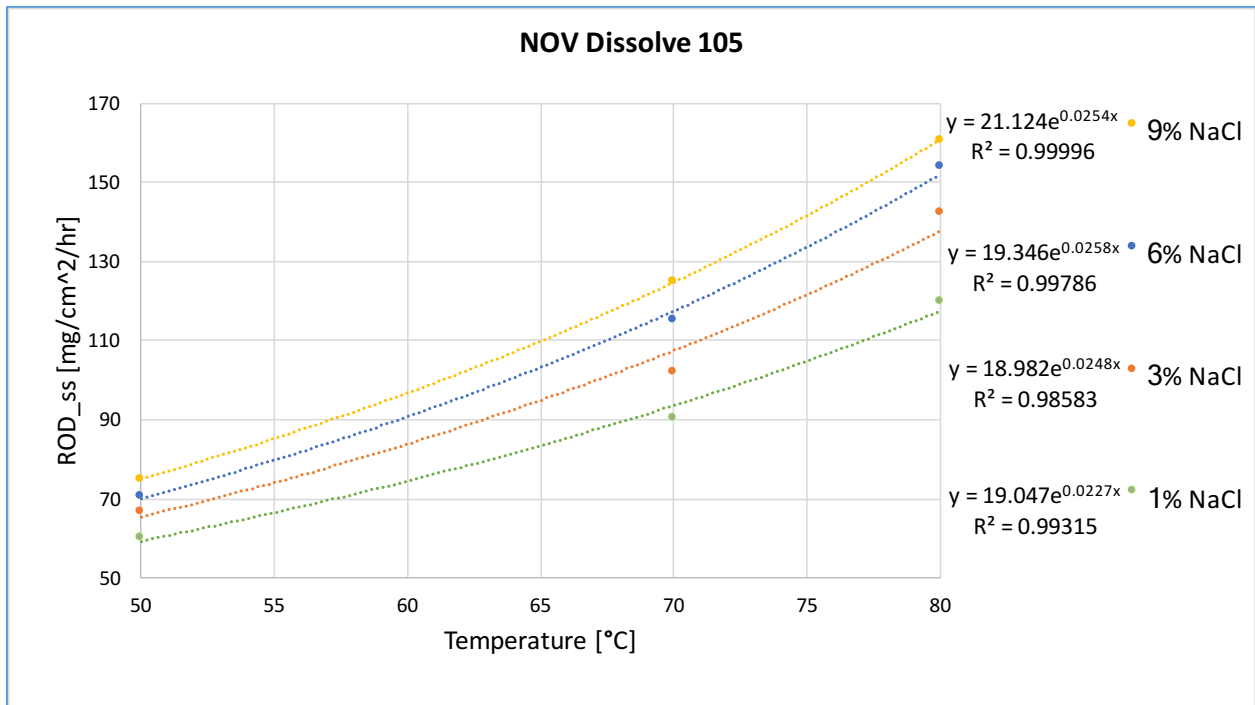


Figure 4-58: Regression analysis equations and trendline modelling ROD_{ss} as a function of temperature when NaCl concentration is constant for NOV Dissolve 105

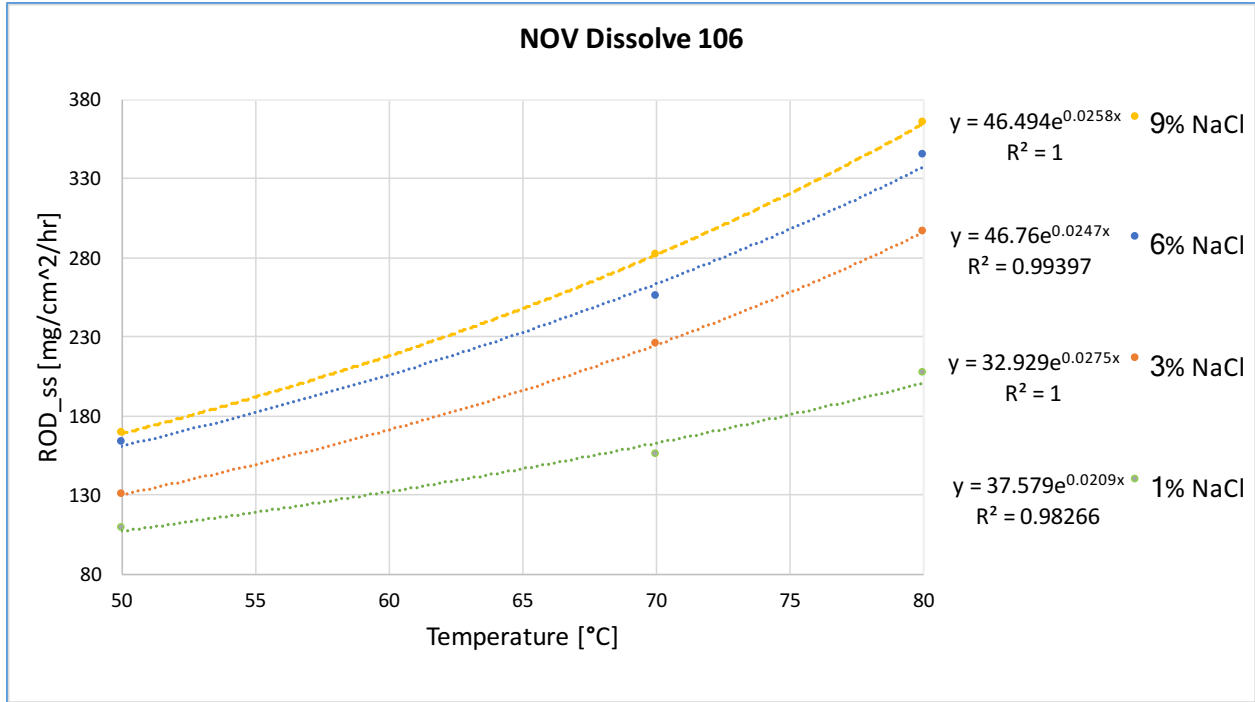


Figure 4-59: Regression analysis equations and trendline modelling ROD_{ss} as a function of temperature when NaCl concentration is constant for NOV Dissolve 106

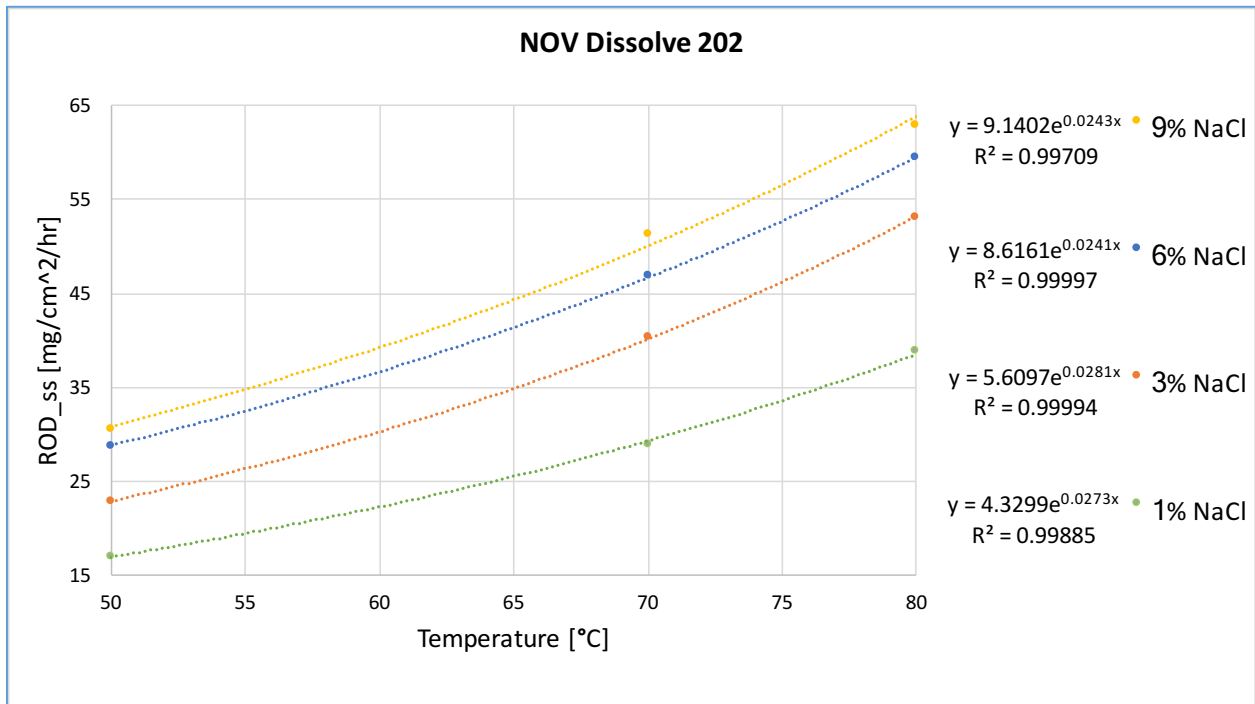


Figure 4-60: Regression analysis equations and trendline modelling ROD_{ss} as a function of temperature when NaCl concentration is constant for NOV Dissolve 202

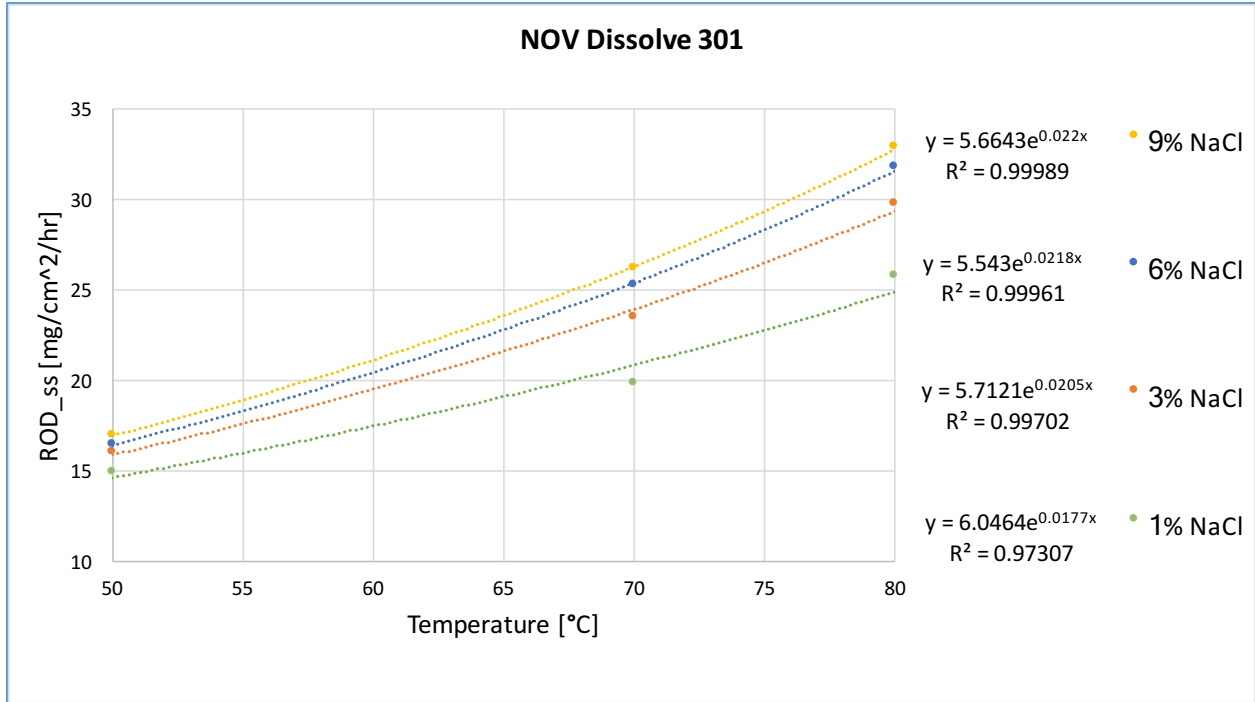


Figure 4-61: Regression analysis equations and trendline modelling ROD_{ss} as a function of temperature when NaCl concentration is constant for NOV Dissolve 301

Based on the above analysis, the relationship between ROD_{ss} and temperature at a given concentration was found to be of the form:

$$ROD_{ss} = f(T) = a_3 * e^{a_4 T}; \text{Constant } C \quad (4.9)$$

where:

- ROD_{ss} : The steady state Rate of Dissolution expressed in $mg/cm^2/hr$
- C : Concentration of NaCl in the test fluid expressed in grams per millilitre
- T : Temperature in $^{\circ}C$
- a_3 and a_4 are constants for a given material at a specific NaCl concentration

Step 3: $ROD_{ss} = f(C, T)$

In Step 1, the steady state Rate of Dissolution was expressed as a function of the NaCl concentration (C) at constant temperature values:

$$ROD_{ss} = f(C) = a_1 * C^{a_2}; \text{Constant } T \quad (4.8)$$

In Step 2, the steady state Rate of Dissolution was expressed as a function of temperature at constant NaCl concentration values:

$$ROD_{ss} = f(T) = a_3 * e^{a_4 T}; \text{Constant } C \quad (4.9)$$

Now in Step 3, the outcomes from the previous steps shall be utilized to develop a combined Dissolve Rate Predictor that expresses the steady state ROD as a simultaneous function of both temperature and concentration:

$$ROD_{ss} = f(C, T)$$

The Curve Fitting Toolbox™ in Matlab (ver. R2015b) was utilized to develop the Dissolve Rate Predictor. Curve Fitting Toolbox™ provides an application and functions for fitting curves and surfaces to data. This toolbox enables one to conduct regression analysis using both linear and nonlinear models. Using this toolbox, one can fit data into standard equations (linear, quadratic, exponential, polynomial etc.) as well as non-standard customised equations [58].

The experimental ROD_{ss} values at the corresponding temperatures and NaCl concentrations (Section 4.4.1) were used as the input data that was to be surface fitted. In addition to the experimental data, the other main input required for the surface fitting process is the equation type that we want to fit the data into. Based on equations 4.8 and 4.9, the following equation form is expected to capture the dependence of ROD_{ss} on both temperature and concentration:

$$ROD_{ss} = f(C, T) = b_1 * C^{b_2} * e^{b_3 T} \quad (4.10)$$

where

- ROD_{ss} : The steady state Rate of Dissolution expressed in $\text{mg}/\text{cm}^2/\text{hr}$
- C: Concentration of NaCl in the test fluid expressed in grams per millilitre

- T: Temperature in °C
- b_1 , b_2 and b_3 are constants for a given material, also referred to in this work as material constants or material coefficients. They are not dependent on temperature or NaCl content.

The above non-standard custom equation was input into Matlab’s Surface fitting tool in order to fit the experimental data and determine the material coefficients. The suitability of this predicted equation to capture the behaviour of ROD_{ss} can be evaluated by the following analysis:

- At a constant temperature value, the term e^{b_3T} becomes a constant. As a result, Eq. 4.10 reduces to $ROD_{ss} = f(C, Constant T) = b_4 * C^{b_2}$, where b_4 is another material constant. This is identical in form to Eq. 4.8 that was generated to capture how ROD_{ss} varies as a function of concentration at constant temperature.
- At a constant concentration value, the term C^{b_2} becomes a constant. Consequently, Eq. 4.10 reduces to $ROD_{ss} = f(T, Constant C) = b_5 * e^{b_3T}$, where b_5 is another material constant. This reduced form is identical in form to Eq. 4.9 that expresses ROD_{ss} as a function of temperature at constant concentration.

Thus, the predicted custom Eq. 4.10 is found to be consistent with the Eq. 4.8 and 4.9 generated in Steps 1 and 2, respectively. Based on this equation, the ROD_{ss} of a given material can be modelled as a function of temperature and NaCl concentration by determining the material constants b_1 , b_2 and b_3 for each specific material. Therefore, Eq. 4.10 was input into the Surface fitting function in Matlab which then determined the best fit material constants based on experimental data. Other inputs to the surface fitting toolbox are listed in Table 5 for reproducibility.

Table 5:Surface fitting options used in Matlab

Fit Options		Definition [58]
Method	Non-Linear Least Squares	Since the custom equation is non-linear in the coefficients.
DiffMinChange	$1e^{-8}$	Minimum change in coefficient value during iterations
DiffMaxChange	0.1	Maximum change in coefficient value during iterations
MaxFunEvals	1000	Maximum number of function evaluations allowed

MaxIter	1000	Maximum number of fit iterations allowed
TolFun	1e ⁻⁸	Termination tolerance used on stopping conditions involving the function (model) value
TolX	1e ⁻⁸	Termination tolerance used on stopping conditions involving the coefficients

First considering material NOV Dissolve 105, the Surface fitting toolbox was used to fit the experimental data into equation 4.10 and the material coefficients were determined as shown in Table 6. The complete Matlab code use to perform the surface fitting and generate the 3D-plots is available in Appendix I.

Table 6: Material coefficients for NOV Dissolve 105

Material Coefficient	Value for Material 105
b ₁	28.75
b ₂	0.1327
b ₃	0.0255
R-square	0.9938

Thus, the equation that predicts the dissolution behaviour, i.e., the Dissolve Rate Predictor of material 105 at different temperatures and NaCl concentrations is as shown below:

$$ROD_{ss} = f(C, T) = 28.75 * C^{0.1327} * e^{0.0255T} \quad (4.11)$$

The high R-squared value of 0.99 indicates that the above equation fits the experimental data very well. Note that Eq. 4.11 is accurate only for temperature values between 50 - 80 °C and NaCl concentrations of 1% - 9%.

Figure 4-62 shows the above equation charted as a 3-Dimensional surface plot with ROD_{ss} as the z-axis. The NaCl concentration and temperature are on the x and y-axes, respectively. The black dots represent the experimental values (some of the experimental values cannot be seen in this figure since they are hidden by the surface plot). The yellow/orange regions of the surface represent high ROD_{ss} values while blue represents regions with low ROD_{ss} values. Also, note that the temperature increases from right to left.

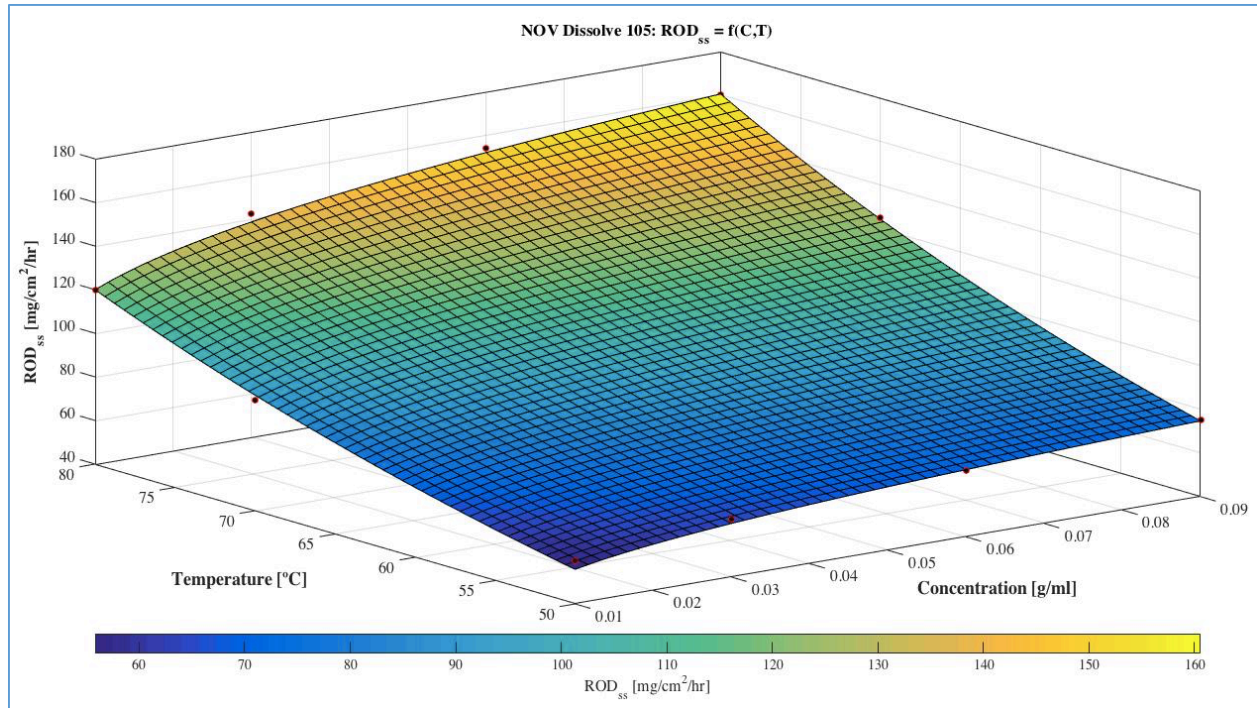


Figure 4-62: 3-D Surface plot showing ROD_{ss} as a function of both temperature and concentration for material 105.

The above 3-D surface plot has been rotated in Figure 4-63 to observe the behaviour in the Z-X plane (ROD_{ss} -Concentration plane). It can be seen that the behaviour of the surface plot in this orientation is very similar to the ROD_{ss} versus concentration plot shown in Figure 4-49. Increasing the concentration of NaCl increases the rate of dissolution process. The dependence of ROD_{ss} on NaCl concentration gradually decreases as the NaCl concentration gets higher. This has been previously discussed in Section 4.2 and 4.4.1.

In Figure 4-64, the 3-D surface plot has been rotated such that the plot can be observed perpendicular to the Z-Y plane (ROD_{ss} -Temperature plane). The variation of the ROD_{ss} in the Z-Y plane is in line with the results charted in Figure 4-50. The dissolution reaction's speed increases with temperature as reflected by the increase in the ROD_{ss} values. Increasing the temperature has a progressively more dominant influence on the steady state ROD at higher temperatures due to the exponential nature of their relationship. This phenomenon is discussed in Section 4.3 and 4.4.1.

Thus, the 3D-surface plot and the corresponding predictive model in Equation 4.11 are consistent with the observations and results in the preceding sections of the thesis.

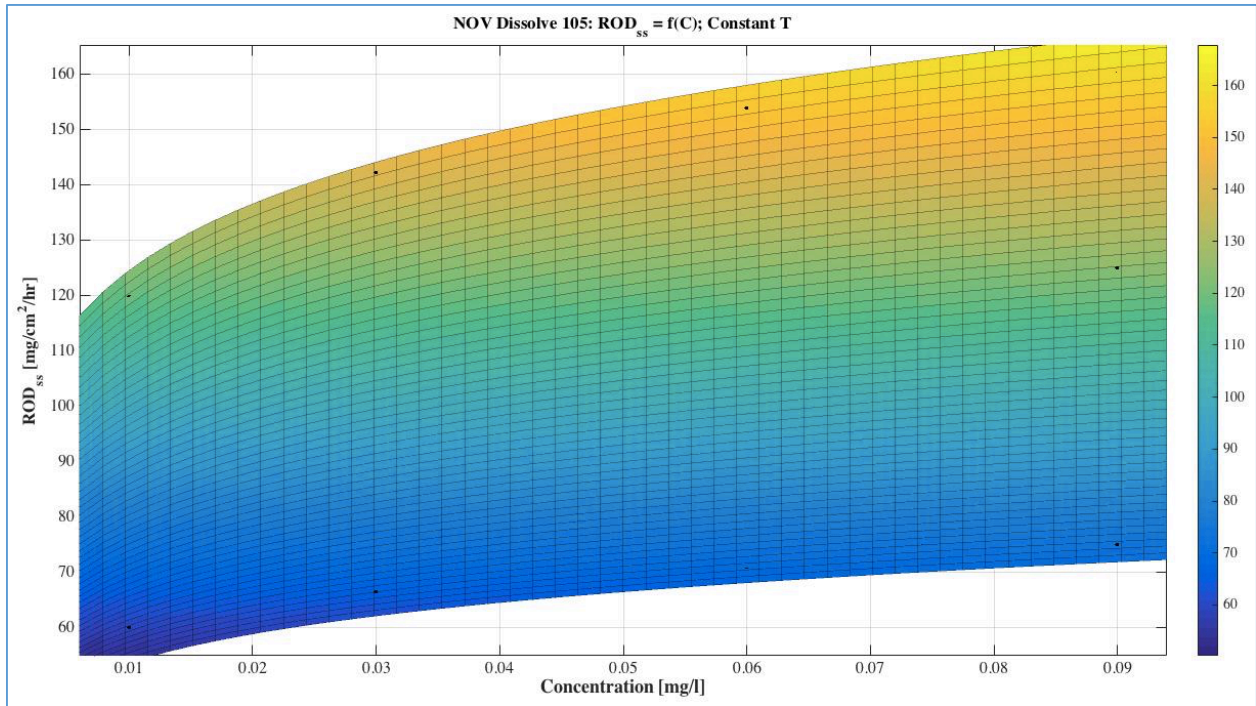


Figure 4-63: Rotated surface plot shown perpendicular to the ROD-Concentration (Z-X) plane for material 105

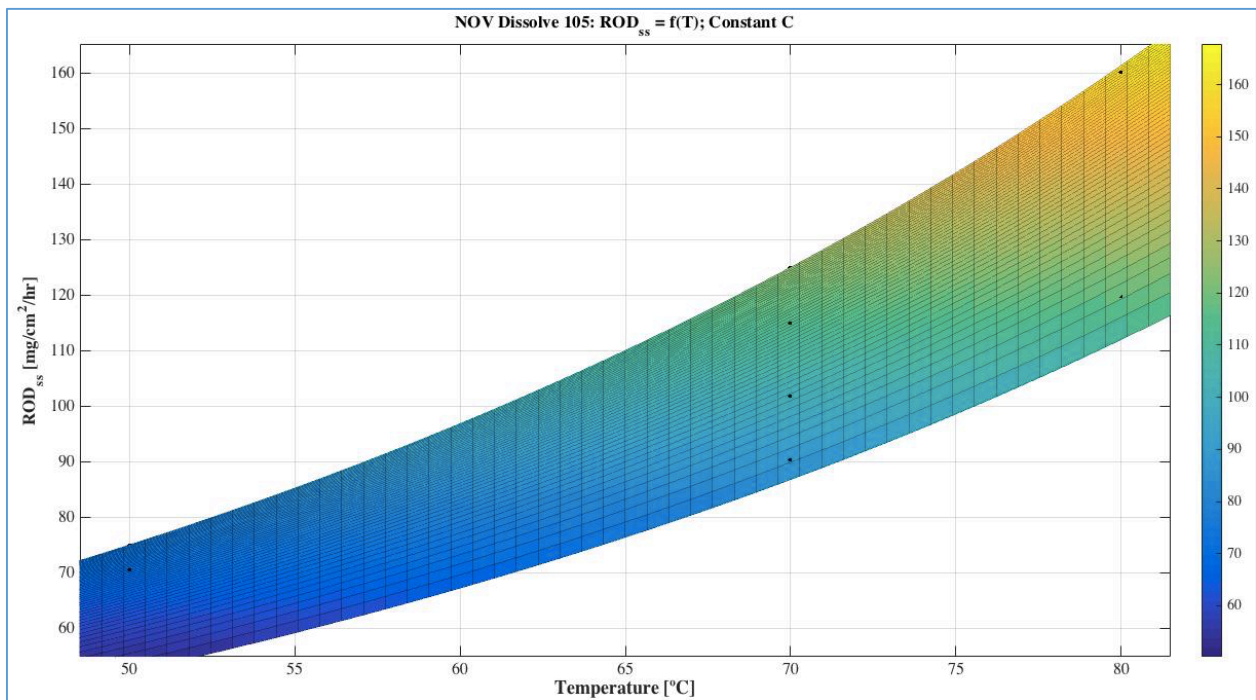


Figure 4-64: Rotated surface plot shown perpendicular to the ROD-Temperature (Z-Y) plane for material 105

The 3-D surface plot and the corresponding Dissolve Rate Predictor equation for the material NOV Dissolve 106 are shown below.

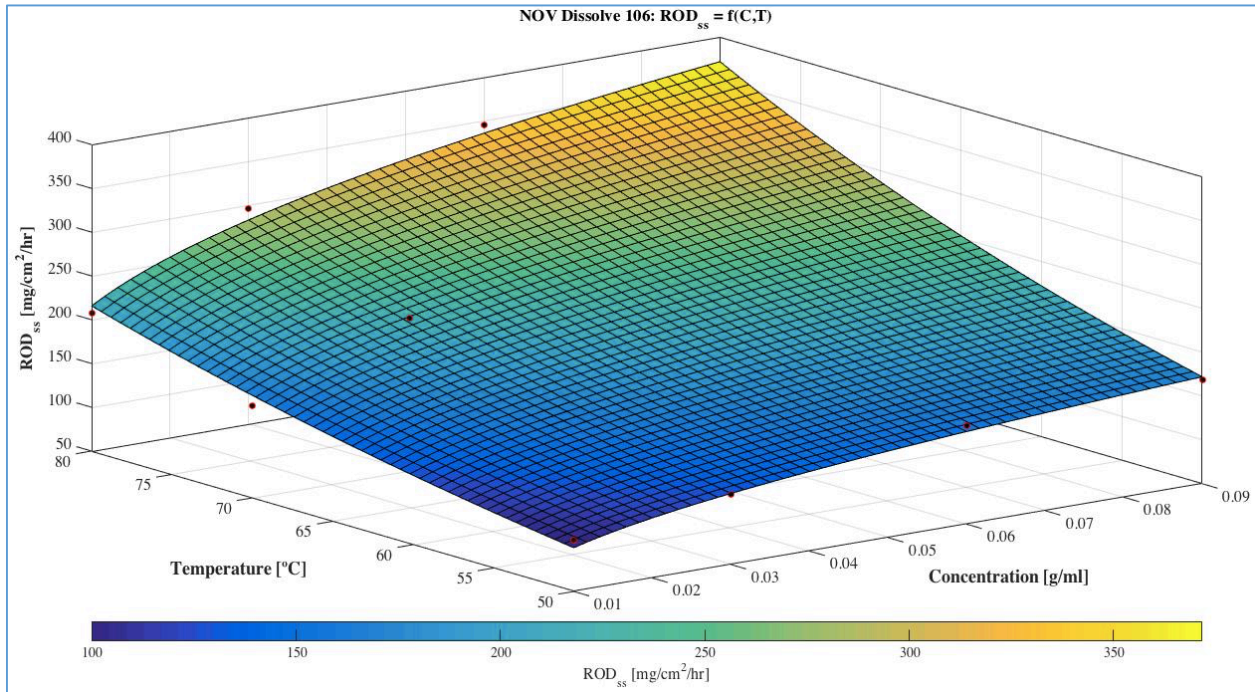


Figure 4-65: Surface plot showing ROD_{ss} as a function of both temperature and concentration for material 106

Table 7: Material coefficients for NOV Dissolve 106

Material Coefficient	Value for Material 106
b_1	86.57
b_2	0.2475
b_3	0.02566
R-square	0.9905

Thus, the equation that predicts the dissolution behaviour, i.e., the Dissolve Rate Predictor of material 106 at different temperatures and NaCl concentrations is as shown below:

$$ROD_{ss} = f(C, T) = 86.57 * C^{0.2475} * e^{0.02566T} \quad (4.12)$$

The 3-D surface plot and the corresponding Dissolve Rate Predictor equation for the material NOV Dissolve 202 are shown below.

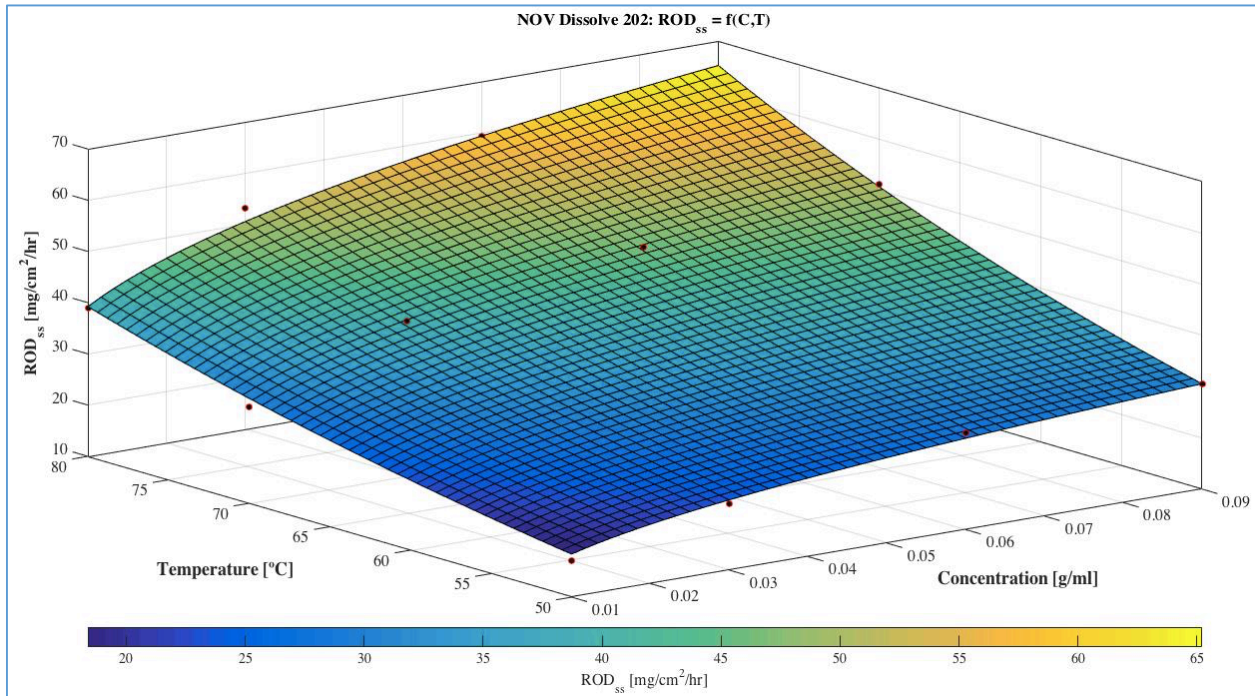


Figure 4-66: Surface plot showing ROD_{ss} as a function of both temperature and concentration for material 202

Table 8: Material coefficients for NOV Dissolve 202

Material Coefficient	Value for Material 202
b_1	15.09
b_2	0.2312
b_3	0.02526
R-square	0.9918

Thus, Dissolve Rate Predictor of material 202 at different temperatures and NaCl concentrations is as shown below:

$$ROD_{ss} = f(C, T) = 15.09 * C^{0.2312} * e^{0.02526T} \quad (4.13)$$

The 3-D surface plot and the corresponding Dissolve Rate Predictor equation for the material NOV Dissolve 301 are shown in this page.

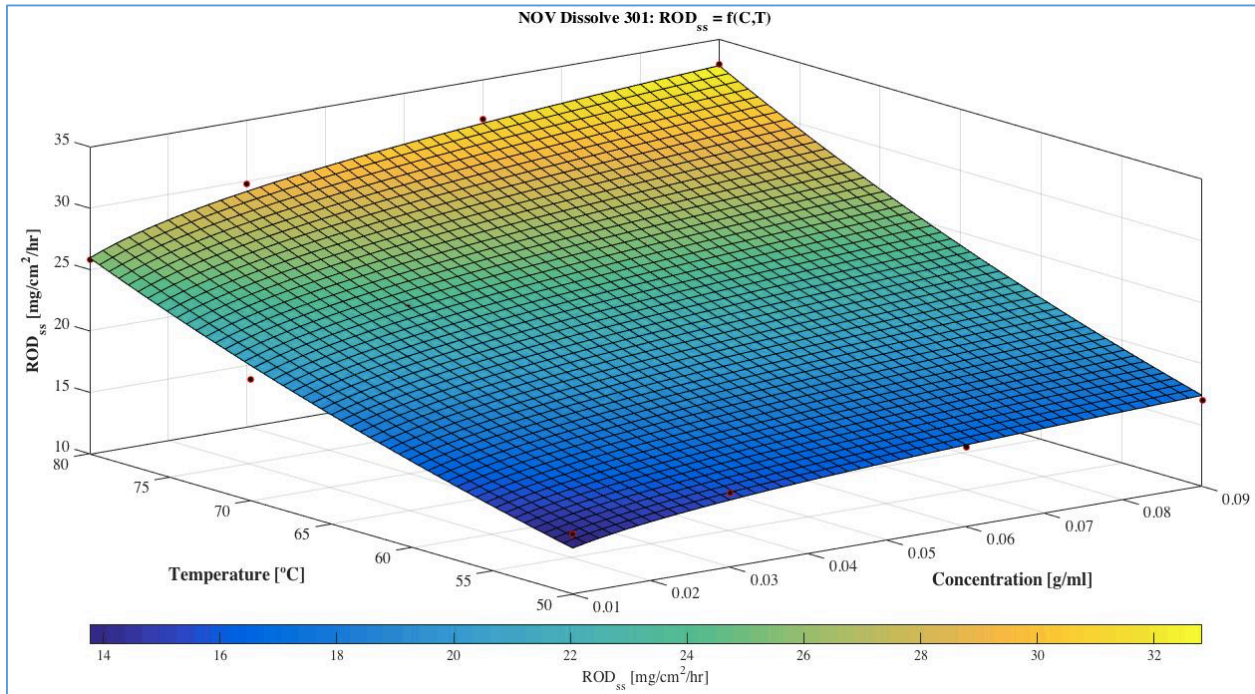


Figure 4-67: Surface plot showing ROD_{ss} as a function of both temperature and concentration for material 301

Table 9: Material coefficients for NOV Dissolve 301

Material Coefficient	Value for Material 301
b_1	7.839
b_2	0.1071
b_3	0.02112
R-square	0.9915

Thus, Dissolve Rate Predictor of material 301 at different temperatures and NaCl concentrations is as shown below:

$$ROD_{ss} = f(C, T) = 7.839 * C^{0.1071} * e^{0.02112T} \quad (4.14)$$

In this section, Dissolve Rate Predictors were developed for each of the four dissolvable materials based on experimental data as summarised in Table 10.

Table 10: Dissolve Rate Predictor Summary

Material	Dissolve Rate Predictor $ROD_{ss} = f(C, T) = b_1 * C^{b_2} * e^{b_3 T}$
NOV Dissolve 105	$ROD_{ss} = f(C, T) = 28.75 * C^{0.1327} * e^{0.0255T}$
NOV Dissolve 106	$ROD_{ss} = f(C, T) = 86.57 * C^{0.2475} * e^{0.02566T}$
NOV Dissolve 202	$ROD_{ss} = f(C, T) = 15.09 * C^{0.2312} * e^{0.02526T}$
NOV Dissolve 301	$ROD_{ss} = f(C, T) = 7.839 * C^{0.1071} * e^{0.02112T}$

The above Dissolve Rate Predictors can be used to determine the steady state Rate of Dissolution of these four materials at a given temperature and NaCl concentration in the test fluid. The predictive model is found to be consistent with the observations and trends discussed in previous chapters (Sections 4.2, 4.3 and 4.4.1).

Note that these predictors are valid in the temperature range between 50 - 80 °C and NaCl concentrations between 1% - 9%. Another point to note is that it is the chloride content which is important for the dissolution process and not necessarily the NaCl content. But the Dissolve Rate Predictor has been set up in terms of NaCl concentration. For an unknown fluid type, by determining its chloride content, an equivalent NaCl concentration can be directly obtained by using equation 4.5.

The objectives achieved and conclusions drawn at the end of Stage IV experiments in Section 4.4 have been summarised below:

- The behaviour of the different dissolvable materials at temperatures between 50 - 80 °C in fluids with NaCl concentrations between 1% - 9% were charted. These were found to be consistent with the results and analysis presented in the Stage I – Stage III experiments.
- An empirical model called the ‘Dissolve Rate Predictor’ was developed by application of regression analysis on the sample dissolution test data. This predictor allows one to predict the steady state Rate of Dissolution of dissolvable materials at given temperature and fluid conditions.

4.5 Dissolvable Ball Selection based on Sample Dissolution

Test Results

In the previous chapter, Dissolve Rate Predictors were developed based on extensive dissolution experiments conducted on cylindrical samples of the four dissolvable materials. The predominant application of dissolvable materials is in the form of spherical balls for stimulation operations as outlined in Section 2.3.1. The sizes of such frac balls can range from 2.0 inches to 4.5 inches. However, owing to the steep prices of these dissolvable balls, the dissolution tests were conducted on small cylindrical samples of dissolvable materials.

In Section 4.1, it was established that the steady Rate of Dissolution (ROD_{ss}) is an intensive material property which is constant for a specific material under given temperature and fluid conditions, and is independent of size or shape. This property shall be used to translate the results from cylindrical sample testing to predict the dissolution behaviour of balls.

In Section 4.5.1, an analytical model has been developed to predict the reduction in diameter of dissolvable balls as a function of time for given temperature and fluid type. This ‘Dissolvable Ball Size Calculator’ is based on the steady state ROD under given conditions. Thereafter, Section 4.5.2 describes a detailed stepwise workflow to select the right dissolvable ball material given the downhole conditions and operational requirements.

4.5.1 Developing a Dissolvable Ball Size Calculator

At present, the primary application of dissolvable materials in the oil and gas industry is in the form of dissolvable balls. In this section, an analytical model has been developed to determine the time dependence of the reduction in diameter of dissolvable balls based on the steady state ROD values.

A fixed ball-seat tubular is run downhole as an integral part of the MSF completion string below fracturing sleeves. Frac balls are circulated down from surface to open the fracturing sleeves before landing on the fixed seat (Figure 2-10). The ball-on-seat system serves as a one-way barrier to isolate fluids and pressures above the ball when pumping stimulation fluids into the reservoir. These applications have been discussed in detail in Section 2.3.

Figure 3-1 shows a ball landed on an NOV i-Seat. The NOV i-Seat consists of a housing made from similar material to that of the completion tubing. A cast iron seat is installed inside this housing. The top and bottom of the i-Seat has premium tubing threads for connecting with the tubing string. After being dropped from the surface, the ball lands on the i-Seat as shown in the figure and the contact area between the ball and the seat is such that it forms a complete seal thereby isolating the pressure above the ball. In this figure, D_{ball} and D_{seat} are used to denote the initial diameter of the ball and inside diameter of the seat.

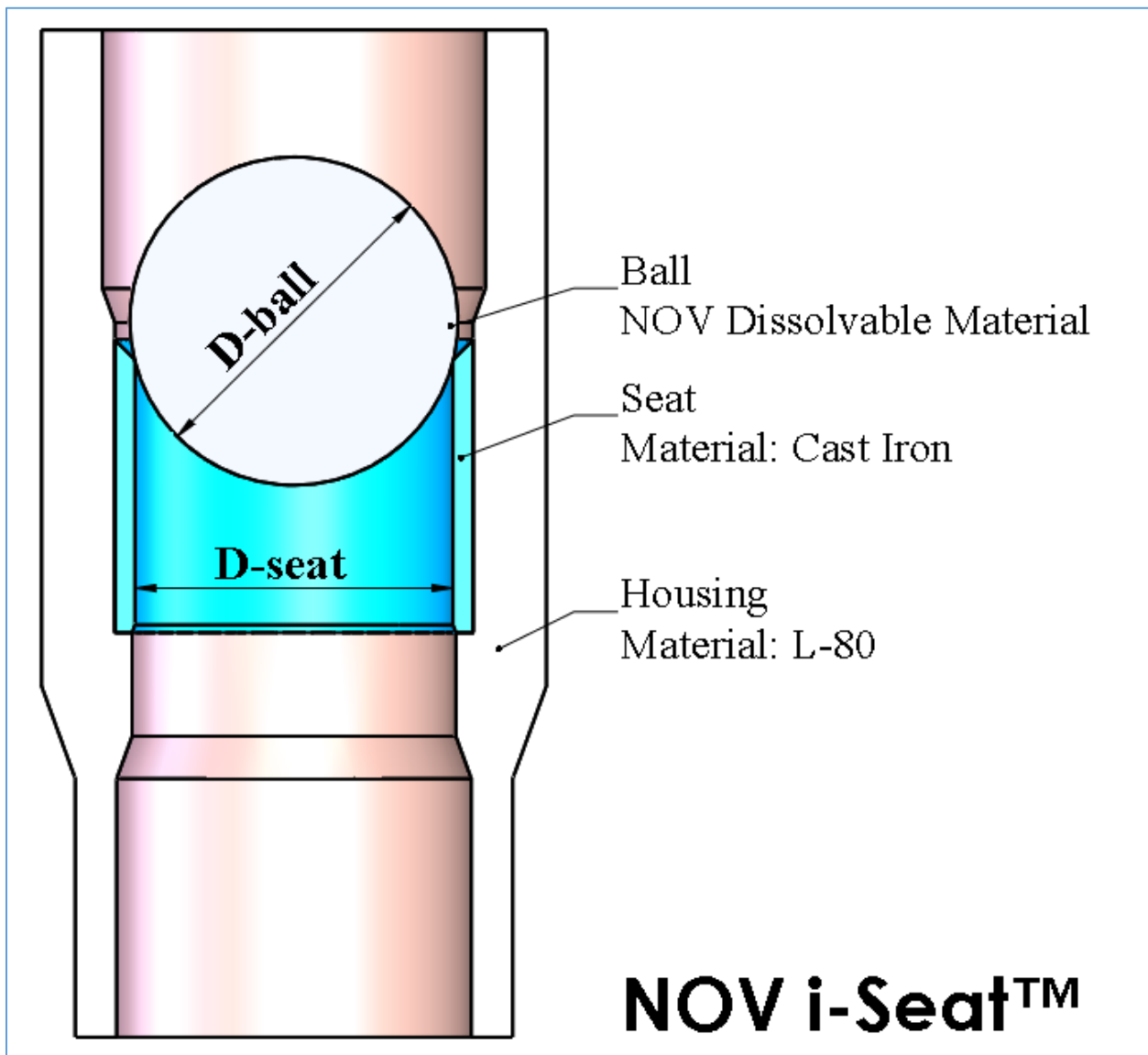


Figure 4-68: Ball shown landed on an NOV i-Seat [28]

The size of the ball is chosen based on the required maximum pressure from above that the ball-seat system is expected to experience. The size of the ball relative to the seat's inner diameter is commonly described by the term 'overlap'. Overlap is defined as follows:

$$Overlap (\%) = \frac{D_{ball} - D_{seat}}{D_{seat}} * 100 \quad (4.15)$$

Ball-seat systems with higher overlaps will be able to withstand higher pressure values before failure. Typical overlap values are between 2% - 4%. In addition to the overlap, the maximum pressure rating of a ball-seat system is also a function of the yield strength and the ultimate tensile strength for metallic balls. Thus, the ball size is chosen such that there is sufficient overlap to be able to achieve the required maximum pressure rating.

When using a dissolvable ball in downhole applications, typical operational requirements are as follows:

- The dissolvable ball is expected to stay on seat for a minimum period, t_{min} , to allow the operator sufficient time to carry out different well operations that require the ball to act as a barrier from above. This minimum period is determined based on the typical times required to carry out the various operations while allowing adequate time to account for unexpected delays.
- The dissolvable ball should not stay on seat for more than a certain maximum period, t_{max} . In other words, by this maximum period, the ball must dissolve enough such that the reduction in its size allows it to pass through the seat. This is to allow subsequent well operations to be carried out or to allow production.

Thus, in this section, an analytical method has been developed to predict the variation in the diameter of dissolvable balls as a function of time based on the Rate of Dissolution (ROD) values. By using this calculator, one can determine how long it takes for a ball to gradually dissolve such that its diameter becomes slightly smaller than the seat inner diameter (D_{seat}). At this point, the ball is expected to pass through the seat.

This ball size calculator is based mainly on the definition of Rate of Dissolution (ROD) presented in Section 4.1. This calculator aims to translate the ROD values into reduction in diameters of the

dissolvable balls, i.e., for a given material how long does it take for the diameter to reduce from an initial value, D_i to a final value, D_f .

It was established in section 4.1 that ROD_{ss} is constant for a given dissolvable material at a specific temperature and test fluid type (NaCl concentration) irrespective of the size or shape of the tested material. Hence, the ROD_{ss} value may be applied to determine the dissolution effect on a ball.

The experimental variation of ROD with time has been previously broken down into a transient period and steady state period in Section 4.1.3. A simplified version is shown in Figure 4-69.

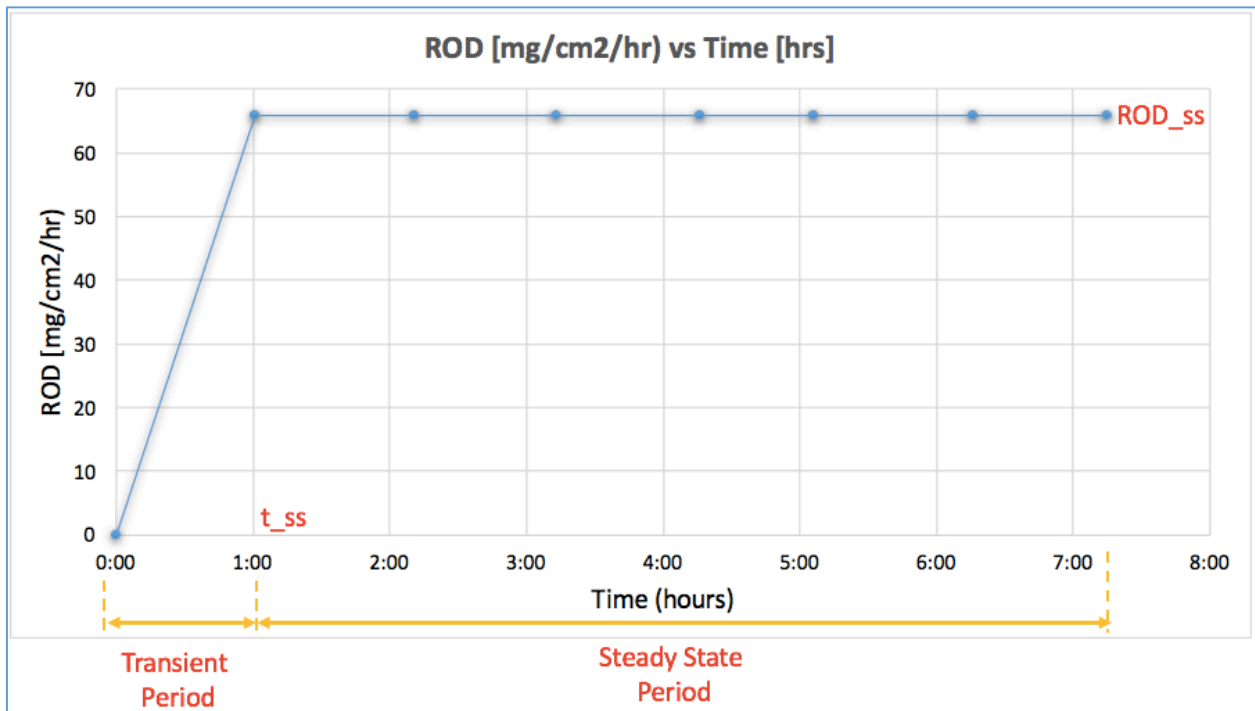


Figure 4-69: Variation of ROD with time under constant temperature and fluid conditions

In this representation, the ROD is seen to be linear until the ‘Time to Reach Steady State’ (t_{ss}) has been reached. Once steady state has been reached, the ROD value is taken as being constant and equal to the steady state value ROD_{ss} until end of the dissolution process (denoted as t_{end}).

This can be represented by the following equations –

$$ROD(t) = \begin{cases} \frac{ROD_{ss}}{t_{ss}} \cdot t, & 0 \leq t \leq t_{ss} \\ ROD_{ss}, & t_{ss} < t < t_{end} \end{cases} \quad (4.16)$$

Objective of Derivation: Based on above model of ROD, the following derivation aims to determine the time dependence of the diameter of a dissolvable ball. Using this calculator, one can predict the total time taken for the diameter of a dissolvable ball to go from an initial value D_i to a final value D_f .

Assumptions:

- i. The dissolution of the ball is uniform and it maintains its spherical shape throughout the dissolution process. This uniformity in shape has been observed during the dissolution tests on the cylindrical samples (Section 4.1.2).
- ii. The average density of the ball remains constant

Derivation:

From equation 4.4, the ROD for a given material under given temperature & fluid can be written as:

$$ROD_t = \frac{|m_t - m_{t-\Delta t}|}{\Delta t \cdot A_t} \quad (4.17)$$

where

- t is the running time counted from when the dissolvable material first contacts the brine
- Δt is the corresponding time interval in hours.
- m is mass in mg
- A is surface area in cm^2

When $\Delta t \rightarrow 0$, by the fundamental theorem of calculus [59], we have:

$$ROD(t) = \frac{dm}{dt} \cdot \frac{1}{A(t)} \quad (4.18)$$

Note that ROD is shown as only a function of time (t) since we are considering a given material under constant temperature and fluid conditions.

The surface area of a sphere, $A(t)$ is a function of time, t and can be expressed as shown below. Note that the diameter is changing and hence, is a function of time as well.

$$A(t) = \pi \cdot D(t)^2 \quad (4.19)$$

The mass of a sphere, $m(t)$ is expressed below based on the standard formula for volume of a sphere. Here, the density, ρ is assumed to be constant.

$$m(t) = \rho \cdot \frac{\pi \cdot D(t)^3}{6} \quad (4.20)$$

Differentiating Eq. 4.20,

$$\frac{dm}{dt} = \rho \cdot \frac{\pi \cdot D(t)^2}{2} \cdot \frac{dD}{dt} \quad (4.21)$$

Substituting equations 4.19 and 4.21 in Eq. 4.18,

$$ROD(t) = -\frac{\rho}{2} \cdot \frac{dD}{dt} \quad (4.22)$$

In order to maintain a positive value of $ROD(t)$, a negative sign has been added to the equation since dD/dt is always negative as the ball's diameters reduces with time.

The diameter of the ball at different times has been denoted by the notations as seen in Table 2.

Table 11: Diameter of the ball at different times

Time	Diameter, D
$t=0$	Initial diameter, D_i
$t=t_{ss}$	Diameter at start of steady state period (or at end of transient period), D_{ss} .
$t=t$	Diameter of the ball at time, t denoted by $D(t)$
$t=t_{end}$	Diameter of the ball is zero, i.e., fully dissolved

Transient phase analysis

In Figure 4-69, first consider the transient state dissolution period, i.e., when $0 \leq t \leq t_{ss}$. In this period, from equation 4.16-

$$ROD(t) = \frac{ROD_{ss}}{t_{ss}} \cdot t \quad (4.23)$$

From equations 4.22 and 4.23, the RHS terms can be equated resulting in:

$$\begin{aligned} -\frac{\rho}{2} \cdot \frac{dD}{dt} &= \frac{ROD_{ss}}{t_{ss}} \cdot t \\ \Rightarrow -dD &= \frac{ROD_{ss}}{t_{ss}} \cdot \frac{2}{\rho} \cdot t \cdot dt \end{aligned}$$

From Table 11, integrating from $t=0$ to $t=t$ where $t \leq t_{ss}$:

$$\begin{aligned} -\int_{D_i}^{D(t)} dD &= \int_{t=0}^{t=t} \frac{ROD_{ss}}{t_{ss}} \cdot \frac{2}{\rho} \cdot t \cdot dt \\ \Rightarrow D_i - D(t) &= \frac{ROD_{ss}}{t_{ss}} \cdot \frac{2}{\rho} \cdot \frac{t^2}{2} \\ \Rightarrow D(t) &= D_i - \frac{ROD_{ss}}{\rho \cdot t_{ss}} \cdot t^2 ; 0 \leq t \leq t_{ss} \end{aligned} \quad (4.24)$$

Equation 4.24 captures the dependence of the ball diameter as a function of time during the transient period.

At $t=t_{ss}$,

$$D(t = t_{ss}) = D_{ss} = D_i - \frac{ROD_{ss}}{\rho} \cdot t_{ss} ; t = t_{ss} \quad (4.25)$$

The diameter at the end of the transient phase, D_{ss} is given by Eq. 4.25. D_{ss} is dependent on ROD_{ss} , density, initial diameter (D_i) and t_{ss} . All of these parameters are constant for a given material at specific temperature and fluid type. Therefore, the diameter at the end of transient phase, D_{ss} is also constant for a specific material under given conditions.

Steady state phase analysis

In Figure 4-69, moving on to the steady state dissolution period, i.e., when $t_{ss} < t \leq t_{end}$, from Eq. 4.16, we have -

$$ROD(t) = constant = ROD_{ss} \quad (4.26)$$

From Equations 4.22 and 4.26, the RHS terms can be equated resulting in:

$$\begin{aligned} -\frac{\rho}{2} \cdot \frac{dD}{dt} &= ROD_{ss} \\ \Rightarrow -dD &= \frac{2}{\rho} \cdot ROD_{ss} \cdot dt \end{aligned}$$

From Table 11, integrating from $t=t_{ss}$ to $t=t$ where $t > t_{ss}$:

$$\begin{aligned} -\int_{D_{ss}}^{D(t)} dD &= \int_{t=t_{ss}}^{t=t} \frac{2}{\rho} \cdot ROD_{ss} \cdot dt \\ \Rightarrow D_{ss} - D(t) &= \frac{2}{\rho} \cdot ROD_{ss} \cdot (t - t_{ss}) \end{aligned}$$

$$\Rightarrow D(t) = D_{ss} - \frac{2}{\rho} \cdot ROD_{ss} \cdot (t - t_{ss}); t_{ss} < t \leq t_{end} \quad (4.27)$$

Substituting for D_{ss} from Eq. 4.25 in Eq. 4.27:

$$\Rightarrow D(t) = D_i - \frac{ROD_{ss}}{\rho} \cdot (2t - t_{ss}); t_{ss} < t \leq t_{end} \quad (4.28)$$

Equation 4.28 captures the variation in ball diameter as a function of time in the steady state period.

The upper limit of time, t_{end} when the ball diameter becomes zero is determined as shown below -

$$D(t = t_{end}) = D_i - \frac{ROD_{ss}}{\rho} \cdot (2t_{end} - t_{ss}) = 0$$

$$\Rightarrow t_{end} = \frac{1}{2} \cdot \left[t_{ss} + \frac{\rho}{ROD_{ss}} \cdot D_i \right] \quad (4.29)$$

Combining Eq. 4.24, 4.28 and 4.29, the diameter of a dissolvable ball at any time, t can be expressed as:

$$D(t) = \begin{cases} D_i - \frac{ROD_{ss}}{\rho \cdot t_{ss}} \cdot t^2, & 0 \leq t \leq t_{ss} \\ D_i - \frac{ROD_{ss}}{\rho} \cdot (2t - t_{ss}), & t_{ss} < t \leq t_{end} \end{cases} \quad (4.30)$$

Equation 4.30 captures the variation in the diameter of a dissolvable ball at any given time, t .

Since one is often interested in estimating the time taken by a ball to reach a given diameter, equation 4.30 can be rearranged to express the time taken by the ball to dissolve to any diameter $D(t)$ as shown below in equation 4.31.

$$t = \begin{cases} \sqrt{(D_i - D(t)) \cdot \frac{\rho}{ROD_{ss}} \cdot t_{ss}}, & D_i \geq D(t) \geq D_{ss} \\ \frac{1}{2} \cdot \left[t_{ss} + \frac{\rho}{ROD_{ss}} \cdot (D_i - D(t)) \right], & D_{ss} > D(t) \geq 0 \end{cases} \quad (4.31)$$

In the above equation, the value of the diameter at end of transient phase, D_{ss} is given by Eq. 4.25.

In case of a ball-seat systems, to determine how long a ball lasts on a seat, it is reasonable to assume that when the diameter of the ball reaches the diameter of the seat, it is expected to pass through seat. Therefore, one can determine the total time required for a ball of initial diameter D_i to pass through a seat of diameter D_{seat} by substituting $D(t) = D_{seat}$ in equation Eq. 4.31 to find the corresponding time, t .

Figure 4-70 plots the diameter of a NOV 105 ball as a function of time by using the analytical models presented in Eq. 4.30 and 4.31. The inputs used to generate this plot are listed below –

- Temperature: 80 °C
- Fluid type: 1% NaCl
- Start of steady state is at $t_{ss} = 1\text{h } 53\text{m}$ or 1.88 hours
- Steady state $ROD_{ss} = 119.96 \text{ mg/cm}^2/\text{hr}$ (Refer to Table 4)
- Density of material = 1.724 g/cc or 1724 mg/cc
- Initial Ball Diameter, $D_i = 3.625 \text{ in.}$ or 9.208 cm

The Matlab code used to generate this plot is available in Appendix II.

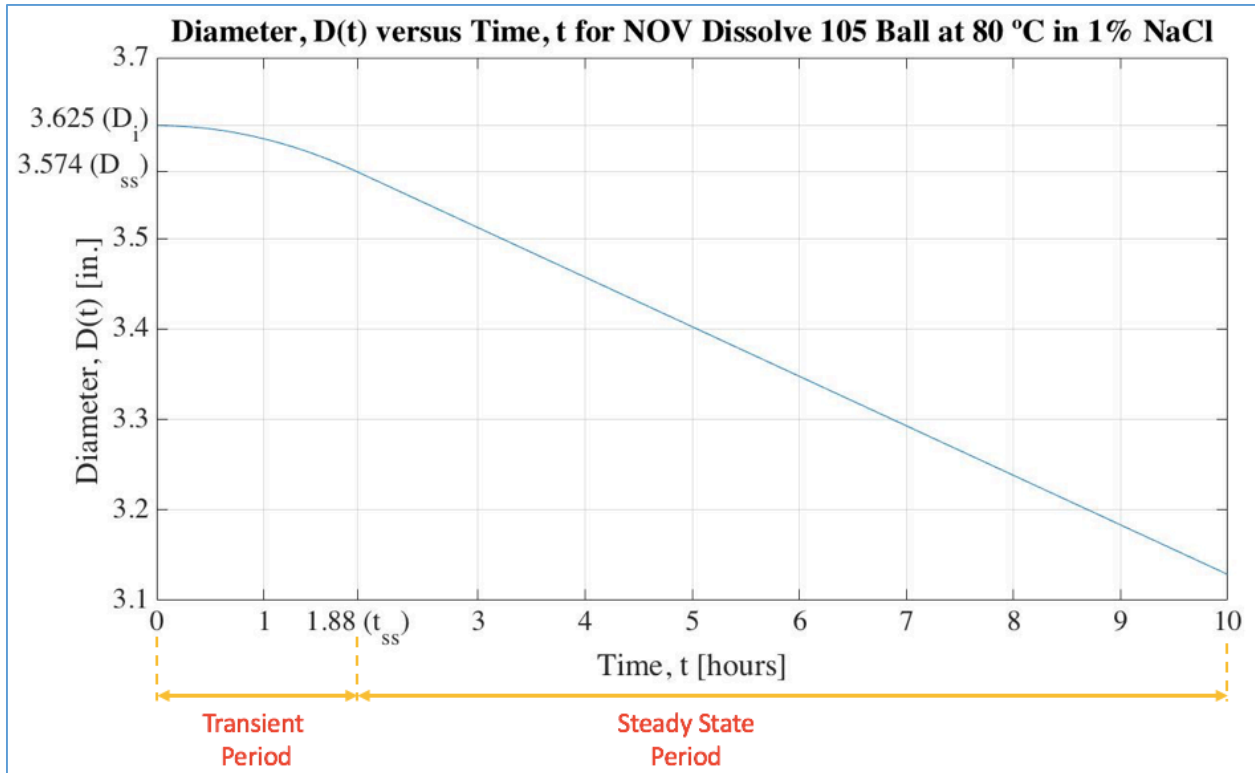


Figure 4-70: Diameter of a 3.625” NOV Dissolve 105 ball as a function of time at 80 °C in 1% NaCl

From its initial value of $D_i = 3.625$ in., the diameter follows a parabolic trend versus time during the transient state period upto $t = t_{ss}$. The diameter at the end of the transient period is $D_{ss} = 3.574$ inches. Beyond t_{ss} , the diameter of the ball follows a steady linear reduction with time. Assuming a scenario where the seat size that the ball sits on is 3.5 in., it can be seen from the plot that the first time that the ball’s diameter will be smaller than 3.5 in. is at 3.22 hours. Thus, for the given ball size, material and downhole conditions, the ball will pass through the seat at ≈ 3.2 hours.

Based on the above analytical model, a dissolvable ball size calculator can be implemented in any program or spreadsheet based on equation 4.31. The calculator’s algorithm and evaluation procedure is summarized below in Table 12.

In conclusion, using the Dissolvable Ball Size Calculator, one can predict the size of a dissolvable ball at various times by making use of their ROD values. This in turn, allows an accurate estimation of how long it takes for a dissolvable ball to pass through a ball-seat with a specified inner diameter.

Table 12: Dissolvable Ball Size Calculator Summary

Inputs
<ul style="list-style-type: none"> • D_i (cm): Initial ball diameter. • D(t) (cm): The desired final ball diameter in cm. In ball-seat systems, the desired final diameter is set to be equal to or slightly smaller than the seat's inner diameter, D_{seat}. This shall allow one to determine the time at which the dissolving ball shall start to pass through the seat. • ρ (mg/cm³): Density of the dissolvable material. • ROD_{ss} (mg/cm²/hr): Steady state Rate of Dissolution of the ball material under the given temperature & NaCl concentration in the fluid. The ROD_{ss} value may be determined directly from cylindrical sample dissolution tests or may be obtained from the Dissolve Rate Predictor developed in Section 4.4.2. • t_{ss} (h): This can be determined from sample dissolution tests at given temperature and fluid conditions. Alternatively, the t_{ss} values for the various dissolvable materials may be recorded at the different conditions and this average t_{ss} value can be used. If this value is not available, an approximate output can be obtained by using t_{ss}=0, i.e., neglecting the transient period and assuming that the dissolution process reaches steady state instantaneously. One must be aware that when using t_{ss}=0, the output time, t shall be slightly lower than reality since one is neglecting the slower dissolution rates during the initial transient period. In other words, we will underpredict the time when the ball goes through the seat.
Calculation Method
<ul style="list-style-type: none"> • Based on Equation 4.31
Outputs
<ul style="list-style-type: none"> • t (h): Total time required by the ball to dissolve to diameter D(t) from initial diameter D_i • Plot of diameter of the dissolvable ball as a function of time for the given temperature and fluid type.

4.5.2 Dissolvable Ball Selection Workflow

In this sub-section, a stepwise workflow is devised to select the correct dissolvable ball material for any given downhole condition and operational requirement. This is done by consolidating the experimental results, empirical models and analytical calculators developed throughout Chapter 4.

The Dissolve Rate Predictor formulated in Section 4.4.2 is an empirical model developed to forecast the steady state Rate of Dissolution (ROD_{ss}) for specific temperature and fluid type based on the sample dissolution tests conducted on different materials. The Dissolvable Ball Size Calculator is an analytical model developed in Section 4.5.1 to simulate the duration that a dissolvable ball lasts on a downhole ball-seat system. These two models form the basis of the Dissolvable Ball Selection Workflow outlined in this sub-section.

By using this workflow, one is able to directly select the dissolvable material type for a ball without spending excessive time and money on performing full-scale testing on expensive dissolvable balls for various combinations of downhole conditions and operational requirements. The main inputs required to initiate this selection process are summarised in Table 13.

Table 13: Inputs required for implementing the Dissolvable Ball Selection Workflow

Inputs to Dissolvable Ball Selection Workflow	
I. Downhole Conditions	<p>a. Downhole Temperature, T</p> <p>This is the temperature of the well at the location of the ball-seat system. The downhole temperature has a major influence on dissolution rates of materials.</p>
	<p>b. Downhole Fluid Type → NaCl concentration, C</p> <p>The chloride concentration in the downhole fluid plays a key role in selection of the dissolvable material type. For a fluid whose chloride content is unknown, chloride meters can be used to directly determine the chloride content in the fluid. This can then be easily expressed in terms of equivalent NaCl concentration using equation 4.5.</p>

II. Operational Requirements	<p>c. Seat Size, D_{seat}</p> <p>This refers to the inner diameter of the seat, D_{seat} and is driven by the allowable restrictions and flow areas in the overall completion design for a well.</p>
	<p>d. Required Pressure Differential → Ball diameter, D_i</p> <p>This refers to the pressure differential from above that the ball-seat system is expected to isolate during the operations. This requirement directly determines the required initial ball diameter to hold a particular pressure based on the necessary overlap that allows the ball to withstand this pressure (Eq. 4.15).</p>
	<p>e. Time Period, t_{min} and t_{max}</p> <p>The dissolvable ball is expected to stay on seat for a minimum period, t_{min}, to allow the operator sufficient time to carry out the different well operations that require the ball to act as a barrier from above. This minimum period is determined based on the typical times required to carry out the various operations while allowing adequate time to account for unexpected delays.</p> <p>The dissolvable ball should not stay on seat for more than a certain maximum period, t_{max}. In other words, by this maximum period, the ball must dissolve enough such that the reduction in its size allows it to pass through the seat. This is to allow subsequent well operations to be carried out or to allow production.</p>

Based on the above inputs, the complete Dissolvable Ball Selection Workflow outlined in Figure 4-71 can be used to select the right material for any given operational and downhole condition.

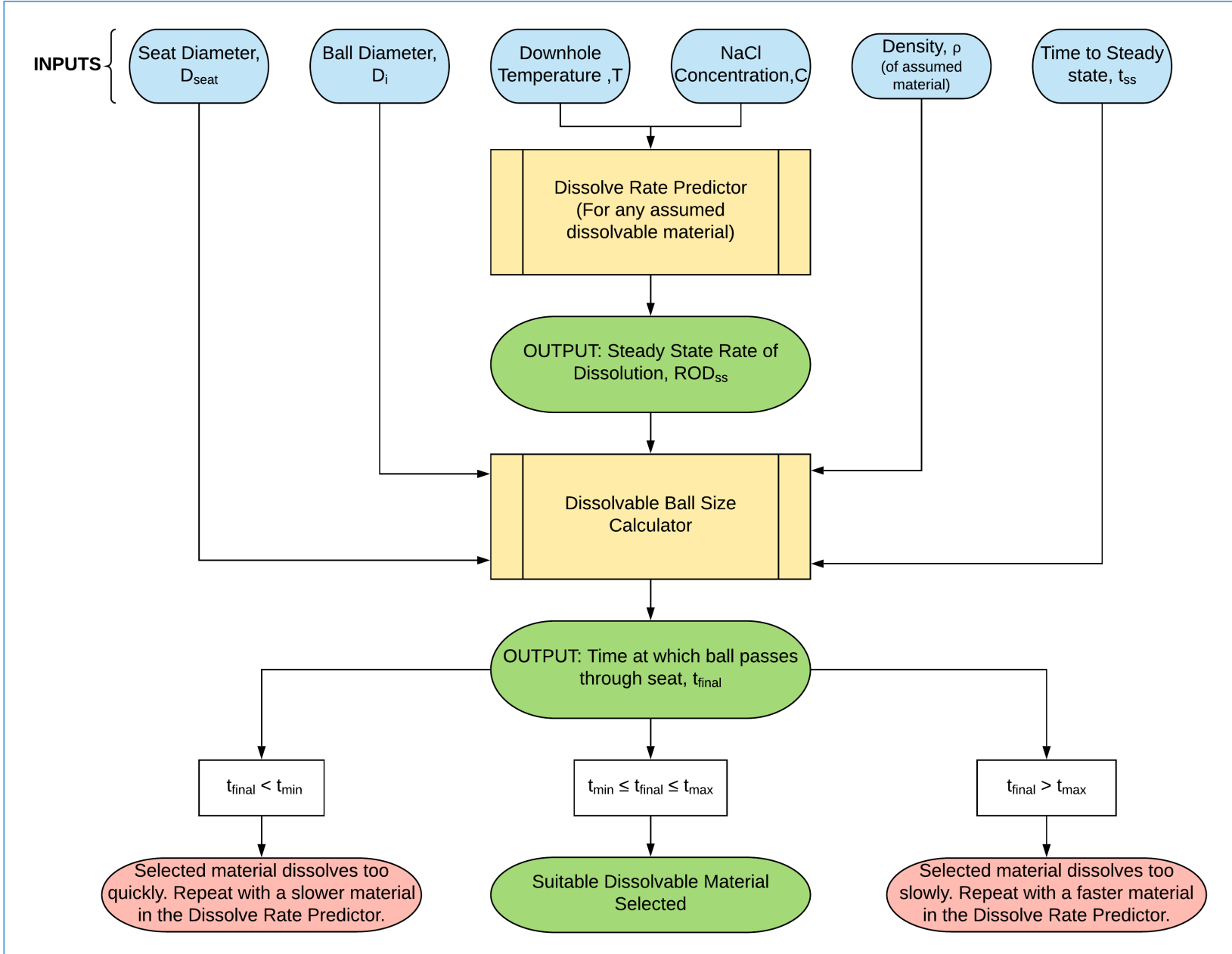


Figure 4-71: Dissolvable Ball Selection Workflow

The general methodology of this workflow is to make an initial assumption of the dissolvable material that might be suitable for a given application. Thereafter, the Dissolve Rate Predictor of that assumed material is used to predict its steady state ROD under the given temperature and fluid conditions. The ROD_{ss} value from the Dissolve Rate Predictor is used as input along with operational requirement inputs to the Dissolvable Ball Size Calculator. This stage of the workflow outputs the time, t_{final} that the dissolvable ball is expected to stay on seat.

If this time falls between the maximum and minimum time period that the ball is required to stay on seat, then the initial assumed dissolvable material is suitable for the given application. If the ball-on-seat time (t_{final}) falls outside the required operational time period, then the initial dissolvable material selection is incorrect. In such a case, a faster or a slower dissolvable material is chosen and the steps of the selection workflow need to be repeated.

The main features and advantages of implementing the Dissolvable Ball Selection Workflow are:

- While this work has only focused on four selected dissolvable materials, the selection approach is transferable and can be applied to other current and to-be-developed dissolvable materials.
- This workflow can be easily implemented in any program to aid companies in selecting the right materials for their application.
- The workflow can be used to quickly identify suitable materials for various applications of dissolvable balls for different combinations of downhole conditions and operational requirements.
- Dissolvable balls are priced high and it is a tedious, time-consuming and expensive process to perform full-scale testing on the numerous dissolvable ball materials for every specific acceptance criteria. Using this workflow, one can quickly narrow down to the most suitable dissolvable material for a given application and perform full-scale testing on just the shortlisted material to validate the selection workflow.

5 Conclusions and Recommendations

5.1 Conclusions

The challenges associated with the removal of traditional frac balls used in sleeve-based multistage stimulation has seen a surge in demand for the use of dissolvable frac balls. Selecting the right dissolvable frac ball for a given operational constraint and downhole condition has been a major barrier to their widespread adoption and commercialization. The present qualification process of dissolvable balls involves multiple iterations of extensive full-scale tests on several materials until the acceptance criteria for the specific application are fulfilled. There is a distinct lack of information in existing scientific literature on how to systematically select the optimal dissolvable ball. The main goal of this thesis was to simplify this tedious selection process.

A series of experiments were conducted on four dissolvable cylindrical samples from NOV to examine the effect of key downhole factors, namely, temperature and NaCl content in the brine. Thereafter, a stepwise workflow is devised that enables the selection of the most suitable dissolvable ball type to fulfil the operator's requirements. The workflow is based on utilizing empirical models formulated from experimental data and applying them in conjunction with analytical models to predict the downhole performance of dissolvable frac balls.

This novel workflow shall eliminate the need for excessive full-scale qualification testing, thereby resulting in substantial cost-savings for the company while drastically improving the overall efficiency and reliability of the selection process.

The main conclusions drawn from different sections of this work have been summarised below.

Stage I - Variations in Critical Parameters during the Dissolution Process

- Rate of Dissolution (ROD) was defined in Equation 4.3 and found to be the most convenient way of expressing the performance of a dissolvable material while accounting for the influences of size, shape, mass loss and surface area.
- Using the definition of ROD, the dissolution reaction was split into a transient period and steady-state period.

- The steady state Rate of Dissolution, ROD_{ss} is found to be an intensive property which remains constant for a given dissolvable material at a specific temperature and test fluid type (NaCl concentration) irrespective of the geometry of the tested material. Therefore, ROD_{ss} was used as the main characteristic parameter to define the speed at which dissolvable materials react with fluids.
- Under given temperature and identical test fluid, NOV Dissolve 106 was found to dissolve the fastest followed sequentially by 105, 202 and 301.

Stage II - Investigating the Effect of Concentration on Dissolution Rate

- Increasing the concentration of NaCl increases the rate of dissolution process as reflected by the increase in the ROD_{ss} values.
- The dependence of ROD_{ss} on NaCl concentration gradually decreases as the NaCl concentration gets higher.
- The above results were rationalized by examining the role of chloride ions in catalyzing the dissolution reaction by removing inhibiting magnesium hydroxide $[Mg(OH)_2]$ layers.
- Chloride ion concentration is a key factor affecting the dissolution behavior and a simple formula was presented to convert NaCl concentration to equivalent chloride ion concentration.
- The dissolvable materials listed in the decreasing order of sensitivity to changes in concentration are: Material 106, 202, 105 and 301.

Stage III - Examining the Effect of Temperature on Dissolution Rate

- The rate of dissolution reaction increases with temperature as reflected by the increase in ROD_{ss} values.
- The dependence of ROD_{ss} on temperatures rises sharply at higher temperatures.
- The above results were explained by means of the collision theory, the role of activation energy as well as the Arrhenius equation. The exponential relationship between ROD_{ss} values and temperature is in accordance with the Arrhenius equation.
- The dissolvable materials listed in the decreasing order of sensitivity to changes in temperature are: Material 202, 105, 106 and 301.

Stage IV - Combined Effect of Temperature and Concentration

- The behaviour of the different dissolvable materials at temperatures between 50 - 80 °C in fluids with NaCl concentrations between 1% - 9% were charted. These were found to be consistent with the results and analysis presented in the Stage I – Stage III experiments.
- An empirical model - ‘Dissolve Rate Predictor’ - was developed for each of the four materials by application of regression analysis to the sample dissolution test data. This predictor allows one to predict the steady state Rate of Dissolution of dissolvable materials at given temperature and fluid condition.

Dissolvable Ball Selection based on Sample Dissolution Test Results

- An analytical model called the ‘Dissolvable Ball Size Calculator’ was developed to simulate the diameter of a dissolvable ball as a function of time. This in turn, allows the prediction of how long it takes for a dissolvable ball to pass through a seat installed in the completion string.
- A stepwise workflow was devised that enables the selection of optimal dissolvable ball material for any given downhole condition and operational requirement.
- This new workflow shall eliminate the need for excessive full-scale tests on various dissolvable ball types for different environments and operational criteria. Consequently, this would result in substantial cost-savings for the company and drastically improve the overall efficiency and reliability of the selection process.
- While the present work has only focused on four chosen materials from NOV, this philosophy may be applied to optimise the qualification process of any dissolvable frac ball application.

5.2 Recommendations

The test fluid used in this work is chloride-based aqueous solution (NaCl salt) since it is one of the most common types of downhole fluids used for circulating down dissolvable frac balls. However, it would be a worthwhile endeavour to examine the effects non-chloride based completion fluids such as aqueous solutions of bromides (calcium bromide, zinc bromide) and formates (potassium formate, cesium formate). The dissolution behaviour in drilling fluids, both oil-based mud (OBM) and water-based mud (WBM), would also be of interest.

The Dissolve Rate Predictor from Section 4.4.2 is generally valid within the experimental boundaries of 50 - 80 °C and NaCl concentrations between 1% - 9%. Increasing the experimental range as well as performing more tests within the given boundaries will be beneficial to improving the accuracy of the empirical models for the different dissolvable materials.

In the present work, experiments were conducted solely on cylindrical dissolvable samples and the analytical model developed in Section 4.5.1 was used to translate the results to predict the reduction in the diameter of dissolvable balls as a function of time. It is recommended that the validity of this analytical model be verified experimentally by conducting similar dissolution tests on dissolvable balls in controlled environments. Discrepancies between the analytical model and experimental results can be addressed by introducing appropriate correction factors into the model.

The petroleum sector has only turned to dissolvable materials since the start of this decade. The main focus of the industry as well as this thesis work has been on dissolvable materials for use in reservoir stimulation applications. Although a handful of other current applications have been documented in Section 2.3.3, the industry has barely scratched the surface. Still, there is a plethora of untapped potential opportunities wherein dissolvable technology can play a vital role. Future works should look into incorporating dissolvable technology into other downhole completion and intervention equipment to increase production and operational efficiency.

Bibliography

- [1] J. L. Gidley, 1st, Ed. *Development geology reference manual: AAPG methods in exploration series, no. 10*. 1993.
- [2] A. A. Daneshy, "Hydraulic Fracturing of Horizontal Wells: Issues and Insights," presented at the SPE Hydraulic Fracturing Technology Conference, Woodlands, Texas, USA, SPE-140134-MS, 2011.
- [3] J. Triepke. (2014). *Well Completion 101 Part 3: Well Stimulation*. Available: <https://info.drillinginfo.com/well-completion-well-stimulation/> [Accessed: March 10, 2018]
- [4] N. Carrejo, J. C. Welch, M. Solfronk, and M. H. Johnson, "Improving Flow Assurance in Multizone Fracturing Treatments in Unconventional Hydrocarbon Reservoirs With High Strength Corrodible Tripping Balls," presented at the SPE Latin America and Caribbean Petroleum Engineering Conference, Mexico City, Mexico, SPE-151613-MS, 2012.
- [5] I. Aviles, M. Marya, T. Reyes Hernandez, T. Dunne, M. Dardis, and J. D. Baihly, "Application and benefits of degradable technology in open-hole fracturing," presented at the SPE Annual Technical Conference and Exhibition, New Orleans, Louisiana, USA, SPE-166528-MS, 2013.
- [6] T. R. Koloy, T. Sorheim, K. Braekke, and P. Lonning, "The Evolution, Optimization & Experience of Multistage Frac Completions in a North Sea Environment," presented at the SPE Annual Technical Conference and Exhibition, Amsterdam, Netherlands, SPE-170641-MS, 2014.
- [7] M. Salah, M. ElSebaee, P. Raouf, and A. Keshishian, "First Application of Cemented Sliding Sleeves With Degradable Drop Ball Technique Optimizes Horizontal Multistage Fracturing Operations in the Middle East: Egypt Western Desert Case Study," presented at the SPE Eastern Regional Meeting, Morgantown, USA, SPE-177284-MS, 2015.
- [8] Z. Xu, G. Agrawal, and B. J. Salinas, "Smart nanostructured materials deliver high reliability completion tools for gas shale fracturing," presented at the SPE Annual Technical Conference and Exhibition, Denver, USA, SPE-146586-MS, 2011.

- [9] Z. Walton, M. Fripp, and M. Merron, "Dissolvable Metal vs. Dissolvable Plastic in Downhole Hydraulic Fracturing Applications," presented at the Offshore Technology Conference, Houston, Texas, USA, OTC-27149-MS, 2016.
- [10] N. Jin and Q. Zeng, "Dissolvable Tools in Multistage Stimulation," presented at the SPE/IATMI Asia Pacific Oil & Gas Conference and Exhibition, Jakarta, Indonesia, SPE-186184-MS, 2017.
- [11] W. Renpu, *Advanced well completion engineering*, 3rd ed. United States of America: Gulf Professional Publishing, 2011.
- [12] K. Furui, D. Zhu, A. D. Hill, E. Davis, and B. R. Buck, "Optimization of Horizontal Well Completion Design," presented at the SPE Annual Technical Conference and Exhibition, Houston, United States of America, SPE-90579-MS, 2004.
- [13] C. Corley and J. Rike, "Tubingless Completions," in *Drilling and Production Practice*, New Orleans, United States of America, API-59-007, 1959: American Petroleum Institute.
- [14] J. A. Aasen, "Lecture Notes - Well Completion Design - Open Hole Gravel pack," ed: Department of Petroleum Engineering, University of Stavanger, 2016.
- [15] J. Bellarby, *Well Completion Design*, 1st ed. United Kingdom: Elsevier, 2009.
- [16] S. Yakeley, E. Wood, and M. J. Knebel, "Contacting the reservoir—Benefits of Horizontal Open-hole Completions," presented at the Offshore Europe, Aberdeen, UK, SPE-124074-MS, 2009.
- [17] R. C. Jones and B. Davis, "A Systematic Approach to the Integration of Upper and Lower Completions: A Strategy for Deep Gas Applications," presented at the SPE Deep Gas Conference and Exhibition, Manama, Bahrain, SPE-131774-MS, 2010.
- [18] M. J. Economides and K. G. Nolte, 3rd, Ed. *Reservoir stimulation*. Prentice Hall Englewood Cliffs, New Jersey (Schlumberger Edition), 2000.
- [19] E. Roach. (2014, March). *Proppant: The Greatest Oilfield Innovation of the 21st Century*. Available: <https://info.drillinginfo.com/proppant-the-greatest-oilfield-innovation/> [Accessed: March 6, 2018]
- [20] G. E. King, "Acidizing Concepts - Matrix vs. Fracture Acidizing," *Journal of Petroleum Technology*, vol. 38, no. 05, SPE-15279-PA, 1986.

- [21] G. Carl, *Drilling and Well Completions*, 1st ed. New Jersey, United States of America: Prentice Hall Publishing Company, 1960.
- [22] B. B. Williams, J. L. Gidley, and R. S. Schechter, *Acidizing Fundamentals*. Dallas, United States of America: SPE Monograph Series, 1979.
- [23] G. Gardiner. (2014, March). *Composites boon from hydraulic fracturing*. Available: <https://www.compositesworld.com/blog/post/composites-boon-from-hydraulic-fracturing> [Accessed: March 8, 2018]
- [24] I. Aviles, M. Dardis, and G. Jacob, "Degradable Alternative to Risky Mill-Out Operations in Plug and Perf," presented at the SPE/ICoTA Coiled Tubing & Well Intervention Conference & Exhibition, The Woodlands, Texas, USA, SPE-173695-MS, 2015.
- [25] S. Co. (2017, March). *Contrast Between Plug And Perf Method And Ball And Sleeve Method For Horizontal Well Stimulation*. Available: <http://info.stonewallco.com/stonewall-horizontal-well-stimulation> [Accessed: March 8, 2018]
- [26] M. Norris, B. Berntsen, L. Skartveit, and C. Teesdale, "Multiple proppant fracturing of horizontal wellbores in a chalk formation: evolving the process in the Valhall Field," *SPE Drilling & Completion*, vol. 16, no. 1, SPE-70133-PA, 2001.
- [27] D. G. Durst, J. T. Harris, J. D. Contreras, and D. R. Watson, "Improved Single-Trip Multistage Completion Systems for Unconventional Gas Formations," presented at the SPE Tight Gas Completions Conference, San Antonio, United States of America, SPE-115260-MS, 2008.
- [28] NOV. (2017). *i-Seat*. Available: https://www.nov.com/Segments/Completion_and_Production_Solutions/Completion_Tools/Lower_Completion/i-Seat.aspx [Accessed: March 1, 2018]
- [29] J. Baihly, J. Johnson, G. Melenyzer, and I. Aviles, "Sleeve Activation Sleeve Activation in Open-hole Fracturing Systems: A Ball Selection Study. SPE Paper 162657," presented at the SPE Canadian Unconventional Resources Conference being held, Calgary, Canada, SPE-162657-MS, 2012.

- [30] I. Seaboard International. (2016). *Seaboard™ AJ7 Ball Catcher*. Available: <https://www.global.weir/products/product-catalogue/seaboard-aj7-ball-catcher/> [Accessed: March 6, 2018]
- [31] O. S. E. Services. (2017). *Ball Catcher*. Available: <http://www.osescanada.com/services-products/ball-catcher/> [Accessed: March 6, 2018]
- [32] C. Mehus, T. Sørheim, P. Lønning, and T. Koløy, "Cemented and Cased Hole Multistage Stimulation Technology Development and Field Wide Implementation in a North Sea Chalk Oilfield," presented at the SPE Annual Technical Conference and Exhibition, Dubai, SPE-181644-MS, 2016.
- [33] G. Wozniak, "Frac Sleeves: Is Milling Them Out Worth the Trouble?," presented at the Tight Gas Completions Conference, San Antonio, Texas, SPE-138322-MS, 2010.
- [34] Z. Walton, J. Porter, M. Fripp, and G. Vargus, "Cost and Value of a Dissolvable Frac Plug," presented at the SPE/ICoTA Coiled Tubing and Well Intervention Conference and Exhibition, Houston, USA, SPE-184793-MS, 2017.
- [35] Halliburton. (2017, March). *Fas Drill® Frac Plug*. Available: <http://www.halliburton.com/en-US/ps/service-tools/drillable-tools/plugs/fas-drill-frac-plug.page> [Accessed: March 10, 2018]
- [36] M. Fripp and Z. Walton, "Degradable Metal for Use in a Fully Dissolvable Frac Plug," presented at the Offshore Technology Conference, Houston, USA, OTC-27187-MS, 2016.
- [37] M. Nichols and A. Eis, "Self-Removing Fracturing Plugs: A Study of Initial Adoption in the Williston Basin," presented at the SPE Oklahoma City Oil and Gas Symposium, Oklahoma City, USA, SPE-185107-MS, 2017.
- [38] S. Takahashi, M. Okura, T. Kobayashi, and T. Takahashi, "Development and Verification of Degradable Sealing Elements for Fully Degradable Frac Plugs," presented at the SPE Asia Pacific Unconventional Resources Conference and Exhibition, Brisbane, Australia, SPE-176917-MS, 2015.
- [39] Halliburton. (2017, March). *Illusion® Frac Plug*. Available: <http://www.halliburton.com/en-US/ps/service-tools/drillable-tools/dissolvable-tools/Illusion-Frac-Plug.page> [Accessed: March 10, 2018]

- [40] Z. Xu, B. M. Richard, and J. H. Kritzler, "Smart Gas Lift Valves Enhance Operation Efficiency of Offshore Wells," presented at the SPE Annual Technical Conference and Exhibition, New Orleans, USA, SPE-166291-MS, 2013.
- [41] N. Carrejo, O. Espinoza, H. Wibowo, and S. Gaudette, "Developing a new high-strength, lightweight material using nano-coated smart materials for oilfield applications," presented at the OTC Brasil, Rio de Janeiro, Brazil, SPE-26282-MS, 2015.
- [42] N. Carrejo, B. Kellogg, S. Gaudette, and J. Barnard, "Using High-Strength Dissolvable Metals to Increase Flow Assurance in High-Temperature and High-Pressure Environments," presented at the SPE Deepwater Drilling and Completions Conference, Bangkok, Thailand, SPE-170561-MS, 2014.
- [43] J. A. Key and D. W. Ball, *Introductory Chemistry -1st Canadian Edition*. Vancouver: BC Campus, 2014.
- [44] R. A. Burns, "Chemical Bonds," in *Fundamentals of chemistry* no. 04; QD33. 2, B8 2003.), 2003.
- [45] P. Taylor and M. Mortimer, *Chemical kinetics and mechanism* (The Molecular World). United Kingdom: Royal Society of Chemistry, 2002.
- [46] J. Clark. (2013). *The Effect of Surface Area on Reaction Rates*. Available: <https://www.chemguide.co.uk/physical/basicrates/surfacearea.html> [Accessed: April 10, 2018]
- [47] A. D. McNaught, A. Wilkinson, M. Nic, J. Jirat, and B. Kosata, *Compendium of chemical terminology*, Version 2.3.3 ed. International Union of Pure and Applied Chemistry, 2014.
- [48] Z. Liu, J. Chen, and Y. Zheng, "Room-temperature synthesis of Mg (OH) 2 nanorods and nanowires in Mg–H₂O–NaCl reaction system," *Micro & Nano Letters*, vol. 8, no. 2, pp. 74-77, 2013.
- [49] D. W. Green and R. H. Perry, *Perry's Chemical Engineer's Handbook*. McGraw-Hill Professional, 1997.
- [50] J. Clark. (2013). *The Collision Theory of Reaction Rates*. Available: <https://www.chemguide.co.uk/physical/basicrates/introduction.html - top> [Accessed: April 10, 2018]

- [51] J. Clark. (2013). *The Effect of Temperature on Reaction Rates*. Available: <https://www.chemguide.co.uk/physical/basicrates/temperature.html> [Accessed: April 10, 2018]
- [52] R. W. Missen, C. A. Mims, and B. A. Saville, *Introduction to Chemical Reaction Engineering and Kinetics*. United States of America: John Wiley & Sons, Inc., 1999.
- [53] M. R. Wright, *Introduction to Chemical Kinetics*. United Kingdom: John Wiley & Sons, Ltd., 2004.
- [54] A. O. Sykes, "An introduction to Regression Analysis," Available: https://chicagounbound.uchicago.edu/law_and_economics/51/ [Accessed: April 10, 2018]
- [55] D. C. Montgomery, E. A. Peck, and G. G. Vining, *Introduction to Linear Regression Analysis*, 5th Ed. ed. (WILEY SERIES IN PROBABILITY AND STATISTICS). United States of America: John Wiley & Sons, 2012.
- [56] J. Frost. (2017, February). *The Difference between Linear and Nonlinear Regression Models*. Available: <http://statisticsbyjim.com/regression/difference-between-linear-nonlinear-regression-models/> [Accessed: April 10, 2018]
- [57] J. O. Rawlings, S. G. Pantula, and D. A. Dickey, S. Edition, Ed. *Applied regression analysis: a research tool*. United States of America: Springer Science & Business Media, 2001.
- [58] Mathworks, "Curve Fitting Toolbox™ User's Guide," United States of America 2017, Available: <https://se.mathworks.com/help/curvefit/?requestedDomain=true> [Accessed: April 10, 2018].
- [59] G. Strang, *Calculus*. MIT - Massachusetts Institute of Technology: Wellesley-Cambridge Press 1991.

Appendix I

Matlab Code for Surface Fitting Experimental Data and Generating 3D-Plots

```
clc
close all
clear all

%% Loading Experimental RODss Data
% the RODss values from the various experiments have been
imported and
% stored as a Matlab workspace file (.mat)
load experimental_data

%% Initialization.

% Initialize arrays to store fits and goodness-of-fit.
fitresult = cell( 4, 1 );
gof = struct( 'sse', cell( 4, 1 ), ...
    'rsquare', [], 'dfe', [], 'adjrsquare', [], 'rmse', [] );

%% Fit: 'NOV Dissolve 105'.
[xData, yData, zData] = prepareSurfaceData( Concentration,
Temperature, ROD_NOV_Dissolve_105 );

% Set up fittype and options.
ft = fittype( 'k*(C^q)*exp(n*T)', 'independent', {'C', 'T'},
'dependent', 'RODss' );
opts = fitoptions( 'Method', 'NonlinearLeastSquares' );
opts.Display = 'Off';
opts.MaxFunEvals = 1000;
opts.MaxIter = 1000;
opts.StartPoint = [0.438744359656398 0.381558457093008
0.765516788149002];
opts.TolFun = 1e-08;
opts.TolX = 1e-08;

% Fit model to data.
[fitresult{1}, gof(1)] = fit( [xData, yData], zData, ft, opts );

% Plot fit with data.
figure( 'Name', 'NOV Dissolve 105' );
h = plot( fitresult{1}, [xData, yData], zData );
%legend( h, 'NOV Dissolve 105', 'ROD NOV Dissolve 105 vs.
Concentration, Temperature', 'Location', 'NorthEast' );
```

```

% Label axes
title('NOV Dissolve 105: ROD_s_s =
f(C,T)', 'FontWeight', 'bold', 'FontSize', 20, 'FontName', 'Times');
xlabel ('Concentration
[g/ml]', 'FontWeight', 'bold', 'FontSize', 16, 'FontName', 'Times')
ylabel('Temperature [°C]', 'FontWeight', 'bold', 'FontSize', 16,
'FontName', 'Times');
zlabel ('ROD_s_s [mg/cm^2/hr]',
'HorizontalAlignment', 'center', 'FontWeight', 'bold', 'FontSize', 16
, 'FontName', 'Times')
grid on
c = colorbar('southoutside');
c.Label.String = ('ROD_s_s [mg/cm^2/hr]');

% Fit: 'NOV Dissolve 106'.
[xData, yData, zData] = prepareSurfaceData( Concentration,
Temperature, ROD_NOV_Dissolve_106 );

% Set up fittype and options.
ft = fittype( 'k*(C^q)*exp(n*T)', 'independent', {'C', 'T'},
'dependent', 'ROD_ss' );
opts = fitoptions( 'Method', 'NonlinearLeastSquares' );
opts.Display = 'Off';
opts.MaxFunEvals = 1000;
opts.MaxIter = 1000;
opts.StartPoint = [25 0.0247 0.2621];
opts.TolFun = 1e-08;
opts.TolX = 1e-08;

% Fit model to data.
[fitresult{4}, gof(4)] = fit( [xData, yData], zData, ft, opts );

% Plot fit with data.
figure( 'Name', 'NOV Dissolve 106' );
h = plot( fitresult{4}, [xData, yData], zData );
%legend( h, 'NOV Dissolve 106', 'ROD NOV Dissolve 106 vs.
Concentration, Temperature', 'Location', 'NorthEast' );
% Label axes
title('NOV Dissolve 106: ROD_s_s =
f(C,T)', 'FontWeight', 'bold', 'FontSize', 20, 'FontName', 'Times');
xlabel ('Concentration
[g/ml]', 'FontWeight', 'bold', 'FontSize', 16, 'FontName', 'Times')
ylabel('Temperature [°C]', 'FontWeight', 'bold', 'FontSize', 16,
'FontName', 'Times');
zlabel ('ROD_s_s [mg/cm^2/hr]',
'HorizontalAlignment', 'center', 'FontWeight', 'bold', 'FontSize', 16
, 'FontName', 'Times')

```

```

grid on
c = colorbar('southoutside');
c.Label.String = ('ROD_s_s [mg/cm^2/hr]');

%% Fit: 'NOV Dissolve 202'.
[xData, yData, zData] = prepareSurfaceData( Concentration,
Temperature, ROD_NOV_Dissolve_202 );

% Set up fitype and options.
ft = fitype( 'k*(C^q)*exp(n*T)', 'independent', {'C', 'T'},
'dependent', 'ROD_ss' );
opts = fitoptions( 'Method', 'NonlinearLeastSquares' );
opts.Display = 'Off';
opts.MaxFunEvals = 1000;
opts.MaxIter = 1000;
opts.StartPoint = [0.585267750979777 0.223811939491137
0.751267059305653];
opts.TolFun = 1e-08;
opts.TolX = 1e-08;

% Fit model to data.
[fitresult{2}, gof(2)] = fit( [xData, yData], zData, ft, opts );

% Plot fit with data.
figure( 'Name', 'NOV Dissolve 202' );
h = plot( fitresult{2}, [xData, yData], zData );
%legend( h, 'NOV Dissolve 202', 'ROD NOV Dissolve 202 vs.
Concentration, Temperature', 'Location', 'NorthEast' );
% Label axes
title('NOV Dissolve 202: ROD_s_s =
f(C,T)', 'FontWeight', 'bold', 'FontSize', 20, 'FontName', 'Times');
xlabel ('Concentration
[g/ml]', 'FontWeight', 'bold', 'FontSize', 16, 'FontName', 'Times')
ylabel('Temperature [°C]', 'FontWeight', 'bold', 'FontSize', 16,
'FontName', 'Times');
zlabel ('ROD_s_s [mg/cm^2/hr]',
'HorizontalAlignment', 'center', 'FontWeight', 'bold', 'FontSize', 16
, 'FontName', 'Times')
grid on
c = colorbar('southoutside');
c.Label.String = ('ROD_s_s [mg/cm^2/hr]');

%% Fit: 'NOV Dissolve 301'.
[xData, yData, zData] = prepareSurfaceData( Concentration,
Temperature, ROD_NOV_Dissolve_301 );

% Set up fitype and options.

```



```

ft = fitype( 'k*(C^q)*exp(n*T)', 'independent', {'C', 'T'},
'dependent', 'ROD_ss' );
opts = fitoptions( 'Method', 'NonlinearLeastSquares' );
opts.Display = 'Off';
opts.MaxFunEvals = 1000;
opts.MaxIter = 1000;
opts.StartPoint = [0.196595250431208 0.251083857976031
0.616044676146639];
opts.TolFun = 1e-08;
opts.TolX = 1e-08;

% Fit model to data.
[fitresult{3}, gof(3)] = fit( [xData, yData], zData, ft, opts );

% Plot fit with data.
figure( 'Name', 'NOV Dissolve 301' );
h = plot( fitresult{3}, [xData, yData], zData);

%legend( h, 'NOV Dissolve 301', 'ROD NOV Dissolve 301 vs.
Concentration, Temperature', 'Location', 'NorthEast' );
% Label axes
title('NOV Dissolve 301: ROD_s_s =
f(C,T)', 'FontWeight', 'bold', 'FontSize', 20, 'FontName', 'Times');
xlabel ('Concentration
[g/ml]', 'FontWeight', 'bold', 'FontSize', 16, 'FontName', 'Times')
ylabel('Temperature [°C]', 'FontWeight', 'bold', 'FontSize', 16,
'FontName', 'Times');
zlabel ('ROD_s_s [mg/cm^2/hr]',
'HorizontalAlignment', 'center', 'FontWeight', 'bold', 'FontSize', 16
, 'FontName', 'Times')
grid on
c = colorbar('southoutside');
c.Label.String = ('ROD_s_s [mg/cm^2/hr]');

```

Appendix II

Matlab Code to generate Figure 4-70 based on the Ball Size Calculator analytical model

```
clc
clear all
close all
%% Inputs

D_i=3.625*2.54; %in cm
rho=1.724; % in sg
ROD_ss=119.96; % in mg/cm2/hr
t_ss=1.88; % in hours

t_start=0; % hrs
t_end=10; % hrs
dt=.001; %time increment

%% Calculation
Di_inches=D_i/2.54;
rho=rho*1000; % converting from g/cc to mg/cc
D_ss = D_i-(ROD_ss*t_ss/rho);

n= 1+((t_end-t_start)/dt);
t=t_start:dt:t_end; %Generating time vector

for i=1:n
    if t(i)<=t_ss
        D(i)=D_i-((ROD_ss*(t(i)^2))/(t_ss*rho));
    else
        D(i)=D_i-((ROD_ss/rho)*((2*t(i))-t_ss));
    end
end

D_inches=D/2.54;

%% Output

% Create figure
figure1 = figure;

% Create axes
axes1 = axes('Parent',figure1);
hold(axes1,'on');
```

```

% Create plot
plot(t,D_inches);

% Create xlabel
xlabel('Time, t
[hours]', 'HorizontalAlignment', 'center', 'FontName', 'Times');

% Create ylabel
ylabel('Diameter, D(t) [in.]', 'HorizontalAlignment', 'center', ...
'FontName', 'Times');

% Create title
title('Diameter, D(t) versus Time, t for NOV Dissolve 105 Ball
at 80 °C in 1% NaCl', ...
'HorizontalAlignment', 'center', ...
'FontWeight', 'bold');

ylim(axes1, [3.1 3.7]);
box(axes1, 'on');
grid(axes1, 'on');
% Set the remaining axes properties
set(axes1, 'FontName', 'Times', 'FontSize', 30, 'XTick', ...
[0 1 1.88 3 4 5 6 7 8 9 10], 'XTickLabel', ...
{'0', '1', '1.88
(t_s_s)', '3', '4', '5', '6', '7', '8', '9', '10'}, 'YTick', ...
[3.1 3.2 3.3 3.4 3.5 3.574 3.625 3.7], 'YTickLabel', ...
{'3.1', '3.2', '3.3', '3.4', '3.5', '3.574 (D_s_s)', '3.625
(D_i)', '3.7'});

```